

Effect of climate change on temperate forest ecosystems

Nederlandse Geografische Studies / Netherlands Geographical Studies

Redactie / Editorial Board

Drs. J.G. Borchert (Editor in Chief)
Prof. Dr. J.M.M. van Amersfoort
Dr. P.C.J. Druiven
Prof. Dr. A.O. Kouwenhoven
Prof. Dr. H. Scholten

Plaatselijke Redacteuren / Local Editors

Dr. R. van Melik,
Faculteit Geowetenschappen Universiteit Utrecht
Dr. D.H. Drenth,
Faculteit der Managementwetenschappen Radboud Universiteit Nijmegen
Dr. P.C.J. Druiven,
Faculteit der Ruimtelijke Wetenschappen Rijksuniversiteit Groningen
Dr. L. van der Laan,
Economisch-Geografisch Instituut Erasmus Universiteit Rotterdam
Dr. J.A. van der Schee,
Centrum voor Educatieve Geografie Vrije Universiteit Amsterdam
Dr. F. Thissen,
Afdeling Geografie, Planologie en Internationale Ontwikkelingsstudies Universiteit van Amsterdam

Redactie-Adviseurs / Editorial Advisory Board

Prof. Dr. G.J. Ashworth, Prof. Dr. P.G.E.F. Augustinus, Prof. Dr. G.J. Borger,
Prof. Dr. K. Bouwer, Prof. Dr. J. Buursink, Prof. Dr. G.A. Hoekveld,
Dr. A.C. Imeson, Prof. Dr. J.M.G. Kleinpenning, Dr. W.J. Meester,
Prof. Dr. F.J. Ormeling, Prof. Dr. H.F.L. Ottens, Dr. J. Sevink, Dr. W.F. Slegers,
T.Z. Smit, Drs. P.J.M. van Steen, Dr. J.J. Sterkenburg, Drs. H.A.W. van Vianen,
Prof. Dr. J. van Weesep

Netherlands Geographical Studies 396

Effect of climate change on temperate forest ecosystems

Reinder Jacob Brolsma

Utrecht 2010

Royal Dutch Geographical Society /
Faculty of Geosciences, Utrecht University

This publication is identical to a dissertation submitted for the degree of Doctor at Utrecht University, The Netherlands. The public defense of this thesis took place on June 25, 2010.

The publication of this thesis has been co-financed by Deltares.

Promotor

Prof. dr. M.F.P. Bierkens, Utrecht University

Co-promotor

Dr L.P.H. van Beek, Utrecht University

Examination committee

Prof. dr. A.J. Dolman, VU University Amsterdam (The Netherlands)

Prof. dr. M. Sivapalan, University of Illinois (United States of America)

Prof. dr. S.E.A.T.M. van der Zee, Wageningen University (The Netherlands)

Prof. dr. J.P.M. Witte, VU University Amsterdam (The Netherlands)

dr. S.C. Dekker, Utrecht University (The Netherlands)

ISBN 978-90-6809-439-8

Copyright © R.J. Brolsma p/a Faculty of Geosciences, Utrecht University, 2010.

Niets uit deze uitgave mag worden vermenigvuldigd en/of openbaar gemaakt door middel van druk, fotokopie of op welke andere wijze dan ook zonder voorafgaande schriftelijke toestemming van de uitgevers.

All rights reserved. No part of this publication may be reproduced in any form, by print or photo print, microfilm or any other means, without written permission by the publishers.

Printed in the Netherlands by A-D Druk – Zeist.

Contents

Figures	9
Tables	11
1 Introduction	13
1.1 Context: Climate change	13
1.2 Eco-hydrology of forest ecosystems	14
1.2.1 Hydrological cycle	14
1.2.2 Carbon cycle	15
1.2.3 Connecting the carbon and hydrological cycle	16
1.3 Influence of groundwater in temperate climate	18
1.4 Adaptation to climate change	18
1.5 Numerical modeling of vegetation	20
1.6 Research questions	23
1.7 Thesis outline	23
2 Groundwater - soil water - vegetation dynamics	25
2.1 Introduction	25
2.2 Methods	27
2.2.1 Model description	27
2.2.2 Plant stress	30
2.2.3 Model runs	32
2.3 Results	33
2.3.1 Hydrological test run	33
2.3.2 Vegetation	34
2.3.3 Influence of rainfall amount	35
2.3.4 Influence of rainfall frequency	38
2.3.5 Slope and aquifer thickness	38
2.4 Discussion and conclusions	40
3 Vegetation competition model for water and light limitation. I: Model description, one-dimensional competition and the influence of groundwater	43
3.1 Introduction	44
3.2 Model description	45
3.2.1 Soil water balance	46
3.2.2 Atmospheric forcing	46
3.2.3 Vegetation growth	48
3.2.4 Temporal upscaling	55
3.2.5 Growth, allocation, allometry and phenology	56
3.3 Results	59

3.3.1	Comparison with fluxdata	59
3.3.2	Light and water competition and the influence of groundwater	62
3.4	Conclusions	67
4	Vegetation competition model for water and light limitation. II: Spatial dynamics of groundwater and vegetation	71
4.1	Introduction	72
4.2	Methods	74
4.2.1	Atmospheric forcing	74
4.2.2	Vegetation model	74
4.2.3	Hydrological model	75
4.2.4	Experiments	79
4.3	Results and discussion	80
4.3.1	Seasonal dynamics	80
4.3.2	Long-term dynamics	81
4.3.3	Sensitivity analysis	83
4.3.4	Influence of variable groundwater level	92
4.4	Conclusions	92
5	Climate change impact on a groundwater-influenced hillslope ecosystem	95
5.1	Introduction	96
5.2	Methods	98
5.2.1	Hydrological model	98
5.2.2	Vegetation model	98
5.2.3	Weather generator	103
5.2.4	Climate change scenario runs	104
5.2.5	Model setup	106
5.3	Results	107
5.3.1	Temperature change	108
5.3.2	Precipitation change	108
5.3.3	Change in atmospheric carbon dioxide	111
5.3.4	Combined effect	111
5.4	Discussion and conclusions	114
6	Synthesis	119
6.1	Groundwater, soil water and vegetation dynamics based on a hydrological approach	119
6.2	Effect of groundwater on vegetation dynamics and hydrological fluxes	121
6.3	Effect of spatio-temporal groundwater dynamics on vegetation growth	124
6.4	Influence of climate change on a groundwater influenced temperate hillslope ecosystem	125
6.5	Vegetation stress in water and light limited forest ecosystems	127
6.6	Implications for other disciplines	128
6.6.1	Ecological modeling	130
6.6.2	Climate modeling	131
6.6.3	Hydrological modeling	131
6.7	Main contributions and insights	132

Appendices	
A Parameters Chapter 3	135
B Parameters Chapter 4	139
Abstract	141
Samenvatting	143
Bibliography	145
Acknowledgements	153
Publications	155
Curriculum Vitae	157

Figures

1.1	Hydrological cycle in a forest.	15
1.2	Carbon cycle in a forest.	16
1.3	Relation of a groundwater gradient and vegetation composition in old growth forest in Białowieża, East Poland.	19
1.4	The way groundwater and vegetation dynamics are simulated in Chapters 2 to 5 and the analysis that has been performed.	24
2.1	Schematic representation of the 2-dimensional hydrological model	27
2.2	Feddes' root water uptake reduction function and Feddes' function converted to static stress function for both vegetation types.	29
2.3	Transpiration of the vegetation along the slope, the relative soil moisture content and the height of the groundwater level for 1, 5, 8 and 15 years after starting the hydrological test run.	34
2.4	Oxygen and water stress for the baseline precipitation scenario	35
2.5	Dynamic oxygen and water stress for the complete system per year for the different locations of the vegetation boundary and different precipitation amount scenarios.	36
2.6	Mean total dynamic stress for the complete system per year for the different locations of the vegetation boundary and different precipitation amount scenarios.	36
2.7	Mean evapotranspiration for the complete system per year for the different locations of the vegetation boundary and different precipitation amount scenarios.	37
2.8	Mean soil moisture content for the complete system per year for the different locations of the vegetation boundary and precipitation amount scenarios.	37
2.9	Interception, evapotranspiration and runoff at the maximum productivity of each precipitation scenario and the influence of changing the amount of rainfall on days that it rains and the influence of changing the number of days that is rains.	39
2.10	Influence of rainfall amount and slope on the location of the boundary between two vegetation types based on the minimum stress criterion.	40
3.1	Scheme used for radiation absorption by trees.	55
3.2	Comparison of measured and modeled fluxes and stomatal conductance for a 5 day period in Hainich forest. Influence of environmental variables on modeled stomatal conductance and evapotranspiration and carbon flux.	60
3.3	Modeled versus measured half-hourly flux data of ET and CO_2 for four five day periods in 2004.	61

3.4	Daily values of measured and modeled fluxes of <i>ET</i> and CO ₂ in Hainich Forest in 2004 using a 10 day running means filter.	62
3.5	Development of biomass and soil moisture of a wet adapted and a drought adapted vegetation type in a case with percolation only and three different groundwater depths on sandy loam.	65
3.6	500 Year average of biomass, evapotranspiration and yearly minimum, maximum and mean soil moisture content along a groundwater gradient for four soil textures.	66
3.7	Influence of groundwater depth on the water balance and biomass for four different soil textures based on 500 year average values.	68
3.8	Dependence of <i>ET</i> on biomass for four soil textures. Biomass and <i>ET</i> are 500 year averages along a gradient of groundwater depths.	69
4.1	An example of the influence of a groundwater gradient on vegetation composition in old growth forest in Białowieża, East Poland	73
4.2	Cross section and block diagram of hydrological model. A schematic representation of the unsaturated fluxes and the groundwater flux	77
4.3	Evapotranspiration, carbon assimilation, groundwater depth and rootzone soil moisture content of vegetation near climax situation at four locations.	82
4.4	Temporal dynamics during a 300 y period of system average variables.	84
4.5	Average groundwater level, rootzone soil moisture content, biomass and evapotranspiration along a hill slope.	85
4.6	Influence of slope angle on biomass for different soil textures.	88
4.7	Influence of aquifer thickness on biomass for different soil textures.	89
4.8	Influence of rainfall amount on biomass for different soil textures.	90
4.9	Influence of rainfall frequency on biomass for different soil textures.	91
4.10	Effect of a constant and a variable groundwater level for different soil textures on biomass.	93
5.1	Simplified representation of the hillslope, aquifer and groundwater.	99
5.2	Outcomes of the PRUDENCE GCM-RCM combinations for the station Eindhoven for the future time period (2071-2100), relative to the baseline period.	106
5.3	The effect of change in temperature on a groundwater controlled forest ecosystem on a slope.	109
5.4	The effect of change in precipitation on a groundwater controlled forest ecosystem on a slope.	110
5.5	The effect of change in atmospheric CO ₂ concentration on a groundwater controlled forest ecosystem on a slope.	112
5.6	Combined effect of change in CO ₂ , temperature and precipitation on a groundwater controlled forest ecosystem on a slope.	113
6.1	Groundwater level, soil moisture content, biomass, evapotranspiration and dynamic vegetation stress along a hillslope for four different soil textures.	129
6.2	Development of biomass and dynamic vegetation stress during an 80 year period within one cell for sandy loam.	130

Tables

2.1	Used soil parameters	31
2.2	Used parameters for vegetation	31
2.3	Influence of slope and aquifer thickness on maximum evapotranspiration, position, minimum stress, minimum soil moisture content, interception and runoff.	39
3.1	Values of parameters to fill lookup table of Tr and A_n .	56
3.2	Soil textures used in simulation runs.	63
3.3	Parameters of the tree species adapted to dry and wet conditions.	63
3.4	Biomass, evaporation, transpiration, flux between soil and ground water and surface runoff for three groundwater levels for four soil textures.	67
4.1	Parameters of the plant functional type adapted to wet and the plant functional type adapted to dry conditions.	76
4.2	Soil physical parameters for different soil textures used in different simulations.	79
4.3	Results of sensitivity analysis for four different soil textures. Effects of precipitation magnitude, precipitation frequency, aquifer thickness and slope angle on biomass, evaporation, transpiration and net precipitation.	86
5.1	Main characteristics of the baseline run and the climate change scenarios.	105
5.2	Parameters of the plant functional types	107
5.3	Averages of biomass and water balance components in the different climate scenarios.	115
5.4	Summary of the outcomes of the different scenarios, compared to the baseline run.	115

1 Introduction

1.1 Context: Climate change

At present global climate change shows a general increase in atmospheric temperature and precipitation. The past 50 years (1956-2005) mean global temperature increased at a rate of 0.10 to 0.16 °C per decade, which is nearly twice the average over the past 100 years. This temperature rise is largely caused by an increase in greenhouse gases in the atmosphere of which CO₂ is the most important. Global atmospheric CO₂ concentration increased from a pre-industrial value of about 280 ppm to 379 ppm in 2005, where the annual increase during the period 1995-2005 was on average 1.9 ppm per year (IPCC, 2007).

Over the next 100 years (2100) the global average temperature is projected to rise 1.1-6.4 °C as a result of increased atmospheric CO₂ concentration. The precipitation amount is expected to increase at high-latitudes, while a decrease is most likely in most subtropical regions (IPCC, 2007). The magnitude of projected climate change depends on the used CO₂ emission scenario (Nakicenovic & Swart, 2000). The SRES A2 emission scenario of the IPCC is often used in climate projections and describes a very heterogeneous world with continuously increasing global population and regionally oriented economic growth. This scenario has the largest CO₂ emission compared to the other IPCC emission scenarios, causing the atmospheric CO₂ concentration to rise from current 370 ppm to 730 ppm in the period 2070-2100 (Nakicenovic & Swart, 2000). Climate projections based on this scenario produce the largest global temperature rise and change in precipitation.

Regional differences of projected climate change, are however large. Projected climate change for north-western Europe in 2100 entails a rise of annual temperature of 3-5 °C, with a larger rise in summer temperatures than winter temperatures. Precipitation is projected to increase in winter and decrease in summer, where the number of wet days decreases (Christensen et al., 2007). Obviously such profound changes in climate will have a large effect on ecosystems.

In this thesis the effect of climate change on a forest ecosystem in the temperate climate zone is investigated.

To better understand long-term effects of climate change it is important to understand the hydrological and carbon cycle of such a forest ecosystem and more importantly how these two are connected. First, an overview is provided of the water and carbon

fluxes in forest ecosystems. Special attention will be paid to the role of groundwater, which is crucial to vegetation dynamics and hydrological fluxes in temperate climates. Then follows a qualitative description of the way both vegetation and hydrology in forest ecosystems may react to climate change. After that a short review is given of different approaches to modeling vegetation. Finally, this chapter ends with the research questions that will be answered in this thesis, followed by the thesis outline.

1.2 Eco-hydrology of forest ecosystems

1.2.1 Hydrological cycle

Figure 1.1 shows a schematic representation of the most important water fluxes within a temperate forest ecosystem. Only the part of the hydrological cycle is shown that directly affects the forest system. The part of the hydrological cycle that is not shown consists of the fluxes within the atmosphere. In general, the most important water flux into the system is precipitation (P). Other influxes can be runoff (R) and groundwater replenishment (Q_v or Q_h) from surrounding areas. Precipitation falls directly onto the ground as throughfall (P_d) or is intercepted by vegetation. Water that is intercepted by leaves, branches and stem evaporates (E_i), or when the interception capacity is exceeded, falls onto the ground as leaf drip (P_{ind}) or runs off as stemflow (P_s). The interception capacity of vegetation largely depends on the amount of leaf area of the vegetation. The evaporation rate strongly depends on atmospheric conditions and canopy structure, i.e., temperature, incoming radiation (Rad), atmospheric vapor pressure deficit (D) and canopy conductance (often split into boundary layer and atmospheric conductance, g_b and g_a).

Depending on the amount of throughfall and the infiltration capacity of the soil, water that reaches the ground either completely infiltrates (I) or ponds on the surface and is turned to runoff (R), after which it either infiltrates further on or accumulates in streams. Water that infiltrates, is 'temporarily stored' in the unsaturated zone. Water in the unsaturated zone either evaporates from the soil surface (E_s), percolates to the groundwater at high soil moisture contents (Q_v) or is taken up by roots (J_w), depending on the vegetation type and prevailing atmospheric and soil moisture conditions. Almost all water that is taken up by roots transpires from the leaves, while a small part can be temporarily stored within the tree's tissue. Transpiration of vegetation again depends strongly on atmospheric and canopy conductance, but also on stomatal conductance g_s . The water flux from the land surface to the atmosphere is thus greatly influenced by vegetation. Vegetation influences the energy and water balance through its physiological properties (in particular, leaf area index, stomatal resistance, and rooting depth), albedo, surface roughness, and its effect on soil moisture (Arora, 2002).

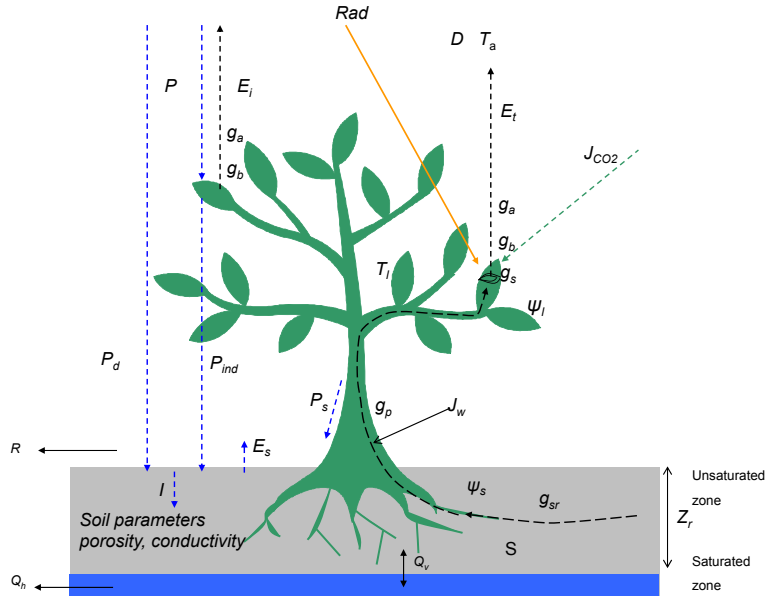


Figure 1.1 Hydrological cycle in a forest showing the following water fluxes and conductances: P , precipitation; P_d , direct throughfall; P_{ind} , indirect throughfall; P_s , stemflow; E_i , interception evaporation; I , infiltration; E_s , soil evaporation; Q_v , vertical soil water flux; Q_h , the horizontal ground-water water flux; J_w , water flux through the tree; E_t , transpiration of the tree; R , runoff; g_{sr} and g_p , soil-root and plant conductance; g_s , g_b and g_a , stomatal, leaf boundary layer and atmospheric conductances. Other fluxes and variables are: Rad , net incoming radiation; J_{CO_2} , CO_2 flux from the atmosphere; D , atmospheric vapor pressure deficit; T_a , air temperature; Ψ_l , leaf water potential; Ψ_s , soil water potential; T_l , leaf temperature; S , water stored in the soil; Z_r , rootzone depth.

1.2.2 Carbon cycle

Figure 1.2 shows the most important carbon fluxes in forest ecosystems. CO_2 from the atmosphere is taken up by vegetation into the leaf through the stomata. Carbon assimilation increases with a higher gradient between atmospheric (c_a) and intercellular (c_i) carbon concentration (inside the leaf). Carbon uptake therefore depends on atmospheric carbon concentration and the atmospheric, boundary layer and stomatal conductance to CO_2 (g_{a,CO_2} , g_{b,CO_2} and g_{s,CO_2}). The delivery of carbon to the leaves for one part determines the carbon assimilation rate.

The carbon assimilation rate of vegetation also depends on biochemical processes which are influenced by the available energy, i.e., solar radiation (photosynthetic active radiation, PAR), leaf temperature (T_l) and the availability of the enzyme Rubisco. Carbon assimilation is either light limited when solar radiation is low (in case of shading or in winter), or Rubisco limited when solar radiation is abundant (sunlit leaves in summer). Assimilated carbon is then stored as carbohydrates.

The other important CO_2 flux is respiration, consisting of autotrophic and heterotrophic respiration. Autotrophic respiration is respiration by the carbon-assimilating species in the ecosystem and can be divided into photorespiration and dark (or mitochondrial) respiration. Photorespiration occurs during photosynthesis in C3 plants. Dark respiration results from plant growth (R_{growth}) and maintenance

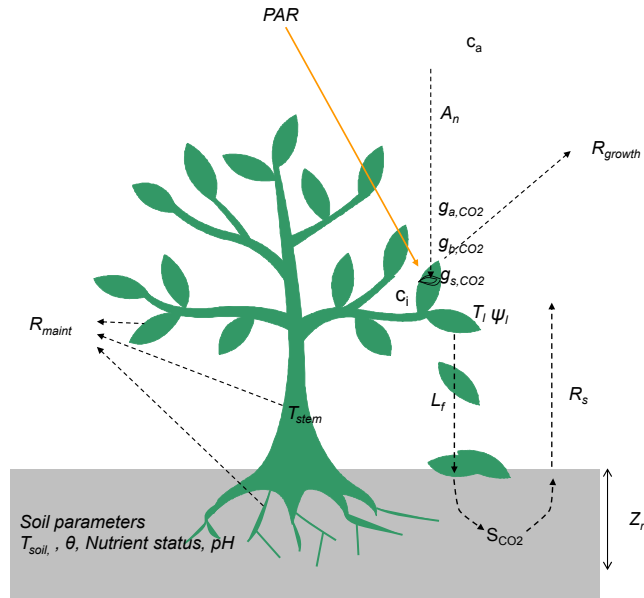


Figure 1.2 Carbon cycle in a forest showing the following fluxes and variables: A_n , net carbon assimilation (carbon assimilation minus photorespiration); g_s,CO_2 , g_b,CO_2 and g_a,CO_2 , stomatal, leaf boundary layer and atmospheric conductances for CO_2 ; R_{maint} , maintenance respiration; R_{growth} , growth respiration; R_s , soil respiration; L_f , leaf fall; c_a , atmospheric carbon concentration; c_i , intercellular carbon concentration. Other variables are: PAR , photosynthetic active radiation; T_l , T_{soil} , T_{stem} , leaf, soil and wood temperature respectively; Ψ_l , leaf water potential; S_{CO_2} , carbon stored in the soil; θ , soil moisture content; pH , acidity; Z_r , the rootzone depth.

(R_{maint}). Growth respiration occurs when providing the energy required by the biosynthesis of new tissues and mainly occurs in the leaves and to a lesser extent in new shoots and roots. Growth respiration is proportional to the growth rate of the plant. Maintenance respiration is the energy required to maintain all tissues and is proportional to the living biomass of the plant. Heterotrophic respiration occurs by all non-carbon assimilating organisms (animals, fungi, bacteria etc). An important part of heterotrophic respiration occurs in the soil, resulting from mineralization of organic matter. This process is called soil respiration (R_s).

Evergreen trees continuously replace older leaves by new ones (L_f), while deciduous trees shed their leaves in winter. Also, fine roots grow new and are shed depending on temperature and soil moisture availability. Plant litter is reworked by small soil organisms to fine soil organic matter and partly mineralized (used as food supply) by micro organisms, bacteria and fungi. The conversion of litter and soil organic matter to CO_2 , i.e. soil respiration, depends very much on soil moisture content and soil temperature (e.g. Reichstein et al., 2003).

1.2.3 Connecting the carbon and hydrological cycle

In a forest ecosystem the carbon and hydrological cycle are closely connected. The most important connections are through the stomatal conductance and the leaf area. The stomatal conductance influences both the transpiration and the carbon flux; when

carbon enters the leaf during carbon assimilation water transpires from the leaf.

The available energy from radiation, atmospheric vapor pressure deficit and atmospheric conductance (which depends on wind speed and atmospheric stability) together determine the atmospheric capacity for evaporation. This means that, whenever the plant opens its stomata to allow CO_2 to enter the leaves, it will also lose a certain amount water to the atmosphere. The loss of water will decrease the leaf water potential (Ψ_l), which causes a gradient in water potential between the soil and the leaf. During favorable soil moisture conditions the plant replenishes this by taking up water through the roots. The flux of water that is maintained, depends on conductances within the soil, between soil and roots, within the plant and finally the stomatal conductance. All these conductances decrease at low water potentials. If the flow of water from the soil to the leaf is large enough to sustain what is lost through evaporation, the leaf water potential will remain more or less constant, and transpiration persists. However, in case the soil becomes drier, the root water uptake diminishes, causing a more negative leaf water potential. If the leaf water potential decreases, the stomata begin to close, stomatal conductance decreases, and eventually the plant will cease to transpire water. This is a defense mechanism of the plant against losing too much water, i.e., wilting. This implies that the plant can no longer take up CO_2 from the atmosphere, inhibiting carbon assimilation and plant growth stops. There are more conditions at which stomata close, such as at low light intensities (in winter and at night) and at high and low temperatures.

Another feedback between transpiration and carbon assimilation is through the leaf temperature. When stomata open during the day transpiration starts. This latent heat flux has a cooling effect on the leaf. The leaf temperature in turn influences the opening of the stomata itself, but also the biochemical activity within the leaf and therefore carbon assimilation.

Additionally, the carbon and hydrological cycle are coupled through soil respiration. Soil respiration is, apart from temperature, also strongly influenced by soil moisture conditions.

Another important link between the hydrological and carbon cycle is through the *LAI* which is largely a function of biomass. A high *LAI* causes a high interception capacity and therefore, under favorable atmospheric circumstances, a high canopy interception evaporation. Also transpiration will be high under favorable atmospheric circumstances, because more radiation is absorbed and the amount of stomata increases. However, high interception evaporation and transpiration lead to drier soil conditions and therefore again limited transpiration, more water stress, closing stomata, and less carbon assimilation. This in turn reduces the amount of leaf area and biomass. These feedbacks cause a dynamic equilibrium to develop between biomass and *LAI* and moisture availability.

Many (hydrological) models use a fixed ratio of assimilation rate and transpiration rate during the season or even during the day. This ratio is called water use efficiency (*WUE*). Based on the description of the connections between the hydrological and carbon cycle it can be seen that using a fixed ratio of assimilation rate and transpira-

tion rate (water use efficiency, *WUE*) during the season or even during the day can lead to large errors in either assimilation or transpiration rates.

1.3 Influence of groundwater in temperate climate

In the temperate climate zone vegetation growth is limited by several factors: light, water and nutrients. Because in temperate climates precipitation exceeds evaporation, groundwater bodies develop with shallow water tables, at least in areas with a permeable substrate. This makes vegetation in a temperate climate if not groundwater controlled certainly groundwater influenced.

In summer periods, the soil moisture content drops as a consequence of increased evapotranspiration due to increased solar radiation and higher temperatures. Soil moisture contents can become so low that evapotranspiration and carbon assimilation are hampered and restrict vegetation growth. The presence of groundwater near the rootzone can (partly) prevent growth reduction. On the other hand if groundwater is too close to the surface (during part of the year), a shortage of oxygen can occur, i.e., oxygen stress (Feddes et al., 1978; Bartholomeus et al., 2008b). Within landscapes with sufficient relief these processes can occur at the same time, as water stress occurs upslope and oxygen stress occurs in the valley.

Different species have adapted to different soil moisture conditions. E.g. *Quercus robur* and *Pinus sylvestris* grow at relatively dry locations and *Betula pubescens* and *Alnus glutinosa* can live at nearly saturated locations, whereas *Fagus sylvatica* can grow in between; this is of course, also depending on substrate and soil type. This differentiation causes a zonation in vegetation along a hillslope to develop, e.g., Figure 1.3 and Falinski & Falinska (1986).

At the same time upslope-downslope interactions can occur, where upslope changes influence downslope processes. For example, forest clearing upslope can temporarily cause more groundwater recharge, and therefore wetter conditions downslope. Changing climate conditions, e.g., a decrease in precipitation, affecting the soil moisture content, can cause vegetation zones to shift up or down along the slope. This shift in its turn can influence the groundwater level along the entire slope. These interactions ask for a coupled approach to study vegetation and groundwater processes.

1.4 Adaptation to climate change

Both vegetation and hydrology are influenced by climate change and both have been subject to many field, experimental and modeling studies. Field studies and experiments show a complex response of vegetation to temperature rise, precipitation change and atmospheric CO₂ rise. These responses occur at different spatial and temporal scales.

The physiological responses of a plant to increased atmospheric CO₂ concentration is

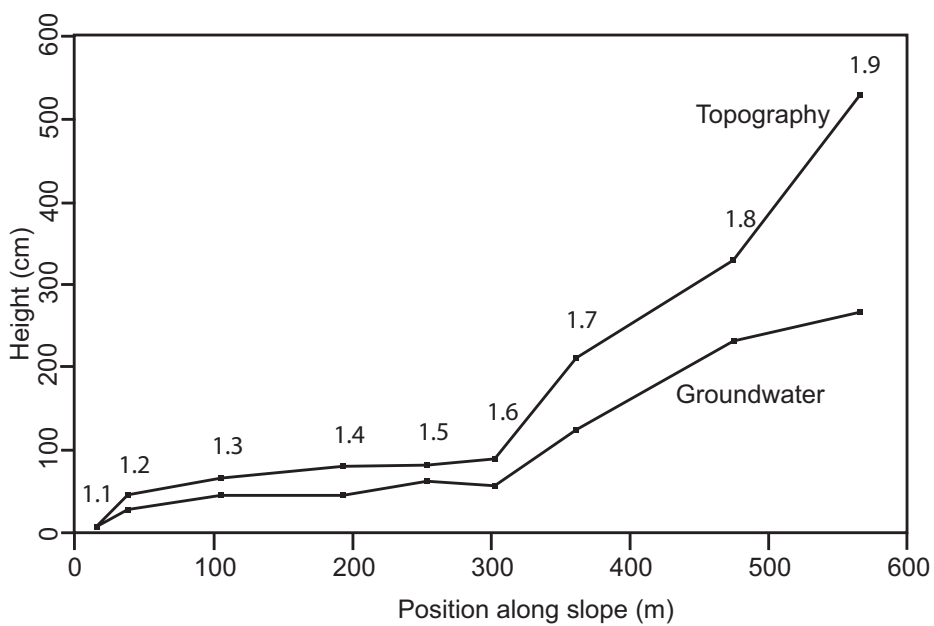
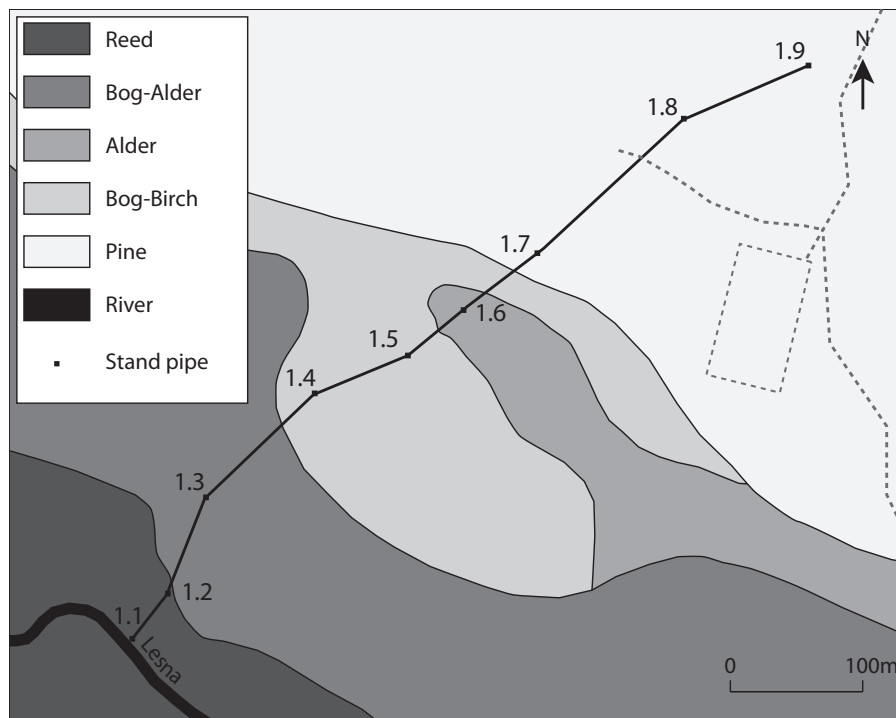


Figure 1.3 Example of the influence of a groundwater gradient (four week average July-August, 2004) on vegetation composition in old growth forest in Białowieża, East Poland (Bosch, 2006).

to reduce its stomatal conductance (e.g. Medlyn et al., 2001; Kruijt et al., 2008). The decrease in stomatal conductance results in reduced transpiration of the plant. At the same time the increase in CO₂ causes higher carbon assimilation rates and net primary production, resulting in a higher biomass, which induces transpiration. Most studies to the increased carbon concentration effect are based on short measurement periods on plants and young (small) trees. The long term effect of increased atmospheric CO₂ concentration on tree species is not clear, also because the interactions with other limiting factors like nutrients and water availability are not well known (Karnosky, 2003).

Temperature rise affects vegetation physiologically by increasing the biochemical activity. Both carbon assimilation and respiration are expected to increase, but the net effect on vegetation growth is unclear and depends also on other environmental conditions (Saxe et al., 2001). Also evapotranspiration is expected to increase as a result of temperature rise, which directly influences hydrology. In case of deciduous trees, a temperature increase also affects phenology, as the growing season is extended. This results in an extended period of carbon assimilation and respiration and thus influences vegetation growth. The change in phenology also affects hydrology as transpiration and interception evaporation are influenced as well. The exact reaction of phenology is however uncertain, because the true mechanisms are not yet understood and the relation between phenology and day length is also strong (Saxe et al., 2001).

Changes in precipitation amount and patterns directly influence hydrology as it determines the amount of water available for interception evaporation, vegetation transpiration and groundwater recharge. Changes in precipitation influence vegetation through soil moisture. This influences (fine) root growth and growth of mycorrhiza and therefore root water uptake. In the longer term, vegetation can respond to for instance drier soil moisture conditions by investing more resources to the root system instead of above ground biomass to enlarge its root system. Periods of droughts also influence LAI and therefore interception evaporation, which again influences the hydrological part of the system.

All these changes in climate conditions also influence the vegetation structure and patterns. Shifts in vegetation zones are expected to occur as a result of temperature rise and changes in precipitation. On a global scale vegetation zones are expected to shift to higher latitudes and on a local scale zones are expected to shift to higher altitudes. Due to changes in precipitation shifts in vegetation can occur, where drought tolerant species replace wet tolerant species and vice versa (Smith et al., 1992; Emanuel et al., 1985).

1.5 Numerical modeling of vegetation

The previous section mentions many feedbacks in the vegetation response to climate change. Field experiments have limitations when trying to quantify the effect of climate change on vegetation systems. This is partly caused by the long response time of vegetation systems to changes in environmental conditions. Therefore long lasting

field experiments have to be conducted. Also the large scale effects on vegetation structure and shifts in zonation are difficult to study, as the complete vegetation system has to be subjected to artificial climate conditions, which is logistically impossible. Geographical substitution can be a solution, where comparable ecosystems (in terms of vegetation type, substrate, exposure, slope angle etc.) at different locations, but with different climate conditions are compared. This approach also has limitations, because it is difficult to isolate the effect of climate, as in reality there will also be simultaneous changes in other environmental conditions.

The effect of climate change on hydrological systems is also far from straightforward. It depends heavily on how vegetation reacts to changes in precipitation, temperature and atmospheric CO₂ concentration. Changes in vegetation affect the hydrological system through changes in interception evaporation and transpiration, while changes in hydrology feed-back on vegetation (Eagleson, 1978). A sound analysis of hydrological sensitivity to climate change thus demands a coupled vegetation-hydrology approach, i.e., eco-hydrological models (Rodriguez-Iturbe, 2000).

Numerical or computer models can help understand and predict the reaction of eco-hydrological systems to climate change. Using numerical models, the often non-linear, vegetation processes and their reaction to climate change can be combined and studied. The many non-linear relationships make the model outcomes highly involved and difficult to predict beforehand. The presence of so many non-linear relations necessitates a vegetation model that is as bio-physically based as possible and a hydrological model that is equally physically sound.

Many vegetation growth models have been developed for and used in climate change studies. Here a short overview is given, without the ambition to be complete. Existing vegetation models that are used to predict climate change effects on vegetation systems are mostly designed to make predictions on a large (global) scale (e.g. Friend et al., 1997; Prentice et al., 1993; Sitch et al., 2003). These models are highly complex in all the processes that they include. However, these models are basically point models and lack many local interactions and feedbacks and as well as interactions between different cells. They do compare well with other point models (e.g. Dufrêne et al., 2005), which are also used to predict the effect of climate change. For instance Davi et al. (2006) used a physiologically based multi-layer model to simulate different forests and the effect of transient climate change up to 2100. They investigated sensitivity of water and carbon fluxes to climate change. As the model that they used was a point model, it contained only one species and did not include groundwater dynamics. Haxeltine et al. (1996) introduced a form of competition in an equilibrium based vegetation model. The competition is based on the predicted net primary production of a certain plant functional type. The species with the highest expected net primary production is selected as the occurring species. Another option to allow for local competition and local scale variations in soil moisture and vegetation competition is using Lotka Volterra type equations (e.g. Arora & Boer, 2006).

Forest gap models (e.g. Botkin et al., 1972; Leemans & Prentice, 1989) simulate forest growth based on growth of individual trees and have been used to determine the effect of climate on forest composition (e.g. Fischlin et al., 1995). Many of these

forest gap models simulate establishment, growth and mortality of individual trees on small patches of land (often 1000m²) as a function of species natural histories and the extrinsic and intrinsic conditions of the stand. These models are however horizontally non-explicit. Forest development at a larger spatial scale is estimated by averaging the successional patterns of these patches from a multitude of simulation runs.

Models such as Forest-BGC (Running & Coughlan, 1988) that are meant to simulate forest growth at the scales of decades to centuries tend to simplify some relationships. Forest-BGC calculates evaporation using Penman-Monteith and a reduction based on the stomatal conductance at low leaf water potentials, that is directly coupled to soil water storage. Assimilation in Forest-BGC is based on a maximum rate and reduction factors for water (based on canopy water content), light nutrients and temperature. Vegetation growth and dynamics are not modeled.

Another class of models consists of models that simulate crop growth. These are meant to simulate crop growth throughout the season. However, they have been applied to natural vegetation at the landscape scale. These models are somewhat more empirical. For instance, the WAVES model (Zhang & Dawes, 1998) as well as the crop growth model WOFOST (Boogaard et al., 1998) (also part of SWAP, van Dam et al. (2008)) calculates transpiration with Penman-Monteith and uses a maximum assimilation rate that is reduced by multiplication factors for soil moisture, nutrients and temperature.

In hydrological models vegetation dynamics are often (over)simplified. Early approaches to include vegetation into hydrological models are most often limited to evapotranspiration and the factors directly influencing it like LAI and soil moisture content (e.g. Abbott et al., 1986a; Wigmosta et al., 1994; Famiglietti et al., 1992). In the field of hydrology an increased interest seems to exist in the effect of vegetation on the water balance. Vegetation models of varying complexity have been developed, but these models mostly focus on water limited systems (e.g. Rodriguez-Iturbe & Porporato, 2004; Daly et al., 2004; Laio et al., 2009; Tamea et al., 2009). One of the recent approaches are based on optimality principles in vegetation functioning (e.g. van der Tol et al., 2008b,a; Schymanski et al., 2009). These models do however all simulate static vegetation and the interaction with groundwater is absent. There are only a few studies combining a vegetation model and a hydrological model. Band et al. (1993) used the Forest-BGC (Running & Gower, 1991) to simulate forest carbon, water and nitrogen budgets at a stand level and combined it with TOPMODEL (Beven, 1979) which is a quasi-distributed hydrological model. However, vegetation in this model is still static in the sense that there is no competition or growth. Other combinations of vegetation and hydrological models seem nonexistent.

To be able to make predictions about the hydrological system under climate change, vegetation dynamics need to be included. Using only predefined response functions as are used in hydrological models neglects effects like increased *LAI*, changes in stomatal conductance (resulting from change in CO₂ concentration) and shifts in vegetation types.

The model that is eventually developed in this study includes many of the men-

tioned omissions in existing models. It operates at a landscape scale, includes lateral hydrological connections through groundwater flow and vegetation dynamics. The latter include, bio-physically based carbon assimilation and transpiration, vegetation growth, inter-species light competition and the response to both water and oxygen stress.

1.6 Research questions

The discussion above shows the complexity of manifold non-linear relations of ecosystem response to climate change and addresses knowledge gaps at the hillslope scale. This thesis especially focuses on the knowledge gaps that arise from the lack of interdisciplinary approaches between hydrological and ecological studies. An integrated approach is used to determine the effect of climate change on groundwater influenced vegetation systems, where vegetation influences hydrology and vice versa. This enables the assessment of the effect of climate change on hydrology including soil moisture dynamics and lateral connections in the landscape through groundwater, in combination with vegetation dynamics including competition for light and water. Hence the following research questions will be answered:

1. Can a quantitative framework, on a hydrological basis, be formulated to understand groundwater, soil water and vegetation dynamics in groundwater influenced ecosystems?
2. What is the influence of the presence of a static groundwater table on vegetation dynamics and water fluxes?
3. What is the effect of spatio-temporal groundwater dynamics on vegetation growth in an eco-hydrological system?
4. What is the effect of climate change on vegetation in a groundwater influenced hillslope ecosystem under temperate climate conditions?
5. To what extent can the concept of water and oxygen stress of vegetation be used in systems that are also light limited?
6. Which findings in this study are important for the disciplines of hydrology, ecology and climatology?

1.7 Thesis outline

The first four research questions will be answered based on studies presented in Chapter 2 to 5. In Chapter 2 a quantitative framework on a hydrological basis is described for understanding groundwater, soil water and vegetation dynamics in groundwater influenced ecosystems, where the groundwater is dynamic but the vegetation static. In Chapter 3 the influence of groundwater on vegetation dynamics and water fluxes in

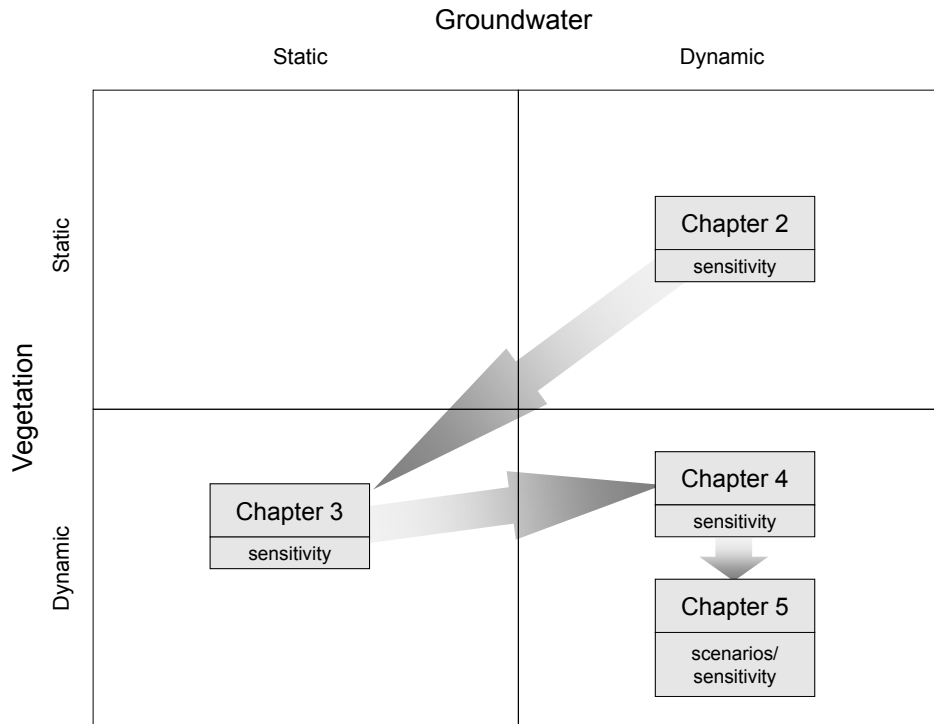


Figure 1.4 Thesis outline. The way groundwater and vegetation dynamics are simulated in Chapters 2 to 5 and the analysis that has been performed.

the hydrological system are shown, based on an advanced dynamic vegetation model and static groundwater. The effect of spatio-temporal groundwater dynamics on vegetation growth in an eco-hydrological system is shown based on the model described in 3 and a dynamic variably saturated hydrological model in Chapter 4. In Chapter 5 the combined model is subsequently used to investigate the effect of climate change on vegetation in a groundwater influenced hillslope ecosystem under temperate climate conditions.

Figure 1.4 provides a diagram of the way groundwater and vegetation are treated in the various chapters; static or dynamic. Also the mode of analysis is indicated, i.e., usage of a sensitivity analysis of environmental parameters or of a climate scenario analysis. It can be seen that the model gradually moves toward a more dynamic and complex model.

In Chapter 6 the first four research questions are discussed based on the results presented in Chapters 2 to 5. Then the last two questions concerning the concept of water and oxygen stress of vegetation in systems that are also light limited and relevance of the findings of this research for the disciplines of hydrology, ecology and climatology are discussed. From these discussions recommendations for further research emerge.

2 Groundwater - soil water - vegetation dynamics in a temperate forest ecosystem along a slope

This chapter has been published as:

Brolsma, R. J. and M. F. P. Bierkens (2007), Groundwater-soil water-vegetation dynamics in a temperate forest ecosystem along a slope. Water Resources Research, 43.

Abstract

Groundwater can have a profound effect on water availability to vegetation in temperate climate regions. Here we attempt to model groundwater, soil water and vegetation dynamics in groundwater controlled ecosystems and assess how these depend on climate and topography. We focus on the possible location of a boundary between two vegetation types on a slope. One vegetation type is adapted to wetter soil moisture conditions and one is adapted to drier conditions. We hypothesized that the vegetation type boundary along the slope in climax state is located where the slope-average evapotranspiration is highest and/or where vegetation stress is minimal. Vegetation stress is a combination of occurring water stress as defined by Porporato et al. (2001) and a newly defined oxygen stress, that results from anaerobic conditions. To study this system we built a 2-dimensional model of saturated-unsaturated flow along a slope in which the abundance of two vegetation types varied along the slope. The results show that boundary between the vegetation types based on maximum evapotranspiration occurs at approximately the same location as that is predicted based on minimum plant stress. When precipitation increases the boundary between the two vegetation types moves up slope. Sensitivity of the location of the vegetation boundary to changes in precipitation decreases with increasing slope angle.

2.1 Introduction

In lowland areas within temperate climate regions, groundwater has a profound effect on the moisture availability to vegetation. Groundwater influences soil moisture

through capillary rise, especially in summer. Recently, many studies have been performed on the interaction between vegetation and soil moisture availability. Many of these studies have been directed to vegetation dynamics and patterning in water limited ecosystems. The multitude of studies can roughly be divided into studies focusing on stochastic soil moisture dynamics and rainfall intermittency (Milly, 1993; Rodriguez-Iturbe et al., 1999; Laio et al., 2001; van Wijk & Rodriguez-Iturbe, 2002; Porporato et al., 2004) and studies focusing on self organized patchiness caused by vegetation-infiltration feedbacks (Klausmeier, 1999; HilleRisLambers et al., 2001; van de Koppel et al., 2002; Rietkerk et al., 2002; von Hardenberg et al., 2001). Also, quite a few studies focus on vegetation patterns in bogs and wetland ecosystems, mainly along the line of feedback mechanisms involving either water logging (Swanson & Grigal, 1988; Couwenberg & Joosten, 2005) or nutrient stress (Rietkerk et al., 2004).

From this review it follows that eco-hydrological studies have so far seldom included groundwater flow and soil water-groundwater interactions and mainly focus on extreme ecosystems like bogs and semi-arid grasslands. Although there is much literature on hillslope hydrology, e.g. (Kirkby, 1978; Brutsaert, 1994; Troch et al., 2003), except for Ridolfi et al. (2003), most eco-hydrological modeling studies have been performed on flat areas, discarding the influence of relief. However, on slopes in temperate climate regions gradients exist from dry soil conditions on upper slopes to wet soil conditions on lower slopes. These gradients cause a change in vegetation type from drought-adapted to vegetation adapted to wet conditions. Redistribution of water and nutrients play an important role in these systems; e.g. upslope hydrological processes influence downslope moisture availability. In this article we will investigate the dynamics of such a gradient type system. We will limit ourselves to water redistribution.

The aim of the research presented here is to provide a quantitative framework for understanding groundwater, soil water and vegetation dynamics in groundwater controlled ecosystems, and to assess how these depend on climate and topography. This is achieved by creating a model to study the interactions between vegetation composition, aquifer thickness and slope angle on vegetation stress, evapotranspiration and soil moisture content.

With this model two optimality assumptions are compared. The first assumption is that ecosystems strive to a maximum transpiration and the second assumption is that ecosystems strive to minimize plant stress. The first assumption is based on the hypothesis that natural selection maximizes the energy flux through the system, so far as compatible with the constraints to which the system is subject (Lotka, 1922), or as formulated by Odum (1983) natural systems tend to maximize the flow of useful energy. We use transpiration as a proxy for energy flow and production. The second assumption is based on Eagleson (1982), suggesting that vegetation canopy density will equilibrate with the climate and soil parameters to minimize the water stress.

Compared to previous work on dynamic modeling of the relation between hydrology and vegetation patterning this study adds a number of novel features. First, we consider lateral groundwater flow and groundwater dependent ecosystems; second, a

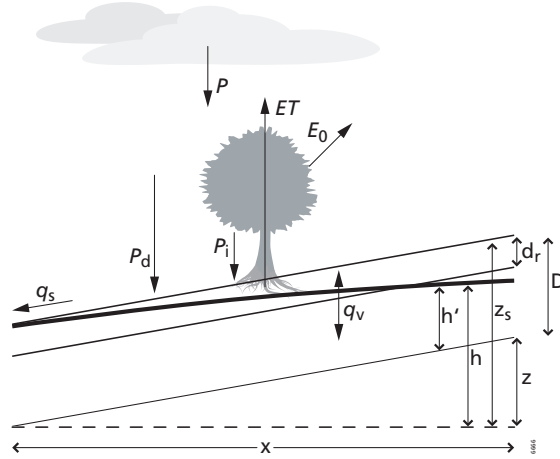


Figure 2.1 Schematic representation of the 2-dimensional hydrological model, also showing the geometry of the slope. The variables are explained in the text.

full gradient of wet-to-dry conditions is considered by analyzing the type-distribution along a slope; third, analogous to water stress (Porporato et al., 2001) we introduce oxygen stress to measure the effect of site conditions becoming too wet for a given plant species; fourth, we analyze how different fitness criteria, i.e. productivity and plant stress, determine the boundary between vegetation types.

The remaining part of the paper is set up as follows. First the developed model will be presented and the model experiments will be described. Then the outcomes of the model experiments will be shown, followed by an investigation of the effects of variations in rainfall input, vegetation composition and slope geometry on the model outcomes.

2.2 Methods

2.2.1 Model description

We developed a quasi 2-dimensional hydrological model to investigate and quantify the influence of slope angle, precipitation input and vegetation composition on the hydrological system. Figure 2.1 gives a schematic overview of this model.

Climatic forcing, interception and evapotranspiration

The climatic input for the model is generated by a stochastic weather generator, developed by Richardson (1981), which generates precipitation, minimum and maximum temperature and wind speed on a daily time step based on statistical properties. We focused on the temperate climate of The Netherlands, which has an average yearly precipitation of 700 mm and an average evapotranspiration of 450 mm. The probability of a wet day varies between 0.43 in June and 0.68 in November. All used parameters for weather generation were for monthly periods and can be found in van der Voet et al. (1996). The other variables needed for calculating evaporation, i.e., radiation

and humidity, were calculated from day number and the simulated temperature using equations summarized in Allen et al. (1998).

Precipitation P [LT^{-1}] can either be intercepted by the vegetation or directly reach the soil surface. This direct throughfall (P_d) is determined by the canopy gap fraction $f_{gap} \cdot P$. Here we have taken $f_{gap}=0.2$, which is the average from van Wijk & Bouten (2001). The intercepted precipitation $(1 - f_{gap}) \cdot P$ evaporates from the canopy and is calculated using the Penman equation for evaporation of open water (E_0 [LT^{-1}]). The maximum interception by the canopy is limited by the interception capacity and the maximum E_0 per day. The water that does not evaporate within one day reaches the soil surface as indirect throughfall P_i [LT^{-1}]:

$$P_i = \begin{cases} 0 & \text{if } (1 - f_{gap})P < \min(E_0, LAI \cdot IntCap/\Delta t) \\ (1 - f_{gap})P - \min(E_0, LAI \cdot IntCap/\Delta t) & \text{if } (1 - f_{gap})P > \min(E_0, LAI \cdot IntCap/\Delta t) \end{cases}, \quad (2.1)$$

in which LAI is the leaf area index (L^2 leaf L^{-2} ground), $IntCap$ is the interception capacity (L^3 L^{-2} leaf) and Δt is the time step at which meteorological forcing is evaluated (1 day in our case). Total throughfall P_n is the sum of direct and indirect throughfall:

$$P_n = P_d + P_i, \quad (2.2)$$

In the model vegetation does not develop in time and is assumed to be in a mature state. The temporal variation of leaf area index (phenology) is modelled based on a temperature index, where LAI increases linearly from LAI_{min} to LAI_{max} as soon as the 10-day average temperature $T10 > 10$ $^{\circ}\text{C}$ and decreases linearly to LAI_{min} again if $T10 < 10$ $^{\circ}\text{C}$. The rate of rise and decline of LAI is taken as $(LAI_{max} - LAI_{min})/30$ [day^{-1}].

No transpiration occurs as long as intercepted water evaporates. Transpiration is calculated using the Penman-Monteith equation and is additionally controlled by the root water uptake and the LAI .

$$ET = \frac{LAI}{LAI_{max}} F(\psi) E_p, \quad (2.3)$$

where ET is transpiration [LT^{-1}], E_p is potential evapotranspiration calculated with Penman-Monteith [LT^{-1}] and $F(\psi)$ is a root water uptake reduction function [-].

Root water uptake occurs from the rootzone and depends on its matric potential ψ [L] and is modelled using the Feddes et al. (1978) root water uptake reduction function. The function is shown in Figure 2.2 for two vegetation types (see hereafter). Note that reduction occurs both in case of very dry soils as well as in case of soil saturation. All vegetation parameters for the two different vegetation types (see section 2.2.2) are given in table 2.1.

Hydrology

The hydrological model aims to describe the flow of water along a hillslope. We used a simplified model, consisting of two coupled zones: a root zone where trees abstract

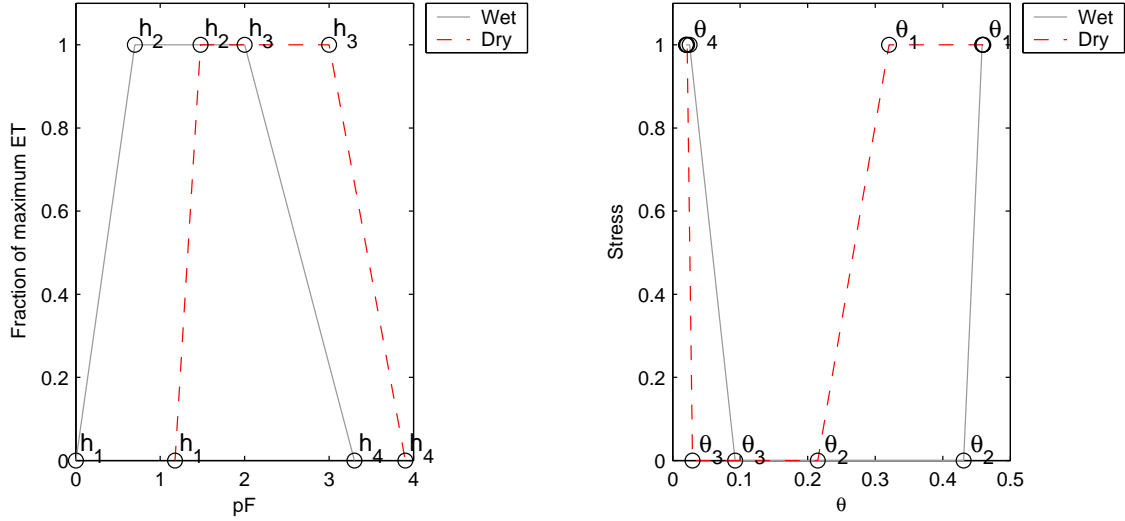


Figure 2.2 Feddes' root water uptake reduction function (left) and Feddes' function converted to static stress function (right) for both vegetation types. Wet and dry refer respectively to the vegetation type adapted to wet and dry soil moisture conditions. $pF = \log(-h)$, where h is in cm.

their water from and a groundwater zone. Although describing subsurface flow using Richards' Equation (Richards, 1931) was preferred, solving Richards' Equation for many hundreds of years taking account of intermittent saturation and drying of soil and the occurrence of (intermittent) seepage zones is still cumbersome in terms of computation time and robustness (i.e. guaranteed convergence). This becomes a problem if many of these centennial-length runs are performed as in this study.

In our simplified model it is thus assumed that flow in the groundwater zone is horizontal only and that a vertical exchange flux exists between the rootzone and the groundwater zone. The assumption of the vertical flux between rootzone and groundwater is warranted if a water table is present such that hydraulic gradients in the rootzone are predominantly vertical and saturation and thus conductivity increases with depth. The assumption of a horizontal flux in the groundwater zone is warranted if the aquifer thickness is large enough and the slope is not too steep.

Figure 2.1 schematically shows the model set up. The model consists of two layers: the (unsaturated) rootzone with vertical flow and the groundwater zone with horizontal flow. The equation describing relative soil saturation s [-] in the rootzone is described by the following ordinary differential equation defined for each location x along the slope:

$$(\theta_s - \theta_r) D_r \frac{ds}{dt} = P_n(t) - q_s(P_n, s) - ET(s, t) + q_v(s, t), \quad (2.4)$$

where s is the relative soil saturation [-] defined as $s = (\theta - \theta_r) / (\theta_s - \theta_r)$ with θ volumetric soil moisture content [-], D_r is the depth of the rootzone [L], θ_s is the volumetric soil moisture content at saturation [-], θ_r is the residual volumetric soil moisture content [-], q_s is the surface runoff [LT^{-1}] and q_v is the vertical exchange flux between the rootzone and groundwater [LT^{-1}], i.e. percolation/groundwater recharge (downward; negative) or capillary rise (upward; positive)

Surface runoff q_s occurs if precipitation exceeds the infiltration capacity which is taken equal to the unsaturated conductivity [LT^{-1}]. In case of rootzone saturation all net input P_n is converted to runoff. Surface runoff is not modelled explicitly, but instantly removed (weak sink) and cumulated as runoff. The vertical exchange flux is modelled by applying Darcy's law:

$$q_v(s, h) = -K(s) \left(\frac{z_s + \psi(s) - h}{z_s - h} \right), \quad (2.5)$$

in which h is the elevation of the groundwater table at location x [L], K is the hydraulic conductivity [LT^{-1}] and z_s is the surface elevation [L]. It can be seen that as long as the matric potential in the rootzone is above $-(z_s - h)$ (i.e. equilibrium) percolation occurs ($q_v < 0$), while if it is smaller than $-(z_s - h)$ we have capillary rise ($q_v > 0$).

Relationships between relative soil saturation, matric potential and unsaturated conductivity are modelled using Mualem-Van Genuchten relationships (van Genuchten, 1980). Soil physical parameters are obtained from Carsel (1988) and are listed in Table 2.1.

Lateral groundwater flow along the slope is modelled with the partial differential equation:

$$n \frac{\partial h'}{\partial t} = K_s \frac{\partial}{\partial x} \left(h' \frac{\partial h'}{\partial x} + h' \tan \alpha \right) - q_v(s; h'), \quad (2.6)$$

where $h' = h - z$ the height of the water table with respect to the aquifer bottom, K_s is the saturated hydraulic conductivity of the subsoil [LT^{-1}], n is the drainable porosity of the subsoil [-] and α is the slope angle.

The coupled equations 2.4, 2.5 and 2.6 are solved by discretizing the slope into a finite number of columns and using a finite-difference scheme which is explicit in time using time steps of 0.01 day (note that the meteorological forcing enters the model as daily averages). With regard to the coupling flux Equation 2.5, we note that during a single integration step the amount of percolation/capillary rise cannot exceed the difference between actual soil moisture store and the soil moisture store that would be obtained in an equilibrium soil moisture profile s_{eq} . So, any location along the slope cannot move from a percolation state to a state of capillary rise or vice versa during a single integration step. It should also be noted that no storage and delay occurs in the flux between rootzone and groundwater. If during the simulation the groundwater table reaches the surface, i.e. a seepage zone develops along the lower parts of the slope (Dunne et al., 1975), the vertical flux becomes a seepage flux (return flow). This seepage is instantly removed and is added to the direct runoff (originating from non-infiltrating throughfall) to form cumulated runoff. Obviously, all throughfall falling on the seepage zone does not infiltrate, but adds to the direct runoff.

2.2.2 Plant stress

In a temperate climate, plants can suffer both from a shortage of water (water stress) as well as from a shortage of oxygen (anaerobic or oxygen stress) (Feddes et al., 1978). The latter occurs at relatively high moisture contents, causing a lack of oxygen, which

Table 2.1 Used soil parameters

Variable	Value	Description	Source
θ_r	0.02	residual soil moisture content	Carsel (1988)
θ_s	0.46	saturated soil moisture content	Carsel (1988)
n	1.89	van Genuchten	Carsel (1988)
α (cm^{-1})	0.075	van Genuchten	Carsel (1988)
K_s (m/d)	1.061	saturated conductivity	Carsel (1988)
r_z (m)	1	thickness rootzone	
D (m)	5	aquifer thickness	

Table 2.2 Used parameters for vegetation

Vegetation type	Wet	Dry
h_1 (m)	-0.01	-0.15
h_2 (m)	-0.05	-0.3
h_3 (m)	-1	-10
h_4 (m)	-20	-80
θ_1	0.4585	0.3204
θ_2	0.4309	0.2150
θ_3	0.0925	0.0294
θ_4	0.0251	0.0215
$IntCap$ (mm)	0.366	interception capacity, per unit leaf area
LAI_{min}	0.01	minimum leaf area index
LAI_{max}	4.1	maximum leaf area index
LAI_{gap}	0.2	gap factor of canopy
k	0.5	plant damage parameter
q	1	nonlinearity parameter for plant stress

is necessary for root water uptake in the rootzone. Porporato et al. (2001) designed a method to calculate water stress. They distinguished between static and dynamic stress. Static stress gauges the "state of stress" of a plant at a given time, while dynamic stress is a measure of total stress that a plant has experienced over a prolonged period of time taking into account the frequency and the mean length of the water stress period that a plant has experienced during a growing season. In analogy to the concept designed by Porporato et al. (2001) we introduce the concept of oxygen stress.

Static stress (Figure 2.2) is stress that a plant experiences without memory of previous stress. The soil moisture content below which static water stress ζ_w begins is equal to θ_3 and maximum static water stress is reached at θ_4 , where static water stress is 1. These correspond to the potentials h_3 and h_4 from the Feddes function. Static oxygen stress ζ_o is calculated in a similar way using θ_1 and θ_2 . The static water and

oxygen stress are formulated as:

$$\zeta_w = \begin{cases} \left(\frac{\theta_3 - \theta_t}{\theta_3 - \theta_4} \right)^q & \text{if } \theta_4 < \theta_t < \theta_3 \\ 1 & \text{if } \theta_t < \theta_4 \end{cases} \quad (2.7)$$

and

$$\zeta_o = \begin{cases} \left(\frac{\theta_1 - \theta_t}{\theta_1 - \theta_2} \right)^q & \text{if } \theta_2 < \theta_t < \theta_1 \\ 1 & \text{if } \theta_t > \theta_1 \end{cases}, \quad (2.8)$$

where θ_t is the soil moisture content at time t and q is a measure of non-linearity of the effects of soil moisture deficit and plant conditions. Since this non-linearity is still poorly understood, q is given the value 1.

The dynamic water stress during an entire growing season is then calculated using (Porporato et al., 2001):

$$Stress_w = \left(\frac{\overline{\zeta_w} \cdot \overline{T_{sw}}}{k \cdot T_{seas}} \right)^{1/\sqrt{n_s}}, \quad (2.9)$$

where $\overline{\zeta_w}$ is the average static water stress of a plant during the period it is under water stress (i.e. for days where $\zeta_w > 0$), T_{seas} is the mean length of a growing season (period during which $LAI > LAI_{min}$), $\overline{T_{sw}}$ is the mean duration of a water stress period, k is a parameter which is a threshold where damage occurs to a plant and n_s is the frequency at which stress occurs. Here dynamic oxygen stress is defined analogously:

$$Stress_o = \left(\frac{\overline{\zeta_o} \cdot \overline{T_{so}}}{k \cdot T_{seas}} \right)^{1/\sqrt{n_s}}, \quad (2.10)$$

where $\overline{\zeta_o}$ is the average static oxygen stress of a plant during the period it is under oxygen stress and $\overline{T_{so}}$ is the mean duration of a oxygen stress period. Total stress is then defined by a multiplicative model of dynamic water and oxygen stress:

$$Stress_{tot} = 1 - (1 - Stress_w) \cdot (1 - Stress_o). \quad (2.11)$$

2.2.3 Model runs

Two vegetation types have been defined, one adapted to wet soil moisture conditions and one favoring dry soil conditions. The vegetation types only differ in their reaction to water availability through root water uptake, i.e. the Feddes parameters (Table 2.2). The vegetation type favoring dry conditions is comparable to *Quercus robur* (oak). The vegetation type favoring wet conditions represents *Alnus glutinosa* (alder). *Alnus glutinosa* has the capability to transport oxygen through its roots to the rootzone, enabling root water uptake under (near) saturated conditions. The abundance of each of the vegetation types is varied along the slopes, between 0% and 100%, whereby the total vegetation coverage is always 100%. The vegetation type favoring the wet conditions is always on the lower part of the slope. We assume a

strict zonation of vegetation to exist (Falinski & Falinska, 1986; Hack & Goodlett, 1960) and therefore no mixture of vegetation types occurs.

The influence of change in climatic forcing is limited to variations in precipitation. The baseline scenario is based on the current rainfall regime of The Netherlands. We studied two cases. In the first case the rainfall amount was changed by multiplying the baseline rainfall amount per day by a factor to obtain two dry scenarios with only 80 and 90% of yearly precipitation, and three wet scenarios with 110, 120 and 130 of yearly precipitation. In the second case we increased the probability of a rainy day after a dry day to increase frequency of rain events, such that again rainfall amounts of 80%, 90%, 100%, 110%, 120% and 130% of the yearly rainfall amount were obtained.

To test if the hydrological model showed the expected dynamic behavior we performed a model run in which we looked at the system's response to a constant forcing, i.e. a constant influx (throughfall) of 2 mm/d and potential evapotranspiration of 1 mm/d. Assuming only oak as vegetation type we calculated the temporal variation along the slope of the following variables: groundwater table, transpiration and rootzone soil moisture content.

To quantify the influence of the main physical parameters of the slope, we varied the slope angle and the thickness of the aquifer. First we performed simulations with three different slope angles: 3, 5 (baseline) and 10% using the baseline rainfall scenario. Secondly the aquifer thickness was investigated using thicknesses of 3, 6 (baseline) and 12 m. Finally we investigated the combined effect of varying slope angle and rainfall amount.

Runs of 150 years were performed where the first 50 years were used as spin up of the system to reach an approximately 'equilibrium' state and were not used in the analysis. Of the last 100 years daily fluxes (evapotranspiration, runoff, q_v and interception), water stress, oxygen stress and soil moisture content were stored.

2.3 Results

2.3.1 Hydrological test run

First we have performed a test run to investigate behavior of the hydrological model. Thereto we applied a constant throughfall of 2 mm/d and a constant potential evapotranspiration of 1 mm/d to the system, starting with an "empty" model. Figure 2.3 shows the resulting temporal development of the groundwater table, soil moisture content and transpiration for $t=1, 5, 8$ and 15 years. It can be seen that after approximately one year the soil moisture content reaches a fixed level, at which it remains approximately constant for five years as a consequence of an almost equilibrium between throughfall, q_v and ET . When groundwater reaches the bottom of the rootzone at the lower part of the slope, the soil moisture content quickly rises above θ_3 causing a reduction in root water uptake and therefore an accelerated increase in moisture content and groundwater rise. After about 13 year an equilibrium is reached, i.e. water that was evaporated first is now discharged from the seepage zone.

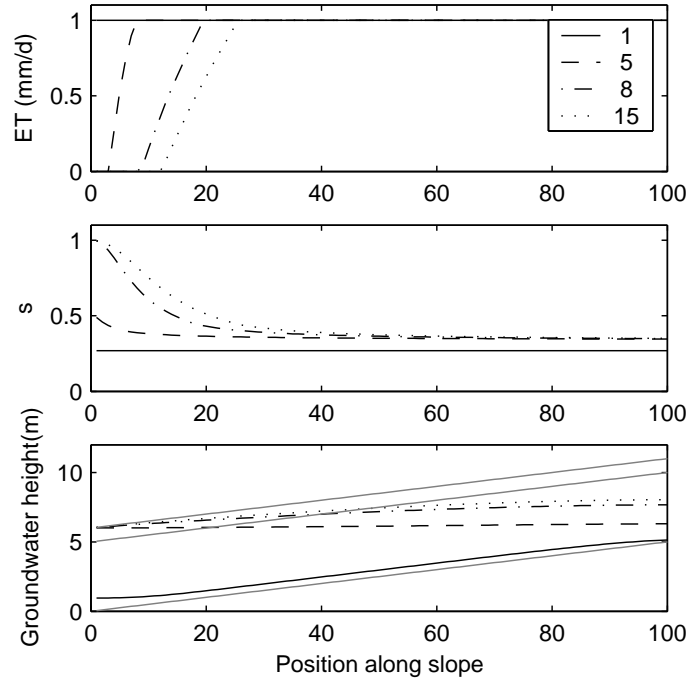


Figure 2.3 The figure at the top shows the transpiration of the vegetation along the slope, the middle figure shows the relative soil moisture content and the figure at the bottom shows the height of the groundwater level for 1, 5, 8 and 15 years after starting the hydrological test run. The grey lines in the figure at the bottom show the lower and upper boundary of the aquifer and the rootzone.

2.3.2 Vegetation

First we compare the different vegetation scenarios (Figure 2.4) focusing on the 100% oak and the 50% oak - 50% alder runs. In both runs water stress is absent on the lowest part of the slope, because the soil moisture content is near saturation or at least above θ_1 . The stress then increases abruptly at 5-6% of the slope. In the 100% oak run the stress increases along the slope to a value of 0.42 and then remains almost constant at the upper part of the slope. In the 50% oak/alder run water stress reaches a value of 0.95 on the part where alder is present, since alder experiences water stress at relatively high soil moisture values. Water stress drops again at the boundary between oak and alder to about 0.42. The maximum value of stress on the upper part of the slope for both the oak and alder vegetation in all runs is approximately the same. Only the run with 100% alder shows less stress which can be explained by the fact that on the higher part of the slope oak, which has a relatively high ET, is not present, causing a higher groundwater level and wetter rootzone conditions down slope.

The oxygen stress is highest for oak causing very high stress on the lowest part of the slope in the runs where oak is present in this part of the slope. Alder only experiences oxygen stress in the lowest 2 cells of the slope, where the soil water content is above θ_1 for a large part of the growing season.

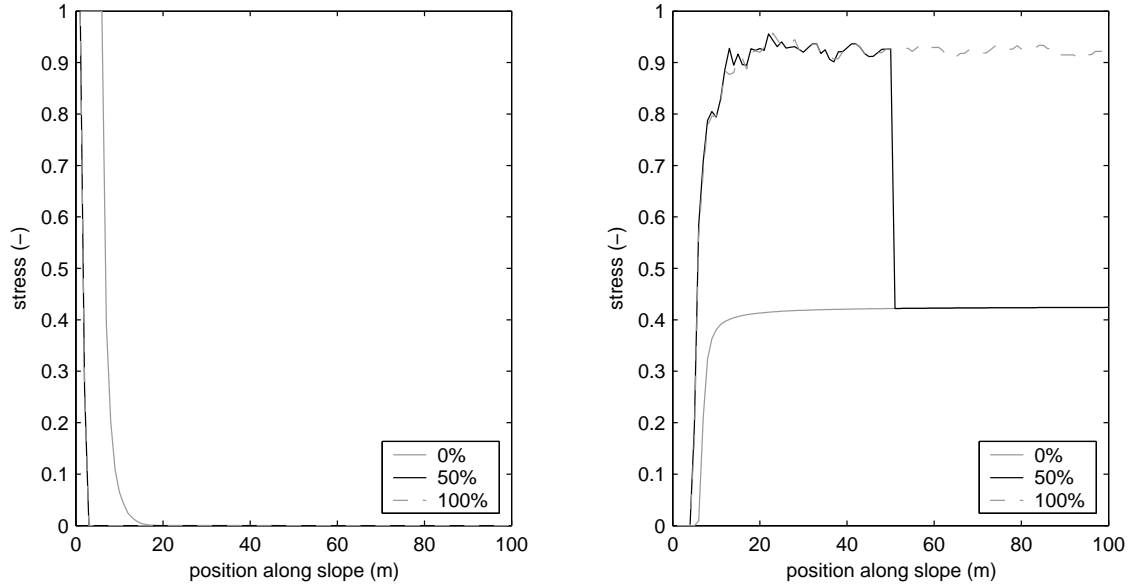


Figure 2.4 The left figure shows the oxygen stress for the baseline precipitation scenario for three different vegetation runs (0, 50 and 100% alder). Position is the location along the slope (0 is lowest point and 100 the highest point). The right figure shows water stress for the same runs.

2.3.3 Influence of rainfall amount

To investigate the influence of rainfall on the vegetation stress and ET we used scenarios with 80, 90 100, 110, 120 and 130% of the actual precipitation, by changing the amount of rain per day, or the number of days it rains. We will first focus on the results of changing the amount of rain per day. Figure 2.5 shows the influence of the location of the vegetation boundary on the water and oxygen stress for the different rainfall scenarios for the system as a whole.

First we will focus on the baseline run (1.0 times normal precipitation). Water stress for the system as a whole, i.e. the spatial mean of the local stress, increases when the boundary between the vegetation types moves up slope, i.e. when the percentage of alder increases. Water stress increases continually when the boundary moves up slope, while oxygen stress decreases. The decrease in oxygen stress mainly occurs at the lower part of the slope where it strongly decreases before stabilizing. The mean oxygen stress for the complete slope is approximately 10 times smaller than the mean water stress. Figure 2.5 also shows that water stress decreases for all vegetation boundary positions with increasing precipitation levels, while the oxygen stress increases.

The combined water-oxygen stress (Figure 2.6) shows a minimum stress value for each of the rainfall scenarios. If we assume that the actual vegetation boundary in climax state is at the position where the ecosystem as a whole experiences minimum stress, we see that this location moves up slope as rainfall increases. A small test, changing the value of q in Equations 2.7 and 2.8 to 2.0 and 3.0, showed only a slight change in magnitude of the stress, but did not show any influence on the location of the boundary where minimum stress occurs.

Similarly one can assume that the vegetation boundary in climax state lies at the

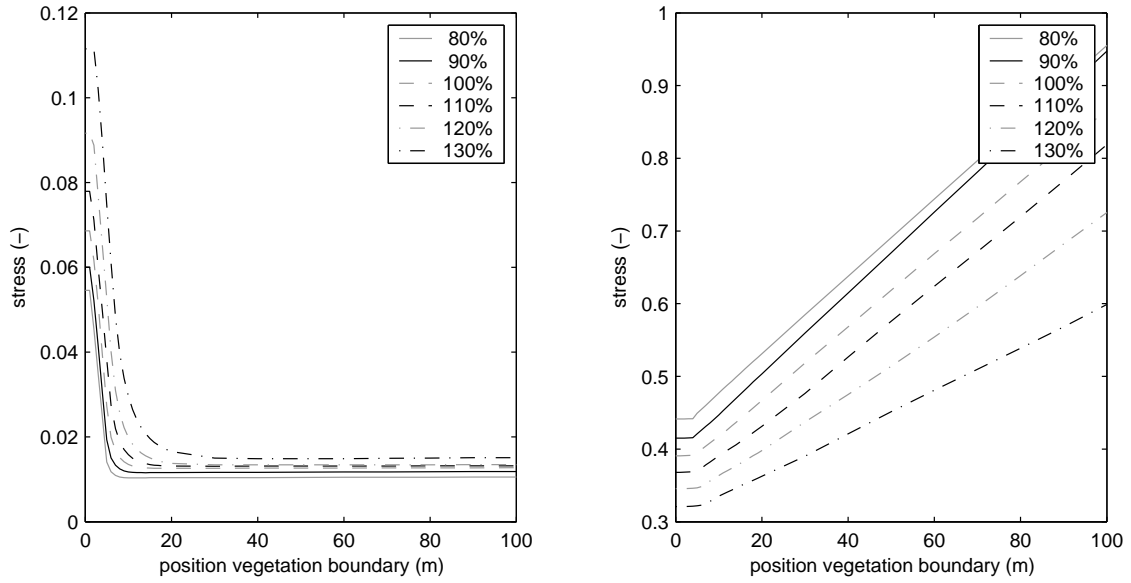


Figure 2.5 Dynamic oxygen stress (left) and water stress (right) for the complete system per year for the different locations of the vegetation boundary and different precipitation amount scenarios.

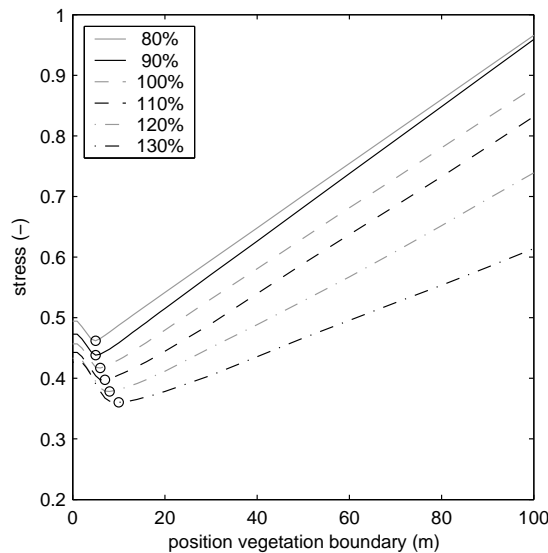


Figure 2.6 Mean total dynamic stress for the complete system per year for the different locations of the vegetation boundary and different precipitation amount scenarios. Circles indicate the minimum values.

location where the ecosystem shows maximum productivity, with maximum evapotranspiration as a proxy. Figure 2.7 shows that this location also moves up the slope as rainfall increases. Comparison of Figures 2.6 and 2.7 shows that both optimality criteria result in similar behavior of the vegetation boundary and almost (but not exactly) the same location of the vegetation boundary for a given rainfall amount. It remains to be seen, whether either of these optimality criteria is found in real ecosystems. They do however lead to comparable results.

Figure 2.8 shows the average soil moisture content of the rootzone of the system as a

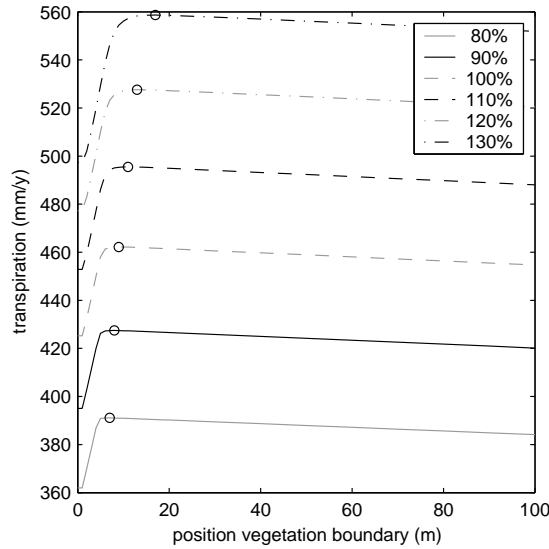


Figure 2.7 Mean evapotranspiration for the complete system per year for the different locations of the vegetation boundary and different precipitation amount scenarios. Circles indicate the maximum values.

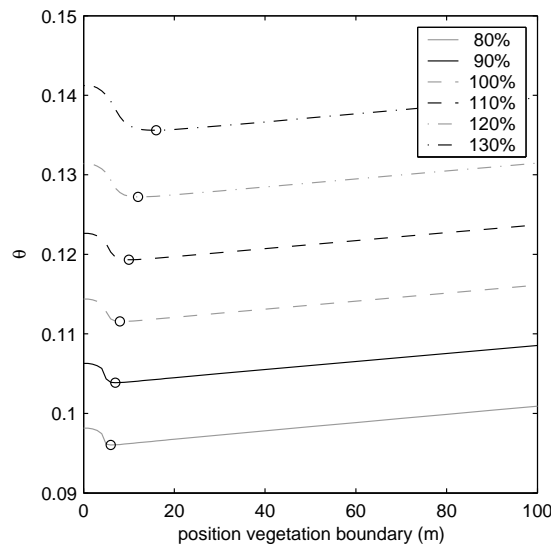


Figure 2.8 Mean soil moisture content for the complete system per year for the different locations of the vegetation boundary and precipitation amount scenarios. Circles indicate the minimum values.

whole, showing that around the location of the vegetation boundary, the ecosystem average soil moisture content is minimal. Although differences are small, this can be attributed to the fact that higher evapotranspiration directly causes lower moisture contents in the rootzone. It is interesting to see that a global optimality criterion as maximum productivity leads to low soil moisture content, fact that can also be deduced from local considerations: individuals must grow as fast as possible and take up as much resources around them as possible to maximize their chances of survival. This then leads to maximum productivity and maximum use of supplied resources for the ecosystem as a whole (Kerckhoff et al., 2004).

Figure 2.9 shows the different fractions of ET , interception (E_0) and runoff for the different rainfall scenarios where the boundary between vegetation type is such that vegetation stress is minimal. For the baseline run the interception is 115 mm, average evapotranspiration along the slope is 461 mm and the total runoff is 129 mm. When precipitation decreases with 20% interception decreases with only 5.2% and if precipitation increases with 30% interception only increases with 5.5%. This may be explained by the limited interception capacity causing more throughfall.

Average evapotranspiration decreases with 15.3% and increases with 20.2% with respectively 80% and 130% of the actual precipitation. In the first case this results from a decrease in throughfall causing a decrease in soil moisture and therefore less root water uptake. The decrease of soil moisture content also causes a decrease in percolation to the groundwater, which results in less runoff (50.1%). The second case is the exact opposite; throughfall, soil moisture content, evapotranspiration and runoff all increase.

2.3.4 Influence of rainfall frequency

To investigate the influence of the frequency of rainfall events we varied the probability of a wet day following a dry day leading to scenarios of 80, 90 100, 110, 120 and 130% of the actual precipitation. The general trend of $Stress$, ET and θ is quite similar as that of increasing the amount of rain per day, and results are not shown. The location of minimum stress is in both cases at approximately the same spot. However the location of maximum ET reacts less in case of increased rainfall frequency. The shifts of the location of minimum soil moisture content between runs are smaller as well.

Figure 2.9 shows that changing the frequency and therefore the number of wet days results in larger changes in interception when compared to changing the rainfall amount per day that it rains. The interception increases proportionately to the increase in rainfall frequency, but when the rainfall amount per day is increased, the interception store is more often exceeded, causing a less than proportionate influence on the interception. Therefore, in the latter case, there is a stronger increase in throughfall and infiltration, which causes a higher soil moisture content, which again results in a stronger increase of ET . Because of the higher soil moisture content, q_v is larger and the change in runoff (seepage) amount is larger too.

2.3.5 Slope and aquifer thickness

Up to now all rainfall scenarios have been run with a slope angle of 5% and a total thickness of the aquifer of 6 meters. To determine the influence of slope angle and aquifer thickness on this system, we conducted runs with slope angles of 3 and 10% and aquifer thicknesses of 3 and 12 meter. The results and a comparison with the baseline scenario can be found in Table 2.3. The main influence of a smaller slope angle of 3% is a decrease of runoff of 21.1 mm/y (16.5%) and an increase of ET with 21.1 mm (4.6%). A larger slope angle of 10% causes an increase of runoff of 17.7 mm

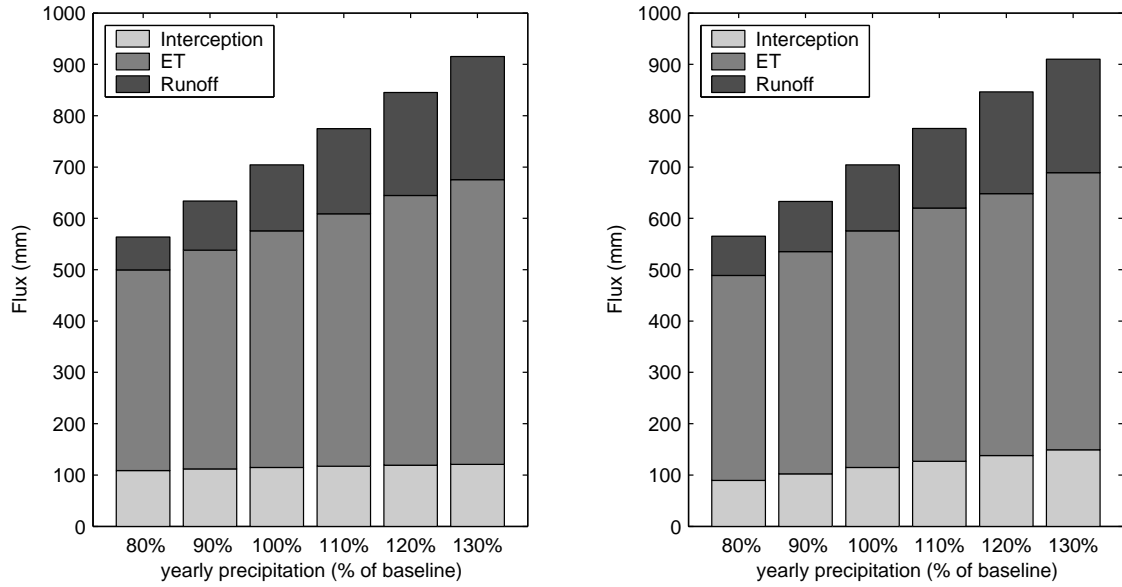


Figure 2.9 Interception, ET and runoff at the maximum productivity of each precipitation scenario. The influence of changing the amount of rainfall on days that it rains and the influence of changing the number of days that is rains.

Table 2.3 Influence of slope and aquifer thickness on maximum evapotranspiration, position, minimum stress, minimum θ , interception and runoff.

	Slope angle(%)			Aquifer thickness(m)		
	3	5	10	3	6	12
Max. evapotranspiration (mm/y)	487	462	444	475	462	457
Position	19	9	4	14	9	8
Min. stress	0.417	0.417	0.425	0.406	0.417	0.411
Position	11	6	3	9	6	6
Minimum θ	0.127	0.112	0.101	0.119	0.112	0.110
Position	19	8	4	13	8	6
Interception (mm/y)	115	115	115	115	115	115
Runoff (mm/y)	107	128	146	116	128	133

(13.8%) and a decrease of ET of (3.8%) for the entire slope. The main influence of doubling aquifer thickness is a decrease in ET of 4.3 mm (0.9%) and an increase of runoff of 3.4%. A thickness half of the normal thickness soil resulted in an increase of ET of 12.4 mm (2.7%) and a decrease in runoff of 9.7%. An increasing slope angle and an increasing aquifer thickness generally lead to higher discharge, drier soils and smaller seepage zones. Consequently the boundary moves down slope.

Figure 2.10 shows the influence of the combined effect of changing slope angle and rainfall amount on the location of the vegetation boundary based on minimum plant stress. It can be seen that a decrease of slope steepness leads to higher vegetation boundaries for all rainfall scenarios. This is caused by a decrease of the water table

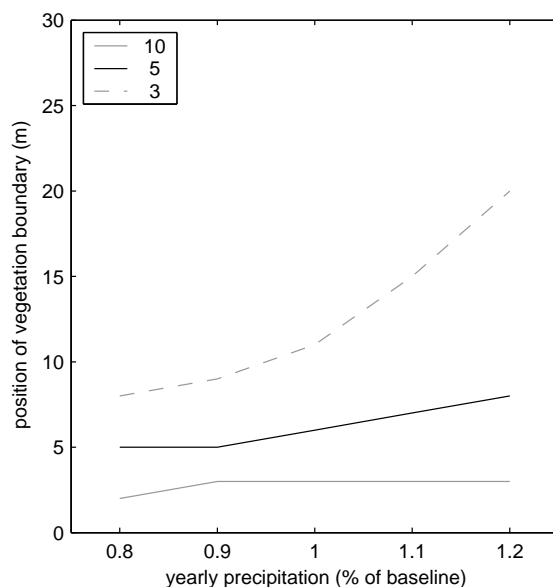


Figure 2.10 Influence of rainfall amount and slope (3, 5 and 10%) on the location of the boundary between two vegetation types based on the minimum stress criterion.

gradient for gentle slopes and therefore lower discharge and higher moisture contents in the rootzone. This results in an increase of oxygen stress rates at the lower part of the slope and a decrease of water stress at the higher part of the slope. The sensitivity of the vegetation boundary to varying rainfall amounts on steeper slopes is less than on gentle slopes. This is because, for gentler slopes a smaller part of the rainfall increase is converted to groundwater runoff leading to a larger increase of soil wetness and a larger upslope shift of the vegetation boundary.

2.4 Discussion and conclusions

A 2-dimensional model of saturated-unsaturated flow along a hill slope was developed to investigate the interaction between hydrology and vegetation in groundwater dependent ecosystems. We focused on the boundary between two vegetation types along a hill slope under varying climatic and topographic conditions.

The concept of water stress as defined by Porporato et al. (2001) has been extended to include oxygen stress. This seems a useful extension for evaluating vegetation stress in groundwater influenced ecosystems. We have defined oxygen stress straightforwardly as the conjugate of the water stress function. Obviously more research and validation using field data is necessary to verify that the proposed oxygen stress function is rightly modelled.

We tested two optimality hypotheses about the location of a location of the vegetation boundary at climax state; first the boundary is there where the ET is at a maximum and second the vegetation boundary is there where total plant stress is at a minimum for the entire system. Our analysis shows that the locations where these criteria are

met, are found at approximately the same location. The position where the maximum evaporation is minimal approximately coincides with the location where slope-average soil moisture is minimal.

As a result of varying precipitation inputs into an ecosystem the position of the boundary between two vegetation types for which ET is maximal moves along the slope. When precipitation increases the boundary moves up slope together with the locations where stress and soil moisture content are minimal. This means that as a result of increased precipitation the abundance of alder increases. In case of an increase in rainfall amount per day, the shifts of the boundary are more pronounced than in case of increasing the amount of wet days. Also the magnitude of the change in amount of ET , $Stress$ and soil moisture are more pronounced. This is caused by the fact that increasing the amount of wet days, mainly increases the interception, which decreases the effect on the other fluxes and the vegetation boundary. Joint sensitivity analysis also shows that the effect of rainfall on the vegetation boundary is more pronounced for gentle slopes than for steep slopes.

This paper presents a first attempt to understand vegetation distribution along a groundwater influenced slope. We only considered static vegetation on a one-dimensional slope where water and indirectly oxygen availability are the limiting factors. Further understanding requires resolving a number of issues, many of which we are working on at this moment. First, extending this approach to a two-dimensional hillslope where actual vegetation patterns can be studied while considering transient vegetation dynamics (i.e. growth and dispersal) will reveal how soil moisture and vegetation patterns interact in space and time. Second, in temperate climate ecosystems such as considered here, water and oxygen stress only partly explain vegetation distribution. Nutrient availability, light competition, forest fire and grazing are important as well and should be included in the model.

Acknowledgments

We acknowledge Stefan Dekker and Thom Bogaard (Utrecht University) for their comments on an early version of this paper. We thank three anonymous reviewers for their comments that helped to greatly improve this paper.

3 Vegetation competition model for water and light limitation.

I: Model description, one-dimensional competition and the influence of groundwater

This chapter has been published as:

Brolsma, R. J., D. Karssenberg and M. F. P. Bierkens (2010), Vegetation competition model for water and light limitation. I: Model description, one-dimensional competition and the influence of groundwater. Ecological Modelling 221, pp. 1348-1363.

Abstract

Vegetation growth models often concentrate on the interaction of vegetation with soil moisture but usually omit the influence of groundwater. However the proximity of groundwater can have a profound effect on vegetation growth, because it strongly influences the spatial and temporal distribution of soil moisture and therefore water and oxygen stress of vegetation. In two papers we describe the behavior of a coupled vegetation-groundwater-soil water model including the competition for water and light. In this first paper we describe the vegetation model, compare the model to measured flux data and show the influence of water and light competition in one dimension. In the second paper we focus on the influence of lateral groundwater flow and spatial patterns along a hillslope. The vegetation model is based on a biophysical representation of the soil-plant-atmosphere continuum. Transpiration and stomatal conductance depend both on atmospheric forcing and soil moisture content. Carbon assimilation depends on environmental conditions, stomatal conductance and biochemical processes. Light competition is driven by tree height and water competition is driven by root water uptake and its water and oxygen stress reaction. The modeled and measured H₂O and CO₂ fluxes compare well to observations on both a diurnal and a yearly timescale. Using an up-scaling procedure long simulation runs were performed. These show the importance of light competition in temperate forests:

once a tree is established under slightly unfavorable soil moisture conditions it can not be outcompeted by smaller trees with better soil moisture uptake capabilities, both in dry as in wet conditions. Performing the long simulation runs with a background mortality rate reproduces realistic densities of wet and dry adapted tree species along a wet to dry gradient. These simulations show that the influence of groundwater is apparent for a large range of groundwater depths, by both capillary rise and water logging. They also show that species composition and biomass have a larger influence on the water balance in eco-hydrological systems than soil and groundwater alone.

3.1 Introduction

Within temperate climate zones vegetation growth is limited by water, light and nutrients. Especially in lowland areas in the temperate climate zone groundwater can have a profound effect on vegetation. This can occur indirectly through influence on the rootzone soil moisture content and directly if groundwater is present within the rootzone itself. Vegetation growth can be limited both as a result of a shortage as well as a surplus of soil moisture, causing either water or oxygen stress. However in most eco-hydrological modeling efforts thus far groundwater is not included (Rodriguez-Iturbe et al., 2007).

Our aim is to determine the influence of groundwater on vegetation dynamics and on the other hand show the effect of using an advanced vegetation model on the water fluxes in the hydrological system. In this series of two articles a model is introduced that is capable of simulating the coupled vegetation, soil water and groundwater dynamics in temperate climates including both water and oxygen stress of vegetation.

Vegetation growth models can be divided into two main groups: The first group consists of models that are based on the soil-plant-atmosphere-continuum (SPAC) (e.g. Friend et al., 1997; Katul et al., 2003; Zavala, 2004; Daly et al., 2004). Carbon assimilation is simulated in a biophysical way, or at least using parameters and variables that have a physical meaning. Photosynthesis and root water uptake, as well as stomatal conductance are modeled explicitly in these models, while variation of ambient variables is taken into account. Due to computational demands these models normally run on a short timescale representing time series lasting at most a few days.

The second group are semi-empirical models (e.g. Parton, 1993; Running & Coughlan, 1988; Potter, 1993) that can run on a time scale from days to centuries. Vegetation growth is usually modeled based on a maximum assimilation or growth rate that depends on species type, irradiance or is calculated using the model of Farquhar et al. (1980). This assimilation rate is then reduced based on empirical reduction functions for water, nutrients and temperature. This group includes the majority of forest growth models.

Although we are interested in long time series (up to a 1000 years) we chose to use a SPAC type approach, because our goal is to create a model that can be used under changing climate conditions. As described by Arora (2002) the simulation of vegetation as a dynamic component of the soil-vegetation-atmosphere continuum in

hydrological models is crucial when studying climate change and transient climate scenarios. Therefore we chose to make the model as physically-based as possible. In order to use a SPAC model on a timescale of 1000 years, an upscaling method was developed that enables us to make long model runs with a daily time step, while still taking into account the non-linearities in the reaction of vegetation in terms of evapotranspiration and carbon assimilation to soil moisture content and (diurnal) variation of atmospheric variables (radiation, temperature and vapor pressure deficit).

The model of Daly et al. (2004) has been used as starting point. This model simulates the soil-plant-atmosphere-continuum and is for the main part physically-based. In order to use this model for vegetation growth and competition in temperate climates the model was expanded with i) light and water competition between vegetation types, ii) oxygen limitation due to high soil moisture contents, iii) growth and respiration of vegetation and iv) climatic forcing by a stochastic weather generator. Furthermore, a temporal upscaling method was applied to make the vegetation model suitable for daily time steps and long time series.

In this first article we describe the adapted vegetation model including one-dimensional water and light competition. To test the model, simulation results of evapotranspiration and carbon dioxide fluxes are compared to eddy covariance measurements. A comparison of fluxes is made based on a daily and a yearly timescale. Using this model the influence of groundwater on the vegetation dynamics and soil moisture content on different time scales as well as the influence of soil texture is determined. The results show the importance of studying vegetation and hydrology including groundwater as an integrated system.

The resulting vegetation model is used as a basis for a spatio-temporal vegetation model coupled to a three-dimensional hydrological model. The second article (Brolsma et al., 2010b) describes the coupling to a dynamic three-dimensional hydrological model. Using that model we describe the influence of spatial groundwater dynamics on vegetation and vice versa. The coupled vegetation-hydrological model will in future research be used to analyze transient climate scenarios.

3.2 Model description

The model described in this first paper is a point model, although it can be used as a component in a spatially distributed model, as will be done in the second paper. Although this is a point model, we chose for a spatial extent of 10*10 m which corresponds to the size of a mature tree. First we describe the soil water balance and the atmospheric forcing. Then we describe the vegetation growth model including carbon assimilation, transpiration, interception, respiration and competition for light and water, as well as the upscaling of these processes. Finally, actual vegetation growth, including allocation, allometry, phenology and mortality of vegetation is described.

3.2.1 Soil water balance

The soil moisture and root water uptake models use a single layer to represent the root zone, with homogeneous soil moisture content. As recently shown by Teuling & Troch (2005) this effectively mimics differential water uptake throughout the root zone throughout the year. The soil moisture model runs on a daily time step. The soil water balance is described by:

$$\frac{d\theta}{dt}Z_r = I - ET - EV + Q_v, \quad (3.1)$$

where θ [-] is soil moisture content, t [s] is time, Z_r [m] root zone depth, I [m s^{-1}] is infiltration, ET [m s^{-1}] is plant evapotranspiration, EV [m s^{-1}] is soil evaporation and Q_v [m s^{-1}] is the vertical exchange flux with the saturated zone. This flux is calculated using:

$$Q_v = K_\theta \frac{\left(-dh_{gw} - \frac{\psi_s}{g\rho_w}\right)}{dh_{gw}}, \quad (3.2)$$

where dh_{gw} [m] is the distance of the groundwater to the center of the rootzone, g [m s^{-2}] is the gravitational acceleration, ρ_w [kg m^{-3}] is the water density, K_θ [m s^{-1}] is the unsaturated soil water conductivity and ψ_s [Pa] is the soil matric potential. K_θ and ψ_s are calculated using Mualem-Van Genuchten relationships (van Genuchten, 1980). Note that the upward flux is positive and the downward flux is negative. With regard to Q_v we note that we limit this flux within one integration time step to the difference between $\theta - \theta_{eq}$, where θ_{eq} is the soil moisture content based on the situation where soil moisture content is in equilibrium with the groundwater level (Broksma & Bierkens, 2007):

$$\theta_{eq} = \frac{\theta_s - \theta_r}{1 + \left[\left(\alpha \frac{dh_{gw}}{\rho_w g}\right)^n\right]^m} + \theta_r, \quad (3.3)$$

in which θ_s [-] and θ_r [-] are the saturated and residual soil moisture content and α , n and m are van Genuchten parameters.

Infiltration (I) is equal to the minimum value of net precipitation, P_{net} [m s^{-1}] and K_θ . When P_{net} exceeds K_θ this is considered as runoff and removed from the cell. The calculation of P_{net} will be described further on. Soil evaporation is assumed to only occur at near saturated conditions ($\theta > \theta_{sat} - 0.01$). When this occurs EV is assumed to be at a potential evaporation rate calculated using the Penman-Monteith equation (Monteith, 1965) for open water conditions.

3.2.2 Atmospheric forcing

The atmospheric parameters that are used in the vegetation model are: minimum and maximum temperature (T_{min} , T_{max}) [$^{\circ}\text{C}$], precipitation (P) [m d^{-1} or $\text{m } 0.5\text{h}^{-1}$], shortwave radiation (Rad_s) [W], longwave radiation (Rad_l) [W] and vapor pressure deficit (D) [-]. The vegetation model runs on a half-hourly time step. If the above listed variables are available on a half-hourly resolution, these data are used directly. In case these are not available at a half-hourly time step, or if vapor pressure deficit

or longwave radiation are not known the following assumptions have been made to obtain half-hourly values.

In these cases, the air temperature during the day is approximated by:

$$T_a = \frac{T_{min} + T_{max}}{2} + \frac{T_{min} - T_{max}}{2} \cos[(t_d - t_s) 2\pi], \quad (3.4)$$

where t_d [day] is time of day and t_s [day] is a the time lag between the time that T_{max} is reached and noon. The vapor pressure deficit is based on the difference between saturated vapor pressure at T_{min} and at T_a according to equations summarized in Allen et al. (1998).

The influence of cloud cover on both long wave radiation, Rad_l [W m^{-2}] and shortwave radiation, Rad_s [W m^{-2}] is estimated using the following two empirical equations by Shuttleworth (1993):

$$Rad_s = \left(a_s + b_s \frac{n}{N} \right) Rad_0, \quad (3.5)$$

where Rad_0 [W m^{-2}] is shortwave radiation at the top of the atmosphere, n [h] is the actual number of sunshine hours per day, N [h] is the maximum sunshine hours per day, a_s [-] is the fraction of Rad_0 on overcast days and $b_s + a_s$ [-] is the fraction of Rad_0 on clear sky days. The net incoming longwave radiation is given by:

$$Rad_l = \sigma T_a^4 (a_e + b_e \sqrt{e_a}) (a_c + b_c \frac{n}{N}), \quad (3.6)$$

where σ is the Stefan Boltzmann constant, T_a [K] is the atmospheric temperature and e_a [Pa] is the vapor pressure. a_e [$\text{k Pa}^{-0.5}$], b_e [-], a_c [-] and b_c [-] are empirical constants.

Short wave radiation over the day is then approximated similarly as in Daly et al. (2004):

$$Rad_d = \frac{4Rad_s}{\delta^2} [-t_d^2 + (\delta + 2t_0)t_d - t_0(t_0 + \delta)], \quad (3.7)$$

where Rad_s [W] is maximum radiation during the day, t_0 [day] is time of sunrise and δ [day] is the day length.

The long simulation runs (1000 years) are performed on a daily basis. Minimum and maximum temperature (T_{min} , T_{max}), precipitation (P) and mean global radiation (Rad_0) are generated by a stochastic weather generator (Richardson, 1981). Added to this generator is a reduction function for radiation to account for the effect of cloud cover. Cloud cover is based on a 50 years time series of measurements of fraction of sunshine by the Royal Netherlands Meteorological Organization (KNMI). Cloud cover data have been divided into bins, based on month number, difference between T_{min} and T_{max} and P . Based on the generated temperature difference and P , a sunshine fraction is drawn randomly from the corresponding bin. Vapor pressure deficit (D) is estimated from equations summarized in Allen et al. (1998) based on T_{min} and T_{max} .

3.2.3 Vegetation growth

To simulate transpiration and assimilation we used the model described in Daly et al. (2004). Here we describe the most important processes and assumptions, as well as the additions and modifications to this model. To allow for competition for light and water, at every location multiple species can grow. In this study we concentrate on a situation with two tree species, which means that understory is not simulated in this study.

The model is based on the single big leaf approach, thus canopy shading and within canopy variation of ambient variables are ignored. Although we are aware of the fact that this can influence both transpiration and growth significantly (e.g. Friend, 2001), to limit calculation times, we did not use a double layer model. Furthermore it is assumed that the plant system acts as a series of steady states, i.e. equilibrium between soil water flux, water flux through the plant and transpiration is reached instantaneously and no storage in the plant is taken into account. The model is sequential in the sense that first transpiration is calculated based on the soil-root-plant conductance and the stomatal conductance. Then the carbon assimilation rate is calculated based on biochemical processes, with the stomatal conductance as a limiting condition.

Transpiration, carbon assimilation, respiration and light interception are calculated on a half hourly time interval. Rainfall interception can be calculated both on a half hourly and on a daily time step. All other processes are calculated on a daily time interval. When the model is run for long simulation runs (longer then 1 year) the model is run on a daily time step. In this case fluxes of transpiration, carbon assimilation and light interception are summed to daily values in an upscaling procedure explained hereafter.

Transpiration

The transpiration module is based on Daly et al. (2004) with one modification to account for oxygen stress due to high soil moisture conditions. Transpiration (ET_{srp}) [m d^{-1}] based on the soil-root-plant conductance and water potential in the soil and the leaf per unit ground area [m s^{-1}] can be described by:

$$ET_{srp} = g_{srp} (\psi_s - \psi_l), \quad (3.8)$$

where g_{srp} [$\text{m Pa}^{-1} \text{s}^{-1}$] is soil-root-plant conductance per unit ground area, ψ_s [Pa] soil water potential and ψ_l [Pa] is the leaf water potential. g_{srp} is described by:

$$g_{srp} = \frac{g_{sr} g_p LAI}{g_{sr} + g_p LAI}, \quad (3.9)$$

where g_p [$\text{m Pa}^{-1} \text{s}^{-1}$] is the plant conductance per unit leaf area, g_{sr} [$\text{m Pa}^{-1} \text{s}^{-1}$] soil-root conductance per unit ground area and LAI [-] is the leaf area index. g_{sr} is calculated using a simplified cylindrical root model that links the distance traveled by water to reach the root to the root zone depth, Z_r [m], and the root area index

RAI [-] using the approach of Katul et al. (2003):

$$g_{sr} = \frac{K_{\theta}\sqrt{RAI}}{\pi g \rho_w Z_r} f_{ox}(\theta), \quad (3.10)$$

where K_{θ} [$\text{m Pa}^{-1} \text{s}^{-1}$] is unsaturated soil water conductivity and $f_{ox}(\theta)$ [-] is a reduction function for wet conditions causing oxygen stress in the rootzone. The last function is added to the function of Katul et al. (2003) and model of Daly et al. (2004) to be able to study the effect of high groundwater levels and water stagnation on vegetation. To account for additional root growth as a consequence of dry soil conditions, the RAI is dependent on soil moisture:

$$RAI = RAI \cdot s^{-a}, \quad (3.11)$$

where a [-] is a parameter that varies from species to species and $s = (\theta - \theta_r) / (\theta_s - \theta_r)$ [-] is the relative soil saturation. The plant conductance depends on leaf water potential ψ_l , because cavitation occurs as a consequence of low water potential in the xylem vessels:

$$g_p = g_{p,max} e[-(-\psi_l/d)^c], \quad (3.12)$$

where $g_{p,max}$ [$\text{m Pa}^{-1} \text{s}^{-1}$] is maximum plant conductance (per unit leaf area), c [-] and d [Pa] are parameters to scale ψ_l .

In wet soil moisture conditions, root water uptake can be limited due to a shortage of oxygen in the rootzone. To account for this effect the reduction function f_{ox} is included. This function is based on Feddes et al. (1978) and Brotsma & Bierkens (2007):

$$f_{ox} = \begin{cases} 1 & \text{if } \theta < \theta_{ox,1} \\ \frac{\theta_{ox,0} - \theta}{\theta_{ox,0} - \theta_{ox,1}} & \text{if } \theta_{ox,1} < \theta < \theta_{ox,0} \\ 0 & \text{if } \theta > \theta_{ox,0} \end{cases}, \quad (3.13)$$

where $\theta_{ox,1}$ is the soil moisture content at which root water uptake declines and $\theta_{ox,0}$ is the soil moisture content at which the water uptake stops.

Transpiration ET_{pm} [m s^{-1}] of plants based on atmospheric demand is determined using the Penman-Monteith equation (Monteith, 1965):

$$ET_{pm} = \frac{(\lambda_w \gamma_w g_{ba} \rho_a D + \Delta AR)}{\rho_w \lambda_w [\gamma_w (\frac{g_{ba}}{g_s LAI} + 1) + \Delta]}, \quad (3.14)$$

where λ_w [J kg^{-1}] is the latent heat of water vaporization, γ_w [Pa K^{-1}] the psychrometer constant, g_{ba} [m s^{-1}] the series of conductances of the boundary layer and the atmosphere (per unit ground area), ρ_a [kg m^{-3}] the air density, D [-] the atmospheric water vapor deficit, Δ [Pa K^{-1}] the slope of the saturated water vapor pressure to temperature relationship, AR [$\text{J m}^{-2} \text{s}^{-1}$] the absorbed long- and shortwave radiation and g_s [m s^{-1}] is the stomatal conductance (per unit leaf area). Since g_{ba} is a series of conductances, it can be calculated using $1/g_{ba} = LAI/g_b + 1/g_a$, where g_b [m s^{-1}] is the conductance to the boundary layer (per unit leaf area) and g_a [m s^{-1}] the conductance to the atmosphere (per unit ground area).

The stomatal conductance depends on radiation, air temperature, leaf water potential and CO₂ concentration. The dependence is calculated using the formulation of Jarvis (1976) which is based on applying reduction functions for the environmental variables reducing a maximum stomatal conductance $g_{s,max}$ [m s⁻¹]:

$$g_s = g_{s,max} f_{Rad}(Rad) f_D(D) f_{T_a}(T_a) f_{\psi_l}(\psi_l) f_{CO_2}(CO_2), \quad (3.15)$$

where $f_{Rad}(Rad)$ [-], $f_D(D)$ [-], $f_{T_a}(T_a)$ [-], $f_{\psi_l}(\psi_l)$ [-] and $f_{CO_2}(CO_2)$ [-] are respectively reduction functions for radiation, vapor pressure deficit, air temperature, leaf water potential and CO₂ concentration in the atmosphere. Daly et al. (2004) shows that the method of Jarvis (1976) leads to similar results as the approach of Leuning (1990).

Reduction of the stomatal conductance as a consequence of vapor pressure deficit is approximated using:

$$f_D(D) = \frac{1}{1 + D/D_x}, \quad (3.16)$$

where D_x is an empirically determined constant (Lohammer in Leuning, 1995). Air temperature influences g_s both at low and high temperatures:

$$f_{T_a}(T_a) = 1 - k_2(T_a - T_{opt})^2, \quad (3.17)$$

in which k_2 [K⁻²] is a sensitivity parameter, T_{opt} [K] is the temperature where g_s is at maximum and T_a [K] is air temperature.

The effect of increasing radiation can be expressed as an exponential function such that stomatal conductance increases at high radiation values:

$$f_{Rad}(Rad) = 1 - \exp(-k_1 Rad), \quad (3.18)$$

where k_1 is a sensitivity parameter (Jones 1992 in Daly et al. (2004)). Finally g_s is directly influenced by leaf water potential, where reduction occurs at low leaf water potentials:

$$f_{\psi_l}(\psi_l) = \begin{cases} 0 & \text{if } \psi_l > \psi_{l_0} \\ \frac{\psi_l - \psi_{l_0}}{\psi_{l_1} - \psi_{l_0}} & \text{if } \psi_{l_0} < \psi_l < \psi_{l_1} \\ 1 & \text{if } \psi_l < \psi_{l_1} \end{cases}, \quad (3.19)$$

where ψ_{l_1} [Pa] is the threshold potential at which the root-to-leaf hydraulic conductance begins to decline, ψ_{l_0} [Pa] threshold potential at which the root-to-leaf hydraulic conductance becomes negligible.

Assuming steady states and no storage, ET_{srp} equals ET_{pm} . Then ET , ψ_l and g_s are solved numerically from equations 3.8, 3.14 and 3.15.

Carbon assimilation

Also for the carbon assimilation module the approach of Daly et al. (2004) is followed. Carbon assimilation is determined by the equilibrium between the assimilation based on stomatal CO₂ conductance, A_{n,g_sba} [mol m⁻² s⁻¹], and the assimilation based on

the carboxylation capacity of the leaf, $A_{n,bio}$ [$\text{mol m}^{-2} \text{s}^{-1}$]. Both are calculated per unit leaf area. The first is described by:

$$A_{n,g_sba} = g_{sba,CO_2}(C_a - C_i), \quad (3.20)$$

where g_{sba,CO_2} [$\text{mol m}^{-2} \text{s}^{-1}$] is the series of stomatal, leaf boundary layer and aerodynamic conductances for CO_2 , C_a [mol mol^{-1}] is carbon concentration at the leaf surface and C_i [mol mol^{-1}] intercellular carbon concentration. It is assumed that the leaf boundary layer and atmospheric conductance are constant. The conductances for CO_2 are related to the conductance for H_2O by $g_{s,CO_2} = g_s/1.6$ [$\text{mol m}^{-2} \text{s}^{-1}$] (per unit leaf area), $g_{b,CO_2} = g_b/1.37$ [$\text{mol m}^{-2} \text{s}^{-1}$] (per unit leaf area) and $g_{a,CO_2} = g_a$ [$\text{mol m}^{-2} \text{s}^{-1}$] (per unit ground area).

The second is modeled according to the model of Farquhar et al. (1980) and extensions summarized in Leuning (1995):

$$A_{n,bio} = A_{n,\psi_l} \min(A_{n,c}, A_{n,q}), \quad (3.21)$$

where A_{n,ψ_l} [-] is a reduction function for carbon assimilation due to low leaf water potential (ψ_l) and $A_{n,c}$ [$\text{mol m}^{-2} \text{s}^{-1}$] and $A_{n,q}$ [$\text{mol m}^{-2} \text{s}^{-1}$] are the rubisco limited and the light limited carbon assimilation rate respectively. The reduction of carbon assimilation due to low ψ_l is modeled by:

$$A_{n,\psi_l} = \begin{cases} 0 & \text{if } \psi_l < \psi_{l,A_{n,0}} \\ \frac{\psi_l - \psi_{l,A_{n,0}}}{\psi_{l,A_{n,1}} - \psi_{l,A_{n,0}}} & \text{if } \psi_{l,A_{n,0}} < \psi_l < \psi_{l,A_{n,1}} \\ 1 & \text{if } \psi_l > \psi_{l,A_{n,1}} \end{cases}, \quad (3.22)$$

in which $\psi_{A_{n,1}}$ [Pa] is the threshold potential at which assimilation reduction caused by chemical action begins to decline and $\psi_{A_{n,0}}$ [Pa] is the threshold potential at which assimilation reduction caused by chemical action becomes negligible.

For light limited conditions biochemical driven carbon assimilation per unit leaf area is calculated using:

$$A_{n,q} = \frac{J C_i - \Gamma^*}{4 C_i + 2\Gamma^*}, \quad (3.23)$$

where J [$\text{mol photons s}^{-1} \text{m}^{-2}$] is the incident electron flux resulting from absorbed photosynthetically active radiation (APAR) and Γ^* [$\text{mol C mol}^{-1} \text{air}$] is the CO_2 compensation point. The CO_2 compensation point depends on temperature as:

$$\Gamma^* = \gamma_0 [1 + \gamma_1(T_l - T_0) + \gamma_2(T_l - T_0)^2], \quad (3.24)$$

where γ_0 , γ_1 and γ_2 are empirical constants, T_0 [K] is the reference temperature and T_l [K] is the leaf temperature.

In rubisco limited conditions carbon assimilation is modeled by:

$$A_{n,c} = V_{c,max} \frac{C_i - \Gamma^*}{C_i + K_c(1 + o_i/K_o)}, \quad (3.25)$$

where $V_{c,max}$ [mol m⁻² leaf s⁻¹] is maximum carboxylation capacity, K_c, K_o [mol mol⁻¹] are Michaelis-Menten constants for CO₂ and O₂ respectively and o_i [mol mol⁻¹] is intercellular oxygen concentration.

The electron flux depends on:

$$k_1 J^2 - (k_2 Q + J_{max}) J + k_2 Q J_{max} = 0, \quad (3.26)$$

where Q [mol photons m⁻² s⁻¹] is the absorbed photosynthetically active radiation (APAR), k_1 [-] determines the shape of the non-rectangular hyperbola, k_2 [mol electrons mol⁻¹ photons] is the quantum yield of whole-chain electron transport and J_{max} [mol photons m⁻² s⁻¹] is the potential rate of whole-chain electron transport. The latter is calculated using:

$$J_{max} = J_{max,0} \frac{\exp\left[\frac{H_{vJ}}{RT_0} \left(1 - \frac{T_0}{T_l}\right)\right]}{1 + \exp\left(\frac{S_v T_l - H_{dJ}}{RT_l}\right)}, \quad (3.27)$$

where $J_{max,0}$ [mol m⁻² s⁻¹] is the maximum electron transport rate at T_0 , T_0 is 293.2K, H_{vJ} [J mol⁻¹] is the energy of activation, S_v [J mol⁻¹ K⁻¹] is an entropy term and H_{dJ} [J mol⁻¹] is the energy of deactivation.

The Michaelis-Menten coefficients [mol mol⁻¹] are given by:

$$K_x = K_{x0} \exp\left[\frac{H_x}{RT_0} \left(1 - \frac{T_0}{T_l}\right)\right], \quad (3.28)$$

where x stands for c and o , K_{x0} [mol mol⁻¹] is the Michaelis-Menten constant at T_0 , R [J K⁻¹ mol⁻¹] is the gas constant and H_x [mol m⁻² s⁻¹] is the activation energy. The maximum carboxylation capacity is given by:

$$V_{c,max} = V_{c,max0} \frac{\exp\left[\frac{H_{vV}}{RT_0} \left(1 - \frac{T_0}{T_l}\right)\right]}{1 + \exp\left(\frac{S_v T_l - H_{dV}}{RT_l}\right)}, \quad (3.29)$$

where $V_{c,max0}$ [mol m⁻² s⁻¹] is the value of $V_{c,max}$ at T_0 , H_{vV} is the energy of activation, S_v [J mol⁻¹ K⁻¹] is an entropy term and H_{dV} [J mol⁻¹] is the deactivation energy.

To evaluate the biochemical parameters J_{max} , K_x and $V_{c,max}$ (eq. 3.27, 3.28 and 3.29) we need the leaf temperature which is calculated from the closure of the leaf energy balance as:

$$T_l = T_a + \frac{AR - \rho_w \lambda_w ET}{c_p \rho g_{ba}}, \quad (3.30)$$

where c_p is the specific heat of air [J kg⁻¹ K⁻¹].

If g_s , ET and ψ_l are calculated T_l can be calculated from Eq. 3.30 after which one can calculate Γ^* , J , K_x , and $V_{c,max}$ from Eq. 3.24, 3.26, 3.28 and 3.29. A_{n,ψ_l} can be calculated from Eq. 3.22. Finally we can solve for C_i by equating Eq. 3.20 to Eq. 3.21. Assuming equilibrium between atmospheric supply of carbon and biochemical assimilation: $A_{n,bio} = A_{n,g_sba}$.

Respiration

To determine the carbon gain and therefore growth of vegetation, also the loss of carbon due to respiration has to be estimated. Total vegetation respiration consists of leaf respiration, above ground wood respiration, fine and coarse root respiration and growth respiration.

Respiration of leaves, stem sapwood, root sapwood, and fine root tissue are modeled according to Sitch et al. (2003); an approach based on Ryan (1991) and Sprugel et al. (1995). In this approach respiration is based on the nitrogen content of different tissues. This nitrogen content is representative of living tissue that respire. Therefore a single nitrogen based respiration coefficient can be used but differentiation is required for the nitrogen content of the different tissues.

For sapwood tissue respiration a distinction is made for above ground respiration, R_{sws} [mol m⁻² s⁻¹], and below ground tissue respiration, R_{swr} [mol m⁻² s⁻¹], for it is temperature dependent. It is given by:

$$R_{sws} = f_{above} \cdot B_{mol} \cdot f_{sw} \frac{r}{cn_w} f(\overline{T_{day}}), \quad (3.31)$$

$$R_{swr} = (1 - f_{above}) \cdot B_{mol} \cdot f_{sw} \frac{r}{cn_w} f(\overline{T_{year}}), \quad (3.32)$$

where r [g C g N⁻¹ d⁻¹] is the respiration coefficient, B_{mol} [mol C m⁻²] is the total species biomass, f_{sw} [-] is the fraction of sapwood, cn_w [g C g N⁻¹] is the C:N ratio of woody tissue, $f(T)$ accounts for the dependency of respiration to temperature and f_{above} [-] is the fraction of above ground woody biomass.

Leaf respiration R_l [mol m⁻² s⁻¹] and fine root respiration R_{fr} [mol m⁻² s⁻¹] are respectively modeled as:

$$R_l = \frac{LAI}{SLA \cdot C_{mass}} \frac{r}{cn_l} f(\overline{T_{day}}), \quad (3.33)$$

$$R_{fr} = \frac{RAI}{SRA \cdot C_{mass}} \frac{r}{cn_{fr}} f(\overline{T_{year}}), \quad (3.34)$$

where C_{mass} [g mol⁻¹] is the mol mass of carbon, cn_l and cn_{fr} are respectively the C:N ratio of leaf and fine root tissue, SRA and SLA are respectively the specific root and leaf area [m² kg⁻¹ leaf]. The temperature dependencies of the respiration of the above and below ground tissue are calculated using a modified Arrhenius equation:

$$f(T) = \exp \left[308.56 \left(\frac{1}{56.02} - \frac{1}{T + 46.02} \right) \right], \quad (3.35)$$

where T [°C] is the temperature.

The total respiration R [mol m⁻² s⁻¹] is the summation of the respiration of all compartments of the tree: $R = R_{sws} + R_{swr} + R_{fr} + R_l$. Net carbon assimilation is then defined as $A_{n,net} = An - R$. Following Ryan (1991) growth respiration is assumed to be a fixed fraction of the net carbon assimilation: $R_{growth} = A_{n,net} * 0.3$ and therefore the assimilate that is available for growth is: $A_{n,growth} = A_{n,net} * (1 - 0.3)$.

Light and water interception

Light absorption is calculated for each species present in a cell. A random / homogeneous distribution of the leaves in space between the top and the base of the crown is assumed, where the base of the crown is located at the middle of the height of the tree. The calculation of radiation absorption is explained based on a case of two trees with overlapping crowns (Fig. 3.1), but it can easily be expanded to cases with more trees. To calculate the absorbed radiation, first the absorption per layer AR_L [W m^{-2}], where L denotes layer number, is calculated based on the total LAI per layer:

$$AR_L = Rad(1 - \alpha) \prod_{l=1}^L (1 - \exp^{-kLAI_l}), \quad (3.36)$$

where α is the albedo [-] and k [-] is the light extinction coefficient and LAI_l [-] is the total LAI of layer l which in the case of two species is:

$$LAI_l = \sum_{i=1}^2 \frac{LAI_{l,i} \cdot dz_l}{dz_{crown,i}}, \quad (3.37)$$

where dz_l [m] is the vertical thickness of the layer, $LAI_{l,i}$ [-] is the leaf area index of tree i in layer l and $dz_{crown,i}$ [m] is the length of the crown of tree i .

Absorbed radiation per tree can now be calculated as the weighted sum of the absorbed radiation per layer. For every tree in the cell the absorbed radiation is:

$$AR_i = \sum_{l=1}^L \frac{LAI_{l,i}}{LAI_l} AR_l. \quad (3.38)$$

Precipitation interception is calculated based on the total LAI of the canopy and than linearly divided between the individual LAI of the tree species that are present. We make the assumption that precipitation falls at a constant rate throughout the given time interval. Part of the precipitation P that reaches the top of the canopy falls on the soil directly as direct throughfall P_d [mm day^{-1}], while part of the precipitation is intercepted P_{int} [mm day^{-1}] depending on the gap fraction f_{gap} :

$$P_{int} = (1 - f_{gap})P. \quad (3.39)$$

The gap fraction is estimated using only the transmittance part of Eq. 3.36:

$$f_{gap} = e^{-kLAI}. \quad (3.40)$$

When running the model on a daily time step we assume that as long as the interception capacity of the canopy is not exceeded and the open water evaporation for a day is not exceeded all water is intercepted:

$$I = E_I = \min(E_O, LAI \cdot I_{cap}/\Delta t, P_{int}), \quad (3.41)$$

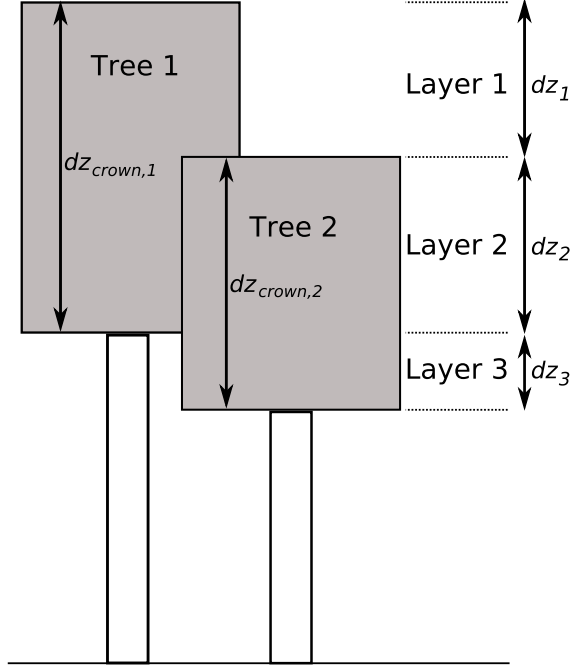


Figure 3.1 Scheme used for radiation absorption by trees. In the model concept the trees do not stand next to each other but the LAI is homogeneously distributed over the cell area, thus LAI does fully overlap horizontally.

where I [mm day^{-1}] is interception, E_I [mm day^{-1}] is evaporation of interception, E_O [mm day^{-1}] is open water evaporation that is calculated using the Penman-Monteith equation (Monteith, 1965) applied to open water, Δt [day] is the time step size and I_{cap} [mm] is the maximum interception capacity.

When running the model on a semi-hourly time step, I is not limited to E_O . This means that the intercepted water from the previous time step that has not yet evaporated is still present in the canopy, thus:

$$I_t = \min(\max(I_{t-\Delta t} + P_{int} - E_O, 0), LAI \cdot I_{cap} / \Delta t), \quad (3.42)$$

where t denotes time and Δt [0.5h] is the time step size. In both cases precipitation that reaches the ground as throughfall is:

$$P_{net} = P - I. \quad (3.43)$$

During the time needed for evaporation of the interception, transpiration is neglected.

3.2.4 Temporal upscaling

To perform long simulation runs, the vegetation model that runs on a time scale of half an hour, has to be scaled up. During the day, meteorological parameters such as radiation, temperature and water vapor pressure deficit vary while they influence transpiration (ET) and carbon assimilation (A_n) in a non-linear way. This means that a simple linear upscaling using average values of the input variables leads to biased

Table 3.1 Values of parameters to fill lookup table of Tr and A_n . Min and Max are the minimum and maximum values of the range for which transpiration and assimilation values have been calculated. Nr of steps indicates the number values between the minimum and maximum value have been calculated. Step size is the interval between the subsequent values of the calculated values of the lookup values. var means that an exponential function is used produce variable step sizes for lookup values.

Parameter	Min	Max	Nr of steps	Step size	Unit
LAI	0.1	5	21	var	[-]
θ	θ_r	θ_{sat}	22	var	[-]
T_{max}	0	40	8	5	[°C]
T_{min}	$T_{max}-30$	T_{max}	7	5	[°C]
Rad_{max}	0	800	20	var	[W m ⁻²]
n/N (cloud coverage)	0	1	6	0.2	[-]
δ (day length)	8	16	5	2	[h]

results. We therefore use the following upscaling procedure. First it is assumed that fluxes during a half hour time interval are constant. An interval of half an hour is chosen, because this corresponds to the eddy-covariance flux measurement integration and report interval. Also, smaller time steps than a half hour would cause a significant increase in computation time, whereas larger time steps would not capture the daily variation. Assuming the daily course in temperature and radiation are as described in equations 3.7 and 3.4, on a daily timescale seven variables influence ET and A_n : T_{min} , T_{max} , Rad , δ (day length), n/N (time fraction cloud coverage), θ and LAI . The range in values of each of these variables is discretized in steps (Table 3.1). Day sums of ET and A_n for all possible combinations of these variables between reasonable bounds are calculated and stored in a lookup table. For LAI and Rad , the step size increases with higher values because the system is most sensitive at lower values. For θ the step size is smaller for both high and low values for the same reason. Because the difference between T_{min} and T_{max} during a day is limited T_{min} is defined relative to T_{max} with a maximum difference of 30°C. When performing long runs, daily values of T_{min} , T_{max} , Rad , δ , n/N , θ and LAI are generated or calculated and the associated ET and A_n is then directly read from the table. The filling of the table takes quite some time (app. 2 days on a PC), requiring the calculation of ET and A_n at half-hourly time step for $21 \cdot 22 \cdot 8 \cdot 7 \cdot 20 \cdot 6 \cdot 5 = 1.55 \cdot 10^7$ parameter combinations. However once filled, long simulation runs (hundreds of years) using realistic A_n and ET values at a daily time step are possible.

3.2.5 Growth, allocation, allometry and phenology

To calculate light competition between trees we need to know the height of the trees H [m] and the LAI . We also need to know the LAI to calculate leaf respiration and carbon allocation. Because these parameters vegetation are difficult to calculate based on bio-mechanical principles, allometric scaling relationships have been used to relate them to biomass per unit area.

The geometry of the trees is based on woody biomass. The woody biomass is divided in above ground biomass B_{above} [kg m^{-2}] and below ground biomass B_{below} [kg m^{-2}]:

$$\begin{aligned} B_{above} &= f_{above}B \\ B_{below} &= (1 - f_{above})B \end{aligned} \quad (3.44)$$

where B [kg m^{-2}] is the dry biomass of the woody parts of the tree, f_{above} [-] is the above ground fraction of biomass. The value of f_{above} is fixed during growth and the same for all species.

The canopy is simplified by assuming that the canopy is homogeneous between its base and its top, where its base is located halfway the top of the canopy and the ground. It is assumed that 40% of the above ground biomass is located in the stem and 60% in the branches. The number of trees per area [trees ha^{-1}] is calculated using:

$$n_{tree} = a_{nr\text{tree}} + b_{nr\text{tree}}e^{-c_{nr\text{tree}}B_{above}}, \quad (3.45)$$

where $a_{nr\text{tree}}$, $b_{nr\text{tree}}$ and $c_{nr\text{tree}}$ are empirical parameters. The function is fitted on data from Jansen et al. (1996). From this it follows that the stem biomass per tree B_{stem} , [kg] is:

$$B_{stem} = \frac{B_{above}10^4}{n_{tree}}, \quad (3.46)$$

where 10^4 is a factor to convert from m^2 to ha [$\text{m}^2 \text{ha}^{-1}$]. When the wood density is known (ρ_{stem} [kg m^{-3}]) the wood volume per tree, V_{stem} [m^3], is:

$$V_{stem} = B_{stem}/\rho_{stem}. \quad (3.47)$$

The diameter of the stem at breast height (D_{stem}) [m] is given by (e.g. Landsberg, 1986):

$$D_{stem} = \left(\frac{B_{stem}}{a_{md}} \right)^{(1.0/b_{md})} / 100, \quad (3.48)$$

where a_{md} and b_{md} are allometric scaling factors and 100 is a factor to convert from cm to m.

Assuming a cylindrical form of the stem of a tree, the height of a tree H_{tree} [m] is given by:

$$H_{tree} = \frac{V_{stem}}{\left(\frac{D_{stem}}{2} \right)^2 \pi}. \quad (3.49)$$

So through equations 3.44 to 3.49 height and number of trees is related to biomass m^{-2} . We assume a fixed relationship between RAI and LAI :

$$RAI = LAI_{max} \cdot RAI_{frac}. \quad (3.50)$$

The maximum LAI depends on the sapwood area (pipe theory Shinozaki in Friend et al., 1997):

$$LAI_{max} = \eta_f Z_{sw}, \quad (3.51)$$

where η_f is the sapwood to foliage ratio [-] and Z_{sw} sapwood area at breast height [m²]:

$$Z_{sw} = f_{sw} D_{stem}^2 \pi / 4, \quad (3.52)$$

where f_{sw} is the fraction of sapwood to total wood. It depends on an allometric scaling factor:

$$f_{sw} = \exp(a_{sw} B_{above}), \quad (3.53)$$

where a_{sw} is a parameter controlling the sapwood area based on the tree biomass. The biomass of the sapwood can then be calculated using:

$$B_{sw} = B_{stem} f_{sw}. \quad (3.54)$$

Phenology depends on the 10 day maximum temperature sum. When this sum exceeds 100 °C leaves start to grow at a maximum growth rate that is a fraction of LAI_{max} :

$$LAI_t = LAI_{t-\Delta t} + LAI_g \cdot LAI_{max} \Delta t, \quad (3.55)$$

where LAI_g [day⁻¹] is the LAI growth rate. The carbon consumed in growth is subtracted from the carbon storage, which can result in a decline in the growth rate when the storage gets depleted. At the end of the growing season, when the 10 day maximum temperature sum becomes lower than 100 °C, leaves start to be shed in a similar way as growth at a fixed rate LAI_d , where the carbon of the leaves is lost.

Carbon allocation is calculated for each species on a daily time step. Each time step carbon assimilate is allocated to a carbon storage compartment [mol]. From the beginning of the growing season, carbon from this storage compartment is used for leaf growth, until LAI_{max} , is reached or until the carbon storage compartment is depleted to 10% of its maximum S . When LAI_{max} is reached the carbon assimilate keeps being allocated to the carbon storage compartment until its maximum capacity. When the carbon storage compartment is filled upto maximum, carbon assimilate is used for biomass growth of the woody parts. Biomass growth of the woody biomass occurs at the above mentioned fractions to the stem and the roots. The amount of carbon used for leaf growth depends on the LAI and SLA :

$$B_{lai} = \frac{LAI}{SLA}, \quad (3.56)$$

where SLA [m² kg⁻¹ leaf] is the specific leaf area index. The capacity of the carbon storage compartment S [kg m⁻²] is limited to a fixed fraction of the sapwood (Friend et al., 1997):

$$S = f_{store} * B_{sw}, \quad (3.57)$$

where f_{store} is the fraction of sapwood that can be used for carbon storage [-]. When the store becomes depleted the tree dies, as it does not have enough storage left to make new leaves the next growing season. Note that the last 10% of the carbon storage can only be used for respiration, not for leaf growth.

Vegetation mortality

As mentioned in the previous paragraph, vegetation dies when the carbon storage becomes depleted. In addition to this assumption a random mortality rate is included to account for death as a result of disease, wind, lightning. Assuming an average tree age of 300 years under unstressed circumstances the probability of dying in a given year is 1/300. This is implemented in the model such that when this happens the biomass of both species in a cell is reset to the initial condition.

3.3 Results

The model has been evaluated on a short timescale by comparing the simulated and measured fluxes of H₂O en CO₂ at 30 minute time intervals. Using the evaluated model long term simulation runs were performed to investigate the influence of light competition and the influence of groundwater on vegetation dynamics. Parameter values for these runs were taken from literature or in some cases submodules were calibrated against data (Appendix A).

3.3.1 Comparison with fluxdata

To evaluate the model we compared model simulations with measured evapotranspiration (*ET*) and CO₂ eddy covariance flux data from Hainich forest in Germany (Knohl et al., 2003). This location was chosen because it is a broadleaf forest and it is located in the temperate climate zone. The dataset also contains data of soil moisture content, atmospheric water vapor concentration, temperature and radiation. The model was run with a 0.5 hour time step corresponding to the integration and reporting interval of the fluxdata. For this runs the soil texture of Hainich Forest is used which is a loamy clay. Its soil physical parameters (Table 3.2) are estimated based on a neural network-based ROSETTA database (Schaap et al., 1998). In this analysis the soil water balance is not calculated and therefore the influence of the groundwater is not included. Instead the measured soil moisture content is used.

Figure 3.2 shows the main environmental input variables, the resulting stomatal conductance and *ET* and CO₂ fluxes in summer for day 180 until day 185 (day one is January first). It can be seen from figure 3.2.g and 3.2.h that the modeled fluxes show a trend that is similar to the measured fluxes. During the day, the *ET* flux is somewhat overestimated by the model. The measured carbon fluxdata show an upward flux during the night, caused by respiration. In the model this flux is underestimated because only autotrophic respiration is included and soil respiration is ignored.

Figure 3.3 shows the modeled versus the measured *ET* and CO₂ flux data for four five day periods. The correlations of *ET* during the growing season are high (R = 0.88 - 0.93). However *ET* fluxes are overestimated by the model especially in spring and autumn. Correlations between the modeled and measured CO₂ flux are higher (R = 0.91 - 0.94) with no apparent bias.

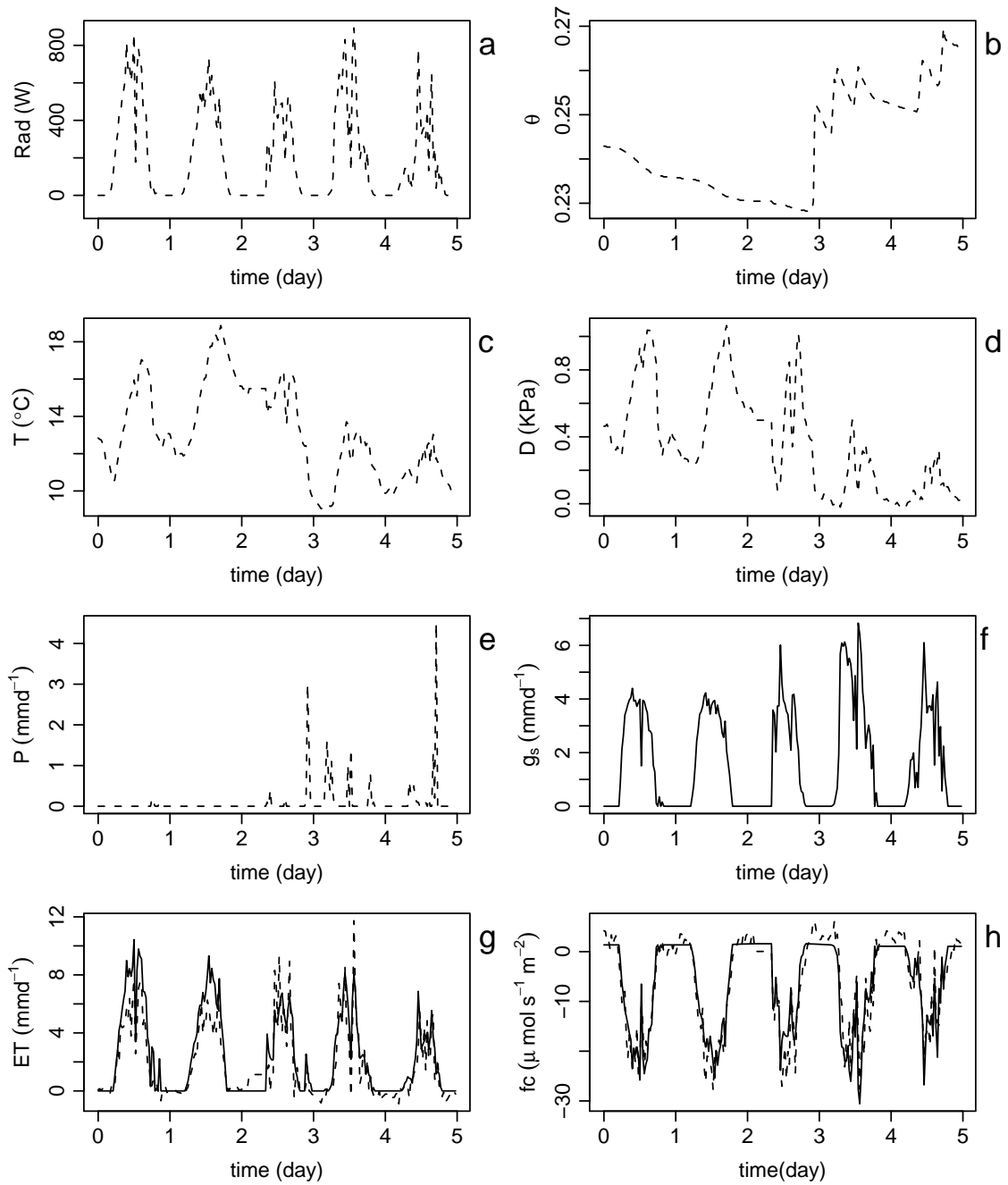


Figure 3.2 Comparison of measured and modeled fluxes and stomatal conductance for a 5 day period (day 181-185, 2004) in Hainich forest. Influence of environmental variables: (a) incoming shortwave radiation, (b) soil moisture content θ of root zone, (c) air temperature, (d) water vapor deficit and (e) precipitation on (f) modeled stomatal conductance and (g) evapotranspiration and (h) carbon flux. Dashed lines, measured values; solid lines, model results.

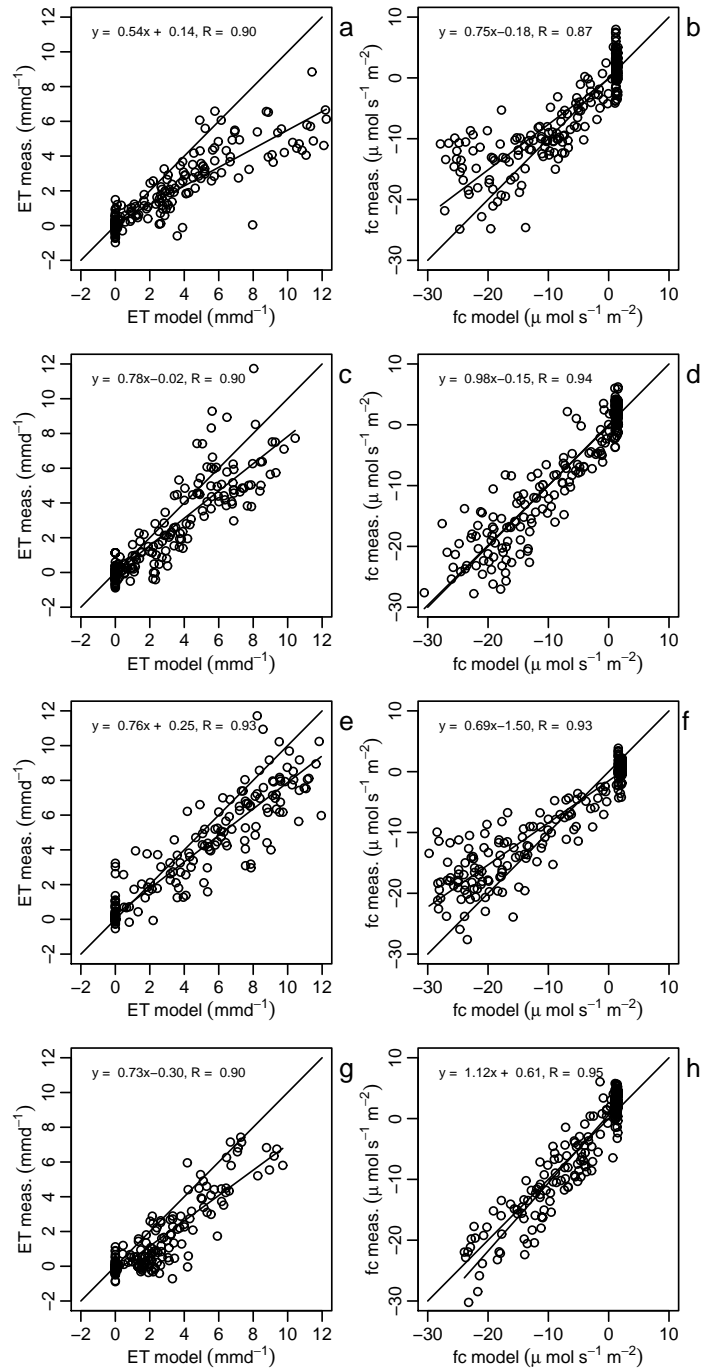


Figure 3.3 Modeled versus measured half-hourly flux data of ET (left) and CO_2 (right) for four five day periods in 2004. Both the 1:1, and the fitted regression line are plotted. Panels (a) and (b), day 150-155; (c) and (d), day 180-185; (e) and (f), day 210-215; (g) and (h), day 240-245. Day 1 is January 1st. Each dot represents one time step of 0.5 h.

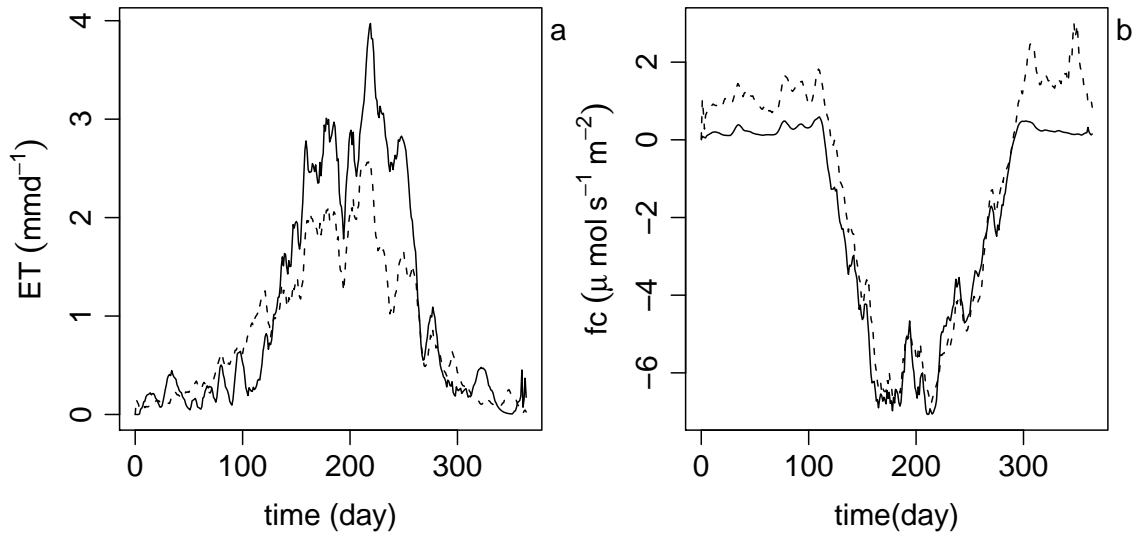


Figure 3.4 Daily values of measured and modeled fluxes of ET (a) and CO_2 (b) in Hainich Forest in 2004 using a 10 day running means filter. Modeled data are plotted as a solid line and measured data are plotted as a dashed line.

We also compared modeled and measured ET and CO_2 on a yearly timescale summing fluxes over a day. Figure 3.4 shows the results for 2004. During summer ET is overestimated by the model. The net modeled CO_2 flux is underestimated during winter. The latter is largely caused by absence of litter decomposition and soil respiration in the model, which is especially apparent in winter.

The cause for the overestimation of ET during summer in the model compared to the measured data is not clear. Causes can be found in one of the many assumptions made in the model. Probable explanations are that the vapor pressure deficit (D) as input for the model is overestimated as it is observed above the canopy of the forest, instead of within the canopy. Also the part of the radiation used for transpiration may be over-estimated by neglecting the heat capacity of the canopy.

3.3.2 Light and water competition and the influence of groundwater

For the long simulation runs of 600 years, climatic forcing by a stochastic weather generator is used, based on Dutch climate conditions, which is characterized by an annual precipitation of 700 mm, a mean summer temperature of 17.7 °C, and a mean winter temperature of 3.4 °C. The long simulation runs have been performed for four different soil textures: loamy sand, sandy loam, sandy clay loam and silty clay loam, of which soil physical parameters are listed in table 3.2. For the long simulation runs a spin-up period of 400 years has been used to obtain equilibrium situation in vegetation and hydrological system. All long simulation runs were performed with a combination of two vegetation species; one which is adapted to dry circumstances (e.g. oak) and one that is better adapted to wet circumstances (e.g. alder). Table 3.3 gives parameters that determine the soil-root-resistance and carbon assimilation

Table 3.2 Soil textures used in simulation runs. θ_{sat} [-] saturated soil moisture content; θ_r residual soil moisture content; K_s [m d⁻¹] saturated conductivity; α [m⁻¹] and n [-] van Genuchten parameters (Carsel, 1988).

Soil texture	θ_{sat} [-]	θ_r [-]	K_s [m d ⁻¹]	α [m ⁻¹]	n [-]
Loamy sand	0.41	0.057	3.50	12.4	2.28
Sandy loam	0.41	0.065	1.06	7.5	1.89
Sandy clay loam	0.39	0.100	0.134	5.9	1.48
Silty clay loam	0.43	0.089	0.0138	10.0	1.23
Loamy clay	0.51	0.102	0.71	1.27	1.38

Table 3.3 Parameters of the tree species adapted to dry and wet conditions.

Parameter	Description	Wet species	Dry species
ψ_0	Leaf water potential below which g_s becomes 0 [Pa]	-0.45e+06	-4.5 e+06
ψ_1	Leaf water potential below which g_s begins to decline [Pa]	-0.005e+06	-0.05 e+06
$\psi_{A_n,0}$	Leaf water potential below which assimilation becomes 0 [Pa]	-0.45e+06	-4.5 e+06
$\psi_{A_n,1}$	Leaf water potential below which assimilation begins to decline [Pa]	-0.05e+06	-0.5 e+06
Ox_0	Soil moisture content above which root water uptake begins to decline [-]	$\theta_{sat}-0.03$	$\theta_{sat}-0.10$
Ox_1	Soil moisture content above which root water uptake becomes 0 [-]	$\theta_{sat}-0.01$	$\theta_{sat}-0.05$

reduction due to low leaf water potential.

Influence of groundwater

To illuminate the role of groundwater in vegetation dynamics we performed simulations for a case in which only percolation occurs and three cases with different groundwater levels that result in fluxes between groundwater and soil water. These simulation runs were performed with sandy loam as soil texture. In the case with percolation only, percolation only occurs when field capacity is exceeded. Percolation rate is then equal to K_θ . Figure 3.5 shows the development of biomass of the two vegetation types in time. In case of a model in which only percolation occurs, biomasses up till 7 kg m⁻² are reached. In this case both the wet and the dry species can grow, although the dry species has a slight advantage.

When a fixed groundwater table is included in the model (Eq. 3.2) a capillary flux from the saturated to the unsaturated zone occurs and results are quite different. In the case where the groundwater is directly underneath the rootzone (0.6 m below the surface) the wet adapted species outcompetes the dry adapted species. A maximum biomass of 28 kg m⁻² is reached and rootzone soil moisture content varies between 0.14 and 0.25. Because of the small distance between the rootzone and the groundwater,

capillary rise in summer is high and water stress is therefore low.

If the groundwater level is deeper (at 1.0 m), soil moisture content decreases as well as the lifetime and biomass of vegetation. The decrease in soil moisture content is a direct effect of the deeper groundwater, increasing the downward flux because of the lower water potential and decreasing capillary rise due to the longer distance between the rootzone and the groundwater. The smaller biomass is a result of the lower soil moisture content. This lower soil moisture content causes a lower ψ_s influencing the $\psi_l - \psi_s$ gradient. At the same time the lower soil moisture content causes a lower K_θ which causes a lower soil-root-plant conductance (g_{srp}). This results in smaller g_s , lower ψ_l and therefore less ET . As a final result A_n becomes smaller. Additionally due to less ET the leaf temperature increases and maintenance respiration increases. The decrease in A_n and increase in respiration finally results in a lower biomass.

When random mortality of vegetation due to diseases, wind or lightning is not included, vegetation in the model still dies after a certain period. As the trees grow larger, the margin between assimilation and maintenance respiration becomes smaller. As a period with favorable assimilation and growth conditions is always followed by a period of less favorable conditions where respiration is larger than assimilation, the chance of the storage being depleted increases when vegetation approaches its maximum biomass.

At a low biomass the LAI per volume of sapwood is higher than at a high biomass. Since carbon storage is a fixed fraction of the sapwood, vegetation with a low biomass has a relatively smaller carbon storage. The effect is that vegetation with a lower biomass due to high stress, is more prone to a depleted carbon buffer and thus lives shorter.

When the groundwater is at 1.5 m the yearly minimum soil moisture content approaches the residual moisture content every year and the average yearly soil moisture content drops slightly. Biomasses remain smaller and circumstances for the dry adapted species become more favorable. Because of the high water retention capacity of sandy loam, the wet species is not yet fully outcompeted.

From the model results it becomes clear that besides the soil moisture content, light competition plays an important role. Once a species has established under unfavorable soil moisture conditions, it cannot be outcompeted by another species with a smaller biomass even if the latter is better adjusted to the current soil moisture conditions. In case that one species dies its biomass is reset to a primordial amount. The other species can have a small advantage because it already has a larger biomass. The difference in biomass after death and the suitability of that species to grow at that location determines whether the species that died can outcompete the other vegetation. This causes the alternation of the two species in time.

Longterm influence of groundwater and soil texture

To determine the combined influence of soil texture and groundwater on soil moisture and vegetation growth, we used a gradient in groundwater levels from 30 cm to

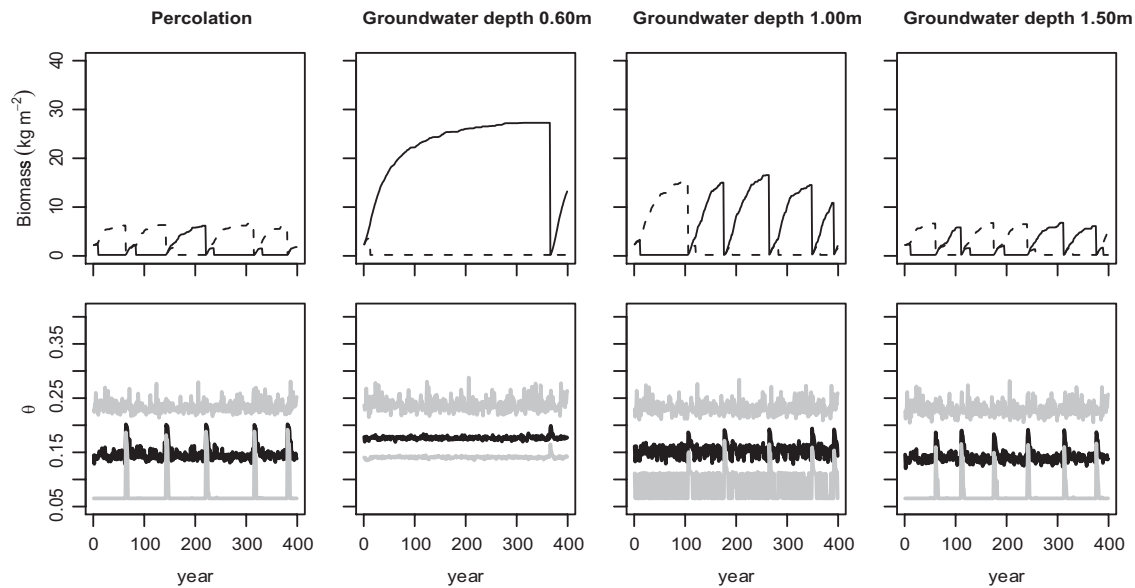


Figure 3.5 Development of biomass (top) and soil moisture (bottom) of a wet adapted and a drought adapted vegetation type in a case with percolation only and three different groundwater depths on sandy loam. Top: solid line, wet adapted vegetation; dashed line, dry adapted vegetation. Bottom: black line, yearly average soil moisture content; gray line, yearly minimum and maximum soil moisture content.

400 cm for four different soil textures. This fixed groundwater level influences both percolation and capillary rise.

Figure 3.6 shows that soil texture and groundwater depth have a large influence on soil moisture content and biomass. The first thing to note is that silty clay loam leads to completely different results than the soil textures with higher conductivities and lower soil water retention capacities. Silty clay loam remains permanently near saturation, only allowing for growth of the wet species. Even this species, does not attain high biomasses due to oxygen stress, but also due to water stress that mainly results from the low soil water conductivity and high water retention capacity. As to be expected, the decrease in soil moisture conductivity and increase in water retention capacity in the sequence of loamy sand, sandy loam and sandy clay loam, causes higher soil moisture contents. The maximum soil moisture content is largely influenced by precipitation and the groundwater recharge at the end of winter, whereas the minimum soil moisture content is mainly influenced by throughfall and the vegetations capability to transpire water from the dry soil in summer.

Vegetation growth on loamy sand, sandy loam and sandy clay loam is rather similar for a groundwater depth less than approximately 70 cm. The proximity of groundwater for all soil textures results in a smaller net flux to the groundwater and therefore relatively high soil moisture contents. The wet vegetation attains approximately the same high biomasses on all soil textures.

At approximately 70 cm the biomass of the wet adapted vegetation drops sharply

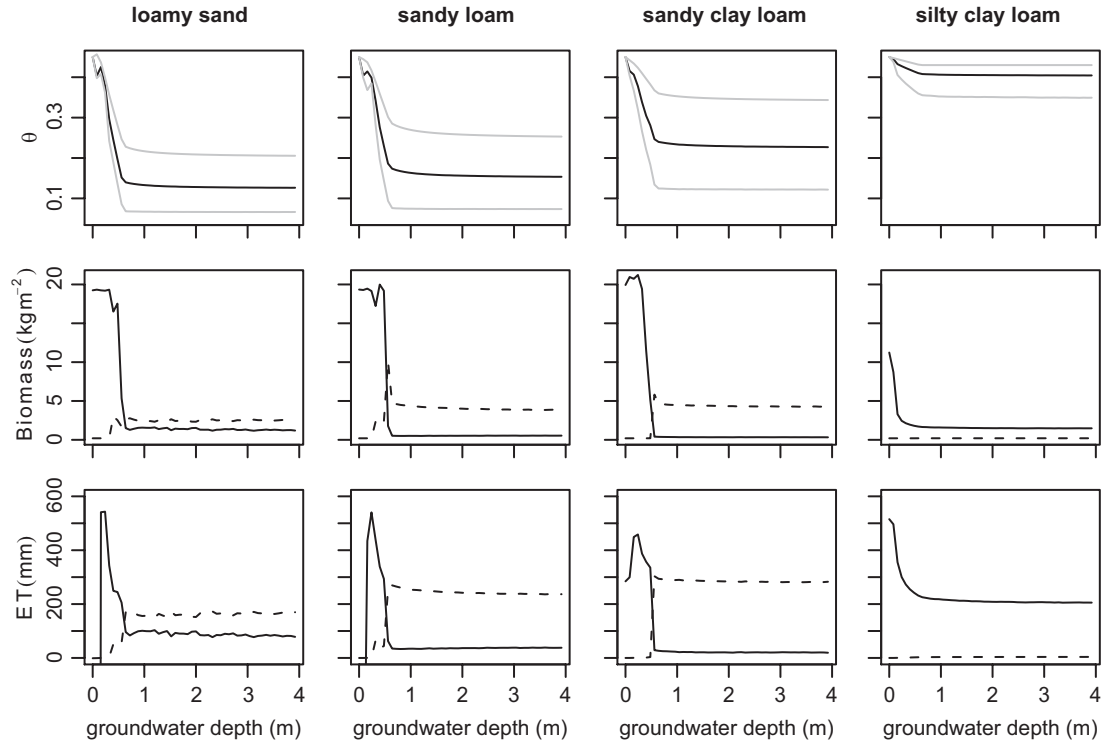


Figure 3.6 500 Year average of biomass, evapotranspiration and yearly minimum, maximum and mean soil moisture content along a groundwater gradient for four soil textures. Biomass and ET : solid line, wet adapted vegetation, dashed line, drought adapted vegetation. Soil moisture content: black line, average, gray line, minimum and maximum.

and the dry species prevails. In reality this drop will not be this abrupt, because the rooting depth is more variable. When groundwater becomes deeper, the soil textures with higher water retention capacities and lower conductivities cause the soil moisture content to be higher and the dry vegetation to obtain slightly higher biomasses. At groundwater levels deeper than 70 cm the wet adapted vegetation on loamy sand reaches relatively high biomasses relative to the wetter sandy loam and sandy clay loam. This is caused by the fact that the dry adapted vegetation experiences more water stress in summer, causing less carbon assimilation and therefore lower biomasses and a shorter lifetime. The wet vegetation therefore receives more radiation giving it more opportunities to grow.

Water balance

To get more insight into the interaction between biomass growth and hydrology we constructed figure 3.7 showing the most important water balance components: evaporation (E), transpiration (Tr), vertical soil water flux (Q_v) and runoff (R) as well as the biomass for each soil texture. For reference table 3.4 provides the water balance for all cases investigated. It is clear that for most deep open soils as considered here the majority of runoff occurs through groundwater. Surface runoff by rain on saturated soils only occurs for impermeable soils (or shallow aquifers as will be shown in

Table 3.4 Biomass (B), Evaporation (E), Transpiration (Tr), flux between soil and ground water (Qv) and surface runoff (R) for three groundwater levels (Gwd) for four soil textures. Mean yearly precipitation per year is 702 mm. 0 and 1 for B , E and Tr denote respectively the wet adapted and the dry adapted vegetation.

Soiltexture	Gwd	B_1	B_2	B	E_1	E_2	E	Tr_1	Tr_2	Tr	Qv	R
loamy sand	0.2	15.8	0.2	16.0	138	9	146	490	0	490	65	0
	0.6	4.4	1.9	6.3	108	55	163	177	64	241	299	0
	1.5	1.4	2.1	3.5	52	74	125	89	141	230	346	0
sandy loam	0.2	16.0	0.2	16.2	138	9	147	398	0	398	156	3
	0.6	1.9	8.9	10.9	41	113	154	69	239	309	239	0
	1.5	0.5	4.0	4.5	25	107	132	34	237	271	299	0
sandy clay loam	0.2	17.2	0.2	17.4	138	9	147	420	0	420	126	17
	0.6	0.5	5.5	6.0	22	117	139	38	284	321	241	0
	1.5	0.4	4.3	4.6	18	111	129	22	273	296	277	0
silty clay loam	0.2	3.5	0.2	3.7	102	9	112	337	0	337	84	338
	0.6	1.8	0.2	2.0	73	11	84	218	2	219	264	269
	1.5	1.5	0.2	1.7	68	12	79	197	3	200	308	230

the companion paper).

The absence of understory (apart from the under growing second species) in the vegetation model influences the water balance. Although the model accounts for soil evaporation under near saturated circumstances, both interception evaporation and transpiration are expected to increase the total evapotranspiration if understory of shadow-tolerant species is accounted.

What is obvious from the results is that there is no clear relation between soil texture and the division between evaporation, transpiration, groundwater recharge and runoff, nor does such a relation exist for groundwater depths. Instead, this division between evapotranspired and infiltrated water strongly depends on the biomass as can be seen in figure 3.8. Note that in this figure both biomass and ET are influenced by groundwater depth. Whether caused by a combination of soil texture and groundwater depth that favors one or both species is of no consequence. As long as total biomass is high, a large part of the precipitation will be evapotranspired instead of discharged through groundwater or surface runoff. This clearly shows the importance of a good representation of vegetation growth for hydrology.

3.4 Conclusions

We have developed a coupled soil moisture - groundwater - vegetation model that is able to simulate the effect of groundwater depth and soil moisture on vegetation growth and vice versa. The model is able to provide estimates of the variation of evapotranspiration (ET) and carbon assimilation (A_n) at hourly, daily and yearly time scales, as well as centennial-scale simulation of forest growth under water and light competition. The results of the 500 year simulation runs clearly demonstrate the importance of light competition in temperate forests: species established under unfa-

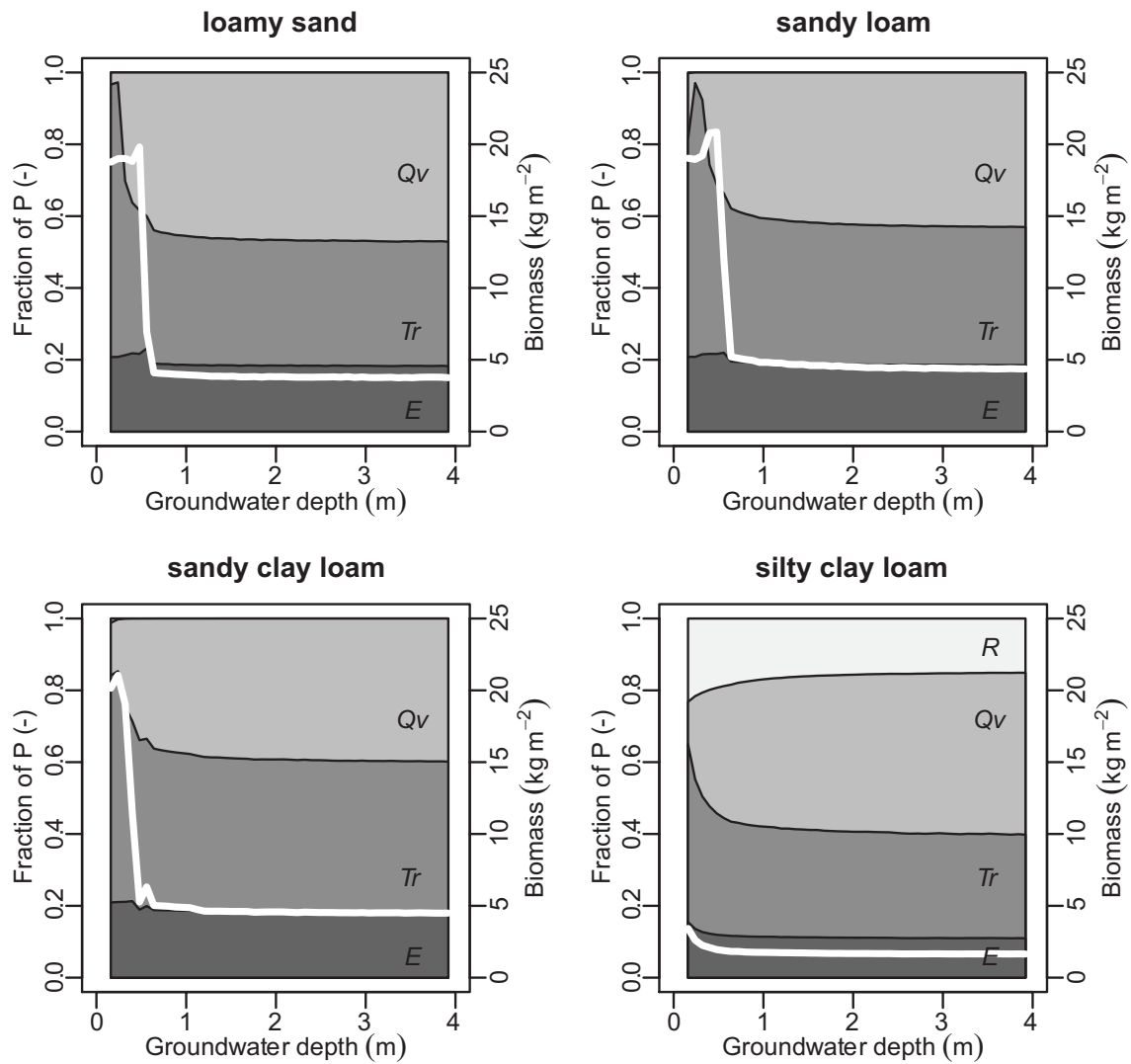


Figure 3.7 Influence of groundwater depth on the water balance and biomass for four different soil textures based on 500 year average values. *E*, evaporation; *Tr*, transpiration; *Qv*, vertical exchange flux between unsaturated zone and groundwater; *R*, surface runoff. Fluxes are given as fraction of precipitation (*P*). The white line represents the biomass.

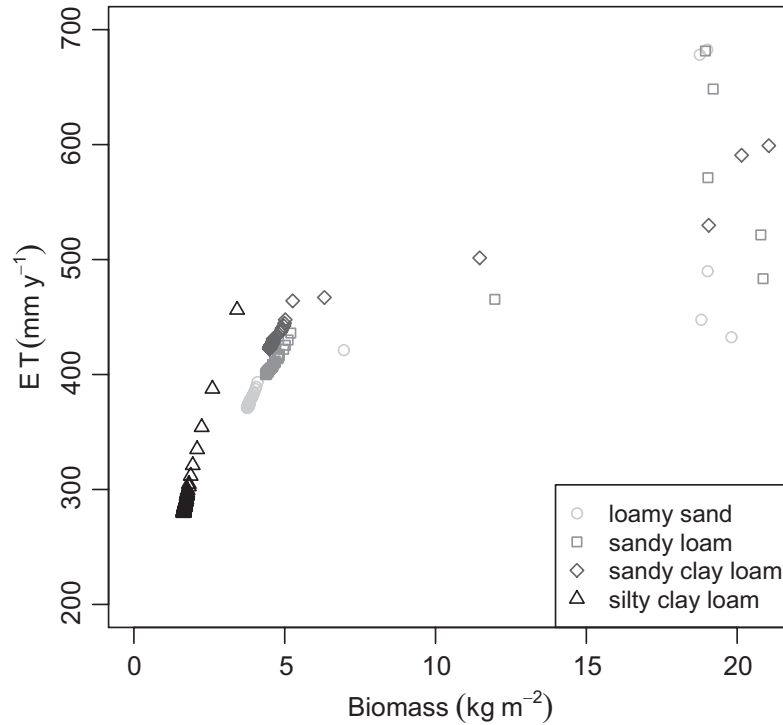


Figure 3.8 Dependence of ET on biomass for four soil textures. Biomass and ET are 500 year averages along a gradient of groundwater depths (0.2-4.0m).

avorable soil moisture conditions can almost not be outcompeted by a smaller species that is better adapted to the local soil moisture regime. Only under extremely wet conditions the wet adapted species can outcompete the dry adapted species, or if the difference in biomass between species is very small, i.e. at a very low biomass, a better adapted smaller species can outcompete taller. The influence of groundwater is present for a large range of groundwater depths, by both capillary rise and possible reduction of percolation to the groundwater, while soil texture is important as well, particularly for higher clay contents. 500 Year simulation runs clearly show that groundwater and soil texture have a large impact on biomass development and species composition, i.e. groundwater depth and soil texture determine what species is most successful. In turn species composition and biomass are important predictors for the long term water balance and therefore energy balance of the eco-hydrological system. This study shows that for ecosystems, models for systems with shallow groundwater can greatly be improved by including fluxes from and to the groundwater. The companion paper will show the influence of incorporating groundwater dynamics.

Acknowledgments

This work was sponsored by the Stichting Nationale Computerfaciliteiten (National Computing Facilities Foundation, NCF) for the use of supercomputer facilities, with financial support from the Nederlandse Organisatie voor Wetenschappelijk Onderzoek (Netherlands Organization for Scientific Research, NWO).

4 Vegetation competition model for water and light limitation. II: Spatial dynamics of groundwater and vegetation

This chapter has been published as:

Brolsma, R. J., L. P. H. van Beek and M. F. P. Bierkens (2010), Vegetation competition model for water and light limitation. II: spatial dynamics of groundwater and vegetation. Ecological Modelling 221, pp. 1364-1377.

Abstract

In temperate climates groundwater can have a profound effect on vegetation, because it strongly influences the spatio-temporal distribution of soil moisture in the rootzone and therefore the occurrence of water and oxygen stress of vegetation. This article focuses on vegetation and groundwater dynamics along a hill slope by developing and evaluating a fully coupled hydrological-vegetation model for a temperate forest ecosystem. The vegetation model is described in part 1 of this series of two papers. To simulate the hydrology an extended version of the saturated-unsaturated hydrological model STARWARS has been used. The coupled model is used to investigate both the short and long-term dynamics for a system of two species. Both compete for light and water where one is adapted to wet conditions and the other to dry conditions. The daily dynamics show that the influence of groundwater is particularly strong in spring when waterlogging occurs due to decreased evapotranspiration in winter. Long simulation runs of 1000 years were performed to study the equilibrium state for the two species. Comparison of simulation results with observations of groundwater depth and vegetation types along a dry-wet gradient in a natural forest shows that a reductionist approach is able to capture these patterns well. Sensitivity analysis shows that the border between wet- and dry adapted species moves upslope with increased rainfall, decreased slope angle and decreased aquifer thickness. These results are similar to previous findings which were based on global maximization of ecosystem evaporation or minimizing ecosystem stress. Comparison of runs with a

fixed and a dynamic groundwater table shows that a dynamic groundwater table facilitates a wider transition zone between vegetation types along the hill slope. In this transition the biomass of vegetation is higher in the case of a dynamic groundwater than in case of a static groundwater table. This underlines the importance of incorporating spatial groundwater dynamics in models of groundwater influenced ecosystems.

4.1 Introduction

Introducing groundwater dynamics in vegetation growth models is important for several reasons. Vegetation growth models that only include soil moisture and omit the presence of a groundwater table miss out on the effect of capillary rise and reduced percolation on soil hydrology (Daly et al., 2009; Laio et al., 2009). Percolation is often only included as sink occurring when a given soil moisture content is exceeded, regardless of the depth of the watertable, while a proximate watertable can dramatically reduce this flux, causing higher moisture contents in the rootzone (e.g. Running & Gower, 1991; Friend et al., 1997; Sitch et al., 2003). This effect is most pronounced in winter, when evaporation and transpiration are minimal. In most vegetation models capillary rise is not included, while this flux can contribute to higher moisture contents, and reduced vegetation water stress. This effect is most pronounced at intermediate soil moisture contents when matric potentials become more negative and the soil water conductivity is still significant.

When lateral groundwater flow is considered, the effect on the vegetation can even be more pronounced. Flow of groundwater from high potential to low potential causes a groundwater gradient along hill slopes. Relative to the soil surface this causes deep groundwater levels upslope and shallow groundwater levels downslope. This in turn results in a soil moisture gradient in the rootzone from low soil moisture contents upslope and high soil moisture contents down slope leading to zonation of vegetation types. Also field research shows that such a gradient in moisture content leads to zonation of vegetation types (e.g. Figure 4.1 and Falinski & Falinska (1986)). The effect of lateral groundwater flow is also apparent when vegetation upslope is disturbed by for example forest fire. Changes in upslope groundwater recharge thus influence downslope moisture conditions and therefore vegetation growth.

In hydrological models on the other hand vegetation dynamics are limited. Evapotranspiration is calculated based on atmospheric conditions and most often a fixed leaf area index (*LAI*). In more advanced models this evapotranspiration is considered to be potential evapotranspiration and a reduction function is used to account for low soil moisture conditions. Sometimes phenology is included in these models to account for seasonality for deciduous trees, but vegetation development over time is usually ignored (e.g. Wigmosta et al., 1995; Abbott et al., 1986a,b).

Our aim is to show the effect of incorporating spatio-temporal groundwater dynamics on simulated vegetation growth in eco-hydrological modeling. We do so by simulating evapotranspiration and vegetation growth in combination with groundwater and soil

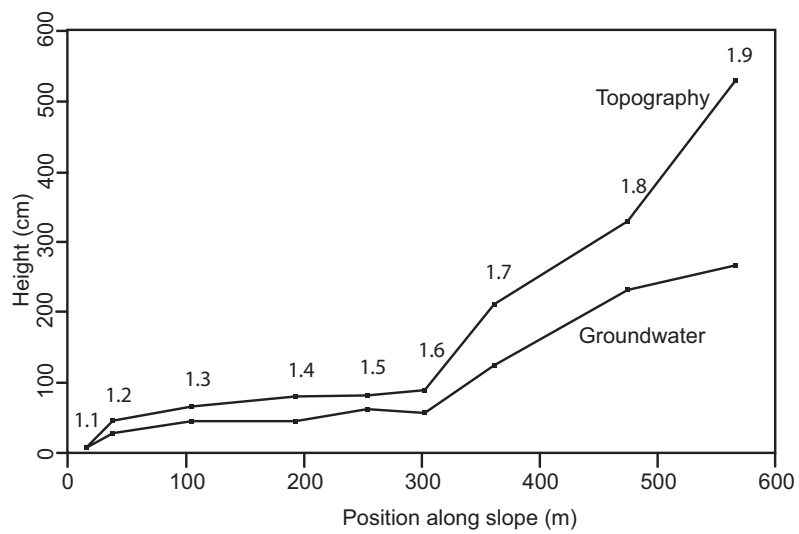
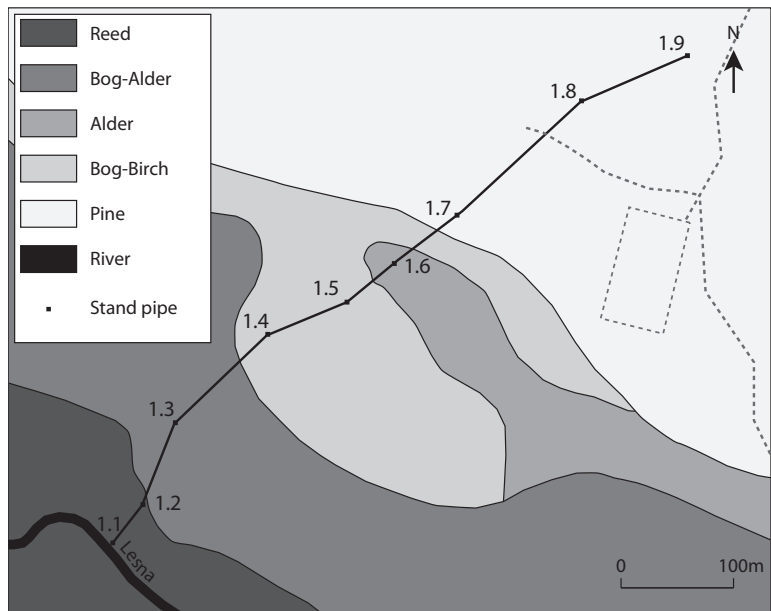


Figure 4.1 An example of the influence of a groundwater gradient (4 week average in July-August, 2004) on vegetation composition in old growth forest in Białowieża, East Poland. (Bosch, 2006).

water dynamics using a bio-physical vegetation model.

In this paper we describe the coupling of the dynamic bio-physical vegetation model and saturated-unsaturated groundwater model. The paper builds on the vegetation competition model described in the companion paper. The fully coupled vegetation-hydrological model is used in long-term simulation runs (1000 years) with simulated meteorological data as input. Using this model in a sensitivity analysis we evaluate the influence of different precipitation climatologies, soil textures and slope angles on long-term vegetation dynamics along a slope. Results of the sensitivity analysis are compared to a previous sensitivity analysis (Brolsma & Bierkens, 2007) where vegetation distribution along the slope was related to maximizing long-term whole ecosystem evaporation or minimizing whole ecosystem stress. Finally we evaluate the influence of a spatio-temporal dynamic groundwater level relative to a static groundwater level as was simulated in the companion paper (Brolsma et al., 2010a).

4.2 Methods

To study vegetation and groundwater dynamics as a combined system we coupled a spatio-temporal dynamic vegetation growth model, as described in the companion paper (Brolsma et al., 2010a), to a saturated-unsaturated hydrological model. The dynamic vegetation model has been extended to 2-dimensions to study spatial interactions that result from lateral groundwater flow. In this article only the main characteristics of and additions to the vegetation model will be explained.

4.2.1 Atmospheric forcing

Atmospheric forcing is produced by a stochastic weather generator, which enables us to generate meteorological conditions for a period of 1000 years. This generator is based on Richardson (1981) and is extended to include for the effect of cloud cover. The statistical parameters are based on Dutch meteorological conditions. These correspond to an annual precipitation of 705 mm and mean summer and winter temperatures of respectively 17.7 °C and 3.4 °C. The generated weather variables are precipitation, P [mm/d], minimum and maximum atmospheric temperature, T_{min} and T_{max} [°C], radiation, Rad [W], vapor pressure, e_a [Pa], and fraction of cloud cover n/N [-]. Cloud cover was included to account for its effect on short- and longwave radiation (see Brolsma et al., 2010a).

4.2.2 Vegetation model

The vegetation model that is described in Brolsma et al. (2010a) is extended to two dimensions resulting in a field based model with a regular grid of square cells of 100 m². This grid corresponds to the size of a mature tree. The hydrological model uses the same grid. Vegetation species competes locally for light, which is determined by tree height, H [m] and leaf area index, LAI [-]. Also competition for water is local

and is determined by root water uptake parameters and root area index, RAI [-]. Spatial interaction between cells is limited to groundwater flow.

The model is based on plant functional types. The differences between the plant functional types are based on their response to soil moisture content. All other vegetation parameters are the same for both species. A low soil moisture content can cause a large negative leaf water potential, ψ_l [Pa], which results in a low plant water conductance. At high soil moisture contents oxygen stress occurs, which also results in reduced root water uptake and reduced leaf water potential. The parameters that control the reaction of plant conductance and assimilation rate to leaf water potential as well as the parameters that control the root water uptake function as a result of high soil moisture contents differ between species. In this case two plant functional types were studied. The first type is better adapted to wet conditions, in which it experiences less stress than the second type, whereas the second type is better adapted to dry conditions. The parameters that differ between the two species are listed in Table 4.1. For simplicity we assume a uniform root distribution within the rootzone.

All vegetation types are assumed to be always present at a primordial biomass in all cells. Regrowth of vegetation after death of one type starts from this primordial biomass. This concept is based on the assumption that a seedbank is always present. The process of dispersal of vegetation is therefore not included. This means that when one vegetation type dies, the other vegetation type has a small advantage because it might already have a slightly higher biomass and LAI . The biomass and LAI of the other species and their suitability to the local soil moisture condition will determine if the species that has died will again outcompete the other.

Carbon assimilation and evapotranspiration are calculated based on the following environmental conditions: soil texture and its corresponding soil physical parameters, soil moisture content θ [-], minimum and maximum atmospheric temperature, T_{min} and T_{max} [°C], radiation, Rad [W], fraction of cloud cover n/N [-], leaf area index, LAI [-], and day length, δ [-]. Since all environmental variables are generated on a daily basis, we assume that precipitation intensity and cloud cover are constant during the day.

4.2.3 Hydrological model

In order to simulate interaction between the hydrological and vegetation dynamics along the slope over an extended period, e.g., 1000 years, a model is required that is capable to adequately capture the spatial and temporal changes in soil moisture and water levels and is at the same time limited in runtime. Such a model was employed here by modifying the STARWARS model (van Beek, 2002). This model was originally developed to simulate the influence of slope hydrology on landslide activity over multiple years. Similar to the original model, the soil profile was discretized into three layers of variable depth to capture several distinct soil layers (Figure 4.2). These layers overlie a semi-impervious lithic contact above which an unconfined perched groundwater level may develop. The unsaturated flow toward this saturated zone was considered to be vertical only as any unsaturated lateral flow will be small;

Table 4.1 Parameters of the plant functional type adapted to wet and the plant functional type adapted to dry conditions.

Parameter	Description	Wet species	Dry species
ψ_0	leaf water potential below which g_s becomes 0 [Pa]	-0.45e+06	-4.5e+06
ψ_1	leaf water potential below which g_s begins to decline [Pa]	-0.005e+06	-0.05e+06
$\psi_{a,0}$	leaf water potential below which assimilation becomes 0 [Pa]	-0.45e+06	-4.5e+06
$\psi_{a,1}$	leaf water potential below which assimilation begins to decline [Pa]	-0.05e+06	-0.5e+06
Ox_0	soil moisture content above which root water uptake begins to decline due to oxygen stress [-]	$\theta_{sat}-0.03$	$\theta_{sat}-0.10$
Ox_1	soil moisture content above which root water uptake becomes 0 due to oxygen stress [-]	$\theta_{sat}-0.01$	$\theta_{sat}-0.05$

Philip (1991) concluded on the basis of a 2-D analytical solution of the Richards Equation that, for a planar slope, the unsaturated lateral flux is negligible for all inclinations below 30°. Even if the lateral unsaturated flux is substantial, the large vertical gradients direct it effectively toward the saturated zone (Jackson, 1992; van Asch et al., 2001).

Contrary to the original model, however, which ignored the matric potential in the unsaturated flow, the vertical unsaturated flow in the present model considers both the elevation and the matric potential. This modification was effectuated to evaluate the importance of capillary rise on the maintenance of vegetation along part of the slope. Also, the current model replaces the original parametrization of the soil water retention curve of Farrell & Larson (1972) with that of van Genuchten (1980).

As shown in Figure 4.2, the vertical discretization of the soil profile includes layers (T_1 to T_3) that are constant in time. Within this soil profile, the height of the water table (WL) can vary depending on the vertical flow from the unsaturated zone, saturated lateral flow and any vertical losses across the semi-impervious bedrock. With fluctuations in the groundwater level, the location of the nodes within the three soil layers will vary (Z_1 to Z_3). If the water level is below or above a particular layer, the node is located at the center of a that layer (Z_1 and Z_3 in Layer T_1 and T_3 in Figure 4.2). If the groundwater level encroaches on the thickness of the unsaturated zone (Figure 4.2), the location is shifted to half the distance between the top of the layer and the top of the water level (Z_2 in layer T_2 in Figure 4.2). The water level itself is located at Z_4 . If the part of the layer is unsaturated, the matric suction, ψ_{i+1} [m], is calculated by means of the Van Genuchten Equation using the mean relative degree of saturation over the unsaturated layer, θ_{E_i} [-]. The total gradient is then calculated as:

$$Grad_i = \frac{\psi_{i+1} - \psi_i}{\Delta Z_i} - 1, \quad (4.1)$$

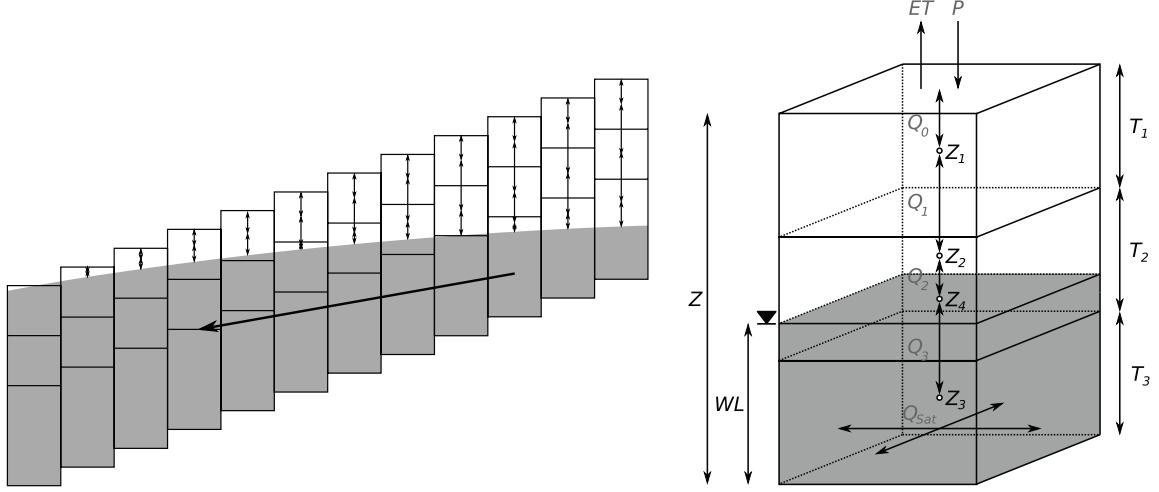


Figure 4.2 Cross section and block diagram of hydrological model. The cross section shows a schematic representation of the unsaturated fluxes (small arrows) and the groundwater flux (large arrow). For all plots of the results of the simulation runs the top of the slope is on the right side of the plots. The block diagram shows the fluxes and calculation nodes in more detail. ET evapotranspiration, P precipitation; T thickness of layer; Z height of calculation node; Q flux; Z thickness of profile; WL water level; Q_{Sat} groundwater flux; subscripts 1-3 denote layer number, 4 denotes the calculation node on top of the groundwater.

where ΔZ_i is the distance between the nodes Z_i and Z_{i+1} or Z_4 and Z_i , if the groundwater table reaches into layer T_i . If so, ψ_{i+1} defaults to zero. The gradient is consequently negative whenever flow is down and positive when upward. If a layer is completely saturated, the corresponding gradient is set to zero thus preventing any unsaturated flow.

The amount of water transferred vertically between layers, Q_i [m], is given by:

$$Q_i = k_{\theta_{E,i}} Grad_i \Delta t, \quad (4.2)$$

where $k_{\theta_{E,i}}$ is the hydraulic conductivity. This estimated hydraulic conductivity is the geometric mean of T_i and the maximum of the hydraulic conductivity of layer T_i and T_{i+1} if the groundwater does not reach into layer T_i . Otherwise, it is the geometric mean of the saturated hydraulic conductivity and the unsaturated hydraulic conductivity for layer T_i .

For each of the unsaturated layers, the water balance is given by:

$$StorMat_{i,t} = StorMat_{i,t-1} + Q_i - Q_{i-1} - TransMat_i, \quad (4.3)$$

where $StorMat$ is the unsaturated matric storage in layer T_i at the present time step, t , and at the previous time step, $t - 1$, updated by the vertical unsaturated fluxes Q_i and Q_{i-1} and the actual transpiration loss, $TransMat_i$, as returned from the vegetation model (all variables in [m] water slice). The corresponding relative degree of saturation, $\theta_{E,i}$ [-], is obtained by dividing the unsaturated storage by the total available pore space in the unsaturated zone.

Special conditions occur at the top of the soil profile and at the top of the groundwater level. First, for the top layer, the transpiration loss is increased by the actual soil evaporation and the influx, Q_0 , is the total net precipitation (direct and indirect throughfall). Second, the outflow from the unsaturated layer overlying the groundwater table is passed on to the saturated zone, Q_{Cap} , which is the capillary rise when directed upward.

Parallel to the changes in the unsaturated zone, the flow in the saturated zone is calculated by evaluating the gradient in both the x- and y-directions of the grid. The total transmissivity over the saturated zone is the weighed saturated hydraulic conductivity per layer, to which end the water level is broken up into the thickness per saturated layer, H_1 to H_3 :

$$Trans = \sum_{i=1}^3 H_i k_{Sat,i}. \quad (4.4)$$

Saturated lateral flow, Q_{Sat} [m^3], along the slope is then governed by the gradient in the $x-$ and $x+$ and $y-$ and $y+$ directions of the grid, which is a ratio of the piezometric head over the grid distance:

$$Q_{Sat} = 1/2 \left(\begin{array}{l} Trans_{x+} \cdot (Z_{WL,x+} - Z_{WL}) - Trans_{x-} \cdot (Z_{WL} - Z_{WL,x-}) \\ + Trans_{y+} \cdot (Z_{WL,y+} - Z_{WL}) - Trans_{y-} \cdot (Z_{WL} - Z_{WL,y-}) \end{array} \right) \Delta t \quad (4.5)$$

where $x+$, $x-$, $y+$ and $y-$ are the locations upstream and downstream along the orthogonal flow directions in the x and y directions, $Trans$ is the corresponding transmissivity and Z_{WL} is the piezometric elevation of the water level relative to a common datum Z_0 .

This leads to a change in saturated storage, $StorSat$ [m], for each grid point. Lateral boundary conditions may vary but in this case no flow boundaries have been imposed along the boundaries of the grid, thus preventing any loss from the saturated zone along the slope other than by exfiltration. The coupling of the saturated and unsaturated flow occurs by first considering the vertical fluxes for the unsaturated zone. If an unsaturated layer experiences a gain and becomes saturated, the saturated storage is updated accordingly and the unsaturated zone becomes absent. Alternatively, any drainage from a fully saturated layer leads to a new unsaturated zone for which the depth and relative degree of saturation comply with the equilibrium profile, thus limiting the risk of dynamic shock in the next time step.

In all calculations of the new storage, care is taken that the fluxes cannot exceed the available storage. Similarly, any upward vertical flux from the unsaturated layer overlying the water table is automatically sustained by extra, upward flow from the saturated zone. Thus, numerical instability can be prevented when the gradient from a very moist but shallow unsaturated zone to the overlying layer is large and the resulting flux would exceed the available storage. The changes in the water balance for the saturated zone includes the vertical exchange between the saturated and unsaturated layer, Q_{Cap} , the lateral saturated flow, Q_{Sat} , and any loss across the lithic contact, Q_4 , which was kept at zero in this case. Each time step the resulting water

Table 4.2 Soil physical parameters for different soil textures used in different simulations (Carsel, 1988).

Soil texture	θ_{sat} [-]	θ_r [-]	K_s [m d ⁻¹]	α [m ⁻¹]	n [-]
loamy sand	0.41	0.057	3.50	12.4	2.28
sandy loam	0.41	0.065	1.06	7.5	1.89
sandy clay loam	0.39	0.100	0.134	5.9	1.48
silty clay loam	0.43	0.089	0.0138	10.0	1.23

level is then reconstituted from the bottom upwards on the basis of the available free pore space. Any saturated storage in excess of the storage capacity of the soil is passed on to the surface as exfiltration and lost.

Through the coupling of vertical unsaturated flow to the saturated zone, the model is more economic than a rigorous 3-D solution of the Richard Equation, with calculation time step sizes in the order of several hours allowing for a simulation period of 1000 years. In this study a time step of 0.1 day (2.4 h) was used in the hydrological model. The coupling between the hydrological model and the vegetation model occurs at the daily time step, with the moisture content and water levels at the end of each day being passed to the calculations for the next day by the vegetation model.

A uniform soil texture is assumed, but the influence of different soil textures is studied with different runs. Soil physical properties are based on Carsel (1988) and are listed in table 4.2.

4.2.4 Experiments

In the simulation experiments presented in the remainder of the paper we first focus on the yearly dynamics, i.e. the dynamics on a daily basis over the period of one year. We especially analyze on the one dimensional (local) dynamics of groundwater, soil water and vegetation and the influence of soil texture. On this short timescale vegetation growth is ignored, but phenology is included in the model. A period of 400 years with stochastically generated weather conditions is used for spin-up of the model, such that vegetation, soil water and groundwater are in an approximate equilibrium. Also the environmental conditions of the studied year were generated stochastically. Based on yearly sums and averages of environmental conditions the year was checked to be not an extreme year for any of the conditions.

Secondly we focus on the long-term dynamics. In this case we simulate 1000 year periods of which the first 400 years are used for spin-up. On this timescale, vegetation growth and mortality are included. These long simulation runs are used to study the influence of soil texture, slope angle, aquifer thickness and precipitation on vegetation and soil and groundwater dynamics. Finally a comparison is made between the system having a dynamic groundwater level and one having a fixed groundwater level.

The settings for the base line scenario are a grid of 50 * 100 square cells of 100 m²

each, which results in a slope length of 500 m and a width of 1000 m. The baseline run has a slope angle of 5 % and the soil texture is sandy loam. The rootzone is defined as the top 60 cm of the soil column, where a homogeneous root distribution is assumed.

Here we follow a mesoscopic deterministic approach, optimizing evaporation and carbon uptake for each location at a sub-daily time scale. In Broolsma & Bierkens (2007) we investigated the effect of slope and rainfall on the distribution of wet- and dry-adapted species. The distribution was modeled from a macroscopic whole system perspective by maximizing either long-term evaporation or minimizing long-term stress. It is interesting to see whether these approaches lead to similar responses of vegetation to changes in slope or rainfall.

4.3 Results and discussion

4.3.1 Seasonal dynamics

Figure 4.3 shows the short time dynamics for climax vegetation at four locations along the slope: near the base, in the transition zone where both species occur with approximately equal biomass, just above this transition zone and at the top of the slope. For this run the settings of the baseline scenario were used. Where groundwater is near the surface, the rootzone soil moisture content remains relatively high throughout the growing season ($\theta > 0.3$). Transpiration is only slightly reduced as a result of a lower matric potential of the soil, but no reduction as a consequence of cavitation in the plant occurs. Therefore interdaily differences are mainly caused by changes in atmospheric circumstances. In this zone the wet adapted species prevails.

When groundwater becomes deeper, but still rises into the rootzone in winter, the rootzone soil moisture content declines and the difference between soil moisture content in winter and summer increases (θ 0.38 in winter and 0.16 in summer). Transpiration and carbon assimilation of the drought adapted species increase, but the wet adapted species still prevails.

Moving even further upslope groundwater becomes deeper and is below the rootzone all year, the rootzone soil moisture content drops further during the growing season and the wet adapted species is outcompeted by the drought adapted species. The drought adapted species can still transpire up till 7 mm/d, but at the end of summer when groundwater is deepest and the soil moisture content becomes low (θ 0.08) transpiration and therefore carbon assimilation become negligible. If groundwater is at a depth of almost 8 m and the influence of groundwater is negligible, the moment that transpiration and carbon assimilation are severely reduced occurs earlier in the season. The difference in soil moisture content and resulting transpiration and carbon assimilation for the situation where groundwater remains just below the rootzone during the year and the situation with deep groundwater is small, although most apparent in spring.

Comparing the dynamics of groundwater and soil moisture in the rootzone, it can be

seen that the deeper the groundwater is the smoother the variations are. The noisy behavior for the shallowest groundwater is caused by the fact that the soil is close to saturation. The storage capacity therefore is very small and small changes of recharge cause large variations in the water table. This effect disappears as the groundwater becomes deeper. Also striking is that the rootzone soil moisture content is tightly coupled to the groundwater on the lowest part of the slope, while the lowest figures show that root zone soil moisture is decoupled, such that its variability increases again because climatic variations (P and ET) are not buffered by capillary rise. The other effect that causes deep groundwater variation to be smoother with depth is that deep groundwater is related to upslope areas where the drainage distance of groundwater to the stream is largest and a slower groundwater system thus exists.

4.3.2 Long-term dynamics

Figure 4.4 shows the temporal variability during a 300 year period of the average whole system biomass, evapotranspiration, carbon assimilation, soil moisture content and groundwater depth. As to be expected the system average groundwater level and soil moisture content increase when the soil water conductivity decreases and water retention capacity increases. The fluctuation for both intermediate soils are larger than for loamy sand and silty clay loam. The evapotranspiration and biomass on the loamy sand is approximately the same for both the wet and the dry adapted species, but the carbon assimilation rate of the dry adapted species is much lower. The wet adapted species occupies only a small part of the slope, but since it is the wettest part ET is relatively high, and since the wet adapted species is well adapted to this part, it reaches a high biomass. Therefore the slope averages are about the same for both species. For sandy loam the soil is wetter, but the biomass of the drought adapted species increases. This is a result of the higher soil water retention capacity that, especially upslope where the dry species prevails, causes the dry species to transpire and assimilate for a longer period in the growing season, i.e. it is the dry adapted species that benefits most from this situation. For the sandy and the silty clay loam the soil becomes even wetter and the biomass of the wet species does increase. This is mainly caused by an expansion of the zone where the wet species dominates, not so much as a result of an increase in the maximum biomass per cell. In extremely dry years carbon assimilation can become smaller than respiration causing vegetation over larger areas to die. After such a dry period, ET and A_n swiftly recover and biomass starts to increase again. This results in fluctuations of the systems biomass, ET and A_n . As a result groundwater level and soil moisture content also fluctuate, where a periods of lower biomass causes higher soil moisture contents and groundwater levels due to increasing groundwater recharge. It is interesting that the dry adapted species is most susceptible to variation in yearly rainfall amount. During dry periods it is the dry species that dies over large areas, while the wet adapted species hardly responds or even increases. The increase in biomass, ET and A_n of the wet species has two reasons: the first direct and most important reason is the increased light availability of the wet adapted species (in a somewhat wetter soil due to less interception evaporation) which temporally results in increased biomass of the wet-adapted species. This occurs mainly upslope. An indirect reason is that the

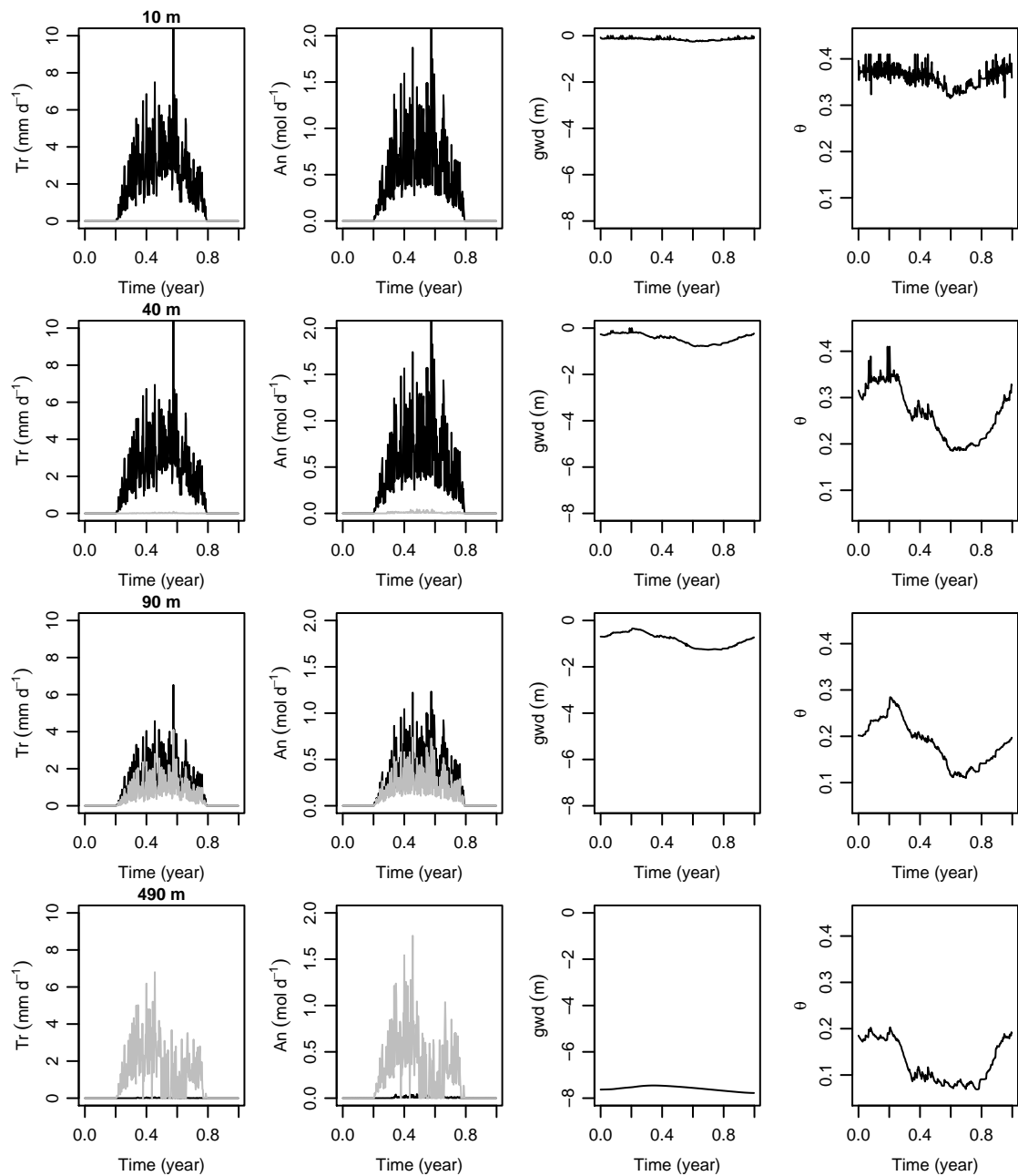


Figure 4.3 Evapotranspiration, carbon assimilation, groundwater depth and rootzone soil moisture content of vegetation near climax situation at four locations at a slope angle of 5%, an aquifer thickness of 8 meter and sandy loam as soil texture. In the evapotranspiration and carbon assimilation plots wet adapted species, black; drought adapted species, gray.

die-back of dry adapted species causes increased groundwater recharge, temporally increasing the zone of shallow water tables downslope and thereby the biomass of the wet-adapted species. This upslope-downslope connection can be observed better with the dynamic content connected to this paper. It shows that a dynamic groundwater table results in true upslope-downslope connections in ecosystem dynamics.

Figure 4.5 shows the 600 year average of groundwater level, soil moisture content, biomass and evapotranspiration of the baseline scenario. The slope results in a groundwater and soil moisture gradient along the slope, where the shallowest groundwater levels and highest moisture contents can be found at the lowest part of the slope. This results in a positive feedback where a high moisture content causes high evapotranspiration and carbon assimilation rates, which causes a larger biomass and *LAI* and therefore even higher carbon assimilation and evapotranspiration rates. The rootzone soil moisture gradient also causes the two vegetation types to develop in two slightly overlapping zones. The wet adapted species develops at the moist base of the slope and the dry adapted species develops upslope, which corresponds to field observations (e.g. Falinski & Falinska (1986); Bosch (2006)).

Strong temporal fluctuations in groundwater and soil moisture content occur which vary along the slope. These fluctuations are caused by the seasonality in the atmospheric forcing and the resulting phenology. The difference between yearly minimum and maximum soil moisture content is small where groundwater is near the surface, i.e. on the lower part of the slope. For deeper groundwater levels the difference between average minimum and maximum soil moisture is larger. The difference is largest in the zone where the rootzone is influenced by capillary rise. Thus moving further upslope the average difference between minimum and maximum soil moisture content becomes smaller again, depending on the soil texture. For loamy sand where the water retention is minimal this difference directly becomes constant whereas for sandy loam and sandy clay loam the difference decrease slowly.

4.3.3 Sensitivity analysis

The hydrological functioning of hill slopes is strongly dependent on slope and subsoil properties, i.e. texture and aquifer thickness as well as climate. It is to be expected that these factors influence the interactions between vegetation growth, species composition and hydrology as well. Therefore we also investigated the effect of different hill slope and hydro-geological characteristics by repeating runs with different slope angle and aquifer thicknesses and rainfall regimes.

Slope angle and aquifer thickness

The slope angle has a major influence on the groundwater gradient (Fig. 4.6 and Tab. 4.3). This is clearly the case for coarse soil textures. This effect results in much lower biomasses for steep slopes in combination with coarse soils and moderately lower biomasses for fine soil textures. The response of the biomass to increased slope angle is thus very non-linear and strongly depends on soil texture.

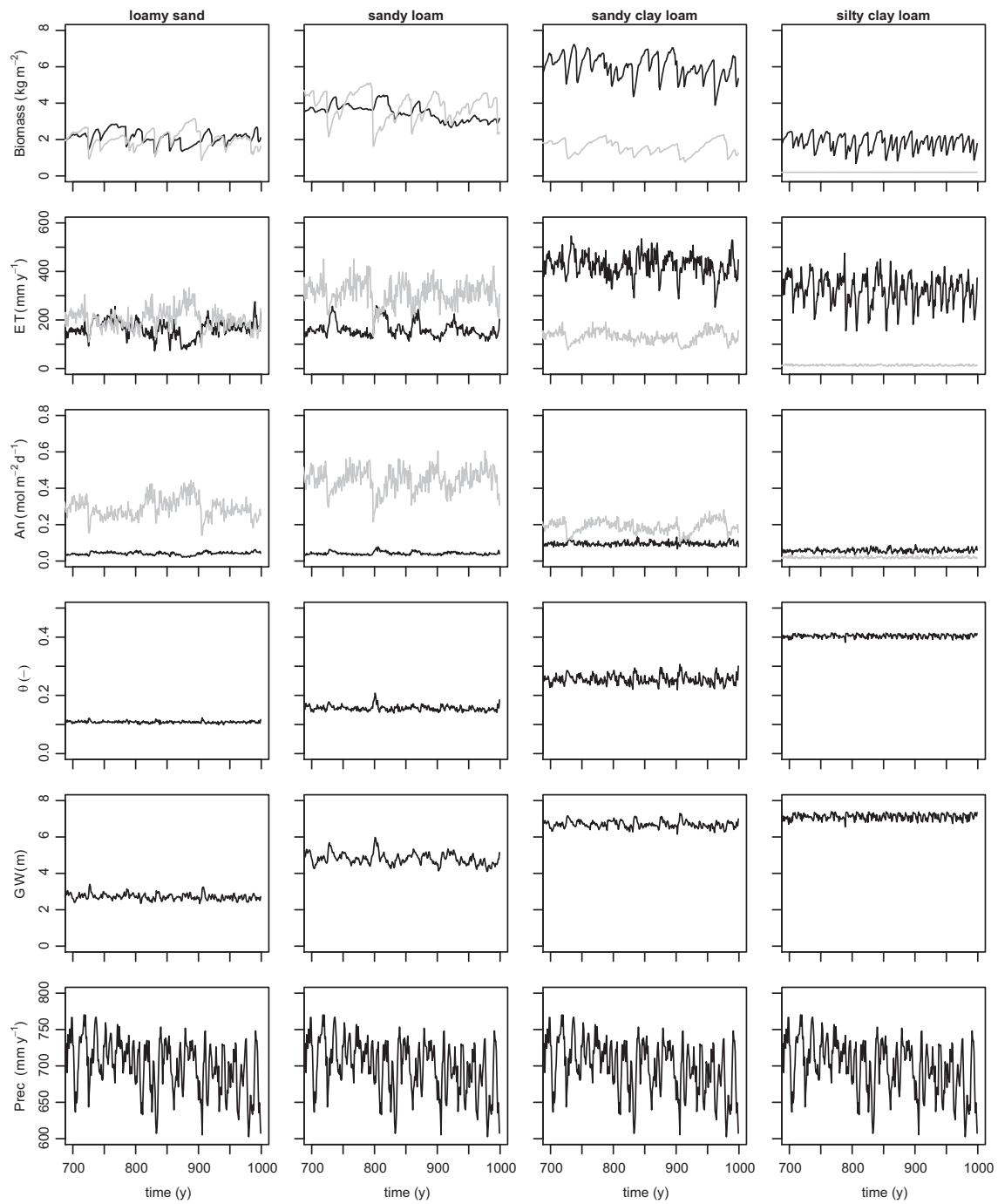


Figure 4.4 Temporal dynamics during a 300 y period of system average variables: Biomass [kg m^{-2}]; evapotranspiration, ET [mm y^{-1}]; carbon assimilation, An [$\text{mol m}^{-2} \text{d}^{-1}$]; soil moisture content θ [-]; groundwater level above impermeable layer, GW [m] and precipitation (5 year running mean), Prec [mm y^{-1}]. Gray line, wet adapted species; black line dry adapted species.

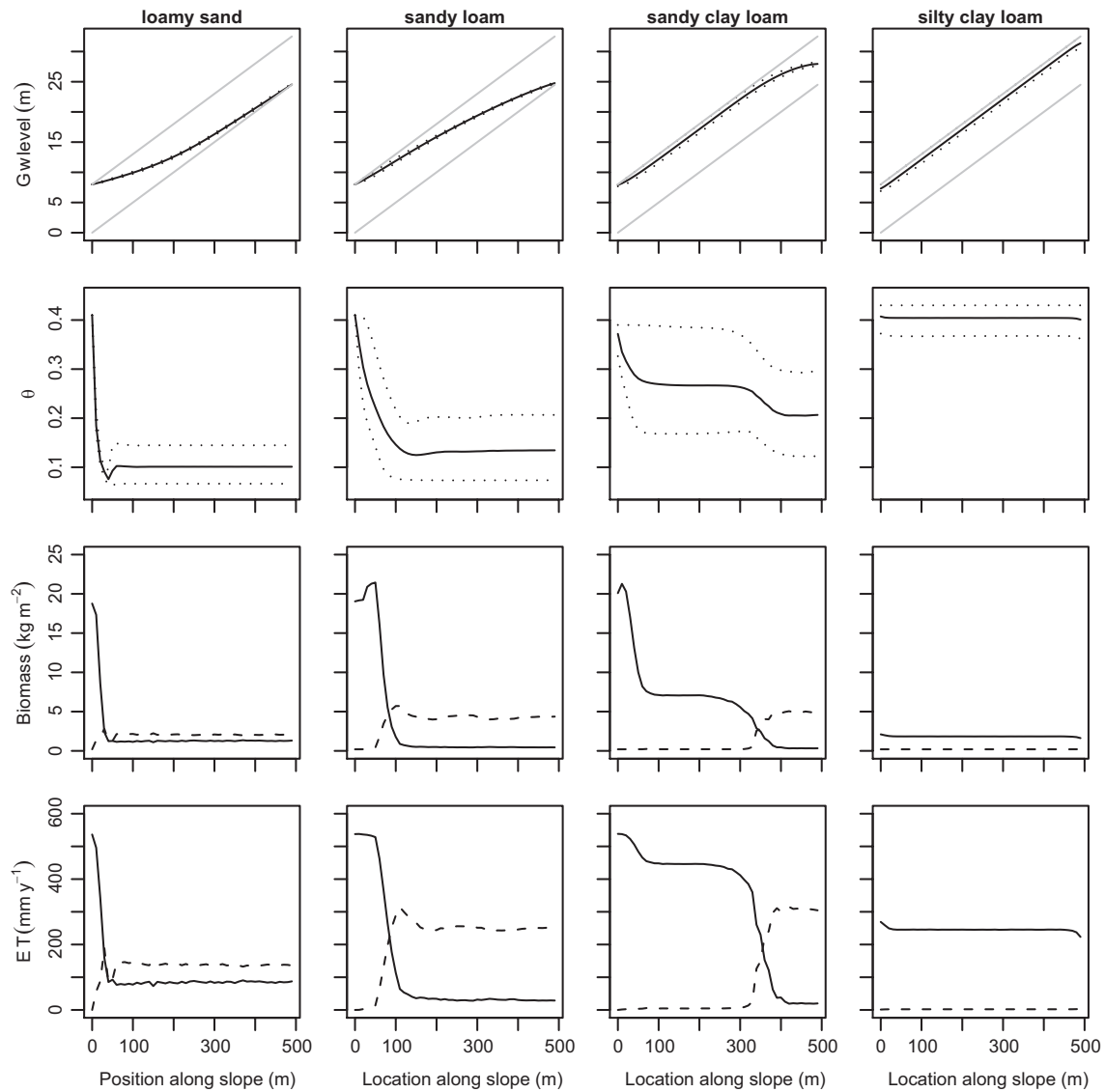


Figure 4.5 Average groundwater level, rootzone soil moisture content, biomass and evapotranspiration along a hill slope. Averages are based on a 600 y period and a slope width of 100 10 m cells. In the groundwater level plot the upper and lower boundary of the aquifer, gray lines. In the groundwater and soil moisture content plot yearly mean values; solid black lines yearly minimum and maximum values, dotted black lines. In the *Biomass* and the *ET* plot the wet adapted vegetation, solid lines; drought adapted vegetation, dashed lines.

Table 4.3 Results of sensitivity analysis for four different soil textures. Effects of precipitation magnitude (P_{mag}), precipitation frequency (P_{freq}), aquifer thickness ($AqTh$)[m] and slope angle ($Slope$)[%] on the following variables are shown: Biomass wet vegetation (B_{wet}), dry vegetation (B_{dry}), total vegetation (B_{tot}), evaporation wet vegetation (E_{wet}), evaporation dry vegetation (E_{dry}), evaporation total vegetation (E_{tot}), transpiration wet vegetation (Tr_{wet}), transpiration dry vegetation (Tr_{dry}), transpiration total vegetation (Tr_{tot}), and net precipitation ($P - ET$). Biomass is given in kg m^{-2} and fluxes in mm y^{-1} .

Rainfall magnitude												
Texture	$\Delta \%$	P	B_{wet}	B_{dry}	B_{tot}	E_{wet}	E_{dry}	E_{tot}	Tr_{wet}	Tr_{dry}	Tr_{tot}	$P - ET$
loamy sand	-10	631.7	2.3	1.4	3.7	63.8	53.5	117.3	129.5	96.1	225.6	288.7
	0	701.8	2.1	2.0	4.1	55.3	70.7	126.0	108.2	132.2	240.4	335.4
	+10	772.0	2.0	2.4	4.4	52.0	81.3	133.2	100.3	155.3	255.5	383.3
sandy loam	-10	631.7	2.8	3.5	6.3	37.2	91.4	128.6	95.9	207.9	303.8	199.3
	+0	701.8	3.5	3.8	7.4	43.6	93.9	137.5	118.0	217.2	335.2	229.2
	+10	772.0	4.7	3.9	8.5	53.7	91.4	145.1	154.8	212.2	367.1	259.9
sandy clay loam	-10	631.7	4.9	1.7	6.7	81.7	46.5	128.2	283.7	108.4	392.1	111.3
	+0	701.8	6.0	1.6	7.6	95.3	41.1	136.5	328.6	92.1	420.8	144.6
	+10	772.0	7.2	1.5	8.7	107.1	36.7	143.8	365.4	78.4	443.8	184.5
silty clay loam	-10	631.7	1.7	0.2	1.9	70.6	11.1	81.6	233.6	2.6	236.2	313.8
	+0	701.8	1.8	0.2	2.0	75.3	11.0	86.4	245.7	2.1	247.8	367.7
	+10	772.0	2.0	0.2	2.2	80.4	11.0	91.4	259.0	1.7	260.7	419.9
Rainfall frequency												
Texture	$\Delta \%$	P	B_{wet}	B_{dry}	B_{tot}	E_{wet}	E_{dry}	E_{tot}	Tr_{wet}	Tr_{dry}	Tr_{tot}	$P - ET$
loamy sand	-10	631.5	2.2	1.6	3.7	55.2	54.3	109.6	120.1	108.8	228.9	293.1
	+0	701.8	2.1	2.0	4.1	55.3	70.7	126.0	108.2	132.2	240.4	335.4
	+10	769.0	2.0	2.5	4.5	57.6	89.2	146.7	99.5	154.9	254.4	367.8
sandy loam	-10	631.5	2.9	3.5	6.4	35.7	84.1	119.8	101.0	209.4	310.4	201.4
	+0	701.8	3.5	3.8	7.4	43.6	93.9	137.5	118.0	217.2	335.2	229.2
	+10	769.0	4.4	3.9	8.3	57.4	98.8	156.2	149.4	211.4	360.8	252.0
sandy clay loam	-10	631.5	5.0	1.7	6.7	77.7	41.1	118.7	294.6	102.3	396.9	115.9
	+0	701.8	6.0	1.6	7.6	95.3	41.1	136.5	328.6	92.1	420.8	144.6
	+10	769.0	7.2	1.5	8.7	114.2	40.7	154.8	359.5	80.5	440.0	174.2
silty clay loam	-10	631.5	1.7	0.2	1.9	65.6	10.3	75.8	236.0	2.8	238.8	316.9
	+0	701.8	1.8	0.2	2.0	75.3	11.0	86.4	245.7	2.1	247.8	367.7
	+10	769.0	2.1	0.2	2.3	89.3	11.8	101.1	264.2	1.6	265.8	402.0
Aquifer thickness												
Texture	$\Delta \%$	$AqTh$	B_{wet}	B_{dry}	B_{tot}	E_{wet}	E_{dry}	E_{tot}	Tr_{wet}	Tr_{dry}	Tr_{tot}	$P - ET$
loamy sand	-50	4.0	2.8	1.6	4.4	64.5	59.9	124.4	139.0	110.1	249.1	328.4
	+0	8.0	2.1	2.0	4.1	55.3	70.7	126.0	108.2	132.2	240.4	335.4
	+50	12.0	2.0	2.0	4.0	55.0	70.6	125.6	106.0	131.4	237.4	338.8
sandy loam	-50	4.0	9.1	2.3	11.4	87.9	55.0	142.9	300.8	122.2	423.0	136.0
	+0	8.0	3.5	3.8	7.4	43.6	93.9	137.5	118.0	217.2	335.2	229.2
	+50	12.0	2.3	4.0	6.4	34.2	101.6	135.8	79.7	230.4	310.2	255.8
sandy clay loam	-50	4.0	6.7	0.7	7.5	114.4	22.7	137.1	400.7	37.7	438.4	126.3
	+0	8.0	6.0	1.6	7.6	95.3	41.1	136.5	328.6	92.1	420.8	144.6
	+50	12.0	5.2	2.4	7.6	77.1	58.5	135.6	258.9	142.6	401.5	164.8
silty clay loam	-50	4.0	1.8	0.2	2.0	74.7	11.1	85.8	242.8	2.2	245.0	371.1
	+0	8.0	1.8	0.2	2.0	75.3	11.0	86.4	245.7	2.1	247.8	367.7
	+50	12.0	1.9	0.2	2.1	75.6	11.0	86.6	247.1	2.1	249.1	366.1
Slope angle												
Texture	$\Delta \%$	$Slope$	B_{wet}	B_{dry}	B_{tot}	E_{wet}	E_{dry}	E_{tot}	Tr_{wet}	Tr_{dry}	Tr_{tot}	$P - ET$
loamy sand	-50	2.5	3.5	1.8	5.3	65.3	63.3	128.5	150.9	118.7	269.5	303.8
	+0	5.0	2.1	2.0	4.1	55.3	70.7	126.0	108.2	132.2	240.4	335.4
	+50	7.5	1.9	2.0	3.9	53.7	71.5	125.2	100.7	133.2	233.9	342.7
sandy loam	-50	2.5	8.9	2.6	11.5	82.6	60.6	143.2	281.1	139.1	420.2	138.4
	+0	5.0	3.5	3.8	7.4	43.6	93.9	137.5	118.0	217.2	335.2	229.2
	+50	7.5	1.8	4.0	5.9	31.8	103.2	135.0	68.8	233.2	302.0	264.8
sandy clay loam	-50	2.5	6.9	0.7	7.7	114.4	22.7	137.1	401.6	38.4	440.0	124.7
	+0	5.0	6.0	1.6	7.6	95.3	41.1	136.5	328.6	92.1	420.8	144.6
	+50	7.5	5.0	2.3	7.3	77.6	57.6	135.2	260.1	139.5	399.6	167.0
silty clay loam	-50	2.5	1.8	0.2	2.0	75.3	11.0	86.3	245.6	2.1	247.7	367.8
	+0	5.0	1.8	0.2	2.0	75.3	11.0	86.4	245.7	2.1	247.8	367.7
	+50	7.5	1.8	0.2	2.0	75.3	11.0	86.4	245.8	2.1	247.9	367.5

Aquifer thickness (Fig. 4.7 and Tab. 4.3) has a similar influence as slope angle, since an increase in water layer increases discharge of water and lower water levels upslope. Again it can be seen that the change in biomass is largest for the intermediate soil textures. The conductivity of loamy sand is so high that a groundwater layer of 4 m is sufficient to discharge all the precipitation surplus through groundwater, which shows from the narrow zone where groundwater is at the surface. The silty clay loam on the other hand can not discharge the precipitation surplus with an aquifer thickness of even 12 m resulting in a wide zone where groundwater is at the surface.

Rainfall intensity and frequency

Changes in rainfall can be caused by changes in rainfall intensities and rainfall frequency. These changes cause a different effect on the ecosystem. The effect of changing rainfall is investigated by repeating runs with a smaller and a larger rainfall amounts. Intensity was investigated by changing the amount of rainfall per day (i.e. at the same frequency but a smaller or larger amount of rainfall on a day that it rains). Frequency was investigated by changing the number of raindays (i.e. same amount of rainfall per day that it rains, but at a higher or lower frequency). Both were varied to plus and minus 10% of the normal amount of rainfall. The influence of different rainfall intensities (i.e. amount of rainfall per day) is shown in figure 4.8 and table 4.3. The total biomass increases with higher rainfall intensities for all soil textures as well as evaporation and transpiration. Although the change in precipitation has only a very small effect on the silty clay loam, and just a slight effect on the drought adapted species in case of the loamy sand, for the intermediate soils (sandy loam and sandy clay loam) an increase in precipitation results in a shift of the zone where the wet and dry species prevail. In this situation the drought adapted species upslope reaches an increased biomass as well. Figure 4.9 and table 4.3 show the effect of different rainfall frequencies on biomass. In this case the effect on the system is much smaller. In case of an increase in precipitation amount, the number of days that the interception capacity is exceeded increases, causing a more than proportional increase in throughfall and therefore more groundwater recharge. If the frequency of rain days increases the interception evaporation increases only proportionally, as well as the throughfall and groundwater recharge.

The sensitivity analysis shows that the border between wet and dry-adapted species moves upslope in case of increased precipitation, smaller slope angles and thinner aquifers. This effect is largest for the intermediate textures. We obtained qualitatively very similar results in previous work (Brolsma & Bierkens, 2007). It is interesting that the latter results were obtained from optimizing a global (whole ecosystem) criterion (minimization of stress or maximization of evaporation) while current results draw from local space-time optimization of evaporation and carbon uptake. We cannot conclude that the system here also leads to global optimization of carbon uptake, net carbon gain (Schymanski et al., 2009) or minimization of stress (Brolsma & Bierkens, 2007). The intermittency of biomass variation over large timescales considered here prevents assessing such an equilibrium metric. However, we do see that the reaction of vegetation zones to varying hill slope morphology and precipitation shows similar

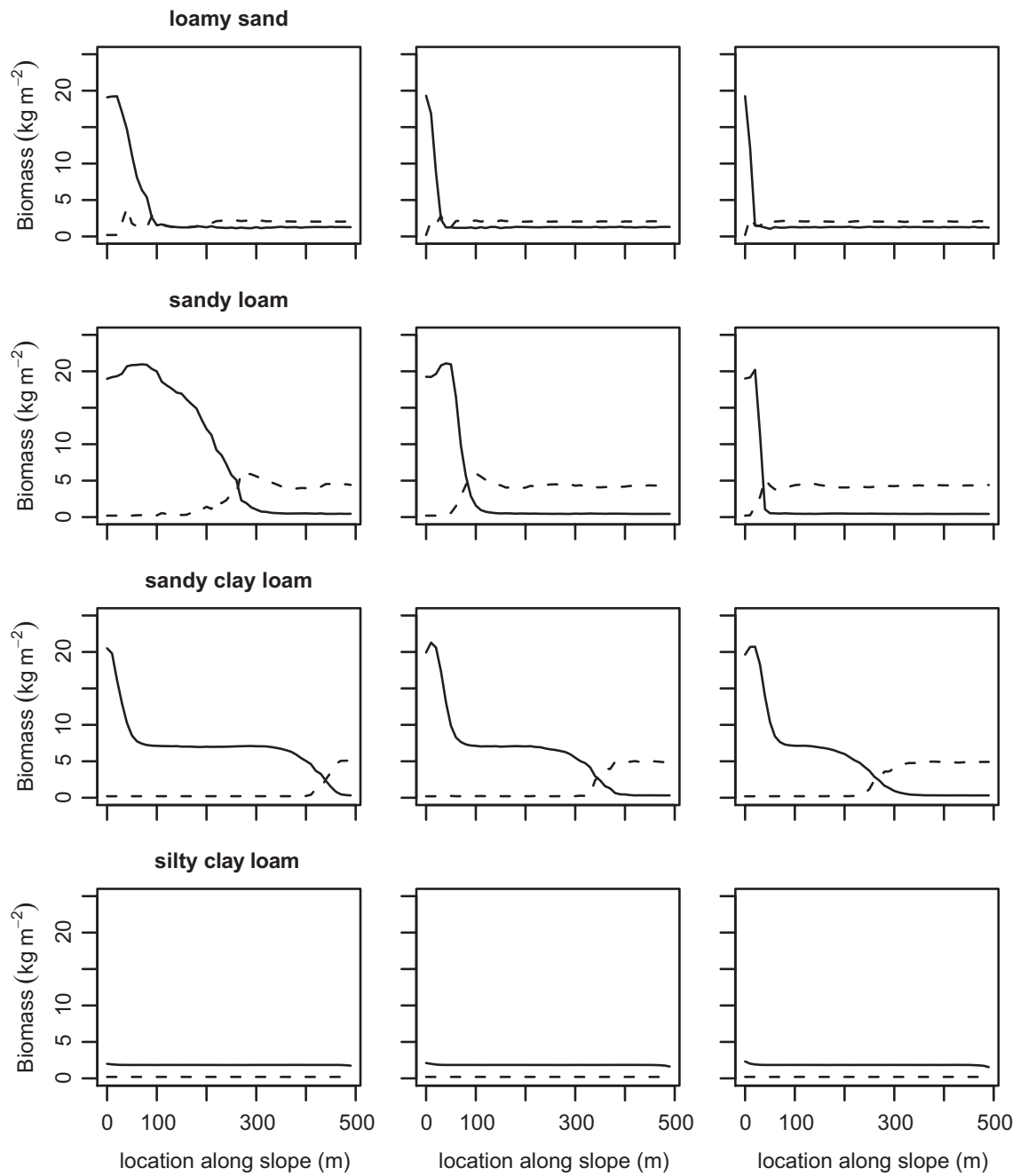


Figure 4.6 Influence of slope angle on biomass for different soil textures. From left to right: slope angle 2.5, 5 (baseline) and 7.5% and from top to bottom loamy sand, sandy loam, sandy clay loam and silty clay loam. Solid lines represent wet adapted vegetation and dashed lines represent drought adapted vegetation. Lines represent average values of 600 years and 100 cells parallel to the slope.

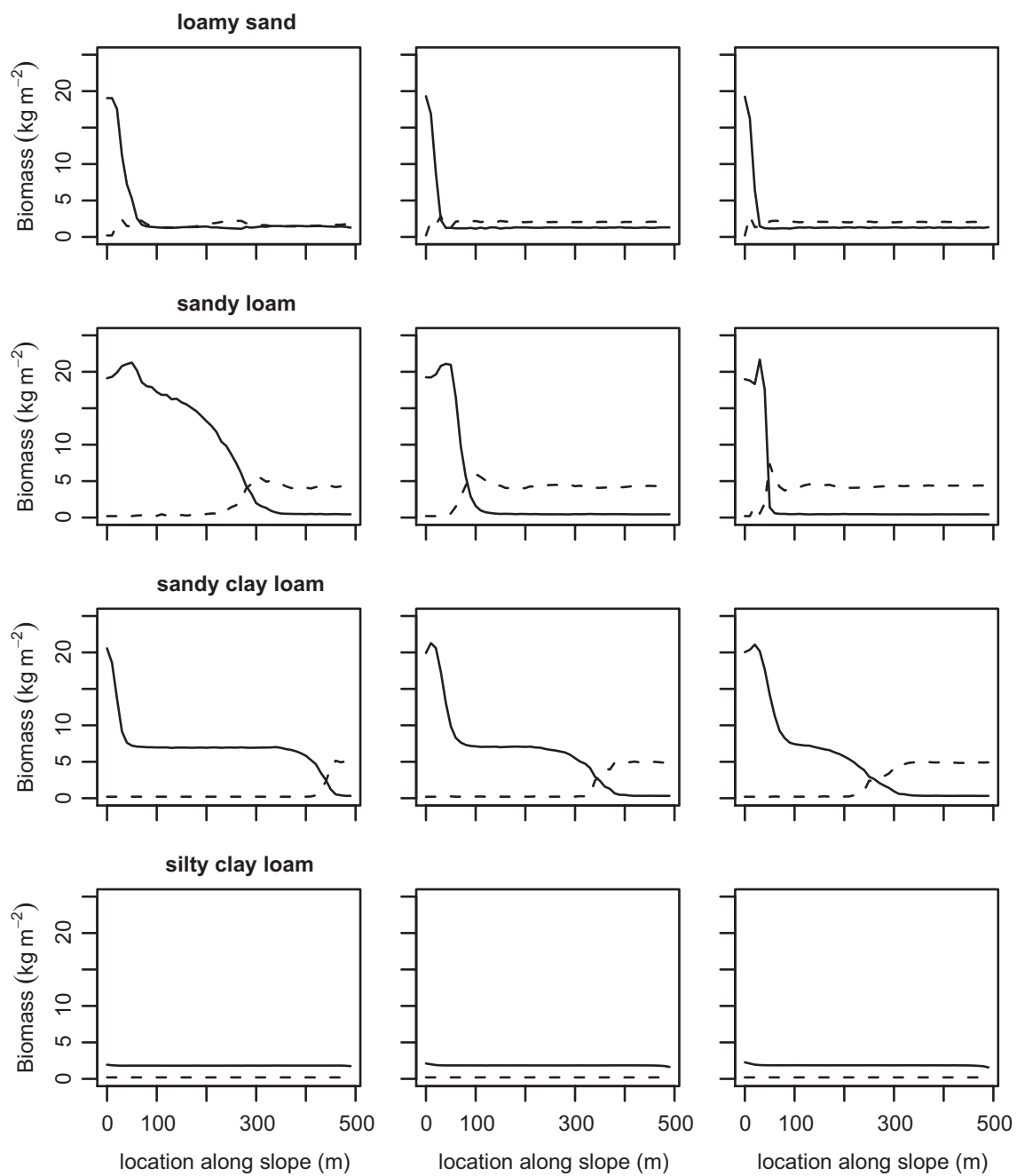


Figure 4.7 Influence of aquifer thickness on biomass for different soil textures. From left to right: 4, 8 (baseline) and 12 m and from top to bottom loamy sand, sandy loam, sandy clay loam and silty clay loam. Solid lines represent wet adapted vegetation and dashed lines represent drought adapted vegetation. Lines represent average values of 600 years and 100 cells parallel to the slope.

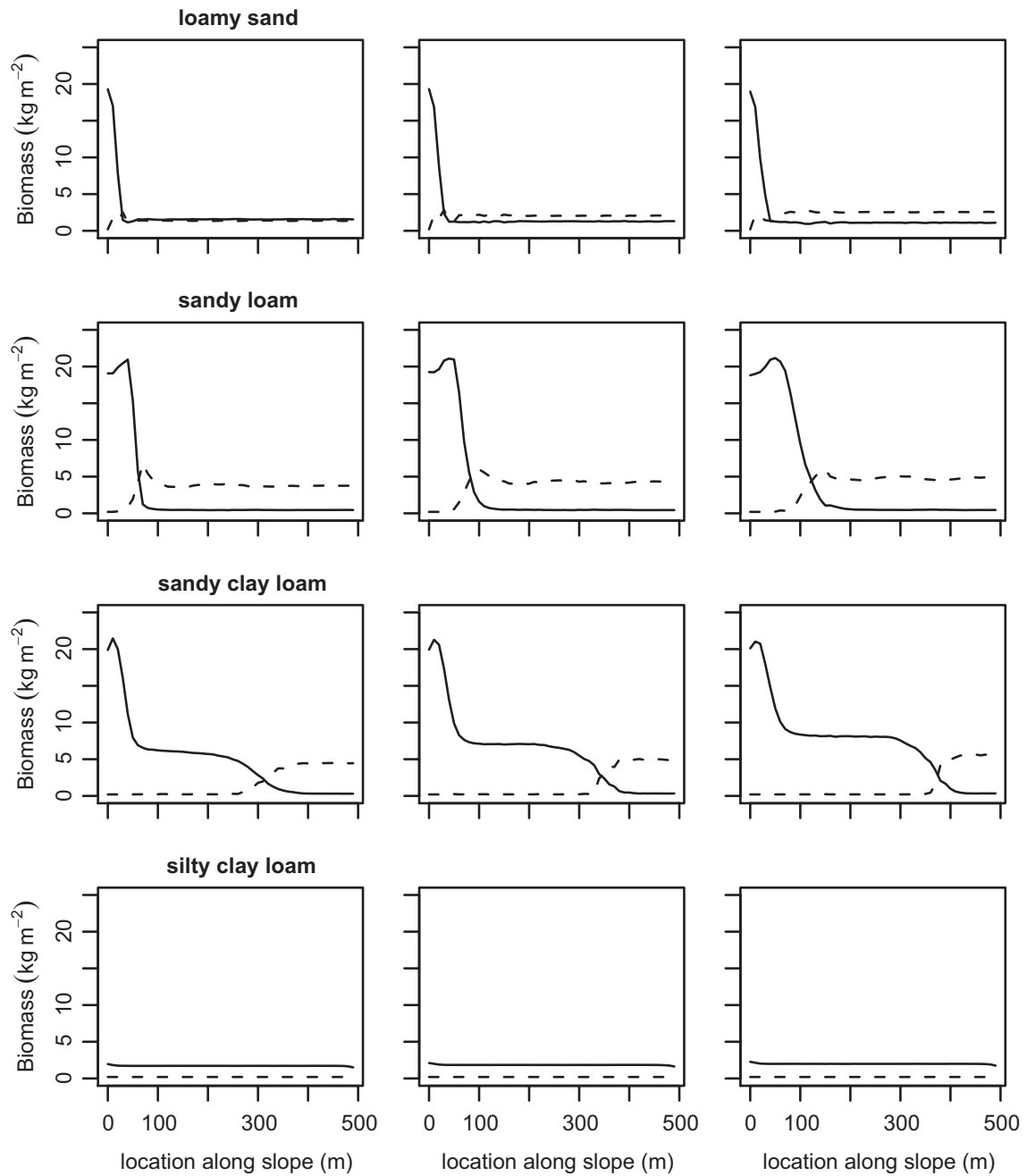


Figure 4.8 Influence of rainfall amount on biomass for four different soil textures. From left to right: 90, 100 and 110% of mean annual precipitation (700mm) and from top to bottom loamy sand, sandy loam, sandy clay loam and silty clay loam. Solid lines represent wet adapted vegetation and dashed lines represent drought adapted vegetation. Lines represent average values of 600 years and 100 cells parallel to the slope.

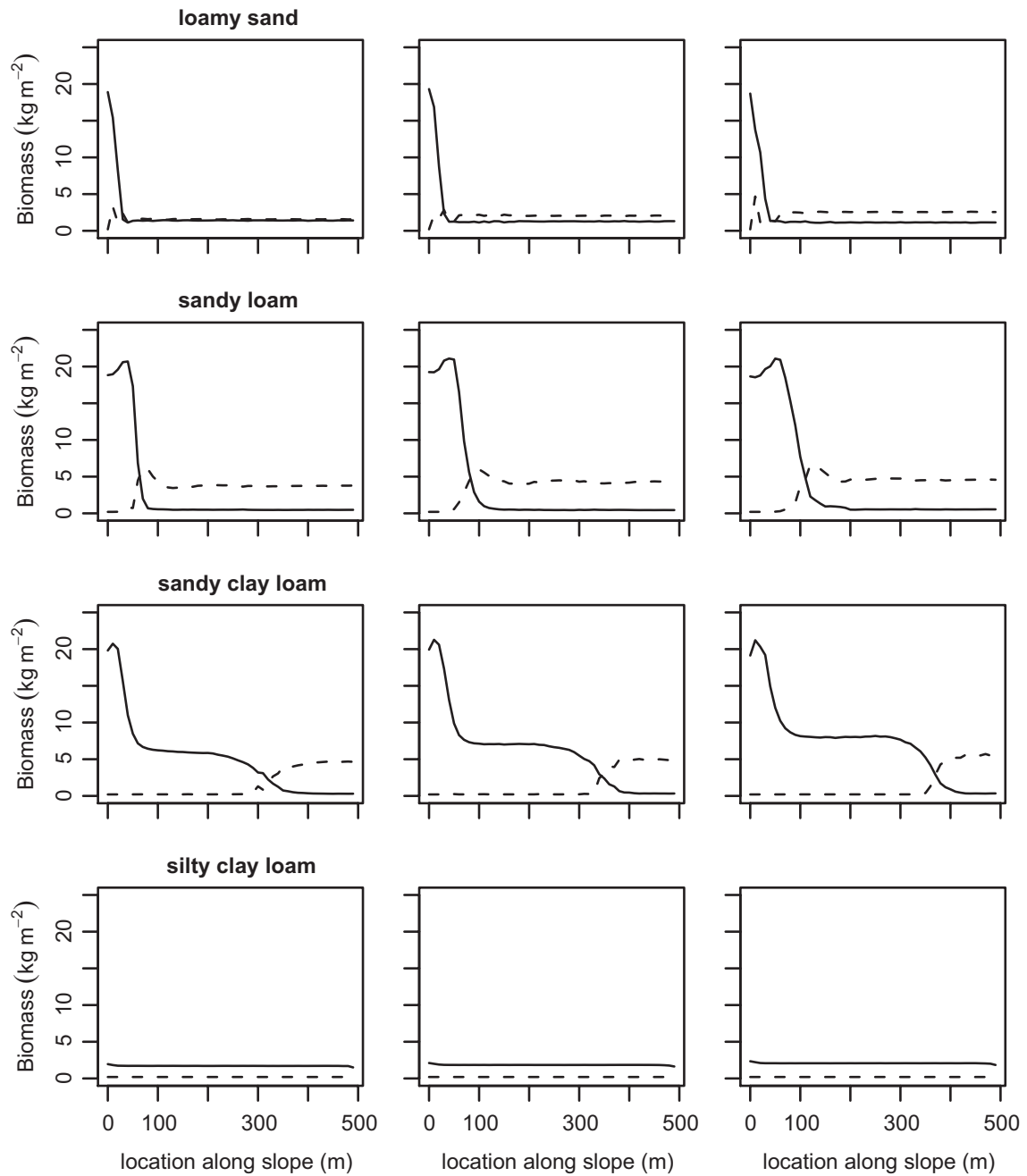


Figure 4.9 Influence of rainfall frequency on biomass for different soil textures. From left to right: 90, 100 and 110% of mean annual rain days (700mm) and from top to bottom loamy sand, sandy loam, sandy clay loam and silty clay loam. Solid lines represent wet adapted vegetation and dashed lines represent drought adapted vegetation. Lines represent average values of 600 years and 100 cells parallel to the slope.

behavior from local space-time optimization as deduced from global scale optimization.

4.3.4 Influence of variable groundwater level

To study the influence of a dynamic groundwater level on vegetation simulation runs with a dynamic and with a static groundwater level were performed. Figure 4.10 shows the long-term (600 year) averages of biomass. In cases where groundwater is near the surface (0.05 m to 0.2 m depending on the soil texture) and in cases where groundwater is deep (deeper than 0.5 to 1.5 m depending on the soil texture) dynamic and static groundwater levels show similar results. The difference between the two groundwater regimes can be found in the zone in between these conditions. In case of a static groundwater level the zone where the wet adapted species prevails and where the drought adapted species prevails is quite abrupt (within 10 cm groundwater depth). In case of a dynamic groundwater regime this zone is much wider (0.5 to 1.5 m depending on the soil texture). This can be explained by a larger temporal fluctuations of soil moisture content. This soil moisture content is favorable for the wet species in spring and for the dry species in summer. In case of the dynamic groundwater regime on sandy clay loam both biomass and ET are slightly higher than in the static groundwater regime. This is because especially in spring the soil moisture content and therefore ET and A_n are higher. This comparison concisely shows how temporal variability can create multiple niches in the same region.

4.4 Conclusions

We created a coupled bio-physical-vegetation growth and variably saturated three dimensional hydrological model to simulate both short-term and long-term vegetation dynamics along a hill slope.

Analysis of the short term dynamics of the model shows that groundwater has a large influence on vegetation productivity (biomass, ET and A_n). Especially when groundwater is near the rootzone groundwater causes a higher soil moisture content in the rootzone and therefore higher transpiration and carbon assimilation rates.

The results of long-term (600 y) simulations provided resemble observations of groundwater depth and vegetation gradients in a natural forest. Longterm dynamics also reveal that die-back of upslope dry adapted vegetation results in an increase in wet adapted vegetation downslope due to increased upslope groundwater recharge. This exemplifies the upslope-downslope connection in these ecosystems.

Sensitivity analysis for three environmental parameters: slope angle, aquifer thickness and rainfall (both magnitude and frequency), shows a great sensitivity of the system to these factors. Both groundwater and vegetation react to these changes. Especially soils with a large capillary fringe zone and moderate conductivity are sensitive to these changes. These finding confirm earlier results from Broksma & Bierkens (2007) that were based on global maximization of evaporation or minimization of plant stress.

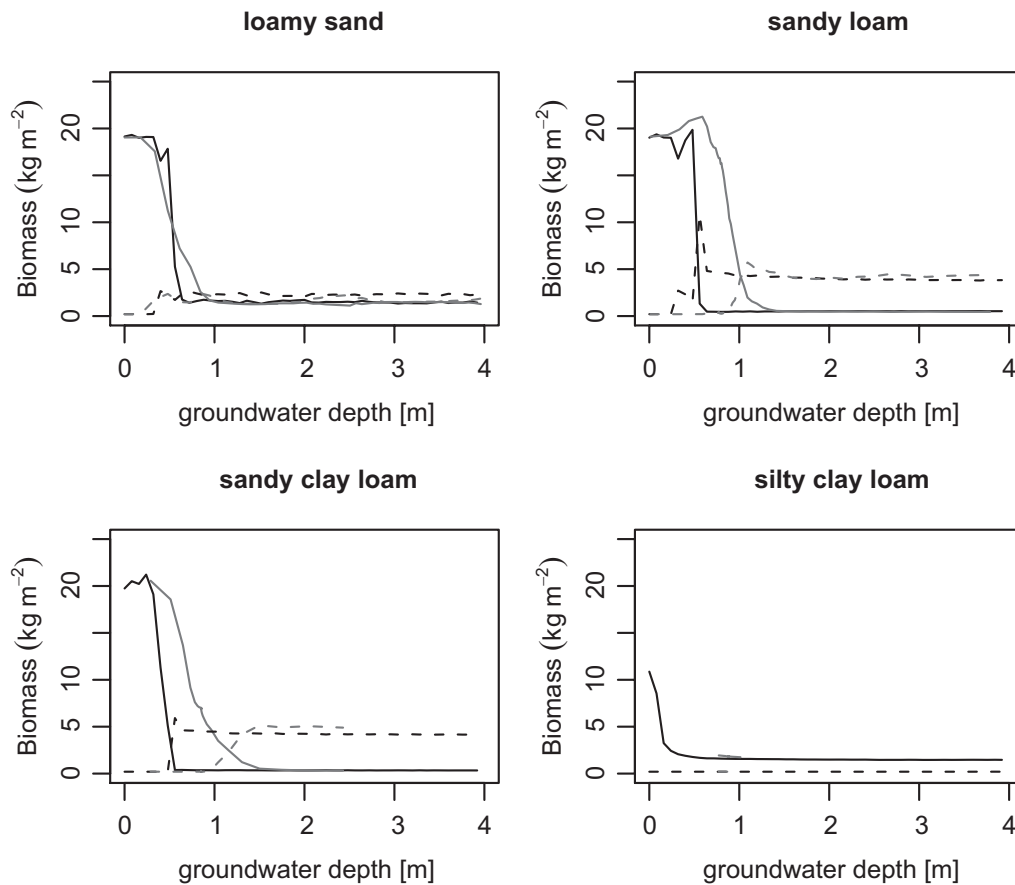


Figure 4.10 Effect of a constant (black) and a variable (gray) groundwater level for four different soil textures on biomass. Solid lines represent wet adapted vegetation and dashed lines represent drought adapted vegetation. Lines represent average values of 600 years and 100 cells parallel to the slope.

The influence of different fixed groundwater levels on vegetation dynamics has already been shown in the companion article in this series of two papers (Brolsma et al., 2010a). Comparison of biomass of simulation runs having these static groundwater levels with simulation runs using a dynamic groundwater model, shows a wider transition zone between the two vegetation types and a higher biomass within this zone for the simulation runs with the dynamic groundwater model. This variation is caused by the temporal dynamics of the groundwater level that results from the climatic forcing and spatial interactions. Together with the upslope-downslope connectivity this result thus shows the importance of using a fully coupled spatio-temporal dynamic groundwater-vegetation model in areas with shallow groundwater.

Acknowledgments

This work was sponsored by the Stichting Nationale Computerfaciliteiten (National Computing Facilities Foundation, NCF) for the use of supercomputer facilities, with financial support from the Nederlandse Organisatie voor Wetenschappelijk Onderzoek (Netherlands Organization for Scientific Research, NWO).

5 Climate change impact on a groundwater-influenced hillslope ecosystem

This chapter has been submitted as:

Brolsma, R. J., M.T.H. van Vliet and M. F. P. Bierkens (2010), Climate change impact on a groundwater-influenced hillslope ecosystem. Water Resources Research.

Abstract

This study investigates the effect of climate change on a groundwater influenced ecosystem on a hillslope consisting of two vegetation types, one adapted to wet and one to dry soil conditions. The individual effects of changes in precipitation, temperature and atmospheric CO₂ concentration are compared to the combined effect of these factors. Change in atmospheric conditions is based on the Netherlands. Projected climate change is obtained from an ensemble of nested global and regional climate models (GCMs and RCMs), representing the IPCC SRES A2 scenario for 2100. For each GCM-RCM combination, change factors were determined and transferred to a stochastic weather generator. All projections show higher temperatures and less annual precipitation. Simulations were performed using an eco-hydrological model, consisting of a dynamic soil-plant-atmosphere-continuum model that is fully coupled to a variably saturated hydrological model, using the stochastic weather data as input. Model results show that increasing atmospheric CO₂ concentration results in higher biomasses due to higher water use efficiency and a decrease in evaporation downslope where vegetation growth is light limited. The change in precipitation regime (drier summers, wetter winters) causes a decreased biomass of especially the dry adapted species and increased upslope groundwater recharge, resulting in groundwater rise and an upward shift of wet adapted vegetation. Temperature rise results in decreased biomass, because respiration increases stronger than carbon assimilation, while increased transpiration causes drier soils and a prolonged period of water limited growth. The combined effect is dominated by the increase in temperature and change in precipitation regime, causing decreased biomass throughout. Surprisingly, the effect on groundwater level depends on the degree by which precipitation distribution changes within the year, showing a drop at a small change and a rise when change is

larger. This study thus shows that climate change effects on hydrology and vegetation are far from straightforward and call for fully coupled eco-hydrological models and upslope-downslope interaction.

5.1 Introduction

Global climate change projections for the 21st century indicate a rise in air temperatures and a general increase in precipitation under increasing CO₂ emissions. However, large regional differences occur, resulting in regions with a decrease in precipitation and a change in distribution of precipitation over the year (Solomon et al., 2007). Field studies and experiments have shown that vegetation reacts in a complex way to climate change and atmospheric CO₂ rise, working at different spatial and temporal scales.

At the scale of individual plants physiological responses will occur. Increased atmospheric CO₂ concentration will result in a reduction of stomatal conductance (e.g. Medlyn et al., 2001; Kruijt et al., 2008), causing a decrease in transpiration of plants. However, at the same time the increase in CO₂ will cause higher carbon assimilation rates and net primary production (NPP), resulting in a higher biomass, which increases transpiration. Studies to this effect are however most often based on short measurement periods on young trees. Long term effects on tree species remain unclear, also because the interactions with other limiting factors like nutrients and water availability are not well known (Karnosky, 2003).

Change in rainfall regime results in change in soil moisture conditions. This in turn will influence (fine) root growth and growth of mycorrhiza and therefore root water uptake. The effect of temperature rise will affect vegetation physiologically by increasing biochemical activity. Therefore carbon assimilation is expected to increase, but at the same time respiration is expected to increase as well. The net effect on vegetation growth remains unclear and will also depend on other environmental conditions (Saxe et al., 2001). At higher temperatures also the phenology will be affected, prolonging the growing season and therefore carbon assimilation, respiration, transpiration and interception evaporation alike. However, the reaction of phenology is uncertain itself, as the true mechanisms are still not understood. For instance the relation between phenology and day length is strong as well (Saxe et al., 2001).

Individual trees react to all of the above changes in atmospheric conditions and resulting changes in soil conditions by changing their growth form, e.g. by increasing the amount of rootmass relative to the above ground biomass as a reaction to water stress. At larger spatial scales shifts in the zonation of vegetation are expected to occur. These shifts are connected to temperature rise and changes in precipitation. Global vegetation models show vegetation zones to shift toward the poles and on local scales to higher altitudes. Landscape scale models show that changes in precipitation result in shifts in the soil moisture regime, which will cause drought tolerant and wet tolerant species to shift up- and downslope (Broksma & Bierkens, 2007).

It can be concluded that the effect of climate change is difficult to investigate in

field experiments, due to the long response time of vegetation systems to change in environmental conditions. Also geographical substitution to investigate climate change has limitations, because it is difficult to extract the individual effect of change of a climate variable, as a consequence of simultaneous change in other environmental conditions.

Using computer models can help understand and predict the reaction of eco-hydrological systems to climate change. The non-linearities in the reaction of vegetation to climate change show the importance of using a bio-physically based vegetation models. The majority of modeling studies that have been performed to assess the influence of climate change on eco-hydrological systems focus on a large (global) scale (e.g. Friend et al., 1997; Prentice et al., 1993; Sitch et al., 2003). These models however omit many local interactions and feedbacks, such as competition for light and local scale variations in soil moisture and groundwater, although vegetation competition is sometimes included using Lotka Volterra type equations (e.g. Arora & Boer, 2006). Hydrological models tend to simplify vegetation dynamics and conversely in ecological models hydrological processes are often over simplified, with Band et al. (1993) as a notable exception.

The effect of climate change on hydrological systems is thus far from straightforward. It depends heavily on how vegetation reacts to changes in precipitation, temperature and atmospheric CO₂ concentration. Changes in vegetation affect the hydrological system due to changes in interception evaporation and transpiration, while changes in hydrology feed-back on vegetation (Eagleson, 1978). A sound analysis of hydrological sensitivity to climate change thus demands a coupled vegetation-hydrology approach, i.e. eco-hydrological models (Rodriguez-Iturbe, 2000).

Up to now, most eco-hydrological models treating both vegetation functioning as well as hydrological processes in a fully coupled mode, are tailored to water limited systems (Rodriguez-Iturbe & Porporato, 2004). However, in temperate climate zones groundwater can have a strong effect on the reaction of vegetation to climate change, because it strongly influences the spatial temporal distribution of soil moisture and therefore water and oxygen stress of vegetation.

Including groundwater dynamics in these models is therefore of great importance (Daly et al., 2009; Rodriguez-Iturbe et al., 2007) and especially spatial dynamics allowing for lateral groundwater flow (Broksma et al., 2010b).

Here we aim to show the effect of climate change on a temperate forest ecosystem using a fully coupled hydrological-vegetation model. To account for most of the above mentioned non-linearities in the reaction of vegetation to climate change and be able to investigate multiple aspects of climate change, we use a bio-physically based vegetation model. The resulting eco-hydrological model includes light competition between two tree-species with different toleration to water and oxygen stress. We particularly focus on the individual effect of temperature, precipitation and CO₂ change and how these compare to the effect of the combination of these factors. Climate input results from 8 regional climate model (RCM) experiments from the PRUDENCE project for current and future (2071-2100) climate under the IPCC SRES A2 scenario (Naki-

cenovic & Swart, 2000). The output of these models is further down-scaled using a stochastic rainfall model and weather generator. The hydrological part consists of a hillslope model including lateral groundwater flow. This way we represent the higher (drier) and lower (wetter) parts of the landscape and their connection through the groundwater system.

5.2 Methods

In this study we use a fully coupled vegetation and variably saturated hydrological model. The vegetation model has been described in detail in Brolsma et al. (2010a) and the hydrological model in Brolsma et al. (2010b). Climate change scenarios, used as input into the coupled eco-hydrological model, have been generated by applying change factors from a selection of RCM experiments of the PRUDENCE project, which were downscaled to local atmospheric forcing using a stochastic rainfall model (Burton et al., 2008) in combination with the stochastic weather generator of Richardson (1981).

5.2.1 Hydrological model

A first full description of the hydrological model, that only included percolation in the unsaturated zone as gravitational flow can be found in van Beek (2002). Modifications to include matric potential driven unsaturated flow including capillary rise are given in Brolsma et al. (2010b). We assume a shallow unconfined aquifer with no-flow boundaries along the borders. This means that water can only leave the system through exfiltration, after which water is instantly removed as runoff from surface of the system. Also infiltration excess runoff is instantly removed from the system. The model (Figure 5.1) consists of three variably saturated layers in which the groundwater level can fluctuate. Lateral fluxes are limited to the saturated zone and vertical fluxes are limited to the unsaturated zone and unsaturated-saturated interface. The vertical Darcy fluxes in the unsaturated zone are based on soil matric potential and unsaturated conductivity, where both depend on soil moisture content using van Genuchten (1980) equations. To increase the numeric stability of the model and allowing relatively large timesteps, every timestep the equilibrium soil moisture content of the layers was calculated based on the layer above. Within one calculation timestep a cell that is wetter than the equilibrium soil moisture content cannot get drier than its equilibrium soil moisture content, and vice versa for cells that are drier than the equilibrium soil moisture content. The horizontal fluxes are modeled with Darcy's equation in two dimensions.

5.2.2 Vegetation model

A full description of the vegetation model is given in Brolsma et al. (2010a). Here only a brief description is given of the main assumptions and equations. The vegetation model is two dimensional and is grid-based, having square cells of 100 m²,

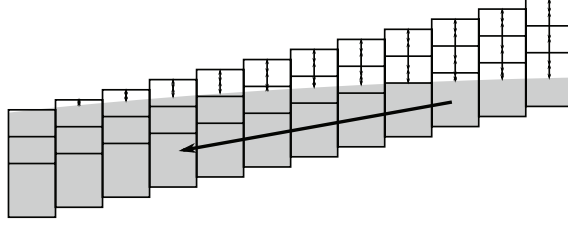


Figure 5.1 Simplified representation of the hillslope, the aquifer and the groundwater.

corresponding to the surface area of the footprint of a mature tree. The model uses plant functional types, that are assumed to be always present at least at a primordial biomass in all cells (i.e. no dispersal modeled). The vegetation model runs on a half-hourly timestep for the calculation of transpiration, carbon assimilation and respiration. However, to produce long-time (century) runs the model is upscaled to daily timesteps (see hereafter).

Transpiration, carbon assimilation and respiration

Simulation of transpiration and carbon assimilation is based on Daly et al. (2004), which is in turn (for the carbon assimilation part) strongly based on the model of Farquhar et al. (1980). Transpiration of vegetation is assumed to be an equilibrium between atmospheric demand and the capacity of the vegetation to provide water to the leaves for transpiration. Atmospheric demand is calculated based on the Penman-Monteith equation (Monteith, 1965):

$$ET_{pm} = \frac{(\lambda_w \gamma_w g_{ba} \rho_a D + \Delta AR)}{\rho_w \lambda_w [\gamma_w (\frac{g_{ba}}{g_s LAI} + 1) + \Delta]}, \quad (5.1)$$

where AR [W m^{-2}] is the absorbed radiation, D [-] the atmospheric vapor pressure deficit, g_s [m s^{-1}] the stomatal conductance, λ_w [J kg^{-1}] the latent heat of water vaporization, γ_w [Pa K^{-1}] the psychrometer constant, Δ [Pa K^{-1}] the slope of the saturated water vapor pressure to temperature relationship, ρ_w [kg m^{-3}] the water density, ρ_a [kg m^{-3}] the air density, LAI [-] the leaf area index and g_{ba} [m s^{-1}] is the series of conductances of the boundary layer and the atmosphere. Note that D and Δ are both functions of temperature.

Stomatal conductance is modeled using the Jarvis (1976) approach, where g_s depends on $g_{s,max}$ through a series of reduction functions related to radiation (Rad), vapor pressure deficit (D), leaf temperature (T_l), atmospheric carbon concentration (CO_2) and leaf water potential (ψ_l) [Pa]. The reduction of g_s due to large negative leaf water potentials is modeled as:

$$f_{\psi_l}(\psi_l) = \begin{cases} 0 & \text{if } \psi_l > \psi_{l_0} \\ \frac{\psi_l - \psi_{l_0}}{\psi_{l_1} - \psi_{l_0}} & \text{if } \psi_{l_0} < \psi_l < \psi_{l_1} \\ 1 & \text{if } \psi_l < \psi_{l_1} \end{cases}, \quad (5.2)$$

where ψ_{l_1} [Pa] is the threshold potential at which the root-to-leaf hydraulic conductance begins to decline, ψ_{l_0} [Pa] threshold potential at which the root-to-leaf hydraulic

conductance becomes negligible. The dependence of g_s to atmospheric CO_2 is based on Kruijt et al. (2008), who determined a decrease in stomatal conductance for woody species of 0.068% per 1 ppm increase in atmospheric CO_2 concentration.

The plants capacity provide water to the leaves is given by:

$$ET_{srp} = g_{srp} (\psi_s - \psi_l), \quad (5.3)$$

where g_{srp} [$\text{m Pa}^{-1} \text{s}^{-1}$] is the soil-root-plant conductance and ψ_s [Pa] the soil water potential. g_{srp} depends on the matric potential and unsaturated conductivity of the soil and the leaf water potential (Daly et al., 2004).

In wet soil moisture conditions, root water uptake can be limited due to a shortage of oxygen in the rootzone. To account for this effect, a reduction function f_{ox} , that limits the soil root conductance, is used (Feddes et al., 1978; Broilmsa et al., 2010a):

$$f_{ox} = \begin{cases} 1 & \text{if } \theta < \theta_{ox,1} \\ \frac{\theta_{ox,0} - \theta}{\theta_{ox,0} - \theta_{ox,1}} & \text{if } \theta_{ox,1} < \theta < \theta_{ox,0} \\ 0 & \text{if } \theta > \theta_{ox,0} \end{cases}, \quad (5.4)$$

where θ [-] is the rootzone soil moisture content $\theta_{ox,1}$ [-] is the soil moisture content at which root water uptake starts to decline and $\theta_{ox,0}$ [-] is the soil moisture content at which the root water uptake stops. Root water uptake is also sensitive to soil temperature as a consequence of respiration reduction (Bartholomeus et al., 2008b). This effect has not been included in this model.

Assuming steady states, atmospheric demand and the plants capacity to provide water to the leaves is in equilibrium. By solving for ψ_l and g_s such that $ET_{srp} = ET_{pm}$ gives the actual transpiration.

Carbon assimilation is based on the equilibrium between the CO_2 flux from the atmosphere through the stomata to the intercellular spaces in the leaf A_{n,g_sba} [$\text{mol m}^{-2} \text{s}^{-1}$] and biochemical demand for CO_2 for photosynthesis $A_{n,bio}$ [$\text{mol m}^{-2} \text{s}^{-1}$]. A_{n,g_sba} depends on stomatal conductance and the gradient in carbon concentration:

$$A_{n,g_sba} = g_{sba,CO_2} (C_a - C_i), \quad (5.5)$$

where g_{sba,CO_2} [$\text{mol m}^{-2} \text{s}^{-1}$] is the series of stomatal, leaf boundary layer and aerodynamic conductances for CO_2 , C_a [mol mol^{-1}] is the carbon concentration at the leaf surface and C_i [mol mol^{-1}] is the intercellular carbon concentration.

$A_{n,bio}$ depends on radiation, leaf temperature and leaf water potential:

$$A_{n,bio} = A_{n,\psi_l} \min(A_{n,c}, A_{n,q}), \quad (5.6)$$

where A_{n,ψ_l} [-] is a reduction function for carbon assimilation due to low leaf water potential (ψ_l) and $A_{n,c}$ [$\text{mol m}^{-2} \text{s}^{-1}$] and $A_{n,q}$ [$\text{mol m}^{-2} \text{s}^{-1}$] are the rubisco limited and the light limited carbon assimilation rate respectively.

The reduction of carbon assimilation due to low ψ_l is modeled by:

$$A_{n,\psi_l} = \begin{cases} 0 & \text{if } \psi_l < \psi_{l,A_{n,0}} \\ \frac{\psi_l - \psi_{l,A_{n,0}}}{\psi_{l,A_{n,1}} - \psi_{l,A_{n,0}}} & \text{if } \psi_{l,A_{n,0}} < \psi_l < \psi_{l,A_{n,1}} \\ 1 & \text{if } \psi_l > \psi_{l,A_{n,1}} \end{cases}, \quad (5.7)$$

in which $\psi_{A_{n,1}}$ [Pa] is the threshold potential at which assimilation reduction caused by chemical action begins to decline and $\psi_{A_{n,0}}$ [Pa] is the threshold potential at which assimilation reduction caused by chemical action becomes negligible.

The light limited carbon assimilation rate is given by:

$$A_{n,q} = \frac{J C_i - \Gamma^*}{4 C_i + 2\Gamma^*}, \quad (5.8)$$

where J [mol photons $\text{m}^{-2} \text{s}^{-1}$] is the incident electron flux resulting from absorbed photosynthetically active radiation (APAR) and Γ^* [mol C mol^{-1} air] is the CO_2 compensation point. In rubisco limited conditions carbon assimilation is calculated by:

$$A_{n,c} = V_{c,max} \frac{C_i - \Gamma^*}{C_i + K_c (1 + o_i/K_o)}, \quad (5.9)$$

where $V_{c,max}$ [mol $\text{m}^{-2} \text{s}^{-1}$] is maximum carboxylation capacity, K_c , K_o [mol m^{-2}] are Michaelis-Menten constants for CO_2 and O_2 respectively and o_i [mol m^{-2}] is atmospheric oxygen concentration. $V_{c,max}$, J , Γ and K_c and K_o all depend on leaf temperature, which is obtained from closing the energy balance. Once g_s and ψ_l are known from the calculation of ET , A_n can be calculated solving $An_{gsba}(C_i) = An_{bio}(C_i)$ for C_i .

To perform long simulation runs (> 100 y), the vegetation model that runs on a time scale of half an hour, has to be upscaled to be used at daily timesteps. During the day, meteorological parameters such as radiation, temperature and water vapor pressure deficit vary while they influence transpiration (ET) and carbon assimilation (A_n) in a non-linear way. Therefore a simple linear upscaling using daily average values of the input variables leads to biased results. On a daily timescale seven variables influence ET and A_n : T_{min} (minimum day temperature), T_{max} (maximum day temperature), Rad (incoming shortwave radiation), δ (day length), n/N (time fraction cloud coverage), θ (rootzone soil moisture content) and LAI . The range in values of each of these variables is discretized in steps (5-22 steps per variable). Half hourly values of ET based on equations 5.1 and 5.3 and A_n based on equations 5.5 and 5.6 are calculated, where at each half-hourly timestep the daily course of T and Rad is accounted for. These half-hourly values of ET and A_n are summed to daily values and stored in a two separate lookup tables, for all possible combinations of the above mentioned seven variables between reasonable bounds. When performing long runs, daily values of T_{min} , T_{max} , Rad , δ , n/N , θ and LAI are generated or calculated and the associated ET and A_n are then directly read from these lookup tables.

Respiration of vegetation depends on biomass that is located in the different compartments of the vegetation (above and below ground woody biomass, leaves and fine roots) and the nitrogen content and temperature of the different compartments. The dependence of respiration on temperature is calculated using a modified Arrhenius equation (*Lloyd and Taylor, 1994 in Sitch et al., 2003*):

$$f(T) = \exp \left[308.56 \left(\frac{1}{56.02} - \frac{1}{T + 46.02} \right) \right], \quad (5.10)$$

where T [$^{\circ}\text{C}$] is the temperature of the compartment.

Finally, carbon assimilate available for growth is defined as:

$$A_{n,growth} = (A_n - Resp_{maint}) \cdot 0.7, \quad (5.11)$$

where $Resp_{maint}$ [mol m^{-2}] is the maintenance respiration calculated according to Sitch et al. (2003) and depending on T according to 5.10 and 0.7 is a factor to account for respiration as a result of growth itself. In (Broksma et al., 2010a) model simulations of daily, and yearly time scale are compared to observations of CO_2 and H_2O , showing good results.

As the studied ecosystem consists of deciduous trees, phenology is included in the model. Phenology is based on the 10 day sum of maximum temperature. When this 10 day sum is larger than 100°C leaves and fine roots start to grow. When the sum is smaller than 100°C after having reached the full LAI leaves and fine roots start to be shed. Leaf and root growth and shedding occur at a fixed rate depending on the LAI and are included in the carbon balance of the vegetation. To model vegetation growth, it is assumed that $A_{n,growth}$ is first moved to the storage compartment, which is a fixed fraction of the sapwood of the wooden parts of the tree. When this compartment is full, excess $A_{n,growth}$ is used for biomass growth. Carbon for leaf and fine root growth are obtained from the storage until a minimum of 10% of carbon in the storage compartment is reached. The last 10% of the carbon storage can only be used for maintenance respiration. When the storage becomes empty, it is assumed that the tree dies. Tree height and maximum LAI are directly related to biomass through allometric functions (Broksma et al., 2010a). The relation between above and below ground biomass is fixed in this model, which means that water or oxygen stress do not affect the growth form of the tree. For simplicity we assume a uniform root distribution within a fixed rootzone of 0.6 m depth. As a consequence the vegetation is not able to adapt to shallow groundwater tables by increasing its root density in the unsaturated part of the rootzone, or to adapt to deeper groundwater tables by rooting deeper to reach the groundwater.

Interception

Assuming a homogeneous canopy within a cell for each species, transmission and therefore interception of light within the canopy are modeled according to Beer's law for light absorption ($1 - e^{-kLAI}$). Light interception mainly depends on tree height and LAI , where both are a function of biomass of the individual vegetation type. Both height and LAI increase with biomass. Precipitation interception is modeled as a bucket model. A gap fraction of the canopy, is used to determine direct throughfall, and indirect throughfall occurs when the maximum interception capacity is exceeded or if the precipitation amount is larger than the potential daily canopy evaporation, based on Penman's open water evaporation.

Competition and mortality

Vegetation competition is only local in the sense that there is only competition for light and water within a grid cell. Light competition is determined by tree height and LAI , where trees with a higher biomass are taller and have a higher LAI and thus catch more light. Competition for water is determined by the plants reaction to large negative leaf water potentials and root water uptake parameters. There are no explicit spatial interactions between cells; only implicit through groundwater flow. A low soil moisture content can cause a large negative leaf water potential, ψ_l [Pa]. This causes cavitation, that leads to lower plant water conductance and therefore lower leaf water potential, lower stomatal conductance, and lower transpiration and carbon assimilation. The parameters that control the reaction of plant conductance and assimilation rate to leaf water potential differ between the species (Table 5.2).

At high soil moisture contents oxygen stress occurs. As a result of oxygen stress root water uptake is hampered, causing again low leaf water potentials. The parameters controlling the root water uptake function at high moisture contents differ between species as well (Table 5.2).

There are two causes of death for vegetation. First of all, vegetation dies when the carbon storage compartment is empty as described above. Secondly, vegetation can die as a consequence of disease, lightning, etc., which is modeled as a stochastic process with a probability of 1/300 per year. Dispersal of vegetation is not included in the model and regrowth of vegetation after death of one vegetation type is based on the concept that a seedbank is present, i.e. when a tree dies, the species starts regrowing the next timestep at primordial biomass.

5.2.3 Weather generator

The vegetation model uses the following daily atmospheric input variables: precipitation amount, minimum and maximum temperature (T_{min} and T_{max}) and net long and incoming short (Rad) wave radiation. Time series of these variables are generated as a stochastic process. Precipitation is simulated using the the stochastic rainfall model RainSim V3 (Burton et al., 2008) in which multi-site time series are sampled from the spatial-temporal Neyman-Scott rectangular pulses process (STNSRP) (Kilsby et al., 2007; Cowpertwait, 1995). Minimum and maximum temperature and clear sky short wave radiation are generated using the Richardson (1981) weather generator and the dependence of long and short wave radiation to cloudiness are based on random sampling of historic cloud cover data (Broksma et al., 2010a).

The baseline run of rainfall is based on the statistical properties of meteorological measurements of the current climate (1961-1990) of 22 stations around Eindhoven. These statistical properties of the rainfall have subsequently been used to generate artificial rainfall series using the RainSimV3 rainfall model (Burton et al., 2008). A more detailed description of the generated rainfall series that are used in our study, is given in van Vliet et al. (submitted).

The generated rainfall series were used as input for the weather simulator by Richard-

son (1981). Usually this simulator determines the occurrence of wet and dry days based on a Markov chain process that is part of the simulator, but in this case we did not use this part of the model and used the simulated wet and dry days and daily rainfall on wet days from the STNSRP model as given.

Parameterization and simulation of the Richardson generator then proceeded as follows. First, for each month mean minimum temperature (T_{min}) and mean maximum temperature (T_{max}) are determined for wet and dry days. Next, crosscovariances of residuals of minimum and maximum temperature are determined separately for each month and conditional to having a wet or a dry day. Conditional to month and having a wet or a dry day, a multivariate normal distribution of T_{min} and T_{max} is assumed to simulate their residuals and add them to the monthly means. Vapor pressure deficit is then estimated from T_{min} and T_{max} assuming dewpoint temperature T_{dew} to be equal to T_{min} according to relationships summarized in Allen et al. (1998). Shortwave radiation is reduced based on cloudiness, which is, together with atmospheric temperature and vapor pressure deficit, used to calculate net incoming long wave radiation (Shuttleworth, 1993).

To simulate cloudiness, cloud cover data for the period 1961-1990 were divided into bins based on month number, rainfall amount and the difference between daily minimum and maximum temperature. Based on month number and predicted rainfall amount and the difference between daily minimum and maximum temperature cloud cover percentages are drawn randomly from the corresponding bin.

5.2.4 Climate change scenario runs

To simulate the effect of climate change we focus on the SRES A2 emission scenario of the IPCC for the period 2071-2100, which describes a very heterogeneous world with continuously increasing global population and regionally oriented economic growth. (Nakicenovic & Swart, 2000). A selection of GCM (general circulation model) and RCM (regional climate model) combinations for the A2 scenario that were generated within the PRUDENCE project (Christensen et al., 2007) were used. The climate change scenarios are based on both the statistical properties of the baseline run and on the monthly changes in statistics calculated from the outputs of the selected GCM-RCM experiments between the baseline period (1961-1990) and future period (2071-2100). In the PRUDENCE project output of several GCMs, forced with the A2 emission scenario, were selected to serve as boundary condition for different RCM runs. An overview of the selected GCM-RCM combinations used in our study is given in 5.1. Boundary conditions of the GCMs HadAM3 and ECHAM4/OPYC have both been used for the runs with the RCMs HIRHAM and RCAO. The RCMs were also run based on the output of a GCM under current climate conditions to produce a baseline run.

Based on differences of the RCM output of the baseline run (1961-1990) and the scenario runs (2071-2100), change factors for mean rainfall, daily rainfall variance, daily skewness coefficient, Pdry (proportion of dry days), daily rainfall lag-1 autocorrelation and mean temperature were determined for each month. A procedure using change

Table 5.1 Main characteristics of the baseline run and the climate change scenarios. Name denotes the name of the scenario used in this article, Period is the time interval for which the rainfall generator has been calibrated, RCM is the regional climate model that has been used to force the rainfall generator (Burton et al., 2008) and weather generator (Richardson, 1981), GCM is the general circulation model that has been used as boundary condition for the RCM, Prec. [mm] is the sum of annual precipitation and Temp. [°C] is the mean annual temperature.

Name	Period	RCM	GCM	Prec.	Temp.
Baseline	1961-1990		data	777	9.7
Arpege	2071-2100	Arpege	HadCM3	759	12.8
HAD-H-P	2071-2100	HadRM3P	HadAM3P	682	13.7
HIRHAM-E	2071-2100	HIRHAM	ECHAM4/OPYC	710	14.6
HIRHAM-H	2071-2100	HIRHAM	HadAM3H	709	13.2
RACMO-H	2071-2100	RACMO	HadAM3H	756	13.0
RCAO-E	2071-2100	RCAO	ECHAM4/OPYC	716	15.1
RCAO-H	2071-2100	RCAO	HadAM3H	734	13.4
REMO-H	2071-2100	REMO	HadAM3H	750	12.9

factors (Kilsby et al., 2007; Fowler et al., 2007) is followed because the RCMs do not sufficiently well reproduce meteorological conditions on short timescales. These changes were then forced on the calculated monthly statistics of the calibrated rainfall model for the selected rainfall gauges around Eindhoven for the actual situation (van Vliet et al., submitted). The timeseries of one location (station Eindhoven) were used as input for the eco-hydrological model, i.e. no spatial fields were used.

The changes in mean temperature per month, based on the RCM outcomes, were added to the average monthly T_{min} and T_{max} assuming both to change at the same rate and the variance to remain the same. The cross covariances of T_{min} and T_{max} residuals were, for a wet and a dry day, assumed to remain constant, as well as the statistical parameters for cloudiness for a given vapor pressure deficit, T_{min} and T_{max} and for wet and dry days.

In all the scenarios the temperature is projected to increase. From figure 5.2 it can be seen that average annual temperature is expected to rise from 9.7 °C to 12.8-15.1 °C. The average temperature increase in winter is around 3 °C and in summer around 5 °C. The RCM runs that are based on the boundary conditions of the ECHAM4/OPYC GCM (HIRHAM-E, RCAO-E) show a larger temperature increase than the ones based on the HadAM3H GCM (HIRHAM-H, RCAO-H).

Average annual precipitation is projected to decrease from a present day 777 mm y⁻¹ to 759-682 mm y⁻¹. As can be seen in figure 5.2 precipitation in summer will decrease, while it increases in winter. This change in precipitation is mainly caused by a decrease in the number of days that it rains, as the amount of rain on rainy days slightly increases all year round. The Had-H-P has the lowest annual rainfall amount. The RCM runs that are based on the ECHAM4/OPYC GCM show a larger change in seasonal precipitation pattern (larger increase in winter and larger decrease in summer) than the RCM runs based on the HadAM3 GCM.

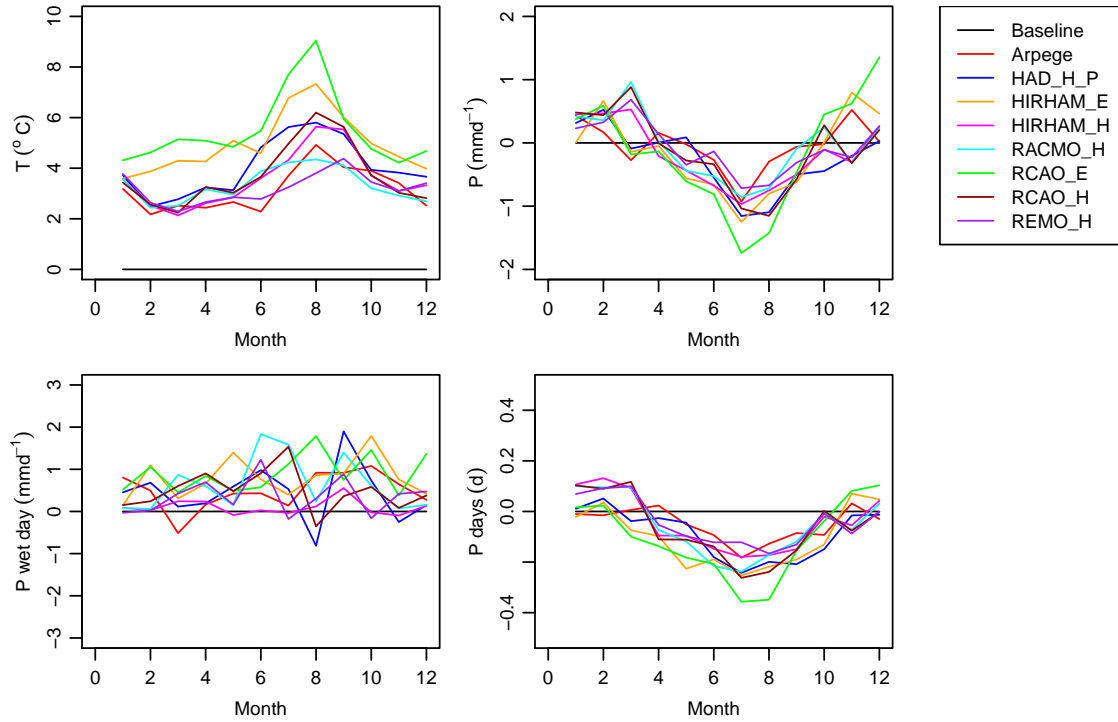


Figure 5.2 Outcomes of the PRUDENCE GCM-RCM combinations for the future time period (2071-2100) for Eindhoven, the Netherlands relative to the baseline period (1961-1990). Upper left panel shows the change in temperature, upper right panel shows the change in daily precipitation amount, lower left panel shows the change in precipitation on days that it rains and lower right panel shows the change in probability that it rains on a single day. P, the amount of precipitation; P wet day, the amount of precipitation on days that with precipitation; Prob. wet day, the probability of a day with precipitation ($P > 0$ mm).

For the baseline run the atmospheric CO_2 concentration is set at 370 ppm. For the period 2071-2100 the CO_2 concentration is assumed to be 730 ppm for all scenarios and is based on the IPCC SRES A2 emission scenarios (Nakicenovic & Swart, 2000).

5.2.5 Model setup

For this study the hydrological model uses in plan-view square cells of 100 m^2 . The thickness of the layers of the hydrological model are from top to bottom of 1, 2 and 5 m, resulting in an aquifer thickness of 8 m. The slope is 50 cells long and 100 cells wide with a slope of 5%. The soil texture is homogeneous and consists of sandy loam (van Genuchten parameters: $\theta_{sat}=0.41$, $\theta_r=0.065$, $K_s=1.06 \text{ m d}^{-1}$, $\alpha=7.5 \text{ m}^{-1}$ and $n=1.89$, (Carsel, 1988)). The hydrological model was run at a timestep of 0.1 day for reasons of stability and the coupling between the vegetation and hydrological model was on a daily basis.

In the vegetation model two plant functional types are defined. The first type is better adapted to wet conditions, in which it experiences less oxygen stress than the second type, whereas the second type is better adapted to dry conditions, in which it

Table 5.2 Parameters of the plant functional type adapted to wet and the plant functional type adapted to dry conditions.

Parameter	Description	Wet species	Dry species
ψ_0	leaf water potential below which g_s becomes 0 [Pa]	-0.45e+06	-4.5 e+06
ψ_1	leaf water potential below which g_s starts to decline [Pa]	-0.005e+06	-0.05 e+06
$\psi_{a,0}$	leaf water potential below which assimilation becomes 0 [Pa]	-0.45e+06	-4.5 e+06
$\psi_{a,1}$	leaf water potential below which assimilation starts to decline [Pa]	-0.05e+06	-0.5 e+06
$O_{x,0}$	soil moisture content above which root water uptake starts to decline [-]	$\theta_{sat}-0.03$	$\theta_{sat}-0.10$
$O_{x,1}$	soil moisture content above which root water uptake becomes 0 [-]	$\theta_{sat}-0.01$	$\theta_{sat}-0.05$

experiences less water stress than the first type. The parameters that differ between the two species are listed in table 5.2.

For every GCM-RCM combination a 1000 year stochastic weather series was produced. The first 400 y were used for spin-up of the eco-hydrological model and the following 600 y were used as results. These results were analyzed by looking at the biomass distribution along the hillslope, average soil moisture content, average groundwater level, average evapotranspiration and the difference between precipitation and evapotranspiration as measure of average groundwater recharge. We simulated changes in P, T and CO₂ separately as well as full climate change, by changing the factors simultaneously. This way we were able to analyze the separate contributions to the combined effect of climate change.

5.3 Results

In this section first the outcomes of the baseline run are described. Then the separate influence of temperature rise, change in precipitation pattern and rise in atmospheric CO₂ concentration on the eco-hydrological system are explained and finally, we describe the effect of expected climate change, by changing all variables simultaneously.

The results of the baseline run are plotted repeatedly in figures 5.3 to 5.6, showing the main variables influencing the water balance and the effect on biomass for the different scenarios. The results are presented as average values of a 600 year period and 100 cells parallel to the slope. In this period a quasi steady state exists in the eco-hydrological system, but spatial and temporal dynamics exist. These are for large part driven by variations in meteorological input. For more information about within year temporal variation we refer to Brotsma et al. (2010b). For reference we also provided dynamic content showing an animation of the 600 y simulation for the baseline run.

The highest biomass (22 kg m^{-2}) is reached by the wet adapted species near the base of the slope. At the base of the slope biomass is slightly lower as a result of oxygen stress. Moving further upslope the biomass of the wet adapted species decreases, while the biomass of the dry adapted species increases. This transition zone is located between 60 and 130 m. Upslope of 130 m the dry adapted species dominates with the highest biomass just upslope of 130 m and a fairly constant biomass of 5 kg m^{-2} along the rest of the slope. Evapotranspiration is also highest downslope and lowest upslope and is almost constant except for the transition zone (60-200 m) in between. This transition zone is wider than the transition zone of the vegetation. This indicates that ET in this zone is not only driven by biomass and vegetation type, but also by the proximity of groundwater and therefore capillary rise or reduced groundwater recharge. Average groundwater and rootzone soil moisture content (0.41-0.12) show a gradient from high to low moving in upslope direction. Due to the assumption of no flow boundaries the groundwater table downslope is at the surface and almost constant.

5.3.1 Temperature change

The effect of temperature change on the eco-hydrological system is shown in figure 5.3 and table 5.3. In all model runs the biomass of both species decreases and the transition zone between species moves downslope. Due to the shift of the transition zone the biomass of the dry species increases in this zone, but total biomass decreases. This coincides with an increase in ET along most part of the slope except for the zone where the shift occurs (80 to 190 m). Because the precipitation amount is equal in all model runs, groundwater recharge shows the opposite pattern of ET . As a result, the groundwater level drops as well as the rootzone soil moisture content. The decrease in soil moisture content is most pronounced in the transition zone, which is caused by the disconnection between groundwater level and the rootzone during a longer period of the year and the shift downward of the drought adapted species that is capable of extracting more water from the soil.

Biomass decreases, because respiration increases faster with an increase in temperature than carbon assimilation in the temperature range between the current climate and the future scenarios. The increase in ET is mostly caused by the increase in vapor pressure deficit (D) and the slope of the vapor pressure curve, (Δ). Both RCM runs based on the ECHAM4/OPYC GCM (HIRHAM-E, RCAO-E) show a stronger temperature increase than the RCM runs based on the HadAM3 GCM (HIRHAM-H, RCAO-H) and therefore have stronger effect on vegetation and hydrology.

5.3.2 Precipitation change

The effect of precipitation on the eco-hydrological system is shown in figure 5.4 and table 5.3. The maximum biomass of the wet adapted vegetation remains approximately the same (20 kg m^{-2}), but the zone where it dominates becomes wider and the overall biomass of wet species increases. However, the maximum biomass as well as the width of the zone of the drought adapted species decreases. Evapotranspira-

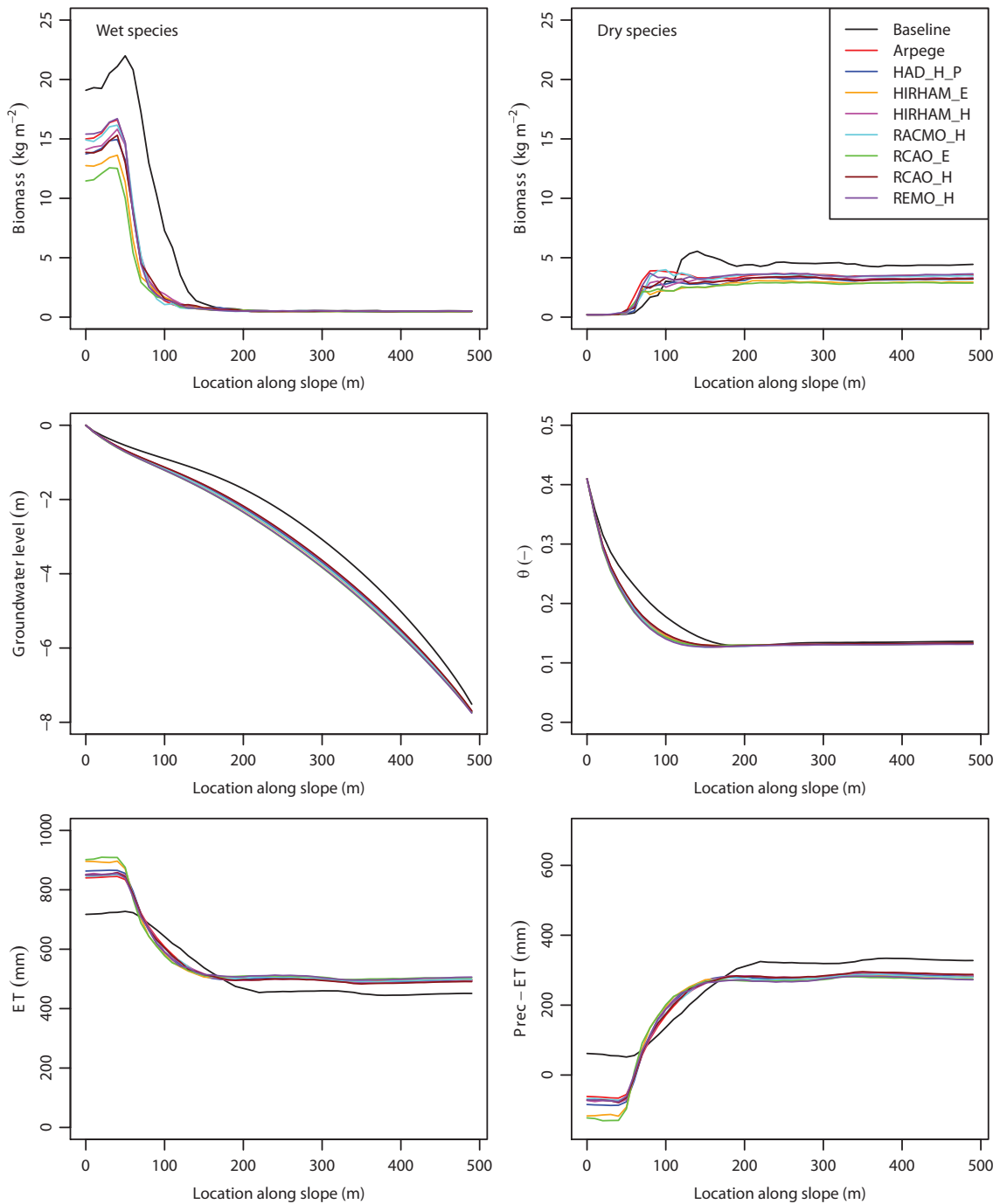


Figure 5.3 The effect of change in temperature on a groundwater controlled forest ecosystem on a slope. Plots show respectively the effect on biomass of the wet adapted and the drought adapted species, groundwater level relative to the surface, rootzone soil moisture content, evapotranspiration and (sub)surface runoff. The lines represent average values of 600 years and 100 cells parallel to the slope. The base of the slope is located at 0 m.

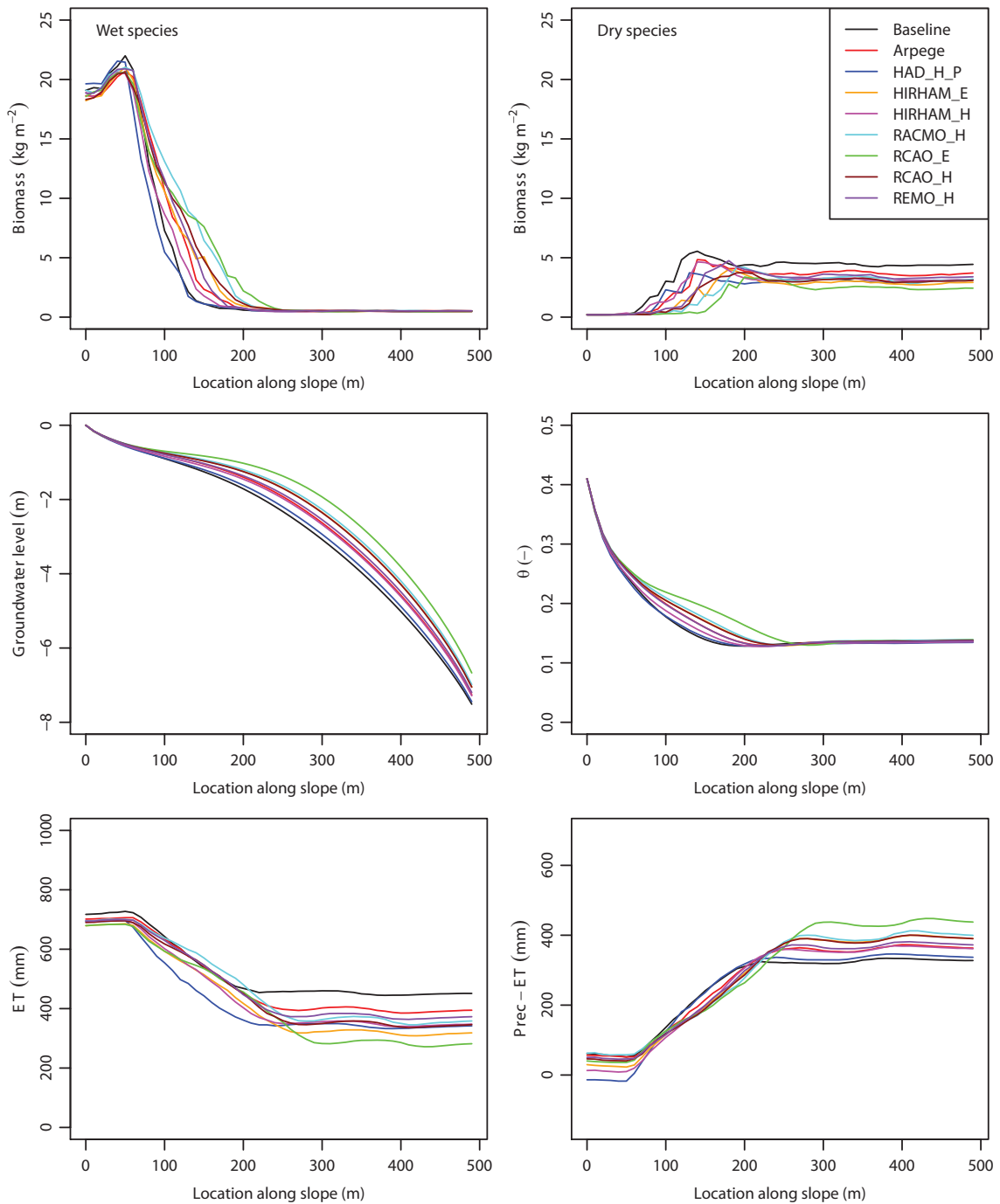


Figure 5.4 The effect of change in precipitation on a groundwater controlled forest ecosystem on a slope. Plots show respectively the effect on biomass of the wet adapted and the drought adapted species, groundwater level relative to the surface, rootzone soil moisture content, evapotranspiration and (sub)surface runoff. The lines represent average values of 600 years and 100 cells parallel to the slope. The base of the slope is located at 0 m.

tion decreases almost everywhere, although upslope much more (50-200 mm) than downslope (20-30 mm). Therefore, the groundwater recharge (that is based on both precipitation and ET) upslope increases whereas downslope it decreases. The groundwater level rises as well as the soil moisture content. The reduction in soil moisture content is especially prominent in the intermediate zone.

The decrease in biomass of the dry species is caused by the decrease in annual precipitation, and especially in summer precipitation when atmospheric demand is highest. This causes more water stress for vegetation, higher leaf temperatures due to less *ET* and more respiration, while due to closure of the stomata the carbon assimilation decreases. Interception evaporation drops in summer because of the decreased precipitation and slightly lower *LAI*. At the same time the amount of precipitation on days that it rains, i.e. the intensity, increases. This results in more throughfall because the interception capacity of the canopy is more frequently exceeded, which is reinforced by decreased *LAI* (biomass). Additionally in winter, when interception evaporation is negligible, precipitation increases. This causes an increase in the annual sum of groundwater recharge and therefore higher groundwater levels and higher average soil moisture contents, especially midslope. This eventually gives room for upslope extension of the zone of wet-adapted species.

5.3.3 Change in atmospheric carbon dioxide

The increase of atmospheric CO₂ content has two opposite effects on evapotranspiration. First, the increasing gradient between atmospheric and intercellular CO₂ causes a larger CO₂ flux into the leaf, resulting in higher assimilation rates and thus a higher biomass. This can be seen throughout the hillslope in figure 5.5 for both dry and wet adapted vegetation. A higher biomass increases evapotranspiration due to an increased transpiration area (*LAI*) and increased interception evaporation. Second, a higher atmospheric CO₂ content results in a reduction of maximum stomatal conductance (7.4 mm d⁻¹ instead of 10 mm d⁻¹) and thus a reduced transpiration per unit leaf area (Kruijt et al., 2008). Figure 5.5 shows that the net effect downslope is a decrease in evaporation. Apparently vegetation growth, i.e. the increase in biomass, is light limited so that it cannot offset the decrease in transpiration due to CO₂ reduced stomatal conductance. Upslope however both effects seem to cancel out. Here, the vegetation growth and evaporation during the summer is water-limited. Due to stomatal closure less water is transpired, which leaves additional water to remain in the soil. This additional water is however immediately used up by the increased biomass which, mainly due to increased interception evaporation, completely compensates the decreased transpiration by reduced stomatal conductance. As can be seen, the effect of CO₂ rise on groundwater level and soil moisture is small, because precipitation is constant and evaporation almost remains the same.

5.3.4 Combined effect

The combined effect of temperature, precipitation and CO₂ change can be seen in figure 5.6 and table 5.3. Biomass will decrease both downslope and upslope for both

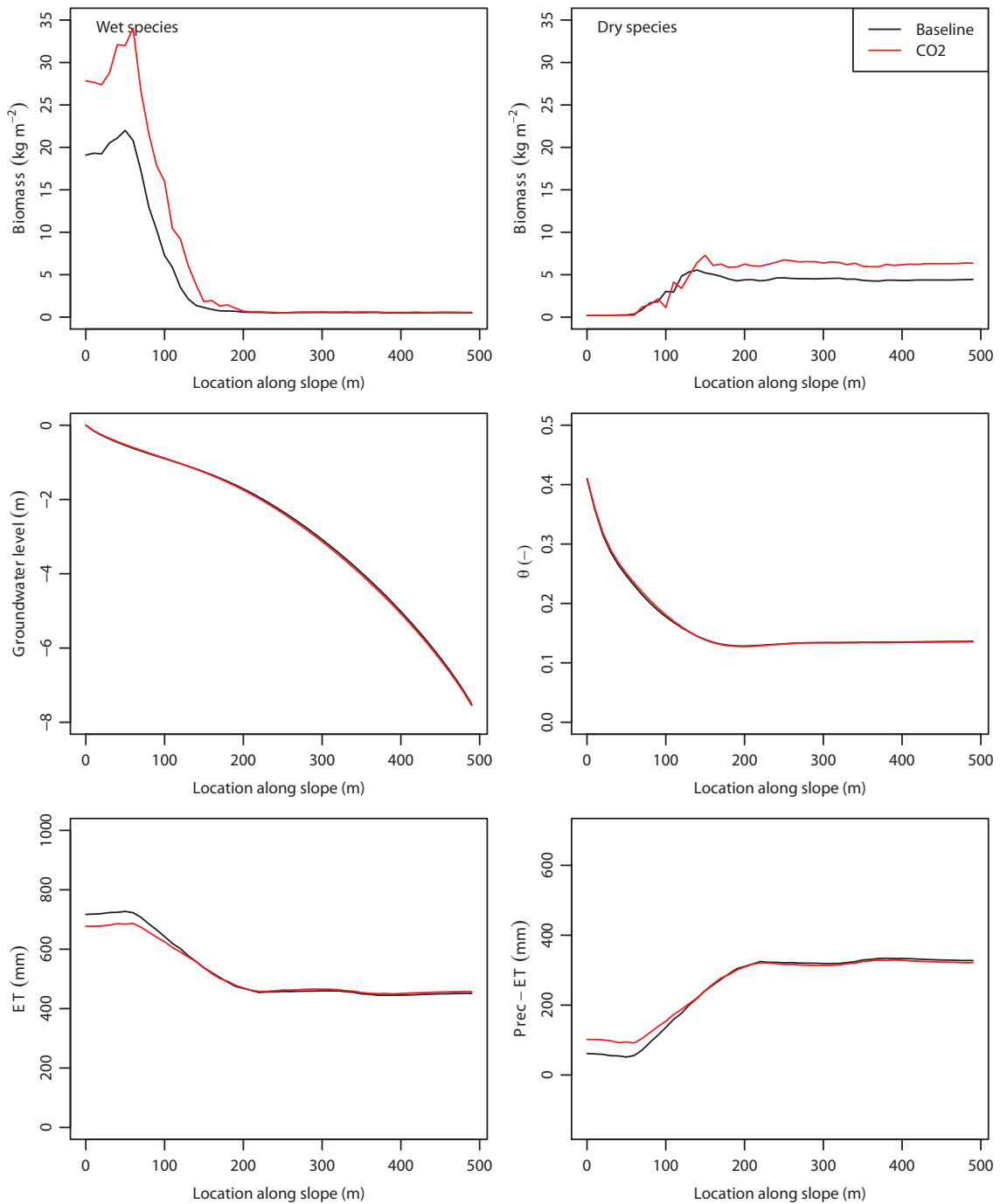


Figure 5.5 The effect of change in atmospheric CO₂ concentration on a groundwater controlled forest ecosystem on a slope. Plots show respectively the effect on biomass of the wet adapted and the drought adapted species, groundwater level relative to the surface, rootzone soil moisture content, evapotranspiration and (sub)surface runoff. The lines represent average values of 600 years and 100 cells parallel to the slope. The base of the slope is located at 0 m.

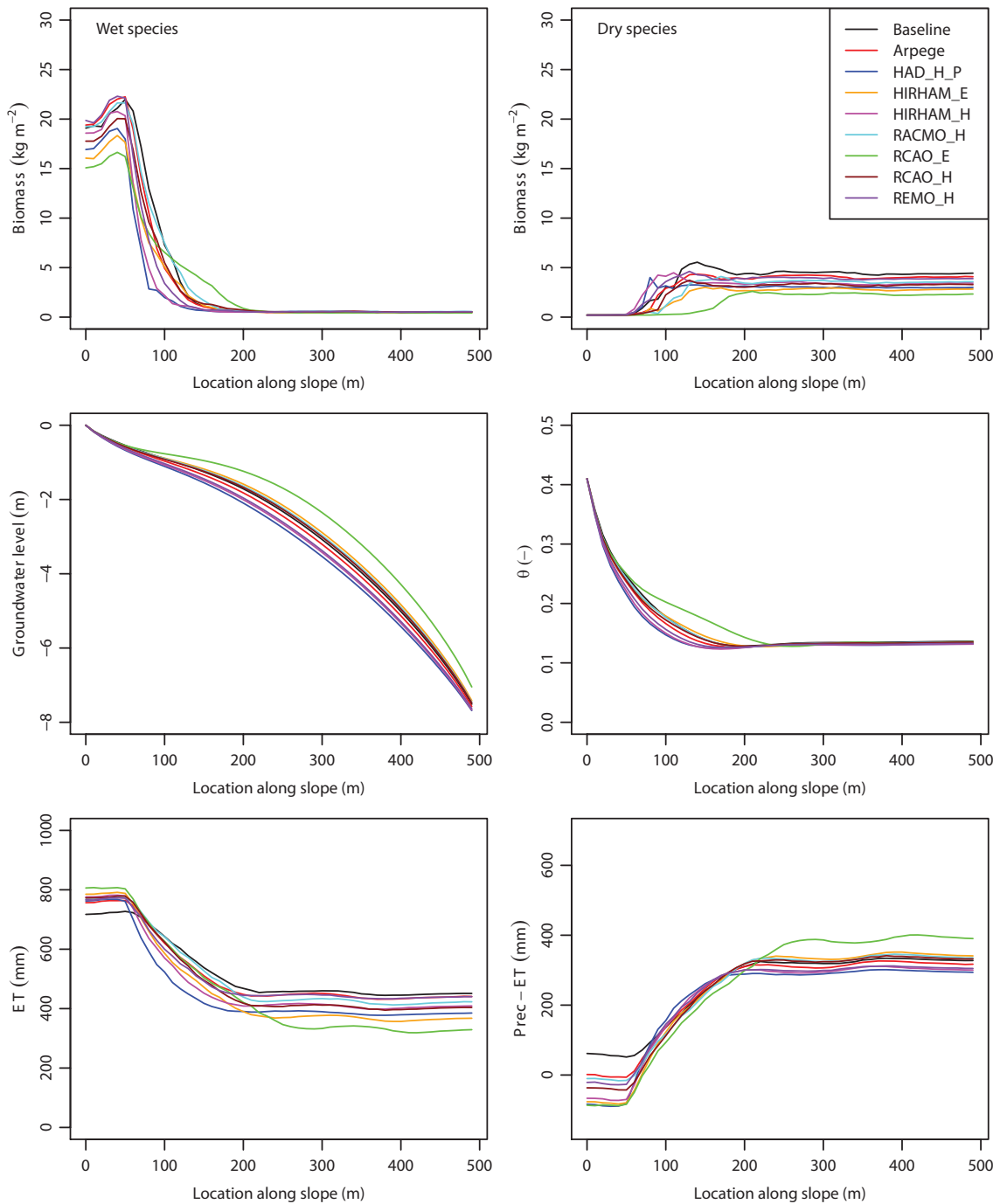


Figure 5.6 Combined effect of change in CO₂, temperature and precipitation on a groundwater controlled forest ecosystem on a slope. Plots show respectively the effect on biomass of the wet adapted and the drought adapted species, groundwater level relative to the surface, rootzone soil moisture content, evapotranspiration and (sub)surface runoff. The lines represent average values of 600 years and 100 cells parallel to the slope. The base of the slope is located at 0 m.

species. Because the influence of precipitation downslope is negligible, the effect of change in temperature is dominant, leading to decreased biomass due to increased respiration. Upslope the dominant factor cannot be recognized as both temperature rise and precipitation change result in a decrease in biomass. Their effect is slightly counterbalanced by the increase in atmospheric CO₂ concentration. Downslope *ET* increases while annual precipitation decreases more, resulting in an evapotranspiration surplus.

Downslope, where vegetation growth is not water limited, the increase in temperature is the main cause for the decrease in biomass due to increased respiration. Upslope, the increase in temperature, the decrease in annual precipitation and increased difference between summer and winter precipitation, cause high water stress and therefore a net reduction in transpiration and carbon assimilation and an increase in respiration, resulting in a lower biomass and *LAI*. For the RCM runs based on the ECHAM4/OPYC GCM, the decrease in biomass is so large that it results in an increase in groundwater recharge upslope and therefore a rise in groundwater level and an increase in rootzone soil moisture content. Surprisingly, the scenarios based on the HadAM3 model show the opposite effect: A smaller increase in temperature and difference between winter and summer precipitation result in a smaller decrease in biomass. Combined with a smaller increase in winter precipitation the net effect is a decrease in groundwater recharge, resulting in a drop in groundwater level and a decrease in soil moisture content.

5.4 Discussion and conclusions

Table 5.4 summarizes the results from the sensitivity analysis showing the effects of climate change and individual change in temperature, precipitation and atmospheric CO₂ on the eco-hydrological variables. We separated the effects downslope and upslope, distinguishing between the zone that is never water limited from the zone that can become water limited in the warm/dry season as well as the RCM runs based on the ECHAM4/OPYC and HadAM3 GCM.

As to be expected, given the lower no-flow boundary condition for groundwater, precipitation change has hardly any effect on downslope groundwater and rootzone soil moisture conditions. As a result, the effect of precipitation on biomass downslope is negligible. Upslope where groundwater levels are deeper, the soil moisture content is lower and the effect of the change in precipitation regime is much larger as vegetation growth is already limited by water availability. Because rootzone soil moisture content downslope is high and hardly changes due to the shallow groundwater table, the effect of CO₂ rise on biomass downslope is large. Upslope the effect is much smaller as water is the limiting factor in vegetation growth. The effect of temperature rise is similar, because the increase in both respiration and carbon assimilation is similar. As a result of a simultaneous change in precipitation, temperature and atmospheric CO₂ concentration, biomass both upslope and downslope decreases, indicating the dominance of the temperature (mostly downslope) and precipitation effect (mostly upslope). Surprisingly the RCM runs based on the ECHAM4/OPYC GCM, show an

Table 5.3 Averages of biomass and water balance components in the different climate scenarios. Effects of temperature rise, change in precipitation pattern, CO₂ concentration and effect of simultaneous change on the following variables: Biomass wet vegetation (B_{wet}), dry vegetation (B_{dry}), total vegetation (B_{tot}), evaporation wet vegetation (E_{wet}), evaporation dry vegetation (E_{dry}), evaporation total vegetation (E_{tot}), transpiration wet vegetation (Tr_{wet}), transpiration dry vegetation (Tr_{dry}), transpiration total vegetation (Tr_{tot}), and net precipitation ($P - ET$). Biomass is given in kg m⁻² and fluxes in mm y⁻¹.

Temperature	P	B_{wet}	B_{dry}	B_{tot}	E_{wet}	E_{dry}	E_{tot}	Tr_{wet}	Tr_{dry}	Tr_{tot}	$P - ET$
Baseline	778.8	4.5	3.7	8.1	56.1	94.6	150.7	157.6	216.5	374.1	254.0
Arpege	778.8	2.7	3.1	5.8	56.8	112.8	169.6	143.5	248.0	391.5	217.7
HAD-H-P	778.8	2.5	2.7	5.2	60.2	107.3	167.5	155.9	238.6	394.5	216.8
HIRHAM-E	778.8	2.3	2.5	4.8	60.8	106.1	167.0	159.6	239.7	399.4	212.5
HIRHAM-H	778.8	2.6	2.8	5.4	59.6	107.7	167.3	153.6	239.1	392.7	218.8
RACMO-H	778.8	2.7	3.0	5.7	57.7	113.5	171.2	145.0	246.9	391.9	215.7
RCAO-E	778.8	2.1	2.4	4.5	60.4	108.9	169.3	156.1	245.0	401.0	208.5
RCAO-H	778.8	2.6	2.8	5.3	58.8	107.3	166.1	153.1	240.1	393.1	219.5
REMO-H	778.8	2.7	3.0	5.7	59.3	115.8	175.1	145.2	245.5	390.7	213.0
Precipitation	P	B_{wet}	B_{dry}	B_{tot}	E_{wet}	E_{dry}	E_{tot}	Tr_{wet}	Tr_{dry}	Tr_{tot}	$P - ET$
Baseline	778.8	4.5	3.7	8.1	56.1	94.6	150.7	157.6	216.5	374.1	254.0
Arpege	757.9	4.9	3.0	7.8	51.8	69.5	121.3	182.4	185.5	367.9	268.7
HAD-H-P	679.0	4.2	2.5	6.7	38.5	54.7	93.3	163.5	173.2	336.7	249.0
HIRHAM-E	708.6	4.9	2.2	7.2	40.7	45.1	85.8	196.1	153.2	349.3	273.5
HIRHAM-H	709.2	4.5	2.7	7.1	44.1	60.7	104.8	171.8	174.8	346.6	257.8
RACMO-H	758.1	5.6	2.3	8.0	50.7	52.1	102.8	215.9	157.7	373.6	281.7
RCAO-E	719.6	5.5	1.8	7.3	41.3	36.0	77.3	222.7	126.4	349.1	293.2
RCAO-H	736.2	5.2	2.4	7.5	47.8	52.1	99.9	203.2	157.4	360.7	275.6
REMO-H	745.1	5.0	2.7	7.7	49.0	61.0	110.0	190.7	175.3	366.0	269.1
CO ₂	P	B_{wet}	B_{dry}	B_{tot}	E_{wet}	E_{dry}	E_{tot}	Tr_{wet}	Tr_{dry}	Tr_{tot}	$P - ET$
Baseline	778.8	4.5	3.7	8.1	56.1	94.6	150.7	157.6	216.5	374.1	254.0
Baseline and CO ₂	778.8	6.9	4.9	11.9	61.5	100.3	161.8	155.7	201.8	357.5	259.5
Total	P	B_{wet}	B_{dry}	B_{tot}	E_{wet}	E_{dry}	E_{tot}	Tr_{wet}	Tr_{dry}	Tr_{tot}	$P - ET$
Baseline	778.8	4.5	3.7	8.1	56.1	94.6	150.7	157.6	216.5	374.1	254.0
Arpege	757.9	4.2	3.3	7.5	57.3	95.2	152.5	157.8	207.0	364.8	240.7
HAD-H-P	679.0	3.1	2.6	5.7	45.0	77.5	122.5	141.0	196.4	337.4	219.1
HIRHAM-E	708.6	3.5	2.2	5.7	48.4	66.3	114.7	175.4	177.9	353.2	240.7
HIRHAM-H	709.2	3.4	3.0	6.4	50.6	93.9	144.5	138.2	203.4	341.6	223.1
RACMO-H	758.1	4.4	2.8	7.3	59.9	84.1	143.9	177.6	190.4	368.0	246.1
RCAO-E	719.6	3.7	1.6	5.4	55.5	52.9	108.4	215.5	138.9	354.4	256.8
RCAO-H	736.2	3.9	2.6	6.6	56.6	81.6	138.2	170.5	186.5	357.0	240.9
REMO-H	745.1	3.9	3.3	7.2	55.1	97.8	152.9	148.3	212.4	360.6	231.6

Table 5.4 Summary of the outcomes of the different scenarios (2071-2100), compared to the baseline run (1961-1990). Downslope refers to the lower 50 m of the slope and upslope to the upper 50 m of the slope, except for the areas (A_{wet} and A_{dry}) which correspond to the entire slope. The results are shown separately for the RCM runs based on the HadAM3 and the ECHAM4/OPYC GCM. B_{wet} , biomass wet adapted species; B_{dry} , biomass dry adapted species; A_{wet} , area wet adapted species; A_{dry} , area dry adapted species; E, evapotranspiration; P-E, precipitation-evapotranspiration; G, groundwater level; θ , soil moisture content. Five classes of change are used: ● large decrease; ● medium decrease; ● no change; ● medium increase; ● large increase.

Change	Model	Downslope						Upslope					
		B_{wet}	A_{wet}	E	P-E	G	θ	B_{dry}	A_{dry}	E	P-E	G	θ
Temperature	HadAM3	●	●	●	●	●	●	●	●	●	●	●	●
	ECHAM4/OPYC	●	●	●	●	●	●	●	●	●	●	●	●
Precipitation	HadAM3	●	●	●	●	●	●	●	●	●	●	●	●
	ECHAM4/OPYC	●	●	●	●	●	●	●	●	●	●	●	●
CO ₂		●	●	●	●	●	●	●	●	●	●	●	●
Combined	HadAM3	●	●	●	●	●	●	●	●	●	●	●	●
	ECHAM4/OPYC	●	●	●	●	●	●	●	●	●	●	●	●

increase in groundwater level and soil moisture content, while the RCM runs based on HadAM3 show a decrease in both variables. This shows that sign of the response can be dependent on the magnitude of the climate change signal and is thus very non-linear in this system.

The results in Table 5.4 also show that the effect of climate change on hydrological variables can be highly non-linear, such that even the sign of change can be different depending on the magnitude of change in temperature and precipitation over the year. Clearly, the combined effect of the three factors temperature, precipitation and CO₂ on the eco-hydrological system is far from straightforward. It depends on the position in the landscape and cannot be simply deduced from the individual effects.

The results also shows the clear presence of spatial interaction. The upslope-downslope interaction, which is most pronounced as a result of change in precipitation regime, where although yearly rainfall decreases, rainfall in winter increases. Decreased upslope biomass and increased rainfall in winter cause the groundwater recharge to increase upslope as a result of increased throughfall in winter. The resulting rise in groundwater level causes wetter conditions downslope and therefore an enlargement of the zone where wet adapted vegetation occurs. This could not have been predicted using a model that does not include lateral groundwater flow. In particular, the non-linear response to magnitude and the upslope-downslope effects, show that predicting the effect of climate change on this temperate ecosystem can be far from straightforward and calls for models that fully couple biophysical vegetation models with the hydrological system. That is, we need eco-hydrological models that are robust under climate change.

We stress that the results show the response of one particular system and one CO₂ emission scenario, although existing of an ensemble of eight projections. Therefore this study cannot be used to draw general conclusions about the effect of climate change in absolute sense. It mostly serves as an example to show the complexity of the response of the system and give directions for future research. Moreover, the validation of the model or comparison of the model as a whole against field data is rather impractical. Experiments with scaled but real vegetation on artificial hillslopes (Hopp et al., 2009; Kleinhans et al., 2010) may be a way to test whether non-linear effects observed in the simulations are a property of the model or of the real system.

Acknowledgments

We would like to thank Dr Stephen Blenkinsop, Aidan Burton and Dr Hayley Fowler of Newcastle University for providing the calculated change factors of precipitation and temperature statistics of the selected RCM experiments and for their assistance with the RainSim V3 rainfall model. Data have been provided through the PRUDENCE data archive, funded by the EU through contract EVK2-CT2001-00132. This work was sponsored by the Stichting Nationale Computerfaciliteiten (National Computing Facilities Foundation, NCF) for the use of supercomputer facilities, with financial support from the Nederlandse Organisatie voor Wetenschappelijk Onderzoek (Nether-

lands Organization for Scientific Research, NWO). We also thank three anonymous reviewers for their constructive comments that helped to improve this paper.

6 Synthesis

In the thesis introduction six research questions were formulated:

1. Can a quantitative framework, on a hydrological basis, be formulated to understand groundwater, soil water and vegetation dynamics in groundwater influenced ecosystems?
2. What is the influence of the presence of a static groundwater table on vegetation dynamics and water fluxes?
3. What is the effect of spatio-temporal groundwater dynamics on vegetation growth in an eco-hydrological system?
4. What is the effect of climate change on vegetation in a groundwater influenced hillslope ecosystem under temperate climate conditions?
5. To what extent can the concept of water and oxygen stress of vegetation be used in systems that are also light limited?
6. Which findings of this study are important for the disciplines of hydrology, ecology and climatology?

The first four questions have partly been discussed in Chapters 2 to 5. A summary of these Chapters and a more elaborate discussion will be given in sections 6.1 to 6.4. The last two questions are based on the outcomes of Chapters 2 to 5. These questions will be discussed in sections 6.5 and 6.6.

6.1 Groundwater, soil water and vegetation dynamics based on a hydrological approach

Where groundwater influences the soil moisture content of the rootzone, it can greatly affect vegetation dynamics and distribution. In Chapter 2 a first attempt was presented to understand the vegetation distribution along a groundwater influenced hillslope. In this case static vegetation on a quasi two-dimensional slope was considered, where water and indirectly oxygen availability were the limiting factors for vegetation productivity.

To provide a quantitative framework on a hydrological basis for understanding groundwater, soil water and vegetation dynamics in groundwater influenced ecosystems, a model simulating evapotranspiration and saturated-unsaturated flow along a hillslope was developed. The effect was shown of two optimality hypotheses about the location of the boundary, in climax state, between two vegetation types that differ in their reaction to water and oxygen stress. The first hypothesis states that the boundary is located at the position where whole system ET is maximized and the second hypothesis states that the vegetation boundary is located where whole system plant stress is minimized.

The concept of plant stress is based on the concept of water stress as defined by Porporato et al. (2001) and has been extended to include oxygen stress. Static water stress occurs when the rootzone soil moisture content is below a certain threshold value and static oxygen stress occurs when the rootzone soil moisture content is above a certain threshold value. Dynamic water and oxygen stress depend on static water and oxygen stress and the duration and frequency of static stress periods. Plant stress is the combination of dynamic water stress and oxygen stress.

The analysis shows that in the system where stress is minimized, the vegetation boundary is located at approximately the same location as in the system where transpiration is maximized. The position where the maximum evaporation is at minimum approximately coincides with the location where slope-average soil moisture is minimal. Due to the limited scope of this study, a conclusion about which hypothesis is more plausible can not be drawn.

The results are in contradiction with the optimality hypothesis of Eagleson (1982) stating that water-limited natural vegetation systems are in stable equilibrium with their climatic and pedologic environments if the canopy density and species act to minimize average water demand stress, i.e. maximize soil moisture content. However, despite the simplicity of the representation of vegetation, the optimality criteria enables mimicking the transposition of vegetation zones in reaction to changing climate and hydro-geology, showing that a wetter climate, less steep slopes and shallower aquifers cause the wet adapted species to move upslope.

The concept of oxygen stress is useful for evaluating plant stress in groundwater influenced ecosystems. However, the response to water stress and oxygen stress are simplified. Both are based on soil moisture conditions, instead of water potentials within the plant. This has the advantage that it avoids modeling the complex and not yet fully understood response of vegetation to soil moisture conditions, but of course also introduces a certain level of empiricism.

It was assumed that oxygen stress occurred at a fixed degree of saturation for all soil textures. Feddes et al. (1978) already indicated that further research to the decrease of root water uptake under wet conditions had to be performed. The authors already mentioned that soil texture and therefore pore space influences the oxygen diffusion in the soil. Hence, more research on the concept of oxygen stress is needed and validation using field data is necessary to verify the proposed oxygen stress function. Furthermore, Bartholomeus et al. (2008a) showed that, based on a plant physiological

and soil physical process-based model, substantial differences in the minimum gas filled porosity of the soil (needed for unstressed root functioning) are related to soil type, soil temperature and soil depth. Consequently, they argue that application of constant values for the minimum gas filled porosity should be avoided, as they may result in large prediction errors of both transpiration and plant growth.

In Chapter 2 it was concluded that further understanding of eco-hydrological systems requires a few additions. Extension of this approach to a two-dimensional hillslope where actual vegetation patterns can be studied, while considering transient vegetation dynamics (i.e. growth and dispersal) will reveal how soil moisture and vegetation patterns interact in space and time. In temperate climate ecosystems such as considered here, water and oxygen stress only partly explain vegetation distribution, as nutrient availability, light competition, forest fire and grazing are important too. Including these processes in the model will improve model predictions. In this study a global optimization criterion was used, because competition was not explicitly included in the model. Local competition, however, may result in a sub-optimal global optimization. Therefore spatial interactions and local vegetation competition should be included.

In Chapter 3 and 4, therefore, a more advanced vegetation model in combination with a hydrological model was used. This made it possible to make evapotranspiration and vegetation growth dependent on plant functioning instead of soil moisture content only, and to include the effect of light limitation. Furthermore, the model was extended to a two-dimensional hillslope where vegetation growth and spatial patterns could be studied and local competition for light and water were included. The effect of nutrient limitation, grazing and forest fire was not investigated as this was outside the scope of this study.

6.2 Effect of groundwater on vegetation dynamics and hydrological fluxes

The proximity of groundwater strongly influences the temporal dynamics of soil moisture and therefore water and oxygen stress of vegetation. For this reason the influence of groundwater on vegetation dynamics and water fluxes in a temperate forest ecosystem controlled by water and light competition was investigated. This was done by developing an advanced vegetation model to simulate coupled dynamics of vegetation, groundwater and soil water including the competition for water and light. First, the effect of the presence of groundwater and more specifically the distance to groundwater was investigated assuming a static groundwater level. In Chapter 3 a comprehensive description is given of the vegetation model, and a comparison is made between modeled and measured H_2O and CO_2 flux data and the influence of local water and light competition was shown. The vegetation model is based on a bio-physical representation of the soil-plant-atmosphere continuum. Transpiration and stomatal conductance both depend on atmospheric forcing and soil moisture content. Carbon assimilation depends on atmospheric conditions, stomatal conductance and biochemical processes.

Light competition is driven by tree height and water competition is driven by root water uptake and the vegetations water and oxygen stress reaction. The modeled and measured H₂O and CO₂ fluxes compare well to observations on both diurnal and yearly timescales.

An up-scaling procedure was introduced enabling simulations at millennium scale. These simulations, with a background mortality rate, reproduced realistic densities of wet and dry adapted tree species along a wet to dry gradient. The results show that the influence of groundwater is apparent for a large range of groundwater depths, both by capillary rise and water logging. The results also show that species composition and biomass have a larger influence on the water balance in eco-hydrological systems than soil and groundwater alone. The simulations demonstrate the importance of light competition in temperate forests: once a tree is established under slightly unfavorable soil moisture conditions, it can not be directly outcompeted by smaller trees with better soil moisture uptake capabilities, both in dry and in wet conditions.

A simulation run with a static groundwater level only explains part of the vegetation and hydrological flux dynamics. The presence of groundwater near the rootzone as a boundary condition causes less variation in soil moisture content, due to percolation and capillary rise, and therefore more biomass, transpiration and interception evaporation. The use of a static groundwater table is of course unrealistic, because the flux from and to the groundwater does not effect the groundwater level itself. In Chapter 4 this assumption is therefore relaxed.

Various important processes that can improve model predictions were not included: (competition for) nutrients, multiple canopy layers, adaptation and resource allocation, competition for space, variable root distribution, phreatophytes and soil formation.

Nutrient limitation and therefore competition for nutrients is not included in the model, although nutrient limitation can have an important role in the competition between species in temperate forest. Especially nitrogen and phosphorus are important, but differences in uptake between species are however not well understood and soil chemical processes would complicate the model and the interpretation of the results.

In this approach the assumption was made of the canopy being a single big leaf. This means that for instance leaf area receives an average amount of solar radiation. In reality there are shaded and non-shaded leaves and a range in between. Also humidity and atmospheric CO₂ concentration vary within the canopy of a tree. This causes individual leaves to respond differently to environmental conditions depending on the location within the canopy of a tree, which influences the functioning of the tree as a whole. As a consequence of location within the canopy different types of leaves can develop. Many studies use multiple layers within the canopy to model especially the shading effect (e.g. Dufrêne et al., 2005; Friend, 1995).

Vegetation tends to invest its resources optimally to capture the most limiting resource as best as possible. Under dry or nutrient poor conditions for instance, a relatively large amount of resources is allocated to the roots, whereas under light lim-

ited conditions more resources are invested in the growth of leaves and stem biomass, increasing canopy height and light capturing capacity. Such adaptive allocation is not modeled. Also, under changing environmental conditions it is hypothesized that biochemical parameters such as V_{max} or J_{max} are adapted to assure optimal growth (Schymanski et al., 2009). Related to this, roots tend to grow where water and/or nutrients are available. This means that trees under wet (shallow groundwater table) conditions have a shallow rooting depth and under dry conditions (deeper groundwater and/or low groundwater recharge) have a deeper rooting depth. We used a fixed rooting depth of 60 cm, which exaggerates the effect of groundwater levels that are just within or underneath the rootzone. This effect is most pronounced in summer when the presence of groundwater within the rootzone significantly reduces vegetation water stress, while in reality the effect of the groundwater level will be more subtle. Especially the absence of taproots of trees when the groundwater table is deep, causes an overestimation of vegetation stress in dry periods, i.e. an underestimation of carbon assimilation and vegetation growth.

Competition for space between individuals was not explicitly simulated. Instead a lumped, height-LAI competition approach was used where leaves and roots are homogeneously distributed in space instead of being distributed in a more clustered configuration. This issue can be overcome by converting the model into an individual based model and explicitly modeling stem, branch, leaf and root growth.

Additionally, phreatophytes were not included in this model. These species are able to transport oxygen from the atmosphere to the rootzone through cavities in their tissues. These species can be mimicked by setting the threshold for oxygen stress tolerance for the wet adapted species at a (nearly) saturated level. However, the maintenance cost of this mechanism has then to be included in the model.

Soil formation, or more specifically, the accumulation of soil organic matter improves the infiltration and water retention capacity of the soil. This is especially important for textures with a high conductivity and low water retention capacity like sand. On the other hand, soil formation in clay soils can largely improve the infiltration capacity. The effect of soil formation is most significant in summer in the area where groundwater tables are deeper. In this situation water stress will decrease, because more water can be stored during winter and this water will be more slowly released to the roots in summer. This will cause increased assimilation rates and therefore more vegetation growth and biomass.

The model results show a relatively low biomass at the dry upslope area of the slope. This is lower than normally observed in the field for temperate climate conditions. This can be explained by the parameterization of the model, the absence of soil formation and the fixed rooting depth as described above. Two other reasons for the low biomass are the relatively low storage capacity at lower biomasses and a lack of water storage in the tree. Due to the allometric relations, the storage capacity at a low biomass is relatively low compared to the carbon that is used for leaf growth and respiration. The storage capacity grows linearly with biomass, while the increase in leaf area with biomass decreases. Therefore older trees have a relatively large storage, making them less prone to stress. The model assumes a quasi steady state, i.e. an

instant equilibrium between root water uptake and transpiration and no storage of water within the tree. This means that transpiration and assimilation react directly to atmospheric and soil moisture conditions. In reality on the scale of a tree, these assumptions are not completely valid. The response in transpiration and assimilation is attenuated, and therefore stress is expected to be less severe. The fact that no water storage in the tree is present results in more acute and probably more severe vegetation stress.

To better understand the value of the presented model a more thorough sensitivity analysis is needed. This will also provide a better understanding of the sensitivity of the system to changes in certain parameters. The separate modules have all been calibrated in other studies, but not all for the system that has been studied here. This study gives directions for further research, and to evaluate possible responses of the system.

6.3 Effect of spatio-temporal groundwater dynamics on vegetation growth

The effect of spatio-temporal groundwater dynamics on vegetation growth was determined, by studying both short-term and long-term vegetation dynamics along a hillslope. This was done using the coupled bio-physical-vegetation growth model as described in Chapter 3 coupled to the variably saturated three dimensional hydrological model as described in Chapter 4.

Analysis of local short term dynamics of the model shows that groundwater has a large influence on vegetation productivity (biomass, transpiration and carbon assimilation). Especially when groundwater is near the rootzone, groundwater causes a higher soil moisture content in the rootzone and therefore higher transpiration and carbon assimilation rates. The results of long-term (600 y) simulations reveal the influence of groundwater on spatial dynamics. Die-back of upslope dry adapted vegetation results in an increase in wet adapted vegetation downslope due to increased upslope groundwater recharge. This highlights the upslope-downslope connection in these ecosystems.

A sensitivity analysis of slope angle, aquifer thickness and precipitation (both magnitude and frequency), showed a great sensitivity of the system to these parameters, where both groundwater and vegetation react to changes. Especially systems with soil textures with a large capillary fringe and moderate conductivity are sensitive. This is in agreement with the results from Chapter 2 that were based on global maximization of evaporation or minimization of plant stress.

A comparison between simulation runs having static groundwater levels and simulation runs having a dynamic groundwater model shows that in case of a dynamic groundwater table a wider transition zone between the two vegetation types develops and that a higher biomass is reached within this zone. Temporal variations of groundwater levels thus create a wider zone of accommodation where competing species can

co-exist. Together with the upslope-downslope connectivity this demonstrates the importance of using a fully coupled spatio-temporal dynamic groundwater-vegetation model in temperate regions with shallow groundwater.

In this model the spatial interactions are limited to groundwater flow. In reality this is of course not the case as additional spatial interactions play a role. For example, in this model only vertical shading was modeled, while in reality trees do also shade neighboring trees, thereby influencing pattern formation. Horizontal competition for water by roots was not accounted for, although this also influences competition and patterns. Finally, variable rooting depth influences spatial patterning, because this causes a less extreme response of vegetation to soil moisture content and therefore a less abrupt transition between the species.

The hydrological part of the model can be extended with a better representation of surface runoff and discharge instead of assuming runoff to be instantly removed from the system. A better representation will for example allow for re-infiltration of runoff water causing wetter soil conditions. Also the simulation of riparian circumstances will then be possible.

6.4 Influence of climate change on a groundwater influenced temperate hillslope ecosystem

In Chapter 5, the effect of climate change on groundwater and vegetation in a temperate forest ecosystem was investigated. Current climate and projections of climate change were based on the situation for the city of Eindhoven, The Netherlands. Climate change projections created using statistical downscaling of an ensemble of GCM-RCM runs for the IPCC SRES A2 scenario for 2100 as performed in the PRUDENCE project (Christensen et al., 2007). The IPCC SRES A2 scenario shows an increase in CO₂ level from present day 370 ppm to 730 ppm in 2100. The average annual temperature of Eindhoven is expected to rise from 9.7 °C to 12.8-15.1 °C, while the average temperature increases about 3 °C in winter and 5 °C in summer. The projections based on the ECHAM4/OPYC GCM show a larger temperature increase than the projections based on the HadAM3H GCM. Precipitation is projected to decrease from present day 777 mm y⁻¹ to 759-682 mm y⁻¹. In summer precipitation will decrease, while in winter it will slightly increase. The decrease in precipitation is mainly caused by a decrease in the number of days that it rains, as the amount of rain on rainy days slightly increases. The projections based on the ECHAM4/OPYC GCM show a larger change in seasonal precipitation pattern (larger increase in winter and larger decrease in summer) than the projections based on the HadAM3H GCM. The GCM-RCM projections were subsequently used to calibrate a stochastic weather generator, which was then used to generate meteorological time series.

First local interactions, comparing the downslope and the upslope response to climate change, are described. Given the no-flow boundary condition for groundwater, change in precipitation regime has hardly any effect on downslope groundwater dynamics and rootzone soil moisture conditions. As a result the effect of precipitation on biomass

is negligible downslope. Upslope, where groundwater levels are deeper and the soil moisture content is lower, vegetation growth is limited by water availability, therefore the effect of change in precipitation regime is larger. As rootzone soil moisture content downslope is largely determined by the lateral groundwater influx, it remains high. Therefore, downslope carbon assimilation is not water limited and the effect of increased CO₂ concentration on biomass downslope is large. Upslope, the effect of elevated CO₂ concentration is much smaller as vegetation growth is water limited. Temperature rise causes respiration to increase more than carbon assimilation. This causes the biomass to decrease both upslope and downslope.

The results also clearly show upslope-downslope interaction. This is most pronounced as a result of change in precipitation regime; while yearly rainfall decreases, rainfall in winter increases. In this case, upslope groundwater recharge increases as a result of increased precipitation in winter in combination with a decrease of upslope biomass (due to increased water stress in summer), resulting in less evapotranspiration in summer. This results in groundwater level rise, which causes wetter conditions downslope and therefore an enlargement of the zone where wet adapted vegetation prevails.

Projected climate change, i.e. simultaneous change in precipitation, temperature and atmospheric CO₂ concentration causes biomass both upslope and downslope to decrease, indicating the dominance of the temperature (mostly downslope) and precipitation effect (mostly upslope). Surprisingly the projections based on the ECHAM4 GCM, show an increase in groundwater level and soil moisture content, while other projections show a decrease in both variables. The sign of the response is dependent on the magnitude of the climate change signal and is thus very non-linear in this system. The results, particularly the non-linear response on magnitude and the upslope-downslope effects, demonstrate that predicting the effect of climate change on this temperate ecosystem is far from straightforward and calls for models that fully couple biophysical vegetation models with the hydrological system. In short, we need eco-hydrological models that are robust under climate change.

These results only show the response of one system and one CO₂ emission scenario, although existing of an ensemble of eight projections. This study cannot be used to draw general conclusions about the effect of climate change in absolute sense. It mostly serves as an example to show the complexity of the response of the system and give directions for future research. As explained in Chapter 5 validation of the model or comparison of the model as a whole against field data is rather impractical. The validation of parts of the model is possible and can further improve predictions. Experiments with scaled but real vegetation on artificial hillslopes (Hopp et al., 2009; Kleinhans et al., 2010) may be a way to test whether non-linear effects observed in the simulations are a property of the model or of the real system.

It would be interesting to make a comparison between different vegetation models on a hillslope scale as has been done for global scale models (e.g. Cramer et al., 2001). Comparison should be made with different combinations of vegetation and hydrological models. Variably saturated hydrological models that are able to produce for long time series within reasonable time are however scarce and temporal upscaling procedures have to be used for most vegetation models.

It would also be interesting to study the effect of transient climate change instead of studying climate change using dynamic equilibrium conditions. In this research we resolved the effect of extreme events (e.g. very dry or wet years) on vegetation dynamics by using long time series (600 y), averaging out these dynamics. Monte carlo type simulations can be used to study the effect of transient climate change, to minimize the effect of extreme conditions during shorter simulation periods (100 y). However, this solution will dramatically increase calculation loads.

6.5 Vegetation stress in water and light limited forest ecosystems

In Chapter 2 it was suggested that minimization of vegetation stress could be used as a global emergent optimization criterion for determining the location of the boundary between different vegetation types. To further investigate minimization of vegetation stress as principle behind zonation in temperate forests, vegetation stress needs to be redefined in such a way that it can also be calculated in the model that was described in Chapters 3 and 4.

Static vegetation stress as defined by Porporato et al. (2001) is only depends on soil moisture content. In the model described in Chapter 3 vegetation stress can not directly be related to soil moisture content alone, because the reduction in transpiration and carbon assimilation is also strongly influenced by atmospheric demand (vapor pressure deficit, air temperature and radiation). Therefore, static vegetation stress is redefined as the reduction of carbon assimilation given the actual atmospheric conditions.

Both under wet and dry conditions root water uptake is restricted, and causes a drop in leaf water potential. Vegetation was defined to be under stress when the leaf water potential drops beneath the value $\Psi_{a,1}$ [Pa], which is the leaf water potential at which carbon assimilation starts to drop. At $\Psi_{a,0}$ [Pa] carbon assimilation completely stops. Static vegetation stress is therefore defined as:

$$\zeta = \begin{cases} 0 & \text{if } \Psi_l > \Psi_{a,1} \\ \left(1 - \frac{A_{n,act}}{A_{n,pot}}\right) & \text{if } \Psi_{a,0} < \Psi_l < \Psi_{a,1} \end{cases}, \quad (6.1)$$

where $A_{n,act}$ [mol m⁻²day⁻¹] is the actual carbon assimilation as calculated by the model and $A_{n,pot}$ [mol m⁻²day⁻¹] is the potential carbon assimilation given the actual atmospheric circumstances and vegetation properties and optimal soil moisture conditions. Different from the model described in Chapter 2 static water and oxygen stress are not calculated separately, as both high and low soil moisture contents cause more negative values of Ψ_l .

As described in Chapter 2 dynamic stress depends on the static stress and the period and the frequency of static stress during the growing season:

$$Stress_{dynamic} = \left(\frac{\zeta T_{stress}}{k T_{season}} \right)^{1/\sqrt{n_s}}, \quad (6.2)$$

where T_{stress} [y] is the mean duration of a stress period during the growing season, k [-] is a threshold value at which damage occurs to a plant, T_{season} [y] is the length of the growing season and n_s [-] is the number of stress periods during the growing season. The growing season is defined as the period during which the LAI is larger than 0.01.

Figure 6.1 shows the average values of groundwater level, soil moisture content, biomass and evapotranspiration over 600 years similar to Figure 4.5 in Chapter 4. Additionally the dynamic vegetation stress is shown. This figure shows that vegetation stress for the drought adapted species is highest downslope in the almost saturated zone, becomes lowest midslope and increases again upslope where the soil becomes dry. The wet species has generally the lowest stress downslope and stress increases moving upslope. Interestingly, upslope the wet species generally experiences the least amount of stress, which is contrary to what is expected based on the plants' reaction to water stress under dry circumstances alone.

Figure 6.2 shows the development of biomass and vegetation stress in time in a cell 400 m from the base of the slope. As expected, from the moment both species start growing the drought adapted species experiences less stress than the wet adapted species. It can also be seen that in this case the wet species starts with a little higher biomass, but the dry species is better adapted to the circumstances and therefore grows slightly faster and keeps up with the wet adapted species. From that moment on the vegetation stress of the wet adapted species drops below the stress of the drought adapted species. As the drought adapted species becomes taller than the wet adapted species, it captures more light, and consequently the ET driven by atmospheric demand increases. This causes a drop in leaf water potential and therefore an increase in vegetation stress. Despite the experienced stress due to a low leaf water potential, the light capture advantage causes higher carbon assimilation and therefore growth rates. At the same time the wet adapted species receives less light, causing a lower ET driven by atmospheric demand and less reduction of leaf water potential and therefore less water stress. This shows that in this situation water and oxygen stress are not sufficient to explain species prevalence. Using the concept of plant stress under circumstances with multiple species, thus asks for an approach which explicitly includes light stress. A further comparison between the models of Chapter 2 and 3 has therefore not been made.

6.6 Implications for other disciplines

In this study the interactions within an eco-hydrological system have been investigated using an eco-hydrological model. This model was forced with atmospheric conditions that were generated by a stochastic weather generator, which was based on global and regional climate models. The results of this study have implications for the individual fields of ecological, hydrological and climatological modeling.

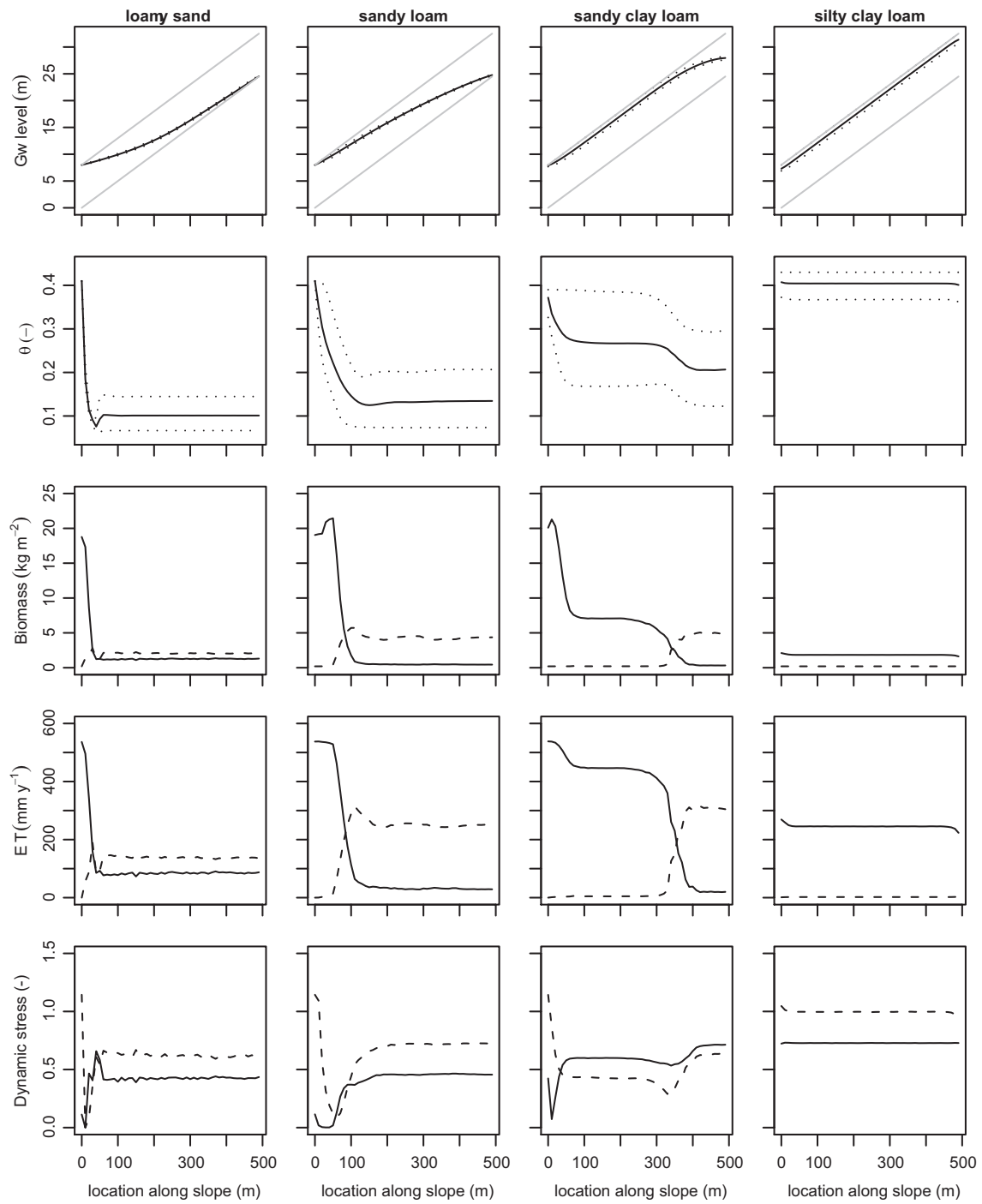


Figure 6.1 Groundwater level (Gw level), soil moisture content (θ), biomass, evapotranspiration (ET) and dynamic vegetation stress (Dynamic stress) along a hillslope for four different soil textures. 600 year and 100 cell (parallel to the slope) average values are shown. In Gw level and θ plot: solid line, average values and dotted line, yearly minimum and maximum values. In biomass, ET and dynamic stress plot: solid line, wet adapted species and dashed line, drought adapted species.

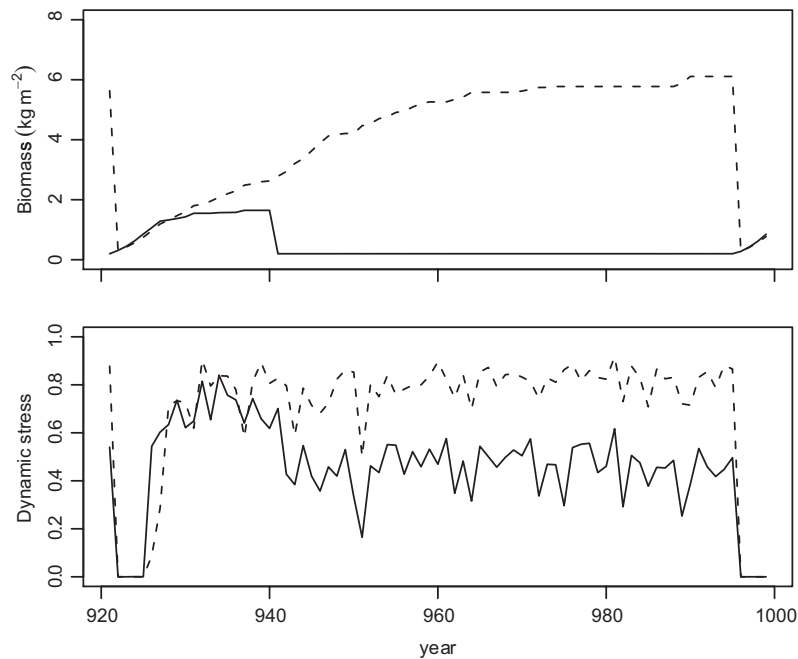


Figure 6.2 Development of biomass and dynamic vegetation stress during an 80 year period within one cell (400 m from the base of the slope) for sandy loam. The first time step shows the death of the previous vegetation. Solid line, wet adapted species and dashed line, drought adapted species.

6.6.1 Ecological modeling

Most ecological models do not account for the influence of groundwater on vegetation, let alone include temporal or spatial groundwater dynamics. As shown in Chapters 2-5 groundwater can have a significant influence on the soil moisture content and therefore on the vegetation.

In Chapter 3 a point model was used to show the influence of a static groundwater level. The presence of a static groundwater level close to the rootzone results in less dry soils in summer and therefore less water stress for vegetation, which results in more biomass. When studying a vegetation system that can be influenced by the presence of groundwater, groundwater needs to be accounted for in the model to correctly simulate carbon and evapotranspiration fluxes and resulting biomass. As groundwater dynamics are difficult to simulate in a 1-dimensional model, a static groundwater level can be used as boundary condition. Alternatively, when groundwater levels are measured in the field, these can be used directly as boundary condition in the model. These options are of course only valid in case one is solely interested in vegetation dynamics and not in hydrological interactions.

Chapter 4 shows the role of groundwater on the spatial distribution of vegetation and the effect of changing environmental conditions. When the same study to the effect on vegetation was conducted based on a static groundwater table, the upslope-downslope effect would be missed and the net ecosystem productivity would be wrongly pre-

dicted. A static groundwater level also narrows the transition zone along a groundwater gradient, and thereby exaggerates the difference between habitats. The simulated effects of climate change on vegetation, as described in Chapter 5, would have been different when the influence of groundwater dynamics, in particular the upslope-downslope interaction had not been included. Especially the non-linear effects of change in precipitation regime on vegetation showing an increase in average groundwater depth and an upward shift of wet-adapted species, could not have been captured by a standard vegetation model.

6.6.2 Climate modeling

Most climate models have a spatial resolution in the order of 1 degree and up. Based on this scale and the effect of within cell heterogeneity it is reasonable to not include lateral groundwater flow in the model. On the other hand, the local effect of groundwater can be significant through the groundwater, soil moisture, evaporation and precipitation feedback (e.g. Bierkens & van den Hurk, 2007; Jiang et al., 2009).

Several climate models, such as ECHAM4/OPYC or HadAM3H do incorporate dynamic vegetation models. However, these models are 1-dimensional and do not include competition other than the prevalence of the plant-functional type with the largest productivity. Several effects would be different if such a 1-dimensional model was to be replaced with a dynamic eco-hydrological model as described in Chapters 3 and 4. First, as shown in Chapter 5, a change of climate could lead to a shift of vegetation types upslope or downslope, which would only change the fraction of a plant functional type within a GCM cell, and not move entire cells. However, this buffering could be accounted for by an intelligent sub-grid parameterization. Moreover, the wet and dry adapted vegetation in the Chapter 5 model may well fall within the same plant functional type, so that effects would be lost. Second, the non-linear response of groundwater recharge, groundwater levels and biomass to changes in rainfall distributions over the year, as demonstrated in Chapter 5, may have an effect on the way climate change affects evaporation and runoff in a GCM cell. This effect may certainly be non-negligible. Finally, a third and most important difference between the eco-hydrological model presented here and current dynamic vegetation models included in climate models is temporal behavior. Even if we assume a seedbank to be present of all species everywhere, it takes decades or even centuries before one vegetation type is replaced by a better adapted species. The feedback of this resilience in vegetation response onto the climate system may therefore be much different from an instantaneous response as is currently used. If GCM runs need to move from equilibrium simulations over time slices to real transient simulations, then spatio-temporal vegetation models such as presented here are a prerequisite.

6.6.3 Hydrological modeling

Hydrology is greatly influenced by vegetation. Chapter 3 to 5 show that vegetation greatly determines the fractioning of water fluxes at the surface, dividing precipitation into throughfall and interception and therefore evaporation. The throughfall that

infiltrates into the soil then either percolates or is taken up by roots. The last one basically depends on the root density, root water uptake capability and the atmospheric demand.

Most hydrological studies use the Penman-Monteith (Monteith, 1965) equation for calculating evapotranspiration. The Penman-Monteith equation yields a reference evapotranspiration. A crop factor needs to be applied to this reference evapotranspiration to correct for the vegetation type, yielding the potential evapotranspiration. To account for reduction of evapotranspiration as a result of dry or wet soil moisture conditions a Feddes et al. (1978) type function needs to be used, resulting in the so called actual evapotranspiration. This formulation is often used in hydrological modeling. Although the Penman-Monteith equation is valid for a large range of atmospheric conditions, reduction of evapotranspiration under more extreme atmospheric conditions, e.g. temperatures higher than 30 °C is not included in the equation. One solution to account for this is using a Jarvis (1976) type formulation of g_s that relates surface resistance to ambient variables including air temperature. However, the Jarvis model relates the surface resistance directly to environmental conditions and not to the plant's physiological state as measured by the leaf water potential. As shown in Chapter 4, including a biophysical vegetation model thus yields a richer response of evaporation to environmental conditions than Penman-Monteith, even if a classic Jarvis model is included.

Using static vegetation is often acceptable in hydrological modeling, when current conditions are simulated. However, if the effect of climate change is modeled, vegetation dynamics will significantly alter, which influences vegetation growth, ET and groundwater recharge and therefore the hydrological system as a whole. Chapter 5 shows that care should be taken when simply implementing static vegetation in climate effect studies. In fact, if the aim is to determine how evaporation, groundwater recharge and groundwater levels are changing, a dynamic vegetation model that is fully coupled to a spatio-temporal hydrological model is required.

6.7 Main contributions and insights

The main contributions to eco-hydrology and new insights provided in this thesis are:

- It provides important new elements of the eco-hydrology of humid groundwater dominated vegetation in a quantitative manner, like oxygen stress and light competition, and is original and unique compared to the eco-hydrology of water-limited systems that dominates literature.
- It shows that feedbacks between vegetation and a hydrological system in which topographically driven groundwater flow is important, result in several counter-intuitive effects when analyzing the effect of climate change, e.g., a decrease in yearly average rainfall may result in an increase of groundwater levels and dominance of wet-adapted species.

- It underlines the importance of using multiple climate projections as input for climate change effect studies, as climate projections that show the same tendency (decrease of annual rainfall, increase of rainfall in winter, decrease of rainfall in summer) but at different intensity can have an opposite effect on groundwater recharge and groundwater levels.
- It is shown that the concept of plant stress as measure of plant fitness (as defined by Porporato et al. (2001)) does not hold if competition for light is involved, unless light stress is included explicitly.

A Parameters Chapter 3

General parameters

Variable	Value	Unit	Description	Source
γ_w	0.0	Pa K ⁻¹	psychrometer constant	Daly et al. (2004)
λ_w	2500000	J kg ⁻¹	latent heat of water vaporization	Daly et al. (2004)
ρ_{air}	1.2	kg m ⁻³	air density	Daly et al. (2004)
ρ_w	1000	kg m ⁻³	water density	-
c_p	1012	J kg ⁻¹ K ⁻¹	air specific heat at constant pressure	Daly et al. (2004)
G	9.81	m s ⁻²	gravitational acceleration	-
P	101325	Pa	air pressure	-
R	8.31	J mol ⁻¹ K ⁻¹	gas constant	-

Atmospheric parameters

wg = from weahter generator

Variable	Value	Unit	Description	Source
δ	-	h	day length	variable
Δ	-	Pa K ⁻¹	slope of the water vapour pressure to temperature	variable
a_s	0.25	-	fraction of Rad_0 on overcast days	Allen et al. (1998)
a_c	0.25	-	empirical constant	Allen et al. (1998)
a_e	0.34	-	empirical constant	Allen et al. (1998)
b_s	0.5	-	empirical constant	Allen et al. (1998)
b_c	0.75	-	empirical constant	Allen et al. (1998)
b_e	-0.14	kPa-0.5	empirical constant	Allen et al. (1998)
C_a	360	mol mol ⁻¹	carbon concentration of atmosphere	Daly et al. (2004)
D	-	Pa	vapor pressure	wg
D_x	0.0077	kg kg ⁻¹	water vapor 'max' deficit	Daly et al. (2004)
e_{max}	-	kPa	saturation vapour pressure at T_{max}	variable
e_{min}	-	kPa	saturation vapour pressure at T_{min}	variable
e_a	-	kPa		variable
N	-	h	maximum number hours of sunshine	wg
n	-	h	actual number of hours of sunshine	wg
P	101325	Pa	air pressure	mean at sealevel
Rad_{max}	-	W	maximum radiation at top of canopy at noon	wg
Rad_l	-	W	longwave radiation	variable
Rad	-	W	actual radiation	variable
T_a	-	°C	actual air temperature	wg
t_{day}	-	h	time of day	variable
$T_{max,C}$	-	°C	maximum air temperature	wg
$T_{max,K}$	-	K	maximum air temperature	wg
$T_{min,C}$	-	°C	minimum air temperature	wg
$T_{min,K}$	-	K	minimum air temperature	wg
$t0$	-	h	time of sunrise	variable

Soil parameters

Variable	Value	Unit	Description	Source
α	see Table 3.2	m	soil physical parameter, van Genuchten	Carsel (1988)
ψ_s	-	Pa	matric potential	var
θ_{sat}	see Table 3.2	-	saturated soil moisture content	Carsel (1988)
θ_r	see Table 3.2	-	residual soil moisture content	Carsel (1988)
θ	-	-	soil moisture content	var
h_{gw}	-	m	depth of groundwater	var
K_θ	-	m s^{-1}	unsaturated conductivity	var
K_{sat}	see Table 3.2	m d^{-1}	saturated conductivity	Carsel (1988)
m	$1 - (1./n)$	-	soil physical parameter, van Genuchten	van Genuchten (1980)
n	see Table 3.2	-	soil physical parameter, van Genuchten	Carsel (1988)
Q_v	-	m s^{-1}	vertical exchange flux between rootzone and groundwater	var
Z_r	0.6	m	soil depth	this article

Vegetation parameters

Variable	Value	Unit	Description	Source
α	0.5	-	fraction reflected radiation	Friend (1995)
Γ^*	-	mol C mol^{-1} air	CO ₂ compensation point	variable
γ_0	34.6e-6	mol mol^{-1}	CO ₂ compensation point	Daly et al. (2004)
γ_1	0.0451	K^{-1}	empirical constant for calculation of Γ	Daly et al. (2004)
γ_2	0.000347	K^{-2}	empirical constant for calculation of Γ	Daly et al. (2004)
$\lambda_{sapwood}$	1	-	sapwood fraction of total stem biomass	variable
ψ_0	-4.5e6	Pa	leaf water potential where g_s becomes 0	Daly et al. (2004)
ψ_1	-0.05e6	Pa	leaf water potential where g_s begins to decline	Daly et al. (2004)
ψ_{a0}	-4.5e6	Pa	leaf water potential where assimilation becomes 0	Daly et al. (2004)
ψ_{a1}	-0.5e6	Pa	leaf water potential where assimilation begins to decline	Daly et al. (2004)
ψ_l	-	Pa	leaf water potential	variable
ρ_{stem}	350	kg m^{-3}	wood density	Schwalm & Ek (2004)
a_{md}	0.1	-	allometric scaling, tree dimension	Zianis & Radoglou (2006)
a_{nrtree}	30	-	allometric scaling, number of trees	this article
a_{sw}	-	kg^{-1}	parameter controlling sapwood area	this article
a	-	-	parameter influencing RAI	variable
An	-	$\text{mol m}^{-2} \text{s}^{-1}$	carbon assimilation	variable
$An_{\psi,l}$	-	-	carbon assimilation reduction due to low ψ_l	variable
An_{bio}	-	$\text{mol m}^{-2} \text{s}^{-1}$	carbon assimilation based biochemical processes	variable
An_{gsba}	-	$\text{mol m}^{-2} \text{s}^{-1}$	carbon assimilation based on stomatal conductance	variable
An_c	-	$\text{mol m}^{-2} \text{s}^{-1}$	carbon assimilation based biochemical capacity, per unit leaf area	variable
An_Q	-	$\text{mol m}^{-2} \text{s}^{-1}$	carbon assimilation based on radiation, per unit leaf area	variable
$APAR$	-	W	absorbed photosynthetic active radiation	variable

Continued on next page

<i>continued from previous page</i>				
Variable	Value	Unit	Description	Source
AR_L	-	W	absorbed radiation of layer L	variable
B_{above}	-	kg	aboveground biomass per cell	variable
B_{lai}	-	kg	biomass of LAI	variable
B_{mol}	-	mol	biomass per cell	variable
$b_{nr\ tree}$	6900	-	allometric scaling, number of trees	this article
B_{sw}	mol	kg	sapwood biomass	variable
b_{tree}	2.5	-	allometric scaling, tree dimension	Zianis & Radoglou (2006)
B_{tree}	-	kg	biomass per tree	variable
$C_{f,root}$	0.3	-	C fraction of root	Foley et al. (1996)
$C_{f,stem}$	0.3	-	C fraction of stem	Foley et al. (1996)
$C_{fraction}$	0.45	-	carbon fraction of dry biomass	Ollinger & Smith (2005)
C_i	-	mol C mol ⁻¹ air	intercellular carbon concentration	variable
$cn_{r\ tree}$	0.43	-	allometric scaling, number of trees	this article
c	2	-	parameter of the vulnerability curve	Daly et al. (2004)
cn_{leaf}	29	-	leaf C:N ratio	Sitch et al. (2003)
cn_{root}	29	-	root C:N ratio	Sitch et al. (2003)
$cn_{sapwood}$	330	-	sapwood C:N ratio	Sitch et al. (2003)
D_{stem}	-	m	diameter of stem	variable
$d_{z,crown,i}$	-	m	thickness of canopy layer L for species i	variable
d	2e6	Pa	parameter of the vulnerability curve	Daly et al. (2004)
E_O	-	m s ⁻¹	open water evapotranspiration	variable
ET_{pm}	-	m s ⁻¹	transpiration according to Penman-Monteith equation	variable
f_{ψ_l}	-	-	leaf water potential reduction function, for g_s	variable
f_{above}	0.8	-	above ground biomass fraction	this article
f_D	-	-	water vapour deficit reduction function, for g_s	variable
f_{gap}	-	-	canopy gap fraction	variable
f_{ox}	-	-	reduction function for oxygen stress	variable
f_{Rad}	-	-	radiation reduction function, for g_s	variable
f_{store}	0.11	-	fraction of sapwood for storage	Friend et al. (1997)
f_{Ta}	-	-	air temperature reduction function, for g_s	variable
$g_{a,CO2}$	g_a/LAI	mol m ⁻² s ⁻¹	atmospheric conductance for CO ₂	Jones in Daly et al. (2004)
g_a	0.02	m s ⁻¹	atmospheric conductance	Daly et al. (2004)
$g_{b,CO2}$	$g_b/1.37$	mol m ⁻² s ⁻¹	leaf boundary layer conductance for CO ₂	Jones in Daly et al. (2004)
g_b	0.02	m s ⁻¹	leaf boundary layer conductance	Daly et al. (2004)
$g_{ba,CO2}$	-	mol m ⁻² s ⁻¹	conductance boundary layer atmosphere	variable
$g_{p,max}$	11.7e-12	m Pa ⁻¹ s ⁻¹	maximum plant conductance	Daly et al. (2004)
$g_{s,CO2}$	$g_s/1.6$	mol m ⁻² s ⁻¹	stomatal conductance for CO ₂	Jones in Daly et al. (2004)
$g_{s,max}$	0.01	ms ⁻¹	maximum stomatal conductance	Breuer et al. (2003)
$g_{sba,CO2}$	-	mol m ⁻² s ⁻¹	series of conductances for CO ₂	variable
g_{srp}	-	m Pa ⁻¹ s ⁻¹	soil root plant conductance	variable
g_s	-	ms ⁻¹	stomatal conductance	variable
H_{dJ}	201000	J mol ⁻¹	deactivation energy for J_{max}	Daly et al. (2004)
H_{dV}	202900	J mol ⁻¹	the energy of deactivation	Daly et al. (2004)
H_{Kc}	59430	J mol ⁻¹	activation energy for k_c	Daly et al. (2004)
H_{Ko}	36000	J mol ⁻¹	activation energy for k_o	Daly et al. (2004)
H_{tree}	-	m	height of tree	variable
H_{vJ}	79500	J mol ⁻¹	activation energy for J_{max}	Daly et al. (2004)
H_{vV}	116300	J mol ⁻¹	the energy of activation	Daly et al. (2004)
I_{cap}	0.0005	m	interception capacity	this article
I_{max}	-	m s ⁻¹	maximum interception	variable
J_{max}	-	mol m ⁻² s ⁻¹	electron flux	variable
$J_{max,0}$	75e-6	mol electrons m ⁻² s ⁻¹	potential rate of whole-chain electron transport at T_0	Daly et al. (2004)

Continued on next page

<i>continued from previous page</i>				
Variable	Value	Unit	Description	Source
J	-	mol photons $s^{-1} m^{-2}$	incident electron flux of APAR	variable
K_{c0}	302e-6	mol mol ⁻¹	Michaelis Menten constant for CO ₂	Daly et al. (2004)
K_{o0}	0.256	mol mol ⁻¹	Michaelis Menten constant for O ₂	Daly et al. (2004)
k_1	0.95	-	shape parameter for calculation of J_{max}	Daly et al. (2004)
k_1	0.005	m ² W ⁻¹	radiation sensitivity constant for Jarvis	Daly et al. (2004)
k_2	0.0016	K ⁻²	temperature sensitivity constant for Jarvis	Daly et al. (2004)
k_2	0.2	mol electrons mol ⁻¹ photons	quantum yield of whole-chain electron transport at T_0 for calculation of J_{max}	Daly et al. (2004)
k	0.5	-	light extinction coefficient	jarvis and leverenz 1983 in Woodward et al. (1995)
LAD	-	m ⁻¹	leaf area density	variable
LAI_d	0.1	m s ⁻¹	LAI decline rate	this article
LAI_g	0.03	m s ⁻¹	LAI growth rate	this article
$LAI_{L,i}$	-	-	LAI of canopy layer L for species I	variable
LAI_L	-	-	LAI of canopy layer L	variable
LAI_{max}	-	-	maximum LAI given biomass	variable
LAI	5.0	-	leaf area index	Breuer et al. (2003)
M_{stem}	-	kg	mass in stem	variable
n_f	5000	m m ⁻¹	foliage to sapwood ratio	this article
N_{Tr}	-	-	number of trees ha ⁻¹	variable
o_i	0.209	mol O air mol ⁻¹	intercellular carbon concentration	Daly et al. (2004)
$OX1_\theta$	0.3	-	soil moisture content where root water uptake begins to decline	this article
$OX2_\theta$	0.4	-	soil moisture content where root water uptake becomes 0	this article
P_{ind}	-	m	indirect precipitation, throughfall	variable
P_{int}	-	m	interception	variable
R_{growth}	0.3* An	mol m ⁻² s ⁻¹	growth respiration	Dufrène et al. (2005)
R_{leaf}	0.015* V_{cmax}	mol m ⁻² s ⁻¹	leaf respiration	variable
r	0.066	g C g N d ⁻¹	tissue respiration rate at 10 °C	Sitch et al. (2003)
RAI_{frac}	1.5	-	RAI-LAI fraction	this article
RAI	-	-	root area index	variable
S_v	650	J mol ⁻¹	entropy term	Daly et al. (2004)
S	-	mol	carbon storage of tree	variable
SLA	37	m ² kg ⁻¹	specific leaf area	Zianis & Radoglou (2006)
T_0	-273	°C	absolute minimum temperature	this article
T_0	293.2	K	optimal temperature for carbon assimilation	Daly et al. (2004)
T_a	-	°C	actual temperature	this article
T_l	-	K	leaf temperature	variable
T_{opt}	298	K	optimal temperature of g_s for Jarvis	Daly et al. (2004)
T_{root}	10	°C	temperature of root	this article
T_{stem}	10	°C	temperature of stem	this article
T_{sum}	100	°C	temperature sum leaf growth	this article
$\overline{T_{day}}$	-	°C	mean day temperature	variable
$\overline{T_{year}}$	-	°C	mean year temperature	variable
$V_{c,max}$	-	mol m ⁻² s ⁻¹	maximum carboxylation rate at T	variable
V_{cmax0}	50e-6	mol m ⁻² s ⁻¹	maximum carboxylation rate at T_0	Daly et al. (2004)
V_{stem}	-	m ³	volume of stem	variable
Z_{sw}	-	m ²	sapwood area at breast height	variable

B Parameters Chapter 4

Groundwater model parameters

variable means variable within run; constant means constant within run

Variable	Value	Unit	Description	Source
$\Delta Z_1, \Delta Z_2, \Delta Z_3$	-	m	distance between nodes	variable
ψ_1, ψ_2, ψ_3	-	m	matric potential of layer	variable
$\theta_{E,1}, \theta_{E,2}, \theta_{E,3}$	-	-	relative degree of saturation of layer	variable
ET	-	m	soil evapotranspiration	variable
$Grad_1, Grad_2, Grad_3$	-	-	gradient in potential between nodes	variable
H_1, H_2, H_3	-	m	water level within layer	variable
$k_{\theta E,1}, k_{\theta E,2}, k_{\theta E,3}$	-	m d ⁻¹	unsaturated hydraulic conductivity of layer	variable
$k_{Sat,1}, k_{Sat,2}, k_{Sat,3}$	-	m d ⁻¹	saturated hydraulic conductivity of layer	constant
P	-	m	precipitation	variable
Q_{Cap}	-	m	capillary rise flux	variable
Q_{Sat}	-	m ³	saturated lateral flux	variable
Q_0	-	m	total net precipitation (direct and indirect throughfall)	variable
Q_1, Q_2, Q_3	-	m	amount of water transferred vertically between layers	variable
Q_4	-	m	loss across the lithic contact	variable
$StorMat_1, StorMat_2, StorMat_3$	-	m	unsaturated matric storage in layer	variable
$StorSat$	-	m	saturated storage	variable
T_1, T_2, T_3	-	m	thickness of layer	constant
t	-	d	time step	constant
$Trans$	-	m ² d ⁻¹	total transmissivity over saturated zone	variable
$TransMat_1, TransMat_2, TransMat_3$	-	m	actual transpiration loss of layer/rootwater uptake	variable
WL	-	m	groundwater level in column, relative to Z_0	variable
$x+, x-, y+, y-$	-	-	locations upstream and downstream along the orthogonal flow directions in x and y directions	constant
Z_{WL}	-	m	piezometric elevation of water level relative to a common datum Z_0	variable
Z_0	0	m	common data at bottom of soil column	constant
Z_1, Z_2, Z_3	-	m	location of calculation node	variable
Z_4	-	m	height of calculation node at groundwater level	variable
Z	-	m	thickness of profile	constant

Other parameters used in the text

wg means from weather generator

Variable	Value	Unit	Description	Source
δ	-	-	day length	variable
ψ_l	-	Pa	leaf water potential	variable
θ	-	-	soil moisture content	variable
e_a	-	Pa	atmospheric vapor pressure	variable
H	-	m	tree height	variable
LAI	-	-	leaf area index	variable
n/N	-	-	fraction of cloud cover	wg
P	-	mm/d	precipitation	wg
Rad	-	$W\ m^{-2}$	radiation	wg
RAI	-	-	root area index	variable
T_{max}	-	$^{\circ}C$	maximum temperature	wg
T_{min}	-	$^{\circ}C$	minimum temperature	wg

Abstract

In temperate climates groundwater can have a strong effect on vegetation, because it can influence the spatio-temporal distribution of soil moisture and therefore water and oxygen stress of vegetation. Current IPCC climate projections based on CO₂ emission scenarios show a global temperature rise and change in precipitation regime, which will affect hydrological and vegetation systems.

This thesis provides a quantitative framework for studying eco-hydrology in groundwater influenced temperate ecosystems. Models with increased complexity have been developed, to investigate the interactions and dynamics of these ecosystems and determine their response to climate change.

The final model combines a dynamic bio-physiologically based vegetation model to simulate vegetation dynamics and competition and a physically-based variably-saturated hydrological model. In this model transpiration and stomatal conductance depend on atmospheric forcing and soil moisture content. Carbon assimilation depends on environmental conditions, stomatal conductance and biochemical processes. Light competition is driven by vegetation height and water competition is driven by root water uptake and the vegetation's response to water and oxygen stress. Modeled and measured atmospheric H₂O and CO₂ fluxes compare well on a diurnal and a yearly timescale. Long term simulations reproduce realistic densities of wet and dry adapted vegetation along a wet to dry gradient. The results clearly show the importance of simulating groundwater on modeled vegetation dynamics. This involves both the presence of groundwater and the upslope-downslope interactions through lateral groundwater connection. The influence of groundwater is apparent for a large range of groundwater depths, by both capillary rise and water logging. The results also show the influence of vegetation dynamics, composition, patterns and biomass on the water balance of a forest ecosystem and therefore groundwater dynamics. Water and oxygen stress can occur simultaneously within a slope and at the same location throughout a year. Light competition is important as the light capturing advantage of established vegetation most often overrules water and oxygen competition.

The response to climate change is investigated by forcing the coupled model with an ensemble of nested global and regional climate models, representing the IPCC SRES A2 scenario for 2100. A stochastic weather generator is calibrated to each GCM-RCM combination. All projections show higher temperatures and less precipitation. Results show that increased atmospheric CO₂ concentration results in higher biomasses due to a higher water use efficiency and less evaporation downslope where vegetation

growth is light limited. Change in precipitation regime (drier summer, wetter winter) causes decreased biomass and increased upslope groundwater recharge, resulting in groundwater rise and an upward shift of wet adapted vegetation. Temperature rise results in a lower biomass, because respiration increases stronger than carbon assimilation, while increased transpiration causes drier soils and prolonged periods of water limited growth. The combined effect of CO₂ and temperature rise change in precipitation regime is dominated by temperature rise and change in precipitation regime, causing a lower biomass. The effect on groundwater level depends on the degree by which precipitation distribution changes, showing a drop at a small difference between summer and winter precipitation and a rise at a large difference. This underlines the importance of investigating multiple climate projections in climate change effect studies.

This study shows that quantifying and understanding the response of temperate forest ecosystems to climate change requires combined physically-based hydrological and bio-physically-based vegetation models.

Samenvatting

Effect van klimaatverandering op gematigde boscosecosystemen

In gematigde klimaatgebieden heeft grondwater een sterke invloed op vegetatie, omdat het de spatio-temporele patronen van bodemvocht en daarmee water- en zuurstofstress van vegetatie kan beïnvloeden. De huidige IPCC-klimaatprojecties, die gebaseerd zijn op CO₂-emissiescenario's laten een globale temperatuurstijging en een verandering in neerslagregime zien. Deze veranderingen zullen effect hebben op hydrologische en vegetatiesystemen. In dit proefschrift wordt een kwantitatief kader gepresenteerd voor het bestuderen van ecohydrologie in grondwaterbeïnvloede gematigde ecosystemen.

Om de interactie en dynamiek van deze systemen te onderzoeken en de reactie op klimaatverandering te bepalen, zijn modellen met toenemende complexiteit ontwikkeld. Het uiteindelijke model combineert een dynamisch biofysisch-gebaseerd vegetatiemodel voor het bestuderen van vegetatiedynamiek en -competitie en een fysisch-gebaseerd verzadigd-onverzadigd hydrologisch model. In dit model zijn transpiratie en stomatale weerstand afhankelijk van atmosferische omstandigheden en bodemvocht. De koolstofassimilatie is afhankelijk van atmosferische omstandigheden, stomatale weerstand en biochemische processen. De competitie voor licht is afhankelijk van vegetatiehoogte en de competitie voor water wordt bepaald door het bodemvochtgehalte en de reactie van vegetatie op water en zuurstofstress.

Gemodelleerde en gemeten atmosferische H₂O- en CO₂-fluxen komen goed overeen op de tijdschaal van een dag en van een jaar. De simulaties op lange termijn reproduceren realistische verdelingen van aan natte en droge omstandigheden aangepaste vegetatie langs een nat-droog-gradiënt. De resultaten tonen duidelijk het belang van het simuleren van grondwater op gesimuleerde vegetatiedynamiek. Dit geldt voor zowel de aanwezigheid als voor de interactie van grondwater tussen hoge en lage gebieden als gevolg van laterale grondwaterstroming. Grondwater heeft een duidelijke invloed over een groot bereik van grondwaterdieptes, door zowel capillaire nalevering als grondwaterstagnatie. De resultaten tonen ook de invloed van vegetatiedynamiek, samenstelling, patronen en biomassa op de waterbalans van een boscosestroom en daarmee op de grondwaterdynamiek. Water- en zuurstofstress kunnen gelijktijdig binnen een helling en op verschillende momenten op dezelfde plaats voorkomen. Het belang van lichtcompetitie komt naar voren in het lichtvoordeel van gevestigde vegetatie dat overheerst boven een mogelijk voordeel door water- of zuurstofcompetitie.

De reactie van ecosystemen op klimaatverandering is onderzocht met behulp van

het hierboven beschreven model. De atmosferische aansturing vindt plaats door een stochastische weergenerator die is aangepast op basis van een ensemble van geneste globale en regionale klimaatmodellen. Dit ensemble is gebaseerd op het A2-scenario IPCC SRES voor 2100. Alle projecties laten hogere temperaturen en minder neerslag zien. De modelresultaten laten zien dat de verhoogde atmosferische CO₂-concentratie leidt tot een hogere biomassa, die veroorzaakt wordt door een hogere efficiëntie van het watergebruik en minder verdamping aan de voet van de helling waar de vegetatiegroei lichtgelimiteerd is. De verandering in neerslagregime (drogere zomers, nattere winters) veroorzaakt een verminderde biomassa en verhoogde grondwateraanvulling hoger op de helling, wat resulteert in grondwaterstijging en helling opwaartse verschuiving van natte vegetatie. De stijging in temperatuur resulteert in een lagere biomassa, omdat de respiratie sterker toeneemt dan de koolstofassimilatie en de verhoogde transpiratie leidt tot drogere bodems en langere periodes van water gelimiteerde groei. Het gecombineerde effect van CO₂- en temperatuurstijging en verandering in neerslagregime wordt overheerst door temperatuurstijging en verandering in neerslagregime, wat leidt tot een lagere biomassa. Het effect op het grondwaterniveau hangt af van de mate van verandering in neerslagverdeling, resulterend in een daling bij een klein verschil tussen zomer- en winterneerslag en een stijging bij een groot verschil. Dit onderstreept het belang van het gebruik van meerdere klimaatprojecties in klimaat effect studies.

Deze studie toont aan dat het kwantificeren en het begrijpen van de reactie van grondwaterbeïnvloede ecohydrologische systemen op klimaatverandering vereist dat gebruikgemaakt wordt van gecombineerde fysisch-gebaseerde hydrologische en biofysisch-gebaseerde vegetatiemodellen.

Bibliography

- ABBOTT, M. B., J. C. BATHURST, J. A. CUNGE, P. E. O'CONNELL & J. RASMUSSEN (1986a), An introduction to the European hydrological system - systeme hydrologique Europeen, SHE, 1: History and philosophy of a physically-based, distributed modelling system. *Journal of Hydrology* 87, pp. 45–59.
- ABBOTT, M. B., J. C. BATHURST, J. A. CUNGE, P. E. O'CONNELL & J. RASMUSSEN (1986b), An introduction to the European hydrological system - systeme hydrologique Europeen, SHE, 2: Structure of a physically-based, distributed modelling system. *Journal of Hydrology* 87, pp. 61–77.
- ALLEN, R., L. PEREIRA, D. RAES & M. SMITH (1998), Crop evapotranspiration. Guidelines for computing crop water requirements. Tech. Rep. 56, FAO.
- ARORA, V. K. (2002), Modeling vegetation as a dynamic component in soil-vegetation-atmosphere transfer schemes and hydrological models. *Reviews of Geophysics* 40, pp. 3–1.
- ARORA, V. K. & G. J. BOER (2006), Simulating competition and coexistence between plant functional types in a dynamic vegetation model. *Earth Interactions* 10.
- BAND, L. E., P. PATTERSON, R. NEMANI & S. W. RUNNING (1993), Forest ecosystem processes at the watershed scale - incorporating hillslope hydrology. *Agricultural and Forest Meteorology* 63, pp. 93–126.
- BARTHOLOMEUS, R. P., J. P. M. WITTE, P. M. VAN BODEGOM & R. AERTS (2008a), The need of data harmonization to derive robust empirical relationships between soil conditions and vegetation. *Journal of Vegetation Science* 19, pp. 799–808.
- BARTHOLOMEUS, R. P., J. P. M. WITTE, P. M. VAN BODEGOM, J. C. VAN DAM & R. AERTS (2008b), Critical soil conditions for oxygen stress to plant roots: Substituting the feddes-function by a process-based model. *Journal of Hydrology* 360, pp. 147–165.
- BEVEN, K. (1979), A sensitivity analysis of the penman-monteith actual evapotranspiration estimates. *Journal of Hydrology* 44, pp. 169–190.
- BIERKENS, M. F. P. & B. VAN DEN HURK (2007), Groundwater convergence as a possible mechanism for multi-year persistence in rainfall. *Geophysical Research Letters* 34.
- BOOGAARD, H., C. VAN DIEPEN, R. ROTTER, J. CABRERA & H. VAN LAAR (1998), WOFOST 7.1 Users guide for the WOFOST 7.1 crop growth simulation model and WOFOST Control Center 1.5. Tech. Rep., DLO Winand Staring Centre.
- BOSCH, S. (2006), Nutrients in the old growth forest of Białowieża, Poland. Master's thesis.
- BOTKIN, D. B., J. F. JANAK & J. R. WALLIS (1972), Some ecological consequences of a computer model of forest growth. *Journal of Ecology* 60, pp. 849–872.
- BREUER, L., K. ECKHARDT & H.-G. FREDE (2003), Plant parameter values for models in temperate climates. *Ecological Modelling* 169, pp. 237–293.
- BROLSMA, R. J. & M. F. P. BIERKENS (2007), Groundwater-soil water-vegetation dynamics in a temperate forest ecosystem along a slope. *Water Resources Research* 43.

- BROLSMA, R. J., D. KARSSENBERG & M. F. P. BIERKENS (2010a), Vegetation competition model for water and light limitation. I: Model description, one-dimensional competition and the influence of groundwater. *Ecological Modelling* 221, pp. 1348–1363.
- BROLSMA, R. J., L. P. H. VAN BEEK & M. F. P. BIERKENS (2010b), Vegetation competition model for water and light limitation. II: Spatial dynamics of groundwater and vegetation. *Ecological Modelling* 221, pp. 1364–1377.
- BRUTSAERT, W. (1994), The unit response of groundwater outflow from a hillslope. *Water Resources Research* 30, pp. 2759–2763.
- BURTON, A., C. G. KILSBY, H. J. FOWLER, P. S. P. COWPERTWAIT & P. E. O’CONNELL (2008), Rainsim: A spatial-temporal stochastic rainfall modelling system. *Environmental Modelling and Software* 23, pp. 1356–1369.
- CARSEL, R. (1988), Developing joint probability distributions of soil water retention characteristics. *Water Resources Research* 5, pp. 755–769.
- CHRISTENSEN, J. H., T. R. CARTER, M. RUMMUKAINEN & G. AMANATIDIS (2007), Evaluating the performance and utility of regional climate models: the PRUDENCE project. *Climatic Change* 81, pp. 1–6.
- COUWENBERG, J. & H. JOOSTEN (2005), Self-organization in raised bog patterning: the origin of microtope zonation and mesotope diversity. *Journal of Ecology* 93, pp. 1238–1248.
- COWPERTWAIT, P. S. P. (1995), A generalized spatial-temporal model of rainfall based on a clustered point process. *Proceedings: Mathematical and Physical Sciences* 450, pp. 163–175.
- CRAMER, W., A. BONDEAU, F. I. WOODWARD, I. C. PRENTICE, R. A. BETTS, V. BROVKIN, P. M. COX, V. FISHER, J. A. FOLEY, A. D. FRIEND, C. KUCHARIK, M. R. LOMAS, N. RAMANKUTTY, S. SITCH, B. SMITH, A. WHITE & C. YOUNGMOLLING (2001), Global response of terrestrial ecosystem structure and function to CO₂ and climate change: results from six dynamic global vegetation models. *Global Change Biology* 7, pp. 357–373.
- DALY, E., A. PORPORATO & I. RODRIGUEZ-ITURBE (2004), Coupled dynamics of photosynthesis, transpiration, and soil water balance. part I: Upscaling from hourly to daily level. *Journal of Hydrometeorology* 5, pp. 546–558.
- DALY, E., Y. ZINGER, A. DELETIC & T. D. FLETCHER (2009), A possible mechanism for soil moisture bimodality in humid-land environments. *Geophys. Res. Lett.* 36.
- DAVI, H., E. DUFRÈNE, C. FRANÇOIS, G. LE MAIRE, D. LOUSTAU, A. BOSC, S. RAMBAL, A. GRANIER & E. MOORS (2006), Sensitivity of water and carbon fluxes to climate changes from 1960 to 2100 in European forest ecosystems. *Agricultural and Forest Meteorology* 141, pp. 35–56.
- DUFRÈNE, E., H. DAVI, C. FRANÇOIS, G. LE MAIRE, V. LE DANTEC & A. GRANIER (2005), Modelling carbon and water cycles in a beech forest. part I: Model description and uncertainty analysis on modelled NEE. *Ecological Modelling* 185, pp. 407–436.
- DUNNE, T., T. MORE & C. TAYLOR (1975), Recognition and prediction of runoff producing zones in humid regions. *Hydrologic Sciences Bulletin* 20, pp. 305–327.
- EAGLESON, P. (1982), Ecological optimality in water-limited natural soil-vegetation systems. 1. theory and hypothesis. *Water Resources Research* 18, pp. 325–340.
- EAGLESON, P. S. (1978), Climate, soil, and vegetation 1. Introduction to water balance dynamics. *Water Resources Research* 14.
- EMANUEL, W. R., H. H. SHUGART & M. STEVENSON (1985), Climatic-change and the broad-scale distribution of terrestrial ecosystem complexes - response. *Climatic Change* 7, pp. 457–460.

- FALINSKI, J. B. & K. FALINSKA (1986), Vegetation dynamics in temperate lowland primeval forests., vol. 8 of *Geobotany*. Dordrecht: Junk.
- FAMIGLIETTI, J. S., E. F. WOOD, M. SIVAPALAN & D. J. THONGS (1992), A catchment scale water-balance model for five. *Journal of Geophysical Research-Atmospheres* 97, pp. 18997–19007.
- FARQUHAR, G. D., S. VON CAEMMERER & J. A. BERRY (1980), A biochemical model of photosynthetic CO₂ assimilation in leaves of C3 species. *Planta* 149, pp. 78–90.
- FARRELL, D. A. & W. E. LARSON (1972), Modelling the pore structure of porous media. *Water Resources Research* 8, pp. 699–706.
- FEDDES, R. A., P. KOWALIK & H. JARADNY (1978), Simulation of field water use and crop yield. In: *Simulation Monographs*, Wageningen: Pudoc, p. 189 p.
- FISCHLIN, A., H. BUGMANN & D. GYALISTRAS (1995), Sensitivity of a forest ecosystem model to climate parametrization schemes. *Environmental Pollution* 87, pp. 267–282.
- FOLEY, J. A., I. C. PRENTICE, N. RAMANKUTTY, S. LEVIS, D. POLLARD, S. SITCH & A. HAXELTINE (1996), An integrated biosphere model of land surface processes, terrestrial carbon balance, and vegetation dynamics. *Global Biogeochemical Cycles* 10, pp. 603–628.
- FOWLER, H. J., S. BLENKINSOP & C. TEBALDI (2007), Linking climate change modelling to impacts studies: recent advances in downscaling techniques for hydrological modelling. *International Journal of Climatology* 27, pp. 1547–1578.
- FRIEND, A. D. (1995), Pgen - an integrated model of leaf photosynthesis, transpiration, and conductance. *Ecological Modelling* 77, pp. 233–255.
- FRIEND, A. D. (2001), Modelling canopy CO₂ fluxes: Are 'big-leaf' simplifications justified? *Global Ecology and Biogeography* 10, pp. 603–619.
- FRIEND, A. D., A. K. STEVENS, R. G. KNOX & M. G. R. CANNELL (1997), A process-based, terrestrial biosphere model of ecosystem dynamics (Hybrid v3.0). *Ecological Modelling* 95, pp. 249–287.
- HACK, J. T. & J. C. GOODLETT (1960), Geomorphology and forest ecology of a mountain region in the central appalachians. U.S. Geological Survey Professional Paper 347, pp. 1–66.
- HAXELTINE, A., I. C. PRENTICE & D. I. CRESWELL (1996), A coupled carbon and water flux model to predict vegetation structure. *Journal of Vegetation Science* 7, pp. 651–666.
- HILLERISLAMBERS, R., M. RIETKERK, F. VAN DEN BOSCH, H. H. T. PRINS & H. DE KROON (2001), Vegetation pattern formation in semi-arid grazing systems. *Ecology* 82, pp. 50–61.
- HOPP, L., C. HARMAN, S. L. E. DESILETS, C. B. GRAHAM, J. J. McDONNELL & P. A. TROCH (2009), Hillslope hydrology under glass: confronting fundamental questions of soil-water-biota co-evolution at biosphere 2. *Hydrology and Earth System Sciences* 13, pp. 2105–2118.
- IPCC (2007), *Climate Change 2007: Synthesis report*. Contribution of working groups I, II and III to the Fourth Assessment Report of the Intergovernmental Panel on Climate Change. Tech. Rep.
- JACKSON, C. R. (1992), Hillslope infiltration and lateral downslope unsaturated flow. *Water Resources Research* 28, pp. 2533–2539.
- JANSEN, J., J. SEVENSTER & P. FABER (1996), *Opbrengst tabellen voor belangrijke boomsoorten in Nederland*. Tech. Rep. IBN 221.
- JARVIS, P. G. (1976), The interpretation of the variations in leaf water potential and stomatal conductance found in canopies in the field. *Philosophical Transactions of the Royal Society London* 273, pp. 593–610.
- JIANG, X. Y., G. Y. NIU & Z. L. YANG (2009), Impacts of vegetation and groundwa-

- ter dynamics on warm season precipitation over the Central United States. *Journal of Geophysical Research-Atmospheres* 114.
- KARNOSKY, D. F. (2003), Impacts of elevated atmospheric CO₂ on forest trees and forest ecosystems: knowledge gaps. *Environment International* 29, pp. 161–169.
- KATUL, G., R. LEUNING & R. OREN (2003), Relationship between plant hydraulic and biochemical properties derived from a steady-state coupled water and carbon transport model. *Plant, Cell and Environment* 26, pp. 339–350.
- KERKHOFF, A. J., S. N. MARTENS & B. T. MILNE (2004), An ecological evaluation of eagleson’s optimality hypotheses. *Funct Ecology* 18, pp. 404–413.
- KILSBY, C. G., P. D. JONES, A. BURTON, A. C. FORD, H. J. FOWLER, C. HARPAM, P. JAMES, A. SMITH & R. L. WILBY (2007), A daily weather generator for use in climate change studies. *Environmental Modelling and Software* 22, pp. 1705–1719.
- KIRKBY, M. J. (1978), *Hillslope hydrology. Landscape systems*, Wiley.
- KLAUSMEIER, C. A. (1999), Regular and irregular patterns in semiarid vegetation. *Science* 284, pp. 1826–1828.
- KLEINHANS, M. G., M. F. P. BIERKENS & M. VAN DER PERK (2010), Hess opinions ”hydrologists, bring out shovels and garden hoses and hit the dirt”. *HESSD* .
- KNOHL, A., E. D. SCHULZE, O. KOLLE & N. BUCHMANN (2003), Large carbon uptake by an unmanaged 250-year-old deciduous forest in central germany. *Agricultural and Forest Meteorology* 118, pp. 151–167.
- KRUIJT, B., J.-P. M. WITTE, C. M. J. JACOBS & T. KROON (2008), Effects of rising atmospheric CO₂ on evapotranspiration and soil moisture: A practical approach for the Netherlands. *Journal of Hydrology* 349, pp. 257–267.
- LAIO, F., A. PORPORATO, L. RIDOLFI & I. RODRIGUEZ-ITURBE (2001), Plants in water-controlled ecosystems: active role in hydrologic processes and response to water stress: Ii. probabilistic soil moisture dynamics. *Advances in Water Resources* 24, pp. 707–723.
- LAIO, F., S. TAMEA, L. RIDOLFI, P. D’ODORICO & I. RODRIGUEZ-ITURBE (2009), Ecohydrology of groundwater-dependent ecosystems: 1. stochastic water table dynamics. *Water Resources Research* 45.
- LANDSBERG, J. (1986), *Physiological ecology of forest production*, vol. XVIII. Academic Press.
- LEEMANS, R. & I. PRENTICE (1989), FORSKA, a general forest succession model. Tech. Rep. 89/2, Institute of Ecological Botany.
- LEUNING, R. (1990), Modelling stomatal behaviour and photosynthesis of eucalyptus grandis. *Australian Journal of Plant Physiology* 17, pp. 159–175.
- LEUNING, R. (1995), A critical appraisal of a combined stomatal-photosynthesis model for C3 plants. *Plant, Cell and Environment* 18, pp. 339–355.
- LOTKA, A. J. (1922), Contribution to the energetics of evolution. *Proceedings of the National Academy of Sciences of the United States of America* 8, pp. 147–151.
- MEDLYN, B. E., C. V. M. BARTON, M. S. J. BROADMEADOW, R. CEULEMANS, P. DE ANGELIS, M. FORSTREUTER, M. FREEMAN, S. B. JACKSON, S. KELLOMAKI, E. LAITAT, A. REY, P. ROBERNTZ, B. D. SIGURDSSON, J. STRASSEMAYER, K. WANG, P. S. CURTIS & P. G. JARVIS (2001), Stomatal conductance of forest species after long-term exposure to elevated CO₂ concentration: a synthesis. *New Phytologist* 149, pp. 247–264.
- MILLY, P. C. D. (1993), An analytic solution of the stochastic storage problem applicable to soil water. *Water Resources Research* 29, pp. 3755–3758.
- MONTEITH, J. L. (1965), Evaporation and environment. *Symposia of the Society for Experimental Biology* 19, pp. 205–234.

- NAKICENOVIC, N. & R. SWART, eds. (2000), IPCC Special Report on Emission 437 Scenarios. Cambridge, UK: Cambridge University Press, 438 edn.
- ODUM, H. T. (1983), *Systems ecology*. New York: Wiley.
- OLLINGER, S. V. & M. L. SMITH (2005), Net primary production and canopy nitrogen in a temperate forest landscape: An analysis using imaging spectroscopy, modeling and field data. *Ecosystems* 8, pp. 760–778.
- PARTON, W. J. (1993), Observations and modeling of biomass and soil organic matter dynamics for the grassland biome worldwide. *Global Biogeochemical Cycles* 7, pp. 785–809.
- PHILIP, J. R. (1991), Hillslope infiltration: planar slopes. *Water Resources Research* 27, pp. 109–117.
- PORPORATO, A., F. LAIO, L. RIDOLFI & I. RODRIGUEZ-ITURBE (2001), Plants in water-controlled ecosystems: active role in hydrologic processes and response to water stress: Iii. vegetation water stress. *Advances in Water Resources* 24, pp. 725–744.
- PORPORATO, A., E. DALY & I. RODRIGUEZ-ITURBE (2004), Soil water balance and ecosystem response to climate change. *American Naturalist* 164, pp. 625–632.
- POTTER, C. S. (1993), Terrestrial ecosystem production: a process model based on global satellite and surface data. *Global Biogeochemical Cycles* 7, pp. 811–841.
- PRENTICE, I. C., M. T. SYKES & W. CRAMER (1993), A simulation model for the transient effects of climate change on forest landscapes. *Ecological Modelling* 65, pp. 51–70.
- REICHSTEIN, M., A. REY, A. FREIBAUER, J. TENHUNEN, R. VALENTINI, J. BANZA, P. CASALS, Y. F. CHENG, J. M. GRUNZWEIG, J. IRVINE, R. JOFFRE, B. E. LAW, D. LOUSTAU, F. MIGLIETTA, W. OECHEL, J. M. OURCIVAL, J. S. PEREIRA, A. PERESSOTTI, F. PONTI, Y. QI, S. RAMBAL, M. RAYMENT, J. ROMANYA, F. ROSSI, V. TEDESCHI, G. TIRONE, M. XU & D. YAKIR (2003), Modeling temporal and large-scale spatial variability of soil respiration from soil water availability, temperature and vegetation productivity indices. *Global Biogeochemical Cycles* 17.
- RICHARDS, L. A. (1931), Capillary conduction of liquids through porous mediums. *Physics* 1, pp. 318–333.
- RICHARDSON, C. (1981), Stochastic simulation of daily precipitation, temperature, and solar radiation. *Water Resources Research* 17, pp. 182–190.
- RIDOLFI, L., P. D'ODORICO, A. PORPORATO & I. RODRIGUEZ-ITURBE (2003), Stochastic soil moisture dynamics along a hillslope. *Journal of Hydrology* 272, pp. 264–275.
- RIETKERK, M., M. C. BOERLIJST, F. VAN LANGEVELDE, R. HILLERISLAMBERS, J. VAN DE KOPPEL, L. KUMAR, H. H. T. PRINS & A. M. DE ROOS (2002), Self-organization of vegetation in arid ecosystems. *American Naturalist* 160, pp. 524–530.
- RIETKERK, M., S. C. DEKKER, M. J. WASSEN, A. W. M. VERKROOST & M. F. P. BIERKENS (2004), A putative mechanism for bog patterning. *American Naturalist* 163, pp. 699–708.
- RODRIGUEZ-ITURBE, I. (2000), Ecohydrology: A hydrologic perspective of climate-soil-vegetation dynamics. *Water Resources Research* 36, pp. 3–9.
- RODRIGUEZ-ITURBE, I. & A. PORPORATO (2004), *Ecohydrology of water-controlled ecosystems*. Cambridge, UK New York, NY, USA: Cambridge University Press.
- RODRIGUEZ-ITURBE, I., P. D'ODORICO, A. PORPORATO & L. RIDOLFI (1999), On the spatial and temporal links between vegetation, climate, and soil moisture. *Water Resources Research* 35, pp. 3709–3722.
- RODRIGUEZ-ITURBE, I., P. D'ODORICO, F. LAIO, L. RIDOLFI & S. TAMEA (2007), Challenges in humid land ecohydrology: Interactions of water table and unsaturated zone with climate, soil, and vegetation. *Water Resources Research* 43.

- RUNNING, S. W. & J. C. COUGHLAN (1988), A general-model of forest ecosystem processes for regional applications. 1. Hydrologic balance, canopy gas-exchange and primary production processes. *Ecological Modelling* 42, pp. 125–154.
- RUNNING, S. W. & S. T. GOWER (1991), FOREST-BGC, a general-model of forest ecosystem processes for regional applications. 2. dynamic carbon allocation and nitrogen budgets. *Tree Physiology* 9, pp. 147–160.
- RYAN, M. G. (1991), Effects of climate change on plant respiration. *Ecological Applications* 1, pp. 157–167.
- SAXE, H., M. G. R. CANNELL, B. JOHNSEN, M. G. RYAN & G. VOURLITIS (2001), Tree and forest functioning in response to global warming. *New Phytologist* 149, pp. 369–399.
- SCHAAP, M. G., F. J. LEIJ & M. T. VAN GENUCHTEN (1998), Neural network analysis for hierarchical prediction of soil hydraulic properties. *Soil Science Society of America Journal* 62, pp. 847–855.
- SCHWALM, C. R. & A. R. EK (2004), A process-based model of forest ecosystems driven by meteorology. *Ecological Modelling* 179, pp. 317–348.
- SCHYMANSKI, S. J., M. SIVAPALAN, M. L. RODERICK, L. B. HUTLEY & J. BERINGER (2009), An optimality-based model of the dynamic feedbacks between natural vegetation and the water balance. *Water Resources Research* 45.
- SHUTTLEWORTH, W. (1993), Evaporation. In: D. Maidment, ed., *Handbook of Hydrology*, New York: McGraw-Hill, p. 4.14.53.
- SITCH, S., B. SMITH, I. C. PRENTICE, A. ARNETH, A. BONDEAU, W. CRAMER, J. O. KAPLAN, S. LEVIS, W. LUCHT, M. T. SYKES, K. THONICKE & S. VENEVSKY (2003), Evaluation of ecosystem dynamics, plant geography and terrestrial carbon cycling in the LPJ dynamic global vegetation model. *Global Change Biology* 9, pp. 161–185.
- SMITH, T. M., R. LEEMANS & H. H. SHUGART (1992), Sensitivity of terrestrial carbon storage to CO₂-induced climate change - comparison of 4 scenarios based on general-circulation models. *Climatic Change* 21, pp. 367–384.
- SOLOMON, S., D. QIN, M. MANNING, Z. CHEN, M. MARQUIS, K. AVERYT, M. TIGNOR & H. MILLER, eds. (2007), IPCC, 2007: Climate Change 2007: The Physical Science Basis. Contribution of Working Group I to the Fourth Assessment Report of the Intergovernmental Panel on Climate Change. Cambridge, New York: Cambridge University Press.
- SPRUGEL, D. G., M. G. RYAN, J. R. BROOKS, K. A. VOGT & T. A. MARTIN (1995), Respiration from the organ level to the stand. In: W. K. Smith & T. M. Hinckley, eds., *Resource Physiology of Conifers*, San Diego: Academic Press, Inc., pp. 255–299.
- SWANSON, D. K. & D. F. GRIGAL (1988), A simulation model of mire patterning. *Oikos* 53, pp. 309–314.
- TAMEA, S., F. LAIO, L. RIDOLFI, P. D'ODORICO & I. RODRIGUEZ-ITURBE (2009), Ecohydrology of groundwater-dependent ecosystems: 2. stochastic soil moisture dynamics. *Water Resources Research* 45.
- TEULING, A. J. & P. A. TROCH (2005), Improved understanding of soil moisture variability dynamics. *Geophysical Research Letters* 32.
- TROCH, P. A., C. PANICONI & E. E. VAN LOON (2003), Hillslope-storage boussinesq model for subsurface flow and variable source areas along complex hillslopes: 1. formulation and characteristic response. *Water Resources Research* 39.
- VAN ASCH, T. W. J., S. J. E. VAN DIJCK & M. R. HENDRIKS (2001), The role of overland flow and subsurface flow on the spatial distribution of soil moisture in the topsoil. *Hydrological Processes* 15, pp. 2325–2340.
- VAN BEEK, R. (2002), Assessment of the influence of changes in land use and climate on

- landslide activity in a Mediterranean environment. Ph.D. thesis, Utrecht University.
- VAN DAM, J. C., P. GROENENDIJK, R. F. A. HENDRIKS & J. G. KROES (2008), Advances of modeling water flow in variably saturated soils with swap. *Vadose Zone Journal* 7, pp. 640–653.
- VAN DE KOPPEL, J., M. RIETKERK, F. VAN LANGEVELDE, L. KUMAR, C. A. KLAUSMEIER, J. M. FRYXELL, J. W. HEARNE, J. VAN ANDEL, N. DE RIDDER, A. SKIDMORE, L. STROOSNIJDER & H. H. T. PRINS (2002), Spatial heterogeneity and irreversible vegetation change in semiarid grazing systems. *American Naturalist* 159, pp. 209–218.
- VAN DER TOL, C., A. J. DOLMAN, M. J. WATERLOO & A. MEESTERS (2008a), Optimum vegetation characteristics, assimilation, and transpiration during a dry season: 2. model evaluation. *Water Resources Research* 44.
- VAN DER TOL, C., A. MEESTERS, A. J. DOLMAN & M. J. WATERLOO (2008b), Optimum vegetation characteristics, assimilation, and transpiration during a dry season: 1. model description. *Water Resources Research* 44.
- VAN DER VOET, P., K. KRAMER & C. VAN DIEPEN (1996), Parameterization of the Richardson weather generator within the European Union. Tech. Rep. 92, DLO Winand Staring Centre.
- VAN GENUCHTEN, M. T. (1980), A closed-form equation for predicting the hydraulic conductivity of unsaturated soils. *Soil Science Society of America Journal* 44, pp. 892–898.
- VAN VLIET, M. T. H., S. BLENKINSOP, A. BURTON & H. J. FOWLER (submitted), A multi-model ensemble of downscaled climate change scenarios for the Dommel catchment, The Netherlands. *Climate Research* .
- VAN WIJK, M. T. & W. BOUTEN (2001), Towards understanding tree root profiles: simulating hydrologically optimal strategies for root distribution. *Hydrology and Earth System Sciences* 5, pp. 629–644.
- VAN WIJK, M. T. & I. RODRIGUEZ-ITURBE (2002), Tree-grass competition in space and time: Insights from a simple cellular automata model based on ecohydrological dynamics. *Water Resources Research* 38.
- VON HARDENBERG, J., E. MERON, M. SHACHAK & Y. ZARMI (2001), Diversity of vegetation patterns and desertification. *Physical Review Letters* 87.
- WIGMOSTA, M. S., L. W. VAIL & D. P. LETTENMAIER (1994), A distributed hydrology-vegetation model for complex terrain. *Water Resources Research* 30, pp. 1665–1679.
- WIGMOSTA, M. S., L. R. LEUNG & E. J. RYKIEL (1995), Regional modelling of climate-terrestrial ecosystem interactions. *Journal of Biogeography* 22, pp. 453–465.
- WOODWARD, F. I., T. M. SMITH & W. R. EMANUEL (1995), A global land primary productivity and phytogeography model. *Global Biogeochemical Cycles* 9, pp. 471–490.
- ZAVALA, M. A. (2004), Integration of drought tolerance mechanisms in mediterranean sclerophylls: A functional interpretation of leaf gas exchange simulators. *Ecological Modelling* 176, pp. 211–226.
- ZHANG, L. & W. DAWES (1998), WAVES, An integrated energy and water balance model. Tech. Rep. No. 31/98, CSIRO Land and Water.
- ZIANIS, D. & K. RADOGLU (2006), Comparison between empirical and theoretical biomass allometric models and statistical implications for stem volume predictions. *Forestry* 79, pp. 477–487.

Acknowledgements

Veel mensen hebben direct of indirect bijgedragen aan mijn proefschrift. Al deze mensen wil ik hartelijk daarvoor danken en een aantal mensen in het bijzonder.

Als eerste wil ik uiteraard mijn promotor Marc Bierkens bedanken. Het initiële voorstel voor dit onderzoek is van jouw hand. In het uiteindelijke proefschrift zijn waarschijnlijk meer eco-physiologische processen beland dan jij aanvankelijk kon vermoeden. Ik wil je daarom bedanken voor het feit dat jij je uiteindelijk grondig hebt willen verdiepen in deze kant van de ecohydrologie. Verder wil ik je uiteraard bedanken voor het lezen en becommentariëren van alle artikelen en mijn proefschrift en voor je eindeloze stroom oplossingen voor uitdagingen die we tegengekomen zijn. Ook waardeer ik je geduld en vertrouwen tijdens het afronden van dit onderzoek. Ondanks onze contrasterende persoonlijkheden kijk ik terug op een goede samenwerking.

Als tweede wil ik mijn copromotor Rens van Beek bedanken. In de eerste plaats voor het hydrologische model STARWARS dat jij ooit voor je eigen proefschrift ontwikkelde met daarin de vlag: matrix stroming aan/uit. Helaas kwam de matrix potentiaal gedreven stroming elders niet meer terug in het model. Zonder dat je er tijd voor had, hebben we deze er toch samen in gebouwd. Daarnaast waardeer ik je input voor het derde artikel en mijn thesis en je kritische blik.

Vervolgens wil ik uiteraard nog de twee andere co-auteurs bedanken voor hun input voor de artikelen: Derek-Jan Karsenberg en Michelle van Vliet. Derek-Jan, je bent er deels in geslaagd mij aan de dynamische programmeertaal PC-Raster–Python te helpen. Mijn modellen runnen in Python; PC-Raster was echter een stap te ver in mijn virtuele wereld met orthogonaal coördinaatsysteem met oorsprong in 0. Michelle van Vliet, uiteraard bedankt voor het genereren van het ensemble van gedownscalede neerslagreeksen.

Natuurlijk wil ik al mijn oud-kamergenoten bedanken voor alle hulp en gezelligheid. Job Spijker je hebt mij goddeels bekeerd tot Latex. Hoewel ik er soms spijt van had, heb ik er in de laatste fase veel profijt van gehad. Wiebe Borren je hebt mij goed op weg geholpen met Python, en in het bijzonder met `array2map.py`. Mijn laatste kamergenoot Wiebe Nijland bedank ik voor de amusante discussies naar aanleiding van je al dan niet gefundeerde mening over alles en natuurlijk de citatie van mijn eerste artikel.

Verder wil ik uiteraard mijn collega's op het departement bedanken voor de gezelligheid, gesprekken en discussies naast de machine waarvan sommigen beweren dat er

koffie uitkomt. Een aantal personen wil ik in het bijzonder noemen. Hanneke Schuurmans; met jou ben ik tegelijkertijd aan een Ph.D. begonnen bij de toen verse professor M.F.P. Bierkens. Wij hebben onder andere gezamenlijk onze verjaardagen op het departement gevierd met borrels en taart. Arien Lam, bedankt voor het beschikbaar stellen van je rekencomputer en het delen van je uitgebreide kennis op het gebied van opensource software en Oliver Schmitz, bedankt voor je ondersteuning in Linux; lokaal en bij het rekencentrum Sara. Verder wil ik nog even mijn oude koffieburen bedanken voor uiteraard de koffie en de gezelligheid: Lara, Derek-Jan, Kor, Hans en Raymond.

Sil en Sita, bedankt voor jullie grote inzet in het veld en de gezelligheid op de camping in Polen. Helaas is slechts weinig van het veldonderzoek in mijn proefschrift beland, maar het heeft mij wel veel inzichten opgeleverd. Furthermore I would like to thank Andrzej Boczon and Janusz Czerepko for their support during our fieldwork in Białowieża, East Poland.

Ik wil Deltares en mijn collega's bij Deltares, bedanken voor de flexibiliteit en steun in de afrondingsfase van mijn proefschrift.

Paranimfen Marijn en Frank, jullie zijn een belangrijke steun voor mij geweest, door ondermeer onze vakanties, bezoeken en het aanhoren van mijn ervaringen in het traject dat promotie heet. Ik heb nu eindelijk meer tijd om met jullie af te spreken in Ispra, NY, Wenen of anders Utrecht, Renkum of Lisse.

Hoewel ik na het aflopen van mijn aio-contract van mijn werk mijn hobby heb gemaakt, waren er toch betere vormen van ontspanning. Prosac (Vintage): Uif, Ate, Ane, Erwin, Martijn, Arnold, Marc, Robert en Mark met jullie deel ik een passie voor boulderen en klimmen of anders in ieder geval een voorliefde voor bier. Daarnaast zijn er natuurlijk Marije, Vincent, Geert-Jan, Josja, Maaïke, Renske, Inka, Maartje en Imke. Met zijn allen hebben jullie een belangrijke bijdrage geleverd in ondersteuning voor het afronden van mijn promotie.

Jacob, Annelies, Anna en Folkert, bedankt voor jullie interesse in mijn onderzoek, inhoudelijk en procesmatig en het vakkundig niet tonen van interesse op momenten dat ik er geen behoefte aan had.

Als laatste wil ik uiteraard Eveline bedanken. Zonder jou was mijn proefschrift mogelijk niet afgekomen. Je zorgde onder andere door een gezonde afwisseling van geduld en motiverend ongeduld voor een goede stimulans. Ik kijk uit naar de periode na het afronden van dit proefschrift waarin ik eindelijk weer meer tijd voor jou en de te lang uitgestelde gezamenlijke verre vakanties heb.

Publications

Articles

Brolsma, R. J., M. T. H. van Vliet, and M. F. P. Bierkens, Climate change impact on a groundwater-influenced hillslope ecosystem. *Water Resources Research*, submitted.

Brolsma, R. J., D. Karssenbergh and M. F. P. Bierkens (2010), Vegetation competition model for water and light limitation. I: model description, one-dimensional competition and the influence of groundwater. *Ecological Modelling* 221, pp. 1348-1363.

Brolsma, R. J., L. P. H. van Beek and M. F. P. Bierkens (2010), Vegetation competition model for water and light limitation. II: spatial dynamics of groundwater and vegetation. *Ecological Modelling* 221, pp. 1364-1377.

Brolsma, R. J., and M. F. P. Bierkens (2007), Groundwater-soil water-vegetation dynamics in a temperate forest ecosystem along a slope, *Water Resources Research*, 43.

Selected presentations

Bierkens, M. F. P., R. J. Brolsma, L. P. H. van Beek, M. T. H. van Vliet (2008), Climate change effects on groundwater dependent temperate forest ecosystems, AGU Fall Meeting, San Francisco, USA.

Brolsma, R. J., L. P. H. van Beek, M. F. P. Bierkens (2008), Climate change effects on groundwater dependent temperate forest ecosystems, EGU General Assembly, Vienna, Austria.

Brolsma, R. J., M. F. P. Bierkens (2007), Climate change effects on temperate forest ecosystems: Putting groundwater into the equation, AGU Fall Meeting, San Francisco, USA.

Bierkens, M. F. P., R.J. Brolsma, S. C. Dekker, M. Rietkerk (2006), Spatio-temporal dynamics of soil, water and vegetation in groundwater dependent ecosystems, HydroEco2006, International multidisciplinary conference on hydrology and ecology, Karlovy Vary, Czech Republic.

Brolsma, R. J., M. F. P. Bierkens (2006), Vegetation dynamics in a groundwater-controlled ecosystem, HydroEco2006, International multidisciplinary conference on hydrology and ecology, Karlovy Vary, Czech Republic.

Brolsma, R. J., M. F. P. Bierkens (2005) Ground-soil water-vegetation dynamics of a groundwater controlled ecosystem along a slope, Sir Mark Oliphant Conference on Thresholds and Pattern Dynamics, Perth, Australia.

Brolsma, R. J., M. F. P. Bierkens (2004), Maximum productivity of vegetation in a simplified soil water - groundwater - vegetation system, EGU, 1st General Assembly, Nice, France.

de Willigen, P., R. Brolsma, W. Bouten, (2002), Infiltration in water repellent soils: measurements and simulations on pore scale, EGS, Nice, France.

Curriculum Vitae

Reinder Jacob Brolsma was born on March 10 1977 in Amsterdam, The Netherlands. In 1996 he finished VWO at Willem Blaeu College in Alkmaar. After this he studied Physical Geography at the University of Amsterdam, graduating in geomorphology. For his M.Sc. thesis he studied the infiltration rate of water drops in water repellent soils using digital imaging. After finishing his study he started his full-time professional career at Royal Haskoning, a major consultancy and engineering company in the Netherlands. There he worked on geo-data management to support large soil research/sanitation projects. Preferring academic research over consultancy he started his Ph.D. research at the department of Physical Geography at Utrecht University, resulting in this thesis entitled: "Effect of climate change on temperate forest ecosystems". After working full-time at his thesis, he continued part-time, while first working at Nelen-Schuurmans and later on at Deltares, the national research institute water, soil and subsurface. Here he performs applied research in the field of sustainable urban water management.

NEDERLANDSE GEOGRAFISCHE STUDIES / NETHERLANDS GEOGRAPHICAL STUDIES

- 365 E HEERE & M STORMS Ormelings cartography; Presented to Ferjan Ormeling on the occasion of his 65th birthday and his retirement as Professor of Cartography – Utrecht 2007: Knag/Faculteit Geowetenschappen Universiteit Utrecht. ISBN: 978-90-6809-407-7, Euro 20,00
- 366 S QUARTEL Beachwatch; The effect of daily morphodynamics on seasonal beach evolution – Utrecht 2007: Knag/Faculteit Geowetenschappen Universiteit Utrecht. 125 pp, 39 figs, 7 tabs. ISBN: 978-90-6809-408-4, Euro 12,50
- 367 R O VAN MERKERK Intervening in emerging nanotechnologies; A CTA of Lab-on-a-chip technology regulation – Utrecht 2007: Knag/Copernicus Institute. 206 pp, 19 box, 35 figs, 12 tabs. ISBN: 978-90-6809-409-1, Euro 20,00
- 368 R M FRINGS From gravel to sand; Downstream fining of bed sediments in the lower river Rhine – Utrecht 2007: Knag/Faculteit Geowetenschappen Universiteit Utrecht. ISBN: 978-90-6809-410-7, Euro 25,00
- 369 W IMMERZEEL Spatial modelling of the hydrological cycle, climate change and agriculture in mountainous basins – Utrecht 2008: Knag/Faculteit Geowetenschappen Universiteit Utrecht. 147 pp, 54 figs, 12 tabs. ISBN: 978-90-6809-411-4, Euro 25,00
- 370 D S J MOURAD Patterns of nutrient transfer in lowland catchments; A case study from northeastern Europe – Utrecht 2008: Knag/Faculteit Geowetenschappen Universiteit Utrecht. 176 pp, 44 figs, 19 tabs. ISBN: 978-90-6809-412-1, Euro 20,00
- 371 M M H CHAPPIN Opening the black box of environmental innovation; Governmental policy and learning in the Dutch paper and board industry – Utrecht 2008: Knag/Copernicus Institute. 202 pp, 41 figs, 30 tabs. ISBN: 978-90-6809-413-8, Euro 22,50
- 372 R P ODDENS & M VAN EGMOND Ormelings atlassen; Catalogus van atlassen geschonken aan de Universiteit Utrecht door de hoogleraren F.J. Ormeling sr. en jr. Utrecht 2008: Knag/Faculteit Geowetenschappen Universiteit Utrechts. ISBN: 978-90-6809-415-2, Euro 15,00
- 373 R VAN MELIK Changing public space; The recent redevelopment of Dutch city squares Utrecht 2008: Knag/Faculteit Geowetenschappen Universiteit Utrecht. 323 pp, 47 figs, 32 tabs. ISBN: 978-90-6809-416-9, Euro 20,00
- 374 E ANDRIESSE Institutions and regional development in Southeast Asia; A comparative analysis of Satun (Thailand) and Perlis (Malaysia) – Utrecht 2008: Knag/Faculteit Geowetenschappen Universiteit Utrecht. 250 pp, 42 figs, 43 tabs, 18 box. ISBN: 978-90-6809-417-6, Euro 25,00
- 375 E HEERE GIS voor historisch landschapsonderzoek; Opzet en gebruik van een historisch GIS voor prekadastrale kaarten – Utrecht 2008: Knag/Faculteit Geowetenschappen Universiteit Utrecht. 231 pp, 73 figs, 13 tabs. ISBN: 978-90-6809-418-3, Euro 30,00
- 376 V D MAMADOUH, S M DE JONG, J F C M THISSEN & J A VAN DER SCHEE Dutch windows on the Mediterranean; Dutch Geography 2004-2008 – Utrecht 2008: Knag/International Geographical Union Section The Netherlands. 104 pp + cd-rom, 38 figs, 9 tabs. ISBN: 978-90-6809-419-0, Euro 10,00
- 377 E VAN MARISSING Buurten bij beleidsmakers; Stedelijke beleidsprocessen, bewonersparticipatie en sociale cohesie in vroeg-naoorlogse stadswijken in Nederland – Utrecht 2008: Knag/Faculteit Geowetenschappen Universiteit Utrecht. 230 pp, 6 figs, 31 tabs. ISBN: 978-90-6809-420-6, Euro 25,00
- 378 M DE BEER, R C L BUITING, D J VAN DRUNEN & A J T GOORTS (Eds.) Water Wegen; Op zoek naar de balans in de ruimtelijke ordening – Utrecht 2008: Knag/VUGS/Faculteit Geowetenschappen Universiteit Utrecht. 91 pp, 18 figs, 1 tab. ISBN: 978-90-6809-421-3, Euro 10,00
- 379 J M SCHUURMANS Hydrological now- and forecasting; Integration of operationally available remotely sensed and forecasted hydrometeorological variables into distributed hydrological models – Utrecht 2008: Knag/Faculteit Geowetenschappen Universiteit Utrecht. 154 pp, 65 figs, 12 tabs. ISBN 978-90-6809-422-0, Euro 15,00
- 380 M VAN DEN BROECKE Ortelius Theatrum Orbis Terrarum (1570-1641); Characteristics and development of a sample of on verso map texts – Utrecht 2009: Knag/Faculteit Geowetenschappen Universiteit Utrecht. 304 pp + cd-rom, 9 figs, 65 tabs. ISBN 978-90-6809-423-7, Euro 30,00
- 381 J VAN DER KWAST Quantification of top soil moisture patterns; Evaluation of field methods, process- based modelling, remote sensing and an integrated approach – Utrecht 2009: Knag/Faculteit Geowetenschappen Universiteit Utrecht. 313 pp, 108 figs, 47 tabs. ISBN 978-90-6809-424-4, Euro 30,00
- 382 T J ZANEN Actie, actie, actie; De vakbeweging in regio Noord-Nederland, 1960-1992 – Utrecht/Groningen 2009: Knag/Faculteit Ruimtelijke Wetenschappen Rijksuniversiteit Groningen. ISBN 978-90-6809-425-1, Euro 30,00

- 383 M PERMENTIER Reputation, neighbourhoods and behaviour – Utrecht 2009: Knag/Faculteit Geowetenschappen Universiteit Utrecht. 146 pp, 10 figs, 19 tabs. ISBN 978-90-6809-426-8, Euro 15,00
- 384 A VISSER Trends in groundwater quality in relation to groundwater age – Utrecht 2009: Knag/Faculteit Geowetenschappen Universiteit Utrecht. 188 pp, 47 figs, 24 tabs. ISBN 978-90-6809-427-5, Euro, 20,00
- 385 B A FURTADO Modeling social heterogeneity, neighborhoods and local influences on urban real estate prices; Spatial dynamic analyses in the Belo Horizonte metropolitan area, Brazil – Utrecht 2009: Knag/Faculteit Geowetenschappen Universiteit Utrecht. 236 pp, 50 figs, 48 tabs. ISBN 978-90-6809-428-2, Euro 25,00
- 386 T DE NIJS Modelling land use change; Improving the prediction of future land use patterns – Utrecht 2009: Knag/Faculteit Geowetenschappen Universiteit Utrecht. 206 pp, 59 figs, 32 tabs. ISBN 978-90-6809-429-9, Euro 25,00
- 387 I J VISSEREN-HAMAKERS Partnerships in biodiversity governance; An assessment of their contributions to halting biodiversity loss – Utrecht 2009: Knag/Copernicus Institute. 177 pp, 4 figs, 4 tabs. ISBN 978-90-6809-430-5, Euro 20,00
- 388 G ERKENS Sediment dynamics in the Rhine catchment; Quantification of fluvial response to climate change and human impact – Utrecht 2009: Knag/Faculteit Geowetenschappen Universiteit Utrecht. 278 pp + addendum, 59 figs, 27 tabs. ISBN 978-90-6809-431-2, Euro 30,00
- 389 M HIJMA From river valley to estuary; The early-mid Holocene transgression of the Rhine-Meuse valley, The Netherlands – Utrecht 2009: Knag/Faculteit Geowetenschappen Universiteit Utrecht. ISBN 978-90-6809-432-9, Euro 25,00
- 390 N L M B VAN SCHAIK The role of Macropore Flow from PLOT to catchment scale; A study in a semi- arid area – Utrecht 2010: Knag/Faculteit Geowetenschappen Universiteit Utrecht. 174 pp, 65 figs, 26 tabs. ISBN 978-90-6809-433-6, Euro 20,00
- 391 B DOUCET Rich cities with poor people; Waterfront regeneration in the Netherlands and Scotland – Utrecht 2010: Knag/Faculteit Geowetenschappen Universiteit Utrecht. 208 pp, 49 figs, 13 tabs. ISBN 978-90-6809-434-3, Euro 25,00
- 392 L PAPE Predictability of nearshore sandbar behaviour – Utrecht 2010: Knag/ Faculteit Geowetenschappen Universiteit Utrecht. 157 pp, 36 figs, 5 tabs. ISBN 978-90-6809-435-0, Euro 17,50
- 393 M M VAN HUIJSTEE Business and NGOs in interaction; A quest for corporate social responsibility – Utrecht 2010: Knag/Copernicus Institute. 176 pp, 4 figs, 8 tabs. ISBN 978-90-6809-436-7, Euro 24,00
- 394 A KOKX Between dreams and reality; Urban governance in the process of Dutch urban restructuring – Utrecht 2010: Knag/Faculteit Geowetenschappen Universiteit Utrecht. 172 pp, 6 figs, 4 tabs. ISBN 978-90-6809-437-4, Euro 20,00
- 395 S VAN ASSELEN Peat compaction in deltas; Implications for Holocene delta evolutions – Utrecht 2010: Knag/Faculteit Geowetenschappen Universiteit Utrecht. ISBN 978-90-6809-438-1, Euro 17,50
- 396 R J BROLSMA Effect of climate change on temperate forest ecosystems – Utrecht 2010: Knag/Faculteit Geowetenschappen Universiteit Utrecht. ISBN 978-90-6809-439-8, Euro 17,95

For a complete list of NGS titles please visit www.knag.nl. Publications of this series can be ordered from KNAG / NETHERLANDS GEOGRAPHICAL STUDIES, P.O. Box 80123, 3508 TC Utrecht, The Netherlands (E-mail info@knag.nl; Fax +31 30 253 5523). Prices include packing and postage by surface mail. Orders should be prepaid, with cheques made payable to Netherlands Geographical Studies. Please ensure that all banking charges are prepaid. Alternatively, American Express, Eurocard, Access, MasterCard, BankAmericard and Visa credit cards are accepted (please specify card number, name as on card, and expiration date with your signed order).